Investigation of the Safety and Efficacy of Nacre for Use in Skin and Wound Repair

Edwin Setiawan Tjandra MSc

School of Animal Biology
10449050

This thesis is presented for the degree of Doctor of Philosophy of The University of Western Australia

2016

THE UNIVERSITY OF WESTERN AUSTRALIA

Abstract

Nacre has been used for both cosmetic and medicinal purposes in many civilizations over thousands of years. The use and widespread belief that nacre can enhance skin appearance and function is supported by only limited scientific evidence. The work presented herein is the result of a study into the preparation, toxicity and efficacy of nacre on skin cells *in vitro*. The aims of this study were to establish a protocol to generate nacre powder with a unimodal particle size distribution, evaluate the safety of inorganic and organic nacre components on skin cells *in vitro* and measure the effects of the organic component of nacre using *in vitro* wound healing models.

One specific issue that has hampered progress with the testing of the biological properties of nacre has been the use of preparations which are inconsistent in size and shape. In the work presented here, a standardised ball milling protocol was developed by varying six parameters: volume of excipient, sample size, grinding ball size, number of balls, speed and duration. The ball milled nacre particle size distribution was measured using a Mastersizer Hydro 2000s. The degrees of zirconium and cadmium contamination, as well as other elements, were quantified using Inductively Coupled Plasma Mass Spectrometry – Atomic Emission Spectrometry. The results demonstrated that the ball milling protocol produced a nacre product that was uncontaminated and consistent in size and shape.

A human immortalized keratinocyte cell line (HaCaT) and a mouse immortalized fibroblast cell line (NIH/3T3) NIH/3T3 fibroblasts) were used to assess the toxicity of nacre produced using the ball milling technique. In addition, for comparison, nacre prepared by other methods such as grinding with mortar and pestle and extraction with

the aid of ionic liquid were included in the study. Comprehensive toxicity testing included MTS assays and live/dead assays to determine the effect of nacre on cell viability qualitatively and quantitatively respectively and a reactive oxygen species (ROS) assay to examine whether nacre induced oxidative stress in skin cell types. The data suggested that milled nacre at a concentration of 0.1 mg/ml was safe and non-toxic to skin derived cell types. The same studies were replicated using media conditioned with 100 mg/ml of the milled particles. This part of the study was to investigate the effects of the organic component of nacre only. Live/dead assays using conditioned media showed no detrimental effects on cell viability and ROS levels were also not affected.

The potential efficacy of nacre on skin wound healing was assessed using *in vitro* models. To this end, a migration assay was used to determine whether nacre affects cell migration and can therefore potentially improve wound closure. Conditioned media containing the organic component of the milled nacre did not have any effect on wound closure. A 'scar in a jar' model was also used to assess the effects of nacre on collagen production. Results showed that the extract from milled nacre increased the quantity of collagen produced by fibroblasts whilst concurrently it did not alter the coherence of collagen produced. Interestingly, cells treated with conditioned media of $CaCO_3$ that acted as a control exhibited similar results.

In conclusion, this research provides a protocol to generate consistently sized nacre particles that are free from contaminants. In addition, the data show that nacre at low concentrations and its organic component are safe and non-toxic to skin cells. Furthermore, organic components of nacre were observed to increase collagen production in the functional assays and simultaneously did not cause the collagen to

lose its coherency. These results suggest that the use of nacre even at high concentrations is safe and may increase collagen production, which would be a potentially desirable effect in cosmetic applications. Further work using the standardized preparation of nacre should be undertaken to better understand the potential of nacre for skin applications.

Table of Contents

List of Figures and Tables

Chapter 1

Chapter 2

Chapter 3

Abbreviations

AD	Anno Domini
ANOVA	Analysis of variance
AP-1	Activator protein 1
ATP	Adenosine triphosphate
BI	Bayesian inference
BMIM/PF6	n-butyl-3-methylimidazolium hexafluorophosphate
BSA	Bovine serum albumin
CA	Caffeic acid
CLA	Conjugated linoleic acid
DCFH-DA	Dichlorodihydrofluorescin diacetate
DNA	Deoxyribonucleic acid
DSC	Differential scanning calorimetry
EDS	Energy dispersive X-ray spectroscopy
EDTA	ethylenediamine tetra-acetic acid
EGCG	epigallocatechin-3-gallate
EGF	Epidermal growth factor
ELISA	Enzyme linked immunosorbent assay
EtBr	Ethidium bromide

FGF	Fibroblast growth factor
FTIR	Fourier transform infrared spectroscopy
HA	Hyaluronic acid
HaCaT	Immortalised human keratinocyte cell line
HMGb-1	High-mobility group box-1
HOFs	Human oral fibroblasts
HOKs	Human oral keratinocytes
ICP MS-AES	Inductively coupled plasma mass spectrometry and atomic emission spectrometry
IL-1	Interleukin-1
IL-1α	Interleukin-1 alpha
IL-1β	Interleukin-1 beta
L929	Permanent mouse fibroblasts cell lines from China Centre for Type Culture Collection
MEF	Mouse embryonic fibroblasts
MMP-1	Matrix mettaloproteinase-1
mRNA	Messenger ribonucleic acid
Nacre G	Nacre grounded with mortar and pestle
Nacre M8	Sample 8 of milled nacre has the lowest contamination of Zr
Nacre M11	Sample 11 of milled nacre has the highest contamination of Zr
Nacre I	Nacre processed with ionic liquid
NGF	Nerve growth factor
NIH/3T3	Immortalised mouse fibroblast cell line
NO	Nitric oxide
NOS	Nitric oxide synthetase
PBS	Phosphate buffered saline
PDGF	Platelet derived growth factor

PHBV	Poly (3-hydroxybutyrate-co-3-hydroxyvalerate)
PMMA	Polymethylmethacrylate
PVA	Polyvynylalcohol
ROI	Region of interest
ROS	Reactive oxygen species
SAP	Superabsorbent polymer
SD	Standard deviation
SEM	Scanning electron microscopy
SOD	Superoxide dismutase
STAT6	Signal transducers and activators of transcription 6
TEM	Transmission electron microscopy
TGA	Thermo gravimetric analysis
TGF-α	Transforming growth factor-alpha
TGF-β	Transforming growth factor-beta
TIMP-1	Tissue inhibitor of metalloperoteinase-1
TNF-α	Tumour necrosis factor-alpha
UV	Ultraviolet
VEGF	Vascular endothelial growth factor
WSM	Water-soluble matrix
XRD	X-ray diffraction

Acknowledgements

Firstly, I would like to acknowledge my gratitude to all of my supervisors for their willingness to accompany me in this PhD training. I am grateful that Prof. Colin Raston took me on board in this nacre project. Prof. Fiona Wood gave inspiration to do research on skin cell. This thesis comes to shape and completion with the positive energy continuously diffused by Dr. Mark Fear and Prof. Sarah Dunlop. When it seems like a dead end, Dr. Fear always ready to suggest additional experiments to keep going forward. Prof. Dunlop is always there to straighten my logic and train me to be a better writer. This PhD project would not be possible without the financial support from Australian Research Council and Pearl Technology Pty Ltd.

Special thanks go to CMCA staff especially Peter Duncan for the technical and analytical support with microscopy. Additionally, I also would like to extend my gratitude for Laura Firth from UWA Centre for Applied Statistics to refresh my old memory about statistics.

I have to acknowledge the friendliness of the colleagues from the Centre for Strategic Nano-Fabrication, especially Dr. Ramiz Boulos, Dr. Jeremiah Toster and Dr. Ben Edwards. Thank you for sharing jokes and motivation that keeps me going in this PhD. Special mention has to go to Andrew Stevenson, my old friend from undergraduate, that helped me a lot in cell culture techniques. I also would like to thank Priyanka Toshniwal from Iyer group. Your readiness to help even in the middle of the night is really appreciated.

Finally, my deepest gratitude to my family especially, my beloved wife Cynthia, my sons Fransiskus and Leonardus, my parents, my parents-in-law and my siblings. To

my wife and sons, thank you for the understanding when I cannot be by your sides. We will have more quality times once this journey is completed. To my parents and parents-in-law, thank you for the care given to my wife and my sons while I am away. To my four siblings, thank you for your words and deeds that made the pressure during the candidature bearable.

Details of Publications and Conference Presentation

Paper published from the data in Chapter 2
Tjandra, E. S., Boulos, A. R., Duncan, P. C. and Raston, C. L., Unfastening pearl nacre nanostructures under shear. *CrystEngComm* **2013**, 15, (35), 6896-6900.

Author contributions: EST, RAB and CLR designed the research; EST performed the research; PCD assisted in TEM; EST, RAB and CLR finalized the manuscript. Overall contribution by EST: 85%

Other papers published during the course of the thesis
1. Agarwal, V., Tjandra, E. S., Iyer, K. S., Humfrey, B., Fear, M., Wood, F. W., Dunlop, S. and Raston, C. L., Evaluating the effects of nacre on human skin and scar cells in culture. *Toxicology Research* **2014**, 3, (4), 223-227.

EST performed the viability and reactive oxygen species assay on HaCaTs. Contribution by EST: 10%

2. Boulos, A. R., Zhang, F., Tjandra, E. S., Martin, A. D., Spagnoli, D. and Raston, C. L., Spinning up the polymorphs of calcium carbonate. *Scientific Reports* **2014**, 4, 3616.

EST assisted in characterization with TEM and SEM. Contribution by EST: 10%

3. Iscla, I., Wray, R., Blount, P., Larkins-Ford, J., Conery, A. L., Ausubel, F. M., Ramu, S., Kavanagh, A., Huang, J. X., Blaskovich, M. A., Cooper, M. A., Obregon-Henao, A., Orme, I., Tjandra, E. S., Stroeher, U. H., Brown, M. H., Macardle, C., van Holst, N., Tong, C. L., Slattery, A. D., Gibson, C. T., Raston, C. L. and Boulos, R. A., A new antibiotic with potent activity targets MscL. *The Journal of Antibiotics* **2015**, 68, 453-462.

EST carried out the cytotoxicity studies on NIH/3T3 and HaCaT cell lines. Contribution by EST: 5%

Poster Presentation
1. Tjandra, E. S., Boulos, R. A. and Raston, C. L., Ultra High Intensity Grinding of Pearl Nacre. ICONN 2012 International Conference on Nanoscience and Nanotechnology 5-9 February 2012, Perth, Western Australia.

Statements of Candidate Contribution

The work presented herein contains no materials, which the author has submitted or accepted for the award of another degree or diploma at any university. To the best of author's knowledge and belief, contains no material previously published or written by another person, except where due reference is made.

Edwin Setiawan Tjandra — Candidate

Prof. Sarah Dunlop — Co-ordinating Supervisor

Faith and reason are like two wings on which the human spirit rises to the contemplation of truth. *Fides et Ratio*, Pope John Paul II.

Chapter 1

Chapter 1: Introduction

1.1. Introduction

Skin is the first and foremost barrier that protects our body against changing temperature[1], ultraviolet (UV) radiation[2], dehydration[3] and infection.[4] Skin not only consists of skin cells but also includes blood vessels, nerve branches, hair follicles and sweat glands. Skin is the largest complex organ[5], and repairing it to its original state after being wounded is a major challenge. In recent years, numerous studies have tested different compounds or devised new strategies that might be beneficial in improving wound healing.[6-11] Nacre is one of the compounds that have been scrutinized in the last decade for its therapeutic effect.[12-14]

Nacre has been used as a medicine since ancient times in China to cure nebula[15] and India to treat gastric acid.[16,17] Other civilizations, such as Mayan Indians used nacre for prosthetic teeth.[18] _Royal families from China, Egypt and Persia were reported to use nacre powder for skin rejuvention.[19] Nowadays, there are many cosmetics from various brands that use pearl as one of their ingredients. They claim that nacre has beneficial effects for skin that ranges from whitening to anti aging. For example, Lorac Cosmetics claim that their lipstick, which contains nacre, can keep lips soft, smooth, supple and naturally rejuvenated.[20] HydroPeptide® Eye Authority claims on their website that crushed pearl can illuminate the eye area to diffuse the appearance of dark circles and eye imperfections while providing antibacterial, detoxification and skin nourishing properties.[21] Oriflame® Giordani Gold Bronzing Pearl claims that the micro pearls contained in it will give the skin a seamless, natural glow and flawless luminescence.[22] Pearl powder is one of the featured ingredients of SWELL™ Oceanic Cooling Mask from SIRCUIT® cosmeceuticals which is claimed to have a soothing, revitalizing and

protective effect on skin.[23] However, there is limited scientific evidence that supports the benefits of nacre on skin.

Nacre is a biomineralised material containing about 95% inorganic material and 5% organic components.[24,25] The inorganic component of nacre is solely composed of calcium carbonate, mostly in the form of aragonite.[25] The 5% organic component is mostly made of polysaccharides and protein fibers[26] which are rich in aspartic acid.[27] Table 1.1 summarizes the macromolecules that have been identified in nacre from *Pinctada* species and they are classified based on their solubility in water.

Table 1.1. Macromolecules from oyster shell *Pinctada* species.

	Soluble	**Insoluble**
Carbohydrate	Chitosan[28]	Chitin[29]
Proteins	AP7[30], AP24[30], MSI31[31], MSI60[31], MSI7[32], Mucoperlin[33], N14[34], N16/ Pearlin[35], Nacrein[36], p10[25], Perline[37], Perlucin[38], Pif[39]	Conchiolin[40], Lustrin A[41], MRNP34[42]
Lipid	----------	Cholesterol[43], cholesterol acetate[43], cholesterol sulfate[43], hydroxylated ceramides[43], nonhydroxylated ceramides[43], fatty acids[43], triglycerides[43],squalene-like lipids[43].

The current study will analyze the effects of different kinds of preparations of nacre on skin cells *in vitro*. It will shed some light on whether the organic or inorganic components of nacre contribute to the beneficial effects of nacre that have been claimed for centuries.

The first step of this study is to generate reproducible nacre product that includes either the organic component alone, inorganic component alone or both. The second step is to test the cytotoxicity of the different kinds of nacre preparations. The last step is to test the efficacy of nacre preparations on skin cell migration, collagen synthesis and collagen coherency.

1.2. Nacre

1.2.1. Source of Oyster

The pearl oysters used for this work were *Pinctada margaritifera*. While pearl is expensive and traded as high-class jewelry[44], its shell is accumulating as waste from the pearl industry. They were supplied by Pearl Technology Pty Ltd, who farms them in the Abrolhos Islands, Western Australia (Fig. 1.1). The common name for *Pinctada margaritifera* is the Black Lipped Pearl Oyster. It is one of the typical suspension-feeding bivalves.[45]

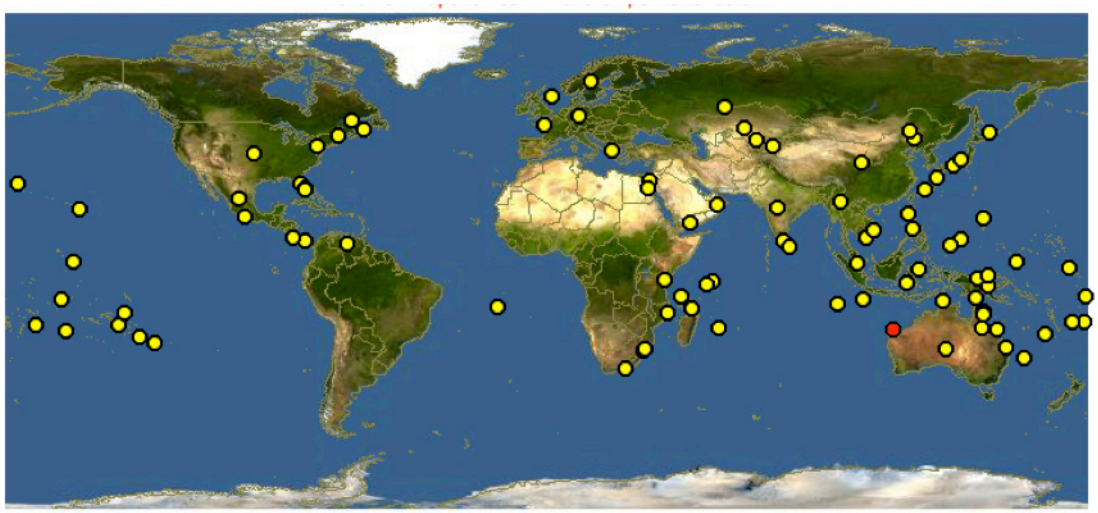

Figure 1.1. World distribution of *Pinctada margaritifera*.[46] *P. margaritifera* can be found in every area marked by the dots. The red dot refers to the location from which *P. margaritifera* nacre was obtained for this study.

1.2.2. Formation of Nacre

Oyster shell has three layers: the outer-most periostracum, consists of decalcified organic conchiolin and the middle layer, the ostracum, consists of prismatic calcite. The inner-most layer, the hypostracum, consists of aragonite tablets arranged in multiple layers which are interleaved by proteins and polysaccharides in the inter lamellar layers so that, collectively, the components form a "brick" (aragonite) and "mortar" (proteins and polysaccharides) structure.[47] This brick-mortar arrangement, which is the source of strength and resilience against fracture[48], is called nacre or mother-of-pearl. Fig. 1.2

shows an illustration of the prismatic calcite and the nacreous aragonite. Nacre is one of the common features in mollusks[49], especially in bivalves such as pearl oyster. Nacre is not only found in the inner shell, but also builds up the outer layer of pearl (see Fig. 1.2).[50]

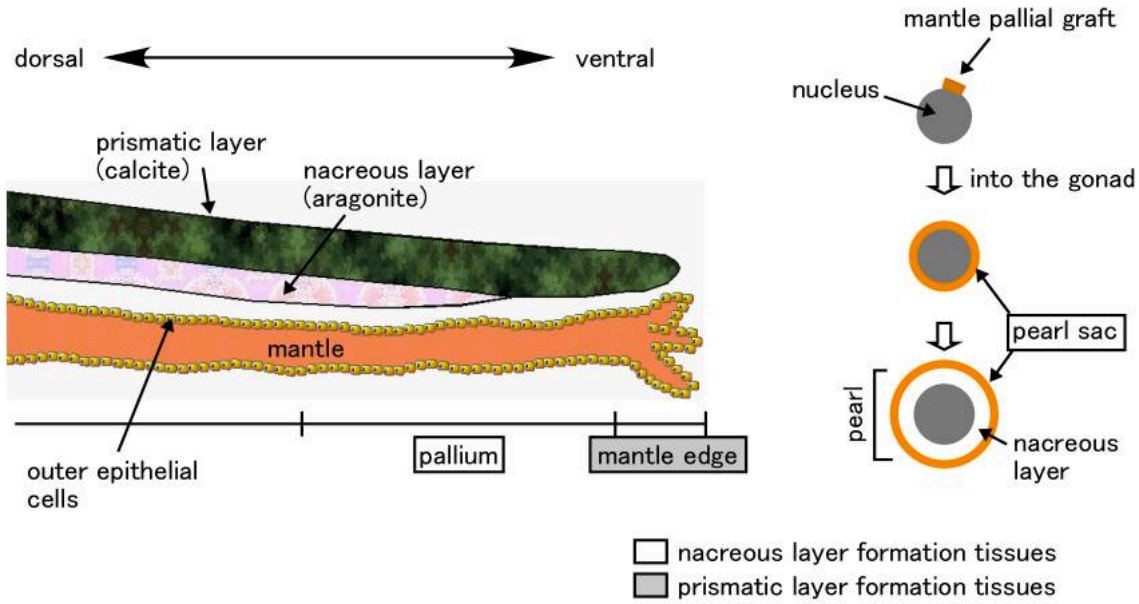

Figure 1.2. Nacre can be found in the inner layer of the shell and at the outer layer of the pearl. The shell is composed of three layers: nacreous layer (aragonite), prismatic layer (calcite) and periostracum (organic). The same layers are secreted at the surface of the pearl: first the organic layer, then prismatic layer and at the exterior nacreous layer.[51]

There are two models of nacre formation that have been described in previous studies (see Fig. 1.3).[52] The first model, called the "compartment model" was proposed by Bevelander and Nakahara (see Fig. 1.3a).[53] In this model, nacre is formed layer by layer in a sequential manner into pre-existing organic compartments. One layer of aragonite tablets is covered by an organic sheet containing proteins and polysaccharides followed by another layer of aragonite and so on. The second model was proposed by Schäffer et al. where the organic inter-lamellar sheets are deposited first to form organic compartments and the aragonite grow through gaps mineral bridges between the organic

inter-lamellar sheets with growth occurring from the inner-most to the outer-most aspect of the forming nacre.[54]

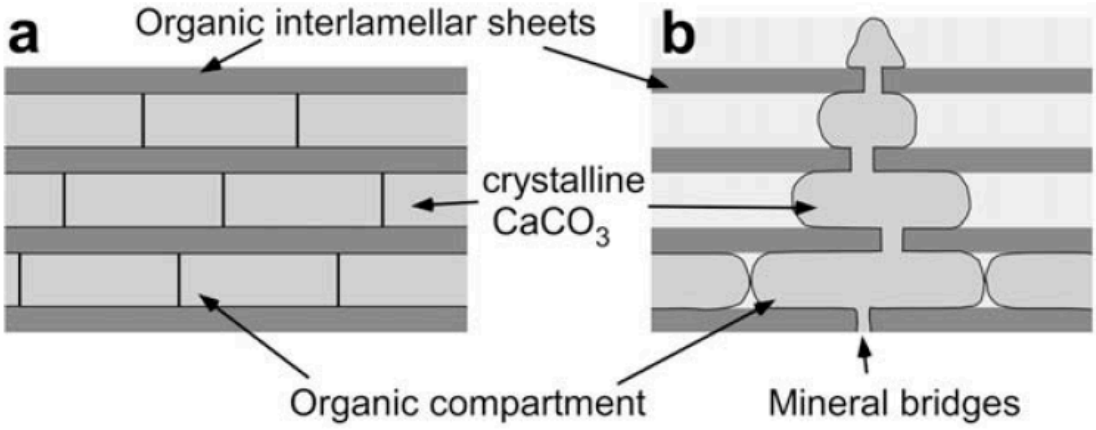

Figure 1.3. Schematic overview of the two major models of nacre formation. a) This model explains nacre formation by precipitation of $CaCO_3$ into pre-existing organic compartments and heteroepitaxial nucleation of $CaCO_3$ on the organic matrix. b) The second model postulates nacre formation by growth through mineral bridges across the pre-existing organic interlamellar sheets.[52]

Rousseau et al. showed that the formation of nacre in *P. margaritifera* follows the second model.[55] A more detailed bottom-up hierarchical formation of nacre of the second model has been well described by Cartwright and Checa (see Fig. 1.4).[56] Nacre formation begins with secretion of molecular polysaccharide chitin (*N*-acetyl-2-glucosamine) by the mantle into the extra-pallial liquid. Chitin then forms crystallites composed of hundreds of polymers. These crystallites in the extra-pallial liquid then form layers of interlamellar membrane. Proteins that have an affinity towards chitin become integrated in and support this membrane. Silk fibroin then aggregates with this membrane. The final stage is the mineralization of this membrane by aragonite. Suzuki et al. found two proteins, Pif 80 and Pif 97, in the organic components of nacre that play important roles in nacre formation.[39] They proposed that Pif 80 and Pif 97 forms a complex in the mantle epithelial cells and are secreted into the extrapallial fluid. Further, they predict that Pif 97 contributes to the formation of the lamellar sheet

through binding with chitin microfibrils to make a larger aggregate with N16 and other proteins. It is Pif 80 that concentrates calcium carbonate and induces aragonite formation.

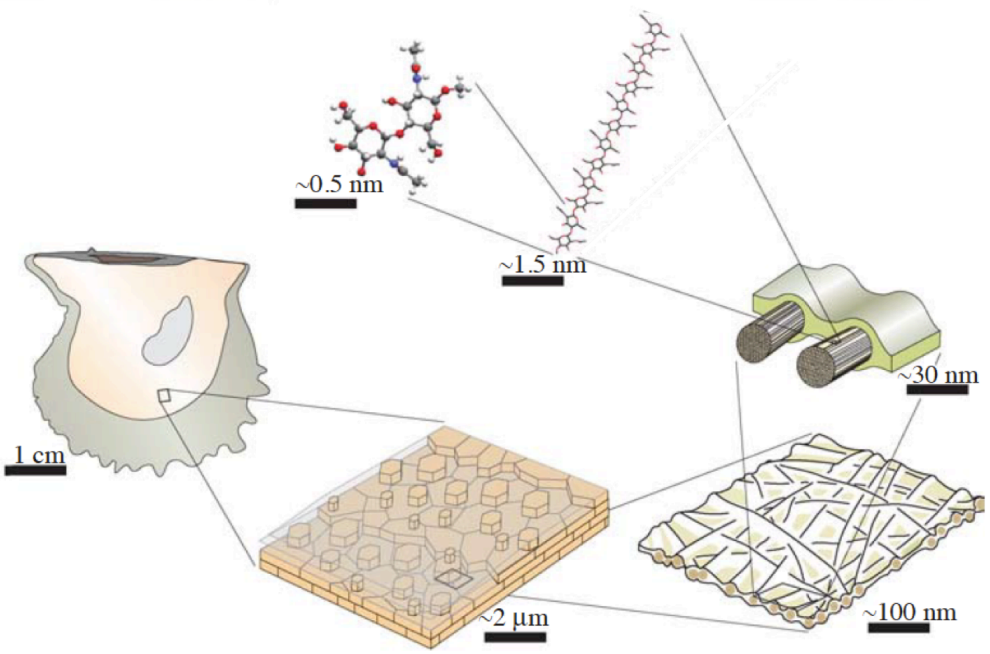

Figure 1.4. Hierarchical construction of nacre. A sketch diagram showing the construction of nacre from a chitin molecule to a shell in bivalves.[56] See text for more detailed explanation.

1.2.3. Nacre – Inspired Materials

The "brick" and "mortar" arrangement gives nacre an exceptional tensile strength up to 110 MN m^{-2}.[49] Nacre has a fracture strength about 3000 times greater than a non-biomineralised $CaCO_3$ (aragonite).[57] This characteristic of nacre has attracted significant interest from material scientists.[50,54,58,59] Nacre architecture provides a framework for the design of many new synthetic materials.[60] Examples include: composite films based on graphene oxide as the bricks and polyvinylalocohol (PVA) as the mortar[61], nanocomposite films composed of TiO_2 as the bricks and polyelectrolytes as the mortar[62], nanoclay sheets coated with soft polymer – polyvinylalcohol (PVA)[63], nacre-mimetic paper with fire shielding properties[64] and clay-based nanocomposites with layered structure using alumina platelets as the bricks and a chitosan polymer as the mortar.[65]

1.2.4. Nacre in Cosmetics

For more than 2000 years, Chinese have crushed pearl into powder for cosmetic use to whiten and smoothen the skin.[66] It was occasionally consumed orally as well by royal and noble families, as it was believed that pearl had an anti-aging effect.[43] However, none of these claims have been proven scientifically. The salt-water pearl is sometimes replaced with cheaper material such as fresh water pearl or nacre from the shell. This practice of using pearl or nacre as skin care is believed to be have been brought to the West by merchants that came from the East to trade.[67] In the West, natural pearl was replaced by other kinds of substance that bear similar physical appearance to the pearl powder, such as bismuth powders[68], zinc oxide[69], or titanium dioxide.[70] Fig. 1.5 shows old and contemporary cosmetic products that contain pearl. Beauty products that claim to contain pearl powder or essence will generally try to convince people that the cosmetic will whiten, smoothen, and slow the aging process of the skin.[71]

Figure 1.5. Cosmetics from 1800s (left) and 2000s (middle-right) that claim their products contain pearl.

An informal survey was undertaken as a complement of this study to investigate the ingredients of 27 cosmetics or skin care products that claim to contain pearl or "pearl essence" either in their product description or ingredients (see Table 1.2). Pearl

essence is not derived from pearl or oyster but can be defined as any compound/s or substance/s that can produce pearl lustre. Some examples include the scales of *Alburnus alburnus*, a type of carp fish[72], and mica. Nowadays, manufactured pearl essence usually coats mica with TiO_2 or Fe_2O_3.[73] Consumers usually take it for granted that "pearl essence" is equal to the pearl itself and that when the pearl is ground up to powder it will still retain its lustre. Lustre from the pearl nacre or nacre from the inner side of the shell is due to the spatial arrangement of the aragonite crystals.[74] So, when the spatial arrangement is compromised in the preparation process the lustre disappears. Pearl essence made from *A. alburnus* scales contain crystals made of guanine and hypoxanthine. They reflect and refract light, thus they exhibit the lustre effect similar to nacre.[75]

Table 1.2. Various skin care products claim to contain pearl or pearl essence. Many of them use mica or any other silicate compounds to create the luminous effect. See text for detail.

No.	Product Name	Pearl	Mica/Silica
1	Revlon 420 Sunlit Jade Colorstay Mineral Eye Shadow	Yes	Yes
2	Alessandro Cream Royal Nutrifying Hand Treatment	Yes	No
3	Alessandro Vital Serum Revitalizing Hand Serum	Yes	No
4	Revlon Color Stay Mineral Brush 020 Petal	Yes	No
5	Anna Sui Loose Compact Powder, 001 Transparent	Yes	Yes
6	Physicians Formula Powder Palette Mineral Glow Pearls	Yes	Yes
7	Lauren Brooke Cosmetiques Silk Veil	Yes	Yes
8	Jouer Mineral Face Powder, Perle D'Ivoire	Yes	Yes
9	Wei East Ageless Pearl Correcting Powder	Yes	Yes
10	Urban Decay Surreal Skin Cream to Powder Foundation, Dream	Yes	Yes
11	BareMinerals Pretty Amazing Lip Color, Allure (Peach)	Yes	Yes
12	LORAC Couture Shine Liquid Lipstick	Yes	Yes
13	Maybelline Color Sensational Lip Color, Plum Perfect	Yes	Yes
14	Bliss The Youth As We Know It Anti Aging Serum	Yes*	Yes
15	Shinto Clinical Wrinkle Shrink	Yes	Yes
16	SIRCUIT Cosmeceuticals SWELL Oceanic Cooling Mask	Yes	No
17	Pearl Professional Anti-Wrinkle Mist from Starmaker	Yes*	Yes
18	HydroPeptide Eye Authority	Yes	Yes
19	L'Oreal Infallible® 24Hr Eye Shadow Endless Pearl	No	Yes
20	Olay Regenerist Micro-Sculpting Cream	No	Yes
21	Avon Rare Pearls Body Powder	No	Yes
22	Clarins White Plus Pearl-to-Cream Brightening Cleanser	No	Yes
23	Neutrogena Instant Nail Enhancer, Pearl Sheen	No	Yes
24	The Body Shop Honey Bronze Brush on Beads	No	Yes
25	Pearl of Youth Pearl Powder	Yes	No
26	Oriflame Giordani Gold Bronzing Pearls	No	Yes
27	Pond's White Beauty Pearl Cleansing Gel	Yes*	No

From the survey in Table 1.2, 20 products listed pearl or its derivatives, e.g. mother of pearl, pearl powder or hydrolyzed pearl in the ingredients list. However, there is no explanation available as to how the pearl powder was produced nor the size range of particles or compounds derived from pearl. It is important to know the uniformity of the particle size of pearl powder across these different skin care products. The particle size might dictate the fate of the pearl powder, whether it stays on top of the epidermis and gets washed away or enters the skin through the hair follicles. The importance of particle size will be discussed further in Chapter 2. There are 3 products that listed "hydrolyzed pearl" in their ingredients list (marked with * in the table). However, there is also no information on the final size range of this hydrolyzed pearl. Product #18 listed "crushed pearl" in the ingredients list. Despite the widespread use of pearl nacre or its derivatives in cosmetics, there is limited evidence of efficacy or consistency in preparation of nacre and its use. Therefore, in order to make progress in understanding properties of nacre scientifically there is a critical need to have a standard protocol for the preparation of nacre from the shell. This aspect is addressed in Chapter 2.

There are 7 products in Table 1.2 that do not mention pearl at all in their ingredients. Interestingly all of the 7 products have one or more silicate compounds including mica. Furthermore, there are only 5 products that do not contain any silicate compounds including mica. It is interesting that many manufacturers added silicate compounds into the product rather than using nacre or natural pearl extracts. It is possible that these manufacturers expect the same effects from the silicate compounds and do not expect the additional expense of adding pearl extract to provide any benefits. Therefore, this study will clarify the safety and efficacy of nacre on skin cells. These aspects are addressed in Chapters 3 and 4. The use of nacre and various pearl essences in cosmetics is also discussed further in the concluding chapter, Chapter 5.

1.2.5. Nacre in Medicine

In many different ancient cultures including in India and China, pearl powder has been prescribed for many different kinds of illness.[15,16,76] Some publications have shown that nacre possesses therapeutic properties, such as preventing and treating myopia in chicks[15], inducing the growth of cutaneous fibroblasts in rats[77], improving repair of the stratum corneum[43], stimulating bone formation *in vitro* and *in vivo*[78], inducing bone repair in the vertebrae of sheep[78,79] and reducing visceral fat in rat[80]. Additionally, Cao et al. claimed that nacre possesses tonic, anti-aging, and anti-radiation actions.[81]

Xu et al. claim that pearl powder could prevent and improve myopia in chicks.[15] A manufactured pearl powder from Jiangxi Province, People's Republic of China was used but no information about the particle size was given. The pearl powder was hydrolysed in distilled water and concentrated to 1 mg/mL. This suspension was dropped on the left eye of chicks that had been manipulated to bring about form-sense-deprived myopia, while the right eye acted as control. The results suggested that calcium and other minerals from nacre could prevent myopia in chicks by preventing the elongation of the axis oculi and change in the diopters of form-sense-deprived myopia. The zinc- and copper- containing minerals also stimulated the activity of superoxide dismutase (SOD) and nitric oxide synthetase (NOS) in the retinopigmental epithelium choroid homogenate in order to hinder oxidation of superoxide.

Lopez's group applied ground nacre to sheep vertebrae and in an *in vitro* study of bone marrow.[78] It was hypothesized that nacre would induce bone formation. Nacre of *P. maxima* obtained from North Australia was used. For the first study, ground nacre powder was mixed with autologous blood and then injected to the lumbar vertebrae. For the *in vitro* study, water-soluble matrix (WSM) from the nacre powder was tested on

bone marrow from male rats aged 40-43 days. The results showed that there was bone formation surrounding the nacre implant and no inflammation was observed. Bone marrow proliferation was reduced when incubated with WSM at a concentration higher than 830μg/mL.

Following the positive results from the above study, an *in vivo* study was performed by injecting ground nacre percutaneously to the vertebrae to investigate the effectiveness of nacre in bone repair.[79] Nacre was compared with polymethylmethacrylate (PMMA), which is commonly used to treat painful lesions in vertebral bone. The study suggested that nacre is better than PMMA in inducing osteogenesis. Furthermore, PMMA was shown to cause necrosis and massive resorption of the trabecular bone. It was demonstrated that nacre provided the beneficial effect through diffusion of the organic matrix following dissolution of the aragonite.

Lopez et al. also implanted ground nacre from *Pinctada maxima* with size about 50 – 100 μm into a pocket between the dermis and hypodermis on the ventral surface of rats at the junction of the thorax and abdomen.[77] They argued that nacre would induce production of collagen from the cutaneous fibroblasts. Their results indeed showed increase secretion of collagens I and III. The inorganic part of nacre, aragonite, was thought not to have an effect since the calcium carbonate control in calcite form did not produce similar results. It was therefore concluded that the organic matrix of nacre was instrumental in inducing collagen secretion. Interestingly, WSM of pearl powder was reported to have an ability to stimulate fibroblast mitosis[76] which is important in wound healing.

The same group extracted lipid from the ground nacre of *P. margaritifera* and applied it to artificially dehydrated skin explants.[43] The lipids extracted were cholesterol, cholesterol sulphate, cholesterol acetate, hydroxylated ceramides, nonhydroxylated ceramides, fatty acids, triglycerides and squalene-like lipids. Their results suggested that nacre lipids improve the repair of the stratum corneum, although it remains unclear which particular lipid is responsible for the effectiveness of the repair.

Table 1.3. Summary of studies using nacre or its derivatives for medical purposes.

No.	Title Study	Model	Results	Nacre
1	Prevention and treatment of myopia with nacre on chicks[15]	Chicks (*in vivo*)	Nacre stimulates SOD and NOS	Nacre powder
2	Stimulation of bone marrow cells and bone formation by nacre[78]	Sheep (*in vivo*)	Nacre induces bone formation	Ground nacre
3	Bone reactions to nacre injected percutaneously into the vertebrae of sheep[79]	Sheep (*in vivo*)	Nacre is better than PMMA in inducing osteogenesis	Ground Nacre
4	Stimulation of rat cutaneous fibroblast[77]	Rats (*in vivo*)	Nacre stimulates mitosis of fibroblasts	Ground Nacre
5	Restoration of stratum corneum with nacre lipids[43]	Skin explant (*ex vivo*)	Nacre lipids improve the repair of stratum corneum	Nacre Lipids

All of the studies above are summarized in Table 1.3. Despite the claims above, the active compound has never been identified. Possibilities include the aragonite itself, the organic component, or both. However, Lopez et al. have excluded the inorganic component, aragonite, as the responsible compound.[77] This conclusion was made largely because any type of calcium carbonate other than aragonite did not exhibit similar results. However, this different result might be due to the different spatial arrangement of calcium carbonate. Although it was not explicitly mentioned as calcite, calcium carbonate obtained from manufacturers is usually in calcite form as it is the most stable polymorph. On the other hand, when nacre as a whole gives a desired therapeutic effect, as in the myopia study, it was largely due to the calcium in nacre. Thus, questions can be raised as to whether calcium from any source could give the

same effect or whether the structure itself is important. Therefore, it is important in any study on nacre to compare nacre with at least one other type of $CaCO_3$, such as calcite or vaterite.

1.3. Skin

Skin is composed of 2 layers, namely, epidermis and dermis (see Fig. 1.6). Although the hypodermis lies underneath the dermis, it is not part of the skin but contains fat and connective tissue and is involved in attaching the skin to bone and muscle. Additionally, the hypodermis contains blood vessels and nerves.

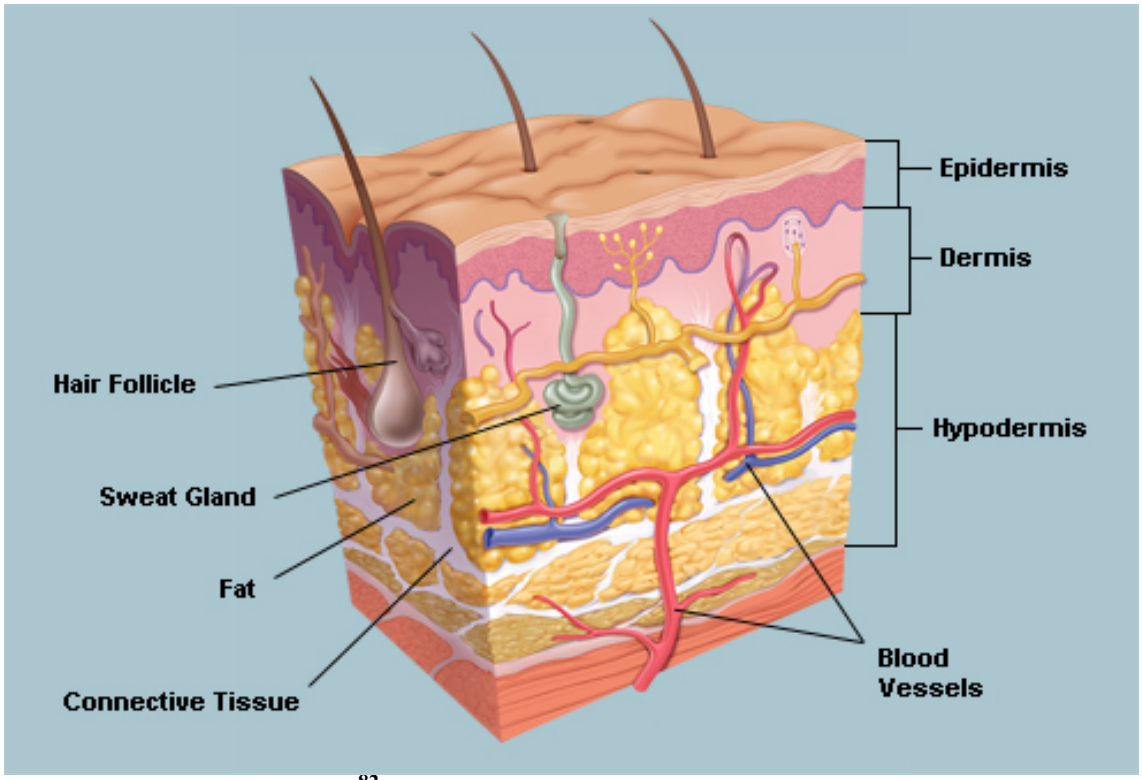

Figure 1.6. Skin structure.[82] There are 2 layers in skin, namely epidermis and dermis.

Skin injury is a daily occurrence that ranges from bruises, scratches, cuts or burns. While bruised and scratched skin normally heals with time on its own, cut or burnt skin may require further treatment.

1.3.1. Structure and Function

1.3.1.1. Epidermis

Epidermis is composed of the following strata from inner to outer, namely, stratum basale, stratum spinosum, stratum granulosum and stratum corneum (see Fig. 1.7). In specific areas such as the soles of the feet or palms of the hand, there is another stratum called the stratum lucidum in between the granulosum and corneum. Keratinocytes are the major cell type that makes up approximately 95% of the cells of the epidermis.[83] The remaining 5% of the epidermis is populated predominantly by Langerhans cells, Merkel cells and melanocytes.[84]

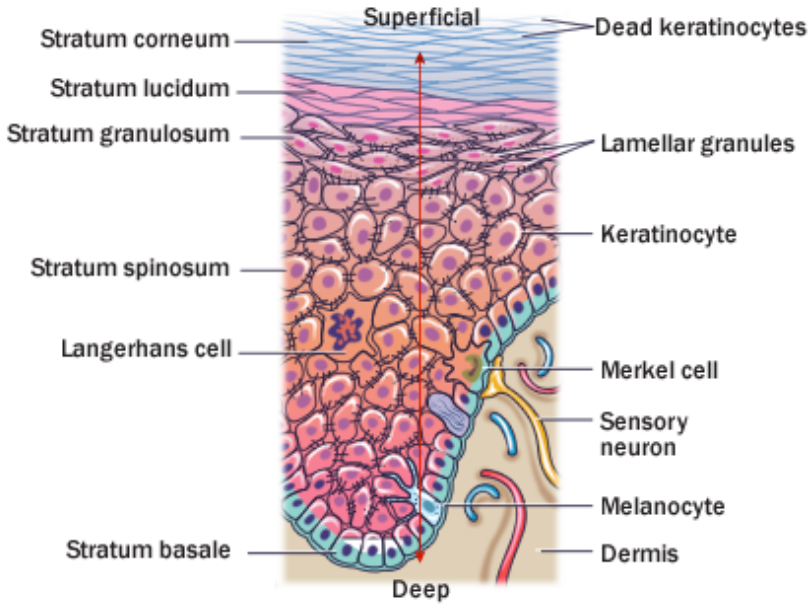

Figure 1.7. Anatomy of epidermis.[85] Epidermis is made of a number of strata from stratum basale at the very deep end to stratum corneum at the most superficial end.

1.3.1.2. Dermis

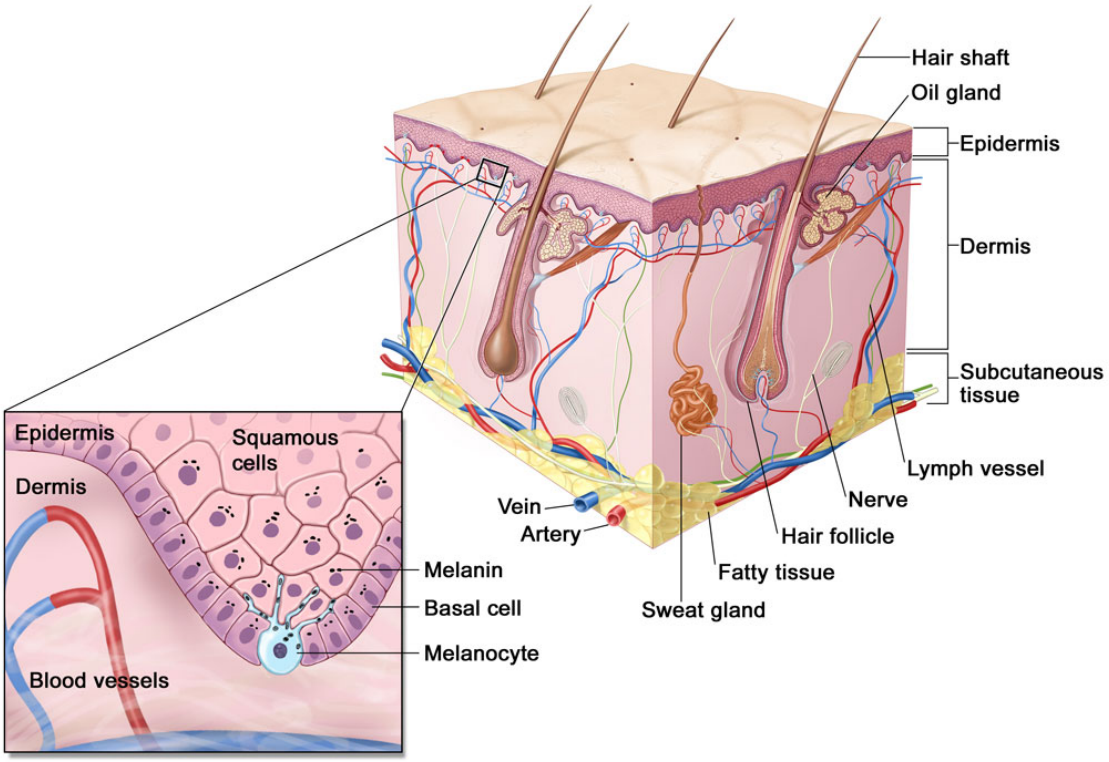

Figure 1.8. Cross section of the dermis.[86] Dermis is a vascularised layer that nourishes both dermis and epidermis layers. The zoom out shows an example of how the blood vessel provides nutrients to the epidermis.

The epidermis does not have blood vessels to nourish itself, i.e. it is avascular.[87] Thus, it needs the dermis as a connective tissue to provide nourishment. In addition to blood vessels, the dermis also contains sweat glands, hair follicles and nerve endings (see Fig. 1.8). The dermis is filled up by collagen and elastin. Both proteins are produced by fibroblasts.[88] Collagen provides strength against strain and traction. Elastin is interwoven amongst collagen fibres to provide resilience and suppleness.[89] The relationship between collagen and scarring will be discussed later in section 1.4.5.

1.3.2. Cell Types

1.3.2.1. Keratinocytes

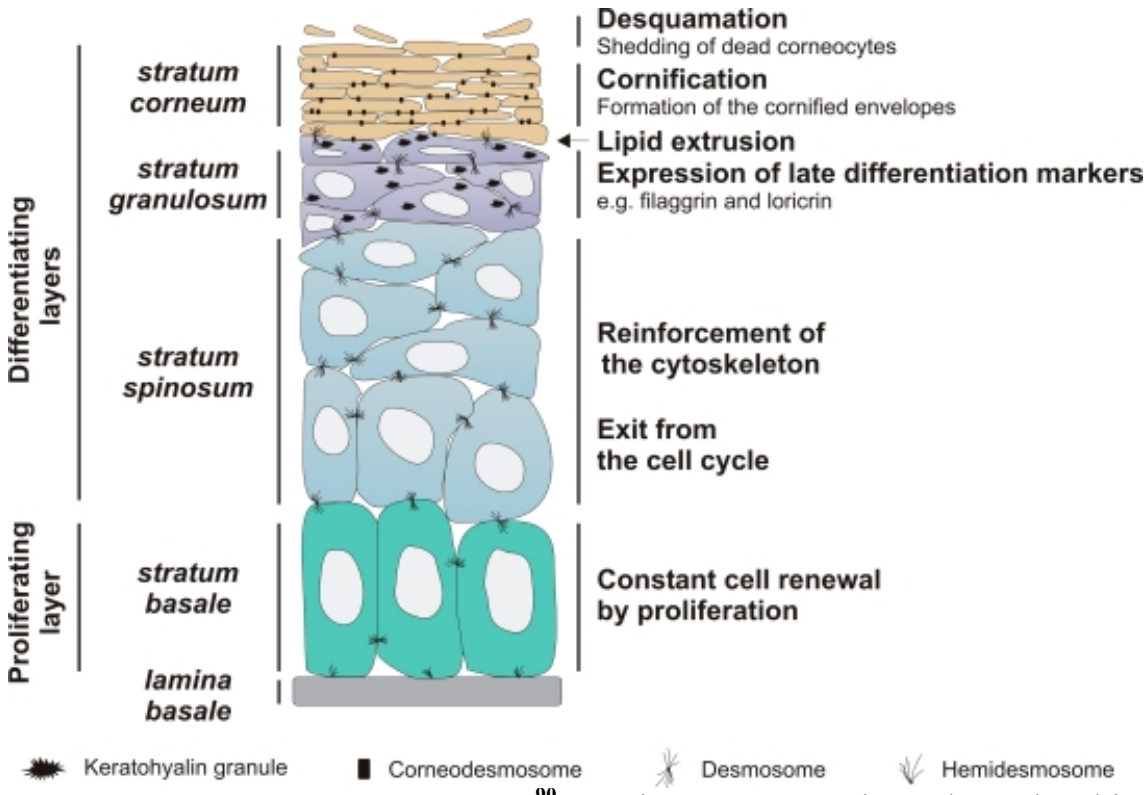

Figure 1.9. Keratinocytes homeostasis.[90] Keratinocytes are continuously produced in stratum basale and then undergo differentiation upward through stratum spinosum and stratum granulosum. The aging keratinocytes are building up stratum corneum.

Homeostasis in the epidermis is maintained by constant proliferation and differentiation of keratinocytes (see Fig. 1.9).[90] Keratinocytes proliferate through mitosis in the stratum basale.[5] Some keratinocytes undergo differentiation first in the stratum spinosum and later in the stratum granulosum.[5] As they differentiate, keratinocytes start producing keratins in the stratum spinosum.[91] Keratins provide skin with its waterproof feature[92,93], and thus maintain its integrity. In the stratum granulosum, keratinocytes are granulated with keratohyalin.[94] Keratohyalin helps the keratins produced in stratum spinosum to be bound together.[95] When these granulated keratinocytes migrate toward the surface and reach stratum corneum, they produce lamellar bodies.[96] These bodies form a hydrophobic layer that gives skin its barrier nature.[97] As a result of the lamellar body production, keratinocytes become anucleated and transform into corneocytes.[96]

They are non-viable keratinocytes that form the stratum corneum.[5] Corneocytes are shed as new dead cells migrate outwards. The removal of corneocytes is called desquamation.[96]

Primary cell lines are often difficult to obtain and maintain. Therefore, a cell line is usually used as a model when investigating the potential effects of specific compounds, such as nacre. In order to solve this problem for keratinocytes, Boukamp et al. stimulated spontaneous transformation of human skin keratinocytes in different culture conditions, one of which gave rise to the HaCaT cell line.[98] HaCaT cells have a stable DNA fingerprint, which was proven by identical DNA fingerprints from passages 6 to 79.[98] HaCaT cells, though immortalized, retain the capacity for normal keratinisation and retain many of the phenotypic features of primary keratinocytes.[98] HaCaT cells are therefore a good model for the study of the impact of nacre on skin epithelial cells.

1.3.2.2. Fibroblasts

Similar to keratinocytes in the epidermis, fibroblasts are the largest cell population in the dermis.[99] The principal function of fibroblasts is to maintain structural integrity of connective tissue, thus they constantly secrete precursors for extracellular matrix.[100,101] Collagen is one of the macromolecules secreted by fibroblasts. Collagen etymology comes from two Greek words, κσλλα (kólla) means "glue" and the suffix -γεν (-gen) means producing.[102] The etymology describes collagen function as glue between two tissues such as skin and muscle or muscle and bone.

1.3.3. Collagen in Cosmetics

Collagen in skin provides its strength, integrity and flexibility.[103] Collagen is constantly synthesized and degraded, but aging shifts the balance toward degradation.[104] UV radiation indirectly causes lower amounts of collagen synthesis by many pathways such as reduction of procollagen mRNA and stimulating production of matrix metalloprotease mRNA.[105] The consequence of aging to skin is visibly apparent in that it loses its aesthetic properties, resilience and elasticity, resulting in loose skin and the most obvious sign of aging, wrinkles.[106] People have always been acutely aware of their appearance, and today anti-aging supplementation and skin care has become a multi-billion dollar industry.[107] In order to quench customer needs, the industry funds substantial research to prevent skin from aging or to reduce the signs of aging.[106] In 2012 it was reported that the total market for anti-aging products and services was valued at US$249.3 billion.[107] Even Google Inc founded Calico a biotechnology company to cure aging.[108]

Many studies approach the problem of skin aging by introducing exogenous collagen, procollagen, or molecules that can affect of the metabolism of collagen. Choi et al. reported that the extract from *Labisia pumila* is able to up-regulate the synthesis of collagen in human foreskin fibroblasts following UV radiation.[105,109] An exogenous collagen cross-linker has been reported to be able to recover tendon functional integrity.[110] Kippenberger claimed that bovine milk induces collagen 1 A1 synthesis by activating signal transducers and activators of transcription 6 (STAT6).[111] Similarly, Obayashi et al. reported that exogenous nitric oxide (NO) increased collagen type I production by up-regulation of pro-collagen I mRNA.[112]

In the clinic, bovine collagen has been used as a filling agent to temporarily replace collagen that is degraded with age.[113] A French-based skin care company, Sederma SA, claims that a fragment of alpha-procollagen I, KTTKS, that is conjugated with palmitoyl could diffuse through the stratum corneum and increase collagen type I synthesis.[114]. Although it has been marketed as Matrixyl this claim needs to be validated by an independent study. In a clinical study, conjugated linoleic acid (CLA) is reported to increase procollagen I production and subsequently improve cellulite grading by dermatologists after 8 and 12 weeks.[115] Extract from amla (*Emblica officinalis* Gaertn.), an Indian medicinal plant, another common ingredient in skin care is reported to be able to control collagen metabolism by suppressing production of matrix metalloproteinase-1 (MMP-1) and up-regulating tissue inhibitor of metalloproteinase-1 (TIMP-1).[116] The last claims need to be verified further by an *in vivo* study. In brief, a methodical approach is necessary to examine the safety and efficacy of a substance in relation to collagen production prior being used in cosmetics.

1.4. Wound Healing

As mentioned at the beginning of this chapter, skin serves as a protective barrier for the body. If the integrity of skin is compromised, it has to be repaired in a timely manner in order to prevent infection, major disability or even death. Wound healing is a complex process that can be divided into 3 phases that overlap, namely: inflammation, re-epithelialisation and remodelling (see Fig. 1.10).

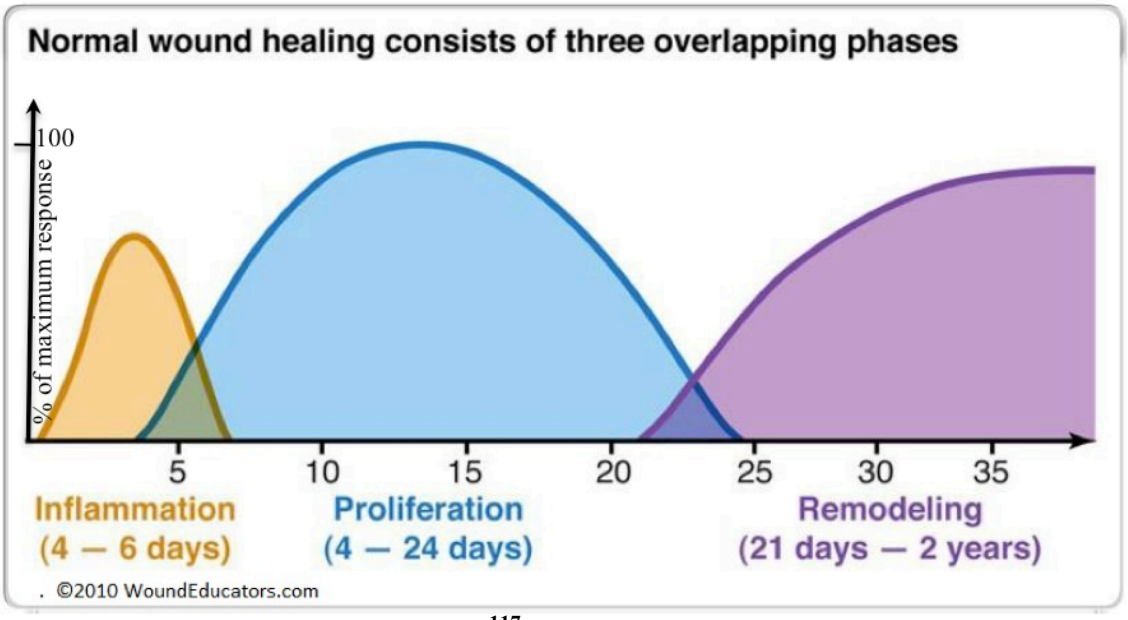

Figure 1.10. Wound healing phases.[117] There are three phases with distinct activities for each phase but yet might overlap in time.

1.4.1. Inflammation

When skin is wounded, the first response is to reach homeostasis. Fig. 1.11 depicts the processes that occur during this stage. Forming a clot prevents further blood loss. The clot is made of fibrin fibres derived from fibrinogen.[118] The fibrin clot serves as a landmark for the circulating inflammatory cells such as neutrophils and monocytes to migrate to the wound bed.[119] Neutrophils usually arrive within minutes after injury and recent findings suggest that neutrophils send out signals to activate surrounding keratinoytes and fibroblasts.[120] Monocytes and macrophages are vital for successful wound healing.[121] Macrophages release a group of growth factors and cytokines, such as fibroblast growth factor (FGF)[122], transforming growth factors-α and -β1 (TGF-α and TGF-β1)[123], vascular endothelial growth factor (VEGF)[124], platelet derived growth factor (PDGF)[125] and interleukins (IL-1α and IL-1β).[120] These molecules enhance the early inflammation signal to recruit more inflammatory cells.[119] Another important task of macrophages is debridement of the wound site, so the wound site can be re-epithelialised without hindrance.

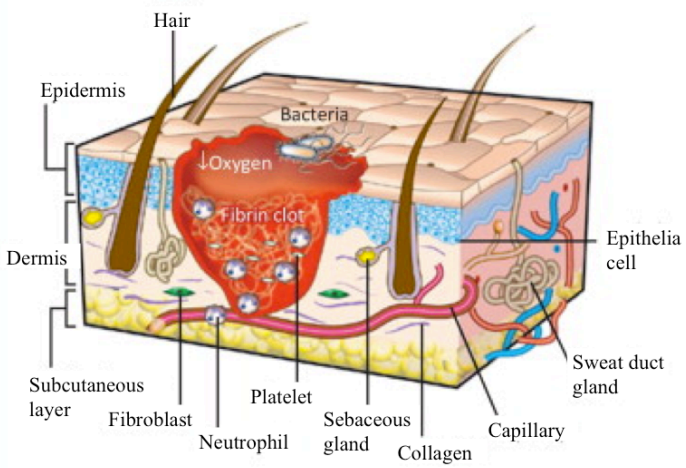

Figure 1.11. Inflammatory phase. Blood clotting happens at this phase, immune cells such as neutrophils are recruited to site and proinflammatory mediators are secreted into the wound.[126]

1.4.2. Re-epithelialisation

Re-epithelialisation begins immediately after injury. Intercellular desmosomes, which lock cells with each other, are dissolved to allow keratinocyte migration.[127] The dissolution includes hemidesmosomes that are used by keratinocytes to attach themselves to the basal lamina.[119] Keratinocytes become flatter and more elongated and they form peripheral cytoplasmic actin filaments.[128] Integrin receptors are expressed by keratinocytes and rearranged in a manner that allows them to interact with the extracellular matrix components, such as fibronectin and vitronectin, in the wound site.[129] The arrangement of integrin receptors dictates the course of keratinocytes in separating the viable cells from the dead ones.[130] The keratinocytes that have reached the wound margin begin to proliferate, while at the same time other keratinocytes migrate to find other edges and some other keratinocytes at the wound edge are in hyper proliferative state.[130] When a layer of keratinocytes has been formed, the migration ceases and keratinocytes revert back to their normal morphology with firm attachment between cells and the underlying dermis.[119]

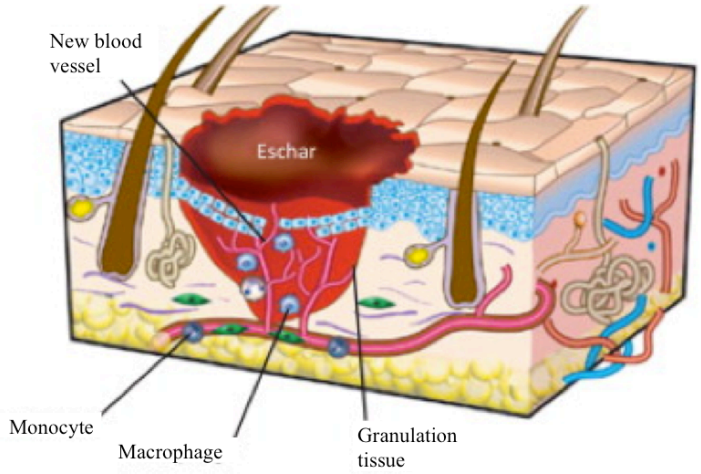

Figure 1.12. Re-epithelialisation phase. Keratinocytes are in proliferative and migratory states until one layer of keratinocytes is formed. [126]

The fibroblasts on the wound margin start to proliferate after being stimulated by FGF, released by neutrophils at the wound site. After 4-5 days post-injury, the fibroblasts migrate through the provisional matrix into the fibrin clot. Fibroblasts then replace the provisional matrix with new extracellular matrix, which is rich with collagen.[131] TGF-β1 is important to promote this activity.[132] The fibroblast-rich matrix is gradually replaced with collagen-rich matrix and becomes a scar.[130,132]

Although re-epithelialisation begins within hours after injury, the epidermal cells at the wound margin only proliferate after 1-2 days post injury.[130] The re-epithelialisation process in adult skin might take between 5 days to 3 weeks (see Fig. 1.10). Wound healing in adults results in scar formation.[133] In contrast, foetal skin has an ability to regenerate.[134] Foetal skin also heals rapidly within 1-7 days.[133] This fact leads to a notion that the time duration for re-epithelialisation is crucial in determining the appearance of the scar at the end of wound healing: the shorter the time, the better the quality of healing or less likely-hood of scarring. Therefore, numerous studies have been performed to find substances or molecules that can accelerate migration of either the epidermal keratinocytes or the dermal fibroblasts or both.

1.4.3. Remodelling

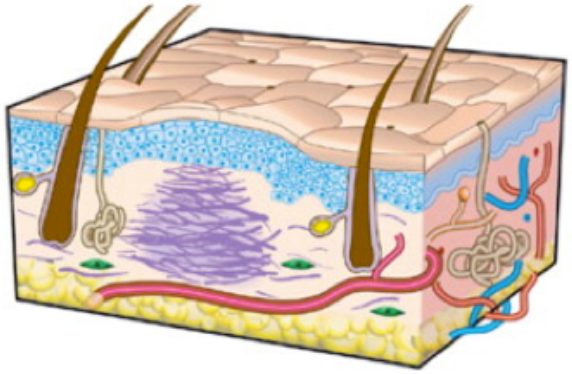

Figure 1.13. Remodelling/maturation phase. In this phase collagen structure is remodelled and wound is contracted.[126]

The remodelling phase is the last phase of wound healing that starts once the re-epithelialisation has ceased and can last up to years. It was mentioned above that the provisional fibroblast-rich matrix was replaced with collagen-rich matrix. The goal of this phase is to remodel this collagen-rich matrix to minimize scar (see Fig. 1.13).

Scarring is not only unaesthetic but also does not have as much strength as normal skin. The maximum tensile strength of scar is only approximately 70% compared to the strength of normal skin.[135,136] The architecture of collagen in scars comprises poorly constructed parallel bundles, unlike the basket-weave arrangement in unwounded skin (see Fig. 1.14)[119]. Therefore, many studies have aimed to find molecules or substances that can prevent the alignment of collagen bundles in parallel. For example, Shah et al. prevented scar tissue formation by injecting neutralizing antibody to TGF-β to the margins of healing dermal wounds in adult rats.[136] The treated wound had less collagen than the control and a more normal architecture.[136] Accordingly, Chapter 4 will investigate the effect of nacre or components of nacre on the amount of collagen produced and collagen architecture.

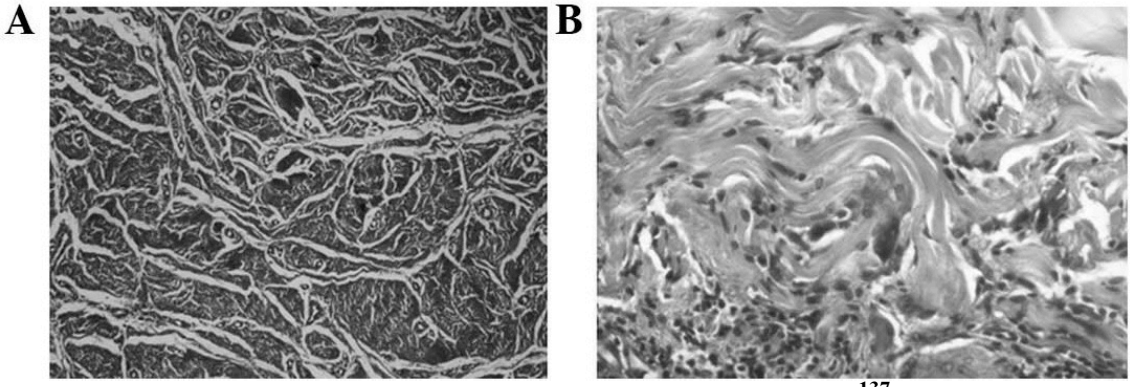

Figure 1.14. Collagen arrangement in scar and normal tissue.[137] Collagen is more aligned to each other in scar tissue (A) compared to a disorder pattern in normal tissue (B). Magnification x100.

1.5. Summary

Nacre has been widely used for cosmetics and medicinal purposes. However, information regarding the uniformity of particle size and a protocol for nacre preparation are limited or not readily available to the public. Thus, it is currently difficult to compare different studies using nacre. There is also no systematic study regarding the toxicity of nacre on skin cells, despite the fact that it has been used extensively in cosmetics. Therefore developing well characterized nacre preparation methodology and a systematic investigation of the potential effects of nacre components on skin cells is required to determine whether nacre is potentially beneficial as a cosmetic or therapeutic for wound repair.

1.6. Experimental Design

Oyster shell is made up of the same nacre as the pearl itself. While pearl is regarded as an expensive gem, the shell is regarded as waste. In the current study, nacre from the shell of *P. margaritifera* will be used to investigate the potential of nacre in wound healing. The main concern of adult wound healing is excessive scarring. Therefore, this study will first explore the best preparation of nacre to be used on skin cells – addressed in Chapter 2. Then, the toxicity of prepared nacre will be assessed in immortalized keratinocytes (HaCaT) and immortalized fibroblasts (NIH/3T3) – addressed in Chapter 3. Subsequently, the potential of nacre or specific components of nacre to minimise scarring in an *in vitro* experimental model of wound healing will be explored – addressed in Chapter 4.

1.6.1. Hypothesis

Nacre contains organic and/or inorganic elements that are beneficial either for cosmetic use or to enhance wound healing.

1.6.2. Specific Aims

Chapter 2

Aim 1: To develop a reproducible and reliable method of nacre preparation for toxicity testing

Questions : What are the parameters required to produce a consistent particle size?

What are the parameters that result in minimal contamination?

Chapter 3

Aim 2: To determine whether nacre is toxic to skin cells *in vitro* using immortalized human keratinocytes (HaCaTs) and immortalized mouse fibroblasts (NIH/3T3)

Questions : Is nacre toxic to skin cells?

Does heavy metal contamination from the ball milling decrease cell viability?

Do different nacre preparations result in different viability?

Chapter 4

Aim 3: To investigate the effects of nacre on wound repair *in vitro*.

Questions : Does organic component of nacre increase the migration rate of fibroblasts and keratinocytes?

Does organic component of nacre reduce the amount of collagen type I deposited by fibroblasts?

Does organic component of nacre increase the randomness of collagen type I orientation to a more 'normal' structure?

1.7. References

1 Oliveira, G., Leverett, J. C., Emamzadeh, M. & Lane, M. E. The effects of heat on skin barrier function and in vivo dermal absorption. *International Journal of Pharmaceutics* **464**, 145-151, doi:http://dx.doi.org/10.1016/j.ijpharm.2014.01.012 (2014).

2 Biniek, K., Levi, K. & Dauskardt, R. H. Solar UV radiation reduces the barrier function of human skin. *Proceedings of the National Academy of Sciences* **109**, 17111-17116, doi:10.1073/pnas.1206851109 (2012).

3 Roberson, E. D. O. & Bowcock, A. M. Psoriasis genetics: breaking the barrier. *Trends in Genetics* **26**, 415-423, doi:http://dx.doi.org/10.1016/j.tig.2010.06.006 (2010).

4 Adamek, M. Ç. *et al.* Cyprinid herpesvirus 3 infection disrupts the skin barrier of common carp (Cyprinus carpio L.). *Veterinary Microbiology* **162**, 456-470, doi:http://dx.doi.org/10.1016/j.vetmic.2012.10.033 (2013).

5 Hänel, K. H., Cornelissen, C., Lüscher, B. & Baron, J. M. Cytokines and the Skin Barrier. *International Journal of Molecular Sciences* **14**, 6720-6745, doi:10.3390/ijms14046720 (2013).

6 Wiegand, C., Abel, M., Ruth, P. & Hipler, U. C. Superabsorbent polymer-containing wound dressings have a beneficial effect on wound healing by reducing PMN elastase concentration and inhibiting microbial growth. *J Mater Sci: Mater Med* **22**, 2583-2590, doi:10.1007/s10856-011-4423-3 (2011).

7 Demiot, C. *et al.* P295 Le candésartan empêche nettement la formation d'un ulcère de pression sans effet bénéfique sur sa cicatrisation chez des souris diabétiques et saines. *Diabetes & Metabolism* **38, Supplement 2**, A100, doi:http://dx.doi.org/10.1016/S1262-3636(12)71397-6 (2012).

8 Lu, B. *et al.* Graphene-based composite materials beneficial to wound healing. *Nanoscale* **4**, 2978-2982, doi:10.1039/c2nr11958g (2012).

9 Wagstaff, M. J. D., Driver, S., Coghlan, P. & Greenwood, J. E. A randomized, controlled trial of negative pressure wound therapy of pressure ulcers via a novel polyurethane foam. *Wound Repair & Regeneration* **22**, 205-211, doi:10.1111/wrr.12146 (2014).

10 Teng, M., Huang, Y. & Zhang, H. Application of stems cells in wound healing—An update. *Wound Repair and Regeneration* **22**, 151-160, doi:10.1111/wrr.12152 (2014).

11 Majtan, J. Honey: An immunomodulator in wound healing. *Wound Repair and Regeneration* **22**, 187-192, doi:10.1111/wrr.12117 (2014).

12 Lee, K. *et al.* Nacre-driven water-soluble factors promote wound healing of the deep burn porcine skin by recovering angiogenesis and fibroblast function. *Mol Biol Rep* **39**, 3211-3218, doi:10.1007/s11033-011-1088-4 (2012).

13 Li, Y.-C., Chen, C.-R. & Young, T.-H. Pearl extract enhances the migratory ability of fibroblasts in a wound healing model. *Pharmaceutical Biology* **51**, 289-297, doi:10.3109/13880209.2012.721130 (2013).

14 Dai, J.-P. *et al.* Effects of pearl powder extract and its fractions on fibroblast function relevant to wound repair. *Pharmaceutical Biology* **48**, 122-127, doi:10.3109/13880200903046211 (2010).

15 Xu, H., Huang, K., Gao, Q., Gao, Z. & Han, X. A study on the prevention and treatment of myopia with nacre on chicks. *Pharmacological Research* **44**, 1-6, doi:10.1006/phrs.2000.0780 (2001).

16 Gopal, R., Vijayakumaran, M., Venkatesan, R. & Kathiroli, S. Marine organisms in Indian medicine and their future prospects. *Natural Product Radiance* **7**, 139-145 (2008).

17 Pal, D., Sahu, C. K. & Haldar, A. Bhasma : The ancient Indian nanomedicine. *Journal of Advanced Pharmaceutical Technology & Research* **5**, 4-12, doi:10.4103/2231-4040.126980 (2014).
18 Bobbio, A. The first endosseous alloplastic implant in the history of man. *Bulletin of the history of dentistry* **20**, 1-6 (1972).
19 Wu, O. in *PR Newswire* (PR Newswire Association LLC, New York, 2003).
20 Lorac. *Lorac Couture Shine Liquid Lipstick*, 2015).
21 HydroPeptide. *Eye Authority: Dark Circles, Puffines, Fine Lines* <http://shop.hydropeptide.com/eye-authority#.Vh5qqChJUfz> (2015).
22 Oriflame. *Giordani Gold Bronzing Pearls*, <http://in.oriflame.com/products/product?code=21632> (2015).
23 SIRCUIT®. *SWELL Ocean Cooling Mask*, <http://sircuitskin.com/inc/sdetail/32524/45981> (2015).
24 Bédouet, L. *et al.* Proteomics Analysis of the Nacre Soluble and Insoluble Proteins from the Oyster Pinctada margaritifera. *Mar Biotechnol* **9**, 638-649, doi:10.1007/s10126-007-9017-1 (2007).
25 Zhang, C., Li, S., Ma, Z., Xie, L. & Zhang, R. A Novel Matrix Protein p10 from the Nacre of Pearl Oyster (*Pinctada fucata*) and Its Effects on Both CaCO3 Crystal Formation and Mineralogenic Cells. *Mar Biotechnol* **8**, 624-633, doi:10.1007/s10126-006-6037-1 (2006).
26 Song, F., Soh, A. K. & Bai, Y. L. Structural and mechanical properties of the organic matrix layers of nacre. *Biomaterials* **24**, 3623-3631, doi:http://dx.doi.org/10.1016/S0142-9612(03)00215-1 (2003).
27 Katti, K. S. & Katti, D. R. Why is nacre so tough and strong? *Materials Science and Engineering: C* **26**, 1317-1324, doi:http://dx.doi.org/10.1016/j.msec.2005.08.013 (2006).
28 Zentz, F. *et al.* Characterization and Quantification of Chitosan Extracted from Nacre of the Abalone Haliotis tuberculata and the Oyster Pinctada maxima. *Mar Biotechnol* **3**, 36-44, doi:10.1007/s101260000042 (2001).
29 Liu, R., Xu, X., Pan, H., Yan, W. & Tang, R. Aragonite crystals formation on nacre substrate. *Journal of Crystal Growth* **351**, 41-46, doi:http://dx.doi.org/10.1016/j.jcrysgro.2012.04.013 (2012).
30 Michenfelder, M. *et al.* Characterization of two molluscan crystal-modulating biomineralization proteins and identification of putative mineral binding domains. *Biopolymers* **70**, 522-533, doi:10.1002/bip.10536 (2003).
31 Sudo, S. *et al.* Structures of mollusc shell framework proteins. *Nature* **387**, 563 - 564 (1997).
32 Zhang, Y. *et al.* A novel matrix protein participating in the nacre framework formation of pearl oyster, Pinctada fucata. *Comp Biochem Physiol B Biochem Mol Biol* **135**, 565 - 573 (2003).
33 Marin, F., Corstjens, P., de Gaulejac, B., de Vrind-De Jong, E. & Westbroek, P. Mucins and Molluscan Calcification: Molecular characterization of mucoperlin, a novel mucin-like protein from the nacreous shell layer of the fan mussel Pinna nobilis (Bivalvia, Pteriomorphia). *Journal of Biological Chemistry* **275**, 20667-20675, doi:10.1074/jbc.M003006200 (2000).
34 Kono, M., Hayashi, N. & Samata, T. Molecular Mechanism of the Nacreous Layer Formation in Pinctada maxima. *Biochem Biophys Res Comm* **269**, 213 - 218 (2000).
35 Miyashita, T. *et al.* Complementary DNA Cloning and Characterization of Pearlin, a New Class of Matrix Protein in the Nacreous Layer of Oyster Pearls. *Mar Biotechnol* **2**, 409-418, doi:10.1007/pl00021687 (2000).

36 Miyamoto, H. *et al.* A Carbonic Anhydrase from the Nacreous Layer in Oyster Pearls. *Proceedings of the National Academy of Sciences of the United States of America* **93**, 9657-9660, doi:10.2307/39766 (1996).
37 McGinty, E. L., Zenger, K. R., Jones, D. B. & Jerry, D. R. Transcriptome analysis of biomineralisation-related genes within the pearl sac: Host and donor oyster contribution. *Marine Genomics* **5**, 27-33, doi:http://dx.doi.org/10.1016/j.margen.2011.08.006 (2012).
38 Blank, S. *et al.* The nacre protein perlucin nucleates growth of calcium carbonate crystals. *Journal of Microscopy* **212**, 280-291, doi:10.1111/j.1365-2818.2003.01263.x (2003).
39 Suzuki, M. *et al.* An Acidic Matrix Protein, Pif, Is a Key Macromolecule for Nacre Formation. *Science* **325**, 1388-1390, doi:10.1126/science.1173793 (2009).
40 Frémy, M. E. *Annales de chimie et de physique* **43**, 45-107 (1855).
41 Shen, X., Belcher, A. M., Hansma, P. K., Stucky, G. D. & Morse, D. E. Molecular Cloning and Characterization of Lustrin A, a Matrix Protein from Shell and Pearl Nacre of Haliotis rufescens. *Journal of Biological Chemistry* **272**, 32472-32481, doi:10.1074/jbc.272.51.32472 (1997).
42 Marie, B. *et al.* Characterization of MRNP34, a novel methionine-rich nacre protein from the pearl oysters. *Amino Acids*, 1-9, doi:10.1007/s00726-011-0932-0.
43 Rousseau, M. *et al.* Restoration of stratum corneum with nacre lipids. *Comparative Biochemistry and Physiology Part B: Biochemistry and Molecular Biology* **145**, 1-9, doi:10.1016/j.cbpb.2006.06.012 (2006).
44 Wu, M., Mak, S. K. K., Zhang, X. & Qian, P.-Y. The effect of co-cultivation on the pearl yield of Pinctada martensi (Dumker). *Aquaculture* **221**, 347-356, doi:http://dx.doi.org/10.1016/S0044-8486(03)00122-4 (2003).
45 Yukihira, H., Lucas, J. S. & Klumpp, D. W. The pearl oysters, Pinctada maxima and P. margaritifera, respond in different ways to culture in dissimilar environments. *Aquaculture* **252**, 208-224, doi:http://dx.doi.org/10.1016/j.aquaculture.2005.06.032 (2006).
46 van Dyk, M. *Pinctada margaritifera*, <http://www.gbri.org.au/Species/Pinctadamargaritifera.aspx?moid=465> (2011).
47 Rousseau, M. *et al.* Dynamics of sheet nacre formation in bivalves. *Journal of Structural Biology* **165**, 190-195, doi:10.1016/j.jsb.2008.11.011 (2009).
48 Pons, A. J. & Karma, A. Helical crack-front instability in mixed-mode fracture. *Nature* **464**, 85-89, doi:http://www.nature.com/nature/journal/v464/n7285/suppinfo/nature08862_S1.html (2010).
49 Currey, J. D. Mechanical Properties of Mother of Pearl in Tension. *Proceedings of the Royal Society of London. Series B. Biological Sciences* **196**, 443-463, doi:10.1098/rspb.1977.0050 (1977).
50 Addadi, L. & Weiner, S. Biomineralization: A pavement of pearl. *Nature* **389**, 912-915 (1997).
51 Kinoshita, S. *et al.* Deep Sequencing of ESTs from Nacreous and Prismatic Layer Producing Tissues and a Screen for Novel Shell Formation-Related Genes in the Pearl Oyster. *PLoS ONE* **6**, e21238, doi:10.1371/journal.pone.0021238 (2011).
52 Jacob, D. E. *et al.* Nanostructure, composition and mechanisms of bivalve shell growth. *Geochimica et Cosmochimica Acta* **72**, 5401-5415, doi:10.1016/j.gca.2008.08.019 (2008).
53 Bevelander, G. & Nakahara, H. in *Biomineralization Mechanisms in Animals and Plants* (eds M Omori & N Watabe) 25-33 (Tokai University Press, 1980).

54 Schäffer, T. E. *et al.* Does Abalone Nacre Form by Heteroepitaxial Nucleation or by Growth through Mineral Bridges? *Chemistry of Materials* **9**, 1731-1740, doi:10.1021/cm960429i (1997).
55 Rousseau, M. *et al.* Sheet nacre growth mechanism: a Voronoi model. *Journal of Structural Biology* **149**, 149-157, doi:10.1016/j.jsb.2004.09.005 (2005).
56 Cartwright, J. H. E. & Checa, A. G. The dynamics of nacre self-assembly. *Journal of The Royal Society Interface* **4**, 491-504, doi:10.1098/rsif.2006.0188 (2007).
57 Jackson, A. P., Vincent, J. F. V. & Turner, R. M. The Mechanical Design of Nacre. *Proceedings of the Royal Society of London. Series B. Biological Sciences* **234**, 415-440, doi:10.1098/rspb.1988.0056 (1988).
58 Song, F. & Bai, Y. Analysis of the strengthening and toughening of a biomaterial interface. *Sci. China Ser. A-Math.* **44**, 1596-1601, doi:10.1007/bf02880799 (2001).
59 Song, F., Zhang, X. H. & Bai, Y. L. Microstructure and Characteristics in the Organic Matrix Layers of Nacre. *Journal of Materials Research* **17**, 1567-1570, doi:doi:10.1557/JMR.2002.0233 (2002).
60 Liu, K. & Jiang, L. Bio-inspired design of multiscale structures for function integration. *Nano Today* **6**, 155-175, doi:http://dx.doi.org/10.1016/j.nantod.2011.02.002 (2011).
61 Li, Y.-Q., Yu, T., Yang, T.-Y., Zheng, L.-X. & Liao, K. Bio-Inspired Nacre-like Composite Films Based on Graphene with Superior Mechanical, Electrical, and Biocompatible Properties. *Advanced Materials* **24**, 3426-3431, doi:10.1002/adma.201200452 (2012).
62 Burghard, Z. *et al.* Nanomechanical Properties of Bioinspired Organic–Inorganic Composite Films. *Advanced Materials* **19**, 970-974, doi:10.1002/adma.200601068 (2007).
63 Walther, A. *et al.* Large-Area, Lightweight and Thick Biomimetic Composites with Superior Material Properties via Fast, Economic, and Green Pathways. *Nano Letters* **10**, 2742-2748, doi:10.1021/nl1003224 (2010).
64 Walther, A. *et al.* Supramolecular Control of Stiffness and Strength in Lightweight High-Performance Nacre-Mimetic Paper with Fire-Shielding Properties. *Angewandte Chemie International Edition* **49**, 6448-6453, doi:10.1002/anie.201001577 (2010).
65 Bonderer, L. J., Studart, A. R. & Gauckler, L. J. Bioinspired Design and Assembly of Platelet Reinforced Polymer Films. *Science* **319**, 1069-1073, doi:10.1126/science.1148726 (2008).
66 Xie, Y. K. *Pearl Science*. 313 (Ocean Press, 1995).
67 Bennett, J. *Pearl Powders*, <http://www.cosmeticsandskin.com/aba/pearl-powders.php> (2014).
68 Askinson, G. W. *Perfumes and cosmetics: Their preparation and manufacture* 5edn, 306 (Crosby Lockwood and Son, 1923).
69 Annotations. *The Lancet* **124**, 375-380, doi:http://dx.doi.org/10.1016/S0140-6736(02)27148-2 (1884).
70 Pearlescent pigments in powder coating. *Focus on Powder Coatings* **2004**, 5-6, doi:http://dx.doi.org/10.1016/S1364-5439(04)00225-4 (2004).
71 *A "Luxury" Cream Made with Precious Pearl Powder, Argireline®, and an Explosion of Vitamins, Minerals, Antioxidants and Amino Acids. Your Skins Dream Cream*, <http://pearl-cream.agedefying-secrets.com/> (2014).
72 Kottelat, M. & Freyhof, J. *Handbook of European Freshwater Fishes*. (Kottelat, 2007).

73 Maile, F. J., Pfaff, G. & Reynders, P. Effect pigments--past, present and future. *Progress in Organic Coatings* **54**, 150-163, doi:http://dx.doi.org/10.1016/j.porgcoat.2005.07.003 (2005).

74 Checa, A. G. & Rodrìguez-Navarro, A. B. Self-organisation of nacre in the shells of Pterioida (Bivalvia: Mollusca). *Biomaterials* **26**, 1071-1079, doi:10.1016/j.biomaterials.2004.04.007 (2005).

75 Pfaff, G. *Special effect pigments*. 2 edn, (Dobler-Druck, 2008).

76 Jian-Ping, D. *et al.* Effects of pearl powder extract and its fractions on fibroblast function relevant to wound repair. *Pharmaceutical Biology* **48**, 122-127 (2010).

77 Lopez, E., Faou, A. L., Borzeix, S. & Berland, S. Stimulation of rat cutaneous fibroblasts and their synthetic activity by implants of powdered nacre (mother of pearl). *Tissue and Cell* **32**, 95-101, doi:10.1054/tice.1999.0091 (2000).

78 Lamghari, M. *et al.* Stimulation of bone marrow cells and bone formation by nacre: in vivo and in vitro studies. *Bone* **25**, 91S-94S (1999).

79 Lamghari, M., Berland, S., Laurent, A., Huet, H. & Lopez, E. Bone reactions to nacre injected percutaneously into the vertebrae of sheep. *Biomaterials* **22**, 555-562, doi:10.1016/s0142-9612(00)00213-1 (2001).

80 Shono, M. *et al.* Reducing Effect of Feeding Powdered Nacre of Pinctada maxima on the Visceral Fat of Rats. *Bioscience, Biotechnology, and Biochemistry* **72**, 2761-2763, doi:10.1271/bbb.80267 (2008).

81 Cao, G., Xu, Z., Wei, H., Yao, S. & Liu, Y. Pearl and mother-of-pearl powder in health-care. *Chin Pharm J* **21**, 635-638 (1996).

82 WebMD. *Picture of The Skin*, <http://www.webmd.com/skin-problems-and-treatments/picture-of-the-skin> (2014).

83 Ramms, L. *et al.* Keratins as the main component for the mechanical integrity of keratinocytes. *Proceedings of the National Academy of Sciences of the United States of America* **110**, 18513-18518, doi:10.1073/pnas.1313491110 (2013).

84 Bigby, M. Atlas of normal human skin. *Archives of Dermatology* **129**, 804-804, doi:10.1001/archderm.1993.01680270148033 (1993).

85 KreativeStudios. *The Epidermis*, <http://kreativestudios.com/Tooltip/05Integument/02epidermis.html> (2015).

86 The-Loudoun-Center. *Skin Anatomy*, <https://www.loudouncenterforplasticsurgery.com/skin-anatomy/> (2015).

87 Linares, H. A. From wound to scar. *Burns* **22**, 339-352, doi:http://dx.doi.org/10.1016/0305-4179(95)00164-6 (1996).

88 Sephel, G. C. & Davidson, J. M. Elastin Production in Human Skin Fibroblast Cultures and Its Decline with Age. *J Investig Dermatol* **86**, 279-285 (1986).

89 Nasrollahi, S. A., Fouladdel, S., Taghibiglou, C., Azizi, E. & Farboud, E. S. A peptide carrier for the delivery of elastin into fibroblast cells. *International Journal of Dermatology* **51**, 923-929, doi:10.1111/j.1365-4632.2011.05214.x (2012).

90 Denecker, G., Ovaere, P., Vandenabeele, P. & Declercq, W. Caspase-14 reveals its secrets. *The Journal of Cell Biology* **180**, 451-458, doi:10.1083/jcb.200709098 (2008).

91 Fuchs, E. Epidermal Differentiation: The Bare Essentials. *The Journal of Cell Biology* **111**, 2807-2814, doi:10.2307/1614286 (1990).

92 Achrai, B. & Wagner, H. D. Micro-structure and mechanical properties of the turtle carapace as a biological composite shield. *Acta Biomaterialia* **9**, 5890-5902, doi:http://dx.doi.org/10.1016/j.actbio.2012.12.023 (2013).

93 McKittrick, J. *et al.* The Structure, Functions, and Mechanical Properties of Keratin. *JOM* **64**, 449-468, doi:10.1007/s11837-012-0302-8 (2012).

94 Brody, I. An ultrastructural study on the role of the keratohyalin granules in the keratinization process. *Journal of Ultrastructure Research* **3**, 84-104 (1959).
95 Nomura, T. *et al.* Unique mutations in the filaggrin gene in Japanese patients with ichthyosis vulgaris and¬†atopic dermatitis. *Journal of Allergy and Clinical Immunology* **119**, 434-440, doi:http://dx.doi.org/10.1016/j.jaci.2006.12.646 (2007).
96 Sticozzi, C. *et al.* Resveratrol protects SR-B1 levels in keratinocytes exposed to cigarette smoke. *Free Radical Biology and Medicine* **69**, 50-57, doi:http://dx.doi.org/10.1016/j.freeradbiomed.2014.01.007 (2014).
97 Wittmann, M., McGonagle, D. & Werfel, T. Cytokines as therapeutic targets in skin inflammation. *Cytokine & Growth Factor Reviews* **25**, 443-451, doi:http://dx.doi.org/10.1016/j.cytogfr.2014.07.008 (2014).
98 Boukamp, P. *et al.* Normal keratinization in a spontaneously immortalized aneuploid human keratinocyte cell line. *The Journal of Cell Biology* **106**, 761-771 (1988).
99 Rnjak, J., Li, Z., Maitz, P. K. M., Wise, S. G. & Weiss, A. S. Primary human dermal fibroblast interactions with open weave three-dimensional scaffolds prepared from synthetic human elastin. *Biomaterials* **30**, 6469-6477, doi:http://dx.doi.org/10.1016/j.biomaterials.2009.08.017 (2009).
100 Kalluri, R. & Zeisberg, M. Fibroblasts in cancer. *Nat Rev Cancer* **6**, 392-401 (2006).
101 Ranzer, M. J., Chen, L. & DiPietro, L. A. Fibroblast Function and Wound Breaking Strength Is Impaired by Acute Ethanol Intoxication. *Alcoholism: Clinical and Experimental Research* **35**, 83-90, doi:10.1111/j.1530-0277.2010.01324.x (2011).
102 Myles, W. M. Ophthalmic etymology. *Survey of Ophthalmology* **37**, 306-309, doi:http://dx.doi.org/10.1016/0039-6257(93)90016-Z (1993).
103 Kahan, V., Andersen, M. L., Tomimori, J. & Tufik, S. Can poor sleep affect skin integrity? *Medical Hypotheses* **75**, 535-537, doi:http://dx.doi.org/10.1016/j.mehy.2010.07.018 (2010).
104 Ravelojaona, V., Robert, L. & Robert, A. M. Effect of cellular aging on collagen biosynthesis: II. Collagen synthesis and deposition by a human skin fibroblast strain over 25 passages. *Archives of Gerontology and Geriatrics* **47**, 368-376, doi:http://dx.doi.org/10.1016/j.archger.2007.08.017 (2008).
105 Murakami, H., Shimbo, K., Inoue, Y., Takino, Y. & Kobayashi, H. Importance of amino acid composition to improve skin collagen protein synthesis rates in UV-irradiated mice. *Amino Acids* **42**, 2481-2489, doi:10.1007/s00726-011-1059-z (2012).
106 Chua, L. S., Lee, S. Y., Abdullah, N. & Sarmidi, M. R. Review on Labisia pumila (Kacip Fatimah): Bioactive phytochemicals and skin collagen synthesis promoting herb. *Fitoterapia* **83**, 1322-1335, doi:http://dx.doi.org/10.1016/j.fitote.2012.04.002 (2012).
107 Elder, M. Antiaging Products and Services: The Global Market. Report No. HLC060B, (BCC Research, Wellesley, 2013).
108 Pollack, A. & Miller, C. C. in *New York TImes* (New York, 2013).
109 Choi, H.-k. *et al.* Labisia pumila extract protects skin cells from photoaging caused by UVB irradiation. *Journal of Bioscience and Bioengineering* **109**, 291-296, doi:http://dx.doi.org/10.1016/j.jbiosc.2009.08.478 (2010).
110 Fessel, G., Wernli, J., Li, Y., Gerber, C. & Snedeker, J. G. Exogenous collagen cross-linking recovers tendon functional integrity in an experimental model of partial tear. *Journal of Orthopaedic Research* **30**, 973-981, doi:10.1002/jor.22014 (2012).

111 Kippenberger, S. *et al.* STAT6-Dependent Collagen Synthesis in Human Fibroblasts Is Induced by Bovine Milk. *PLoS ONE* **10**, e0131783, doi:10.1371/journal.pone.0131783 (2015).
112 Obayashi, K., Akamatsu, H., Okano, Y., Matsunaga, K. & Masaki, H. Exogenous nitric oxide enhances the synthesis of type I collagen and heat shock protein 47 by normal human dermal fibroblasts. *Journal of Dermatological Science* **41**, 121-126, doi:http://dx.doi.org/10.1016/j.jdermsci.2005.08.004 (2006).
113 Baumann, L. Skin ageing and its treatment. *The Journal of Pathology* **211**, 241-251, doi:10.1002/path.2098 (2007).
114 Guttman, C. Studies demonstrate value of procollagen fragment. *Cosmetic Surgery Times* **5**, 34 (2002).
115 Al-Bader, T. *et al.* Effect of cosmetic ingredients as anticellulite agents: synergistic action of actives with in vitro and in vivo efficacy. *Journal of Cosmetic Dermatology* **11**, 17-26, doi:10.1111/j.1473-2165.2011.00594.x (2012).
116 Fujii, T., Wakaizumi, M., Ikami, T. & Saito, M. Amla (Emblica officinalis Gaertn.) extract promotes procollagen production and inhibits matrix metalloproteinase-1 in human skin fibroblasts. *Journal of Ethnopharmacology* **119**, 53-57, doi:http://dx.doi.org/10.1016/j.jep.2008.05.039 (2008).
117 Swezey, L. *Phases of Wound Healing-Part 1*, <http://woundeducators.com/phases-of-wound-healing/> (2014).
118 Clark, R. A. F. 3-50 (Plenum, New York, 1996).
119 Martin, P. Wound Healing--Aiming for Perfect Skin Regeneration. *Science* **276**, 75-81, doi:10.1126/science.276.5309.75 (1997).
120 Hübner, G. *et al.* Differential regulation of pro-inflammatory cytokines during wound healing in normal and glucocorticoid-treated mice. *Cytokine* **8**, 548-556, doi:http://dx.doi.org/10.1006/cyto.1996.0074 (1996).
121 Leibovich, S. J. & Ross, R. The role of the macrophage in wound repair. A study with hydrocortisone and antimacrophage serum. *The American Journal of Pathology* **78**, 71-100 (1975).
122 Werner, S. *et al.* Large induction of keratinocyte growth factor expression in the dermis during wound healing. *Proceedings of the National Academy of Sciences of the United States of America* **89**, 6896-6900 (1992).
123 Frank, S., Madlener, M. & Werner, S. Transforming Growth Factors 1, 2, and 3 and Their Receptors Are Differentially Regulated during Normal and Impaired Wound Healing. *Journal of Biological Chemistry* **271**, 10188-10193, doi:10.1074/jbc.271.17.10188 (1996).
124 Brown, L. F. *et al.* Expression of vascular permeability factor (vascular endothelial growth factor) by epidermal keratinocytes during wound healing. *The Journal of Experimental Medicine* **176**, 1375-1379, doi:10.1084/jem.176.5.1375 (1992).
125 Eriksson, A., Siegbahn, A., Westermark, B., Heldin, C.-H. & Claesson-Welsh, L. PDGF α- and β-receptors activate unique and common signal transduction pathways. *THE EMBO Journal* **11**, 543-550 (1992).
126 Stein, C. & Küchler, S. Targeting inflammation and wound healing by opioids. *Trends in Pharmacological Sciences* **34**, 303-312, doi:http://dx.doi.org/10.1016/j.tips.2013.03.006 (2013).
127 Goliger, J. & Paul, D. Wounding alters epidermal connexin expression and gap junction-mediated intercellular communication. *Mol Biol Cell* **6**, 1491-1501 (1995).

128 Gabbiani, G., Chaponnier, C. & Hüttner, I. Cytoplasmic filaments and gap junctions in epithelial cells and myofibroblasts during wound healing. *The Journal of Cell Biology* **76**, 561-568, doi:10.1083/jcb.76.3.561 (1978).
129 Larjava, H., Salo, T., Haapasalmi, K., Kramer, R. H. & Heino, J. Expression of integrins and basement membrane components by wound keratinocytes. *The Journal of Clinical Investigation* **92**, 1425-1435, doi:10.1172/jci116719 (1993).
130 Singer, A. J. & Clark, R. A. F. Cutaneous Wound Healing. *New England Journal of Medicine* **341**, 738-746, doi:doi:10.1056/NEJM199909023411006 (1999).
131 Welch, M. P., Odland, G. F. & Clark, R. A. Temporal relationships of F-actin bundle formation, collagen and fibronectin matrix assembly, and fibronectin receptor expression to wound contraction. *The Journal of Cell Biology* **110**, 133-145, doi:10.1083/jcb.110.1.133 (1990).
132 Clark, R. A., Nielsen, L. D., Welch, M. P. & McPherson, J. M. Collagen matrices attenuate the collagen-synthetic response of cultured fibroblasts to TGF-beta. *Journal of Cell Science* **108**, 1251-1261 (1995).
133 Coolen, N. A., Schouten, K. C. W. M., Boekema, B. K. H. L., Middelkoop, E. & Ulrich, M. M. W. Wound healing in a fetal, adult, and scar tissue model: A comparative study. *Wound Repair and Regeneration* **18**, 291-301, doi:10.1111/j.1524-475X.2010.00585.x (2010).
134 Ferguson, M. W. J. & Sharon, O. K. Scar-Free Healing: From Embryonic Mechanisms to Adult Therapeutic Intervention. *Philosophical Transactions: Biological Sciences* **359**, 839-850, doi:10.2307/4142114 (2004).
135 Levenson, S. *et al.* The healing of rat skin wounds. *Annals of Surgery* **161**, 293-308 (1965).
136 Shah, M., Foreman, D. M. & Ferguson, M. W. J. Control of scarring in adult wounds by neutralising antibody to transforming growth factor Œ≤. *The Lancet* **339**, 213-214, doi:10.1016/0140-6736(92)90009-r (1992).
137 Chen, X. *et al.* Application of acellular dermal xenografts in full-thickness skin burns. *Experimental and Therapeutic Medicine* **6**, 194-198, doi:10.3892/etm.2013.1114 (2013).

Chapter 2

Chapter 2: Optimization of Nacre Tablet Preparation - Generation of Uniform Nacre Tablets

2.1. Introduction

In recent years, there have been several studies in the literature reporting the application of nacre in the cosmetics industry[1] as well as a potential therapeutic in wound healing.[2] In particular Lee et al. have shown that water soluble components of nacre are able to promote wound healing in porcine skin with deep second degree burns.[3] However, to date, to the best of the author's knowledge, there have been no reports on using the inorganic component of nacre, i.e. aragonite, for personal skin products or wound care dressings.

One of the key issues in comparing different studies that use nacre is the lack of consistency in the preparations, for example in terms of size of the particles and composition, as well as information about contamination. The production of more consistent preparations will allow more accurate measurements of safety and efficacy. The main focus of this thesis is to determine whether nacre is safe to be used as a product in personal skin products and/or wound care dressings and whether there are beneficial effects of using nacre.

As described in the Introduction, nacre is composed of both organic and inorganic components.[4] There are therefore a number of different types of preparations that can be produced i.e. those containing exclusively the inorganic components, the organic ones or a mixture of both. The simplest and most straightforward preparation method uses grinding with a mortar and pestle to physically break down the nacre. The products generated by this method still have both organic and inorganic components.

Pure aragonite tablets have been previously produced from nacre by dissolving the organic matrix in shell nacre using an ionic liquid, n-butyl-3-methylimidazolium hexafluorophosphate [BMIM][PF_6].[5] In order to separate the organic matrix, nacre is usually decalcified with acid, such as formic acid, acetic acid or ethylenediamine tetra-acetic acid (EDTA).[6,7] Alternatively, some of the organic components that are water soluble can be obtained through water extraction.[8] Using purified water to extract the organic component has greater merit as some proteins might become denatured in the presence of acid. On the other hand, not all of the organic components in the matrix are soluble in water.

2.2. Production of nacre powder through grinding

In the historical examples given above, descriptions of nacre preparations are not available. However, nacre was presumably ground manually using a mortar and pestle but the uniformity of the particle size or lack thereof is unknown. In the current industrial era, processing devices are employed to grind nacre.

Table 2.1. Preparations of nacre through grinding.

No.	Author	Year	Preparation Method	Product Size
1	Lamghari et al.[9]	1999	Grinding with unknown machine	50-150 μm
2	Lopez et al.[10]	2000	Grinding with unknown machine	50-100 μm
3	Rousseau et al.[11]	2006	Grinding with unknown machine	50-100 μm
4	Chen et al.[12]	2008	Dry cryo-nanonization grinding	84nm-29 μm*
5	Drai and Guillot[13]	2011	Planetary ball-milling	<100 nm

* 84 nm is a mean diameter for nanonized pearl powder, 29 μm is mean diameter for micronized pearl powder.

Table 2.1 summarises a number of publications reporting the preparation of nacre using various grinding methods. The products have particle sizes ranging from 150 μm to less than 1 nm. To put this in context, natural nacre aragonite tablets are approximately 5 – 15 μm in diameter.[14] In order to produce desired effects in the dermal layer, nanoparticles may need to cross the epidermis. Theoretically, for nacre powder to

be effective as skin care, the particle size needs to be smaller than 40 nm to be able to penetrate epidermis.[15] This penetration would be important for the nacre to have a direct interaction with dermal cells and therefore a direct effect on their activity. However, it may be that non-penetrating particles could have an indirect effect through the keratinocytes or other physical changes to the skin environment. Additionally, Bos and Meinardi argued that the molecular weight of a compound must be smaller than 500 Daltons to allow skin absorption through stratum corneum in the epidermis.[16] Thus, the molecular weight of any organic molecules from nacre should be less than 500 Daltons for skin absorption. Alternatively, nacre particles could be absorbed through skin appendages, especially hair follicles.[17] Through this pathway, particle size can be much larger than 40 nm depending on the size of the hair follicle which can vary depending on the site in the body.[18] The size is certainly larger than the aragonite tablet size mentioned above (nacre tablet: 5 – 15 μm vs average of hair follicles in forehead: 66 μm). See Fig. 2.1. Therefore, whole aragonite tablets might be absorbed through hair follicles, whereas the finer powder that is smaller than 40 nm might be absorbed both through hair follicles and corneal layers.

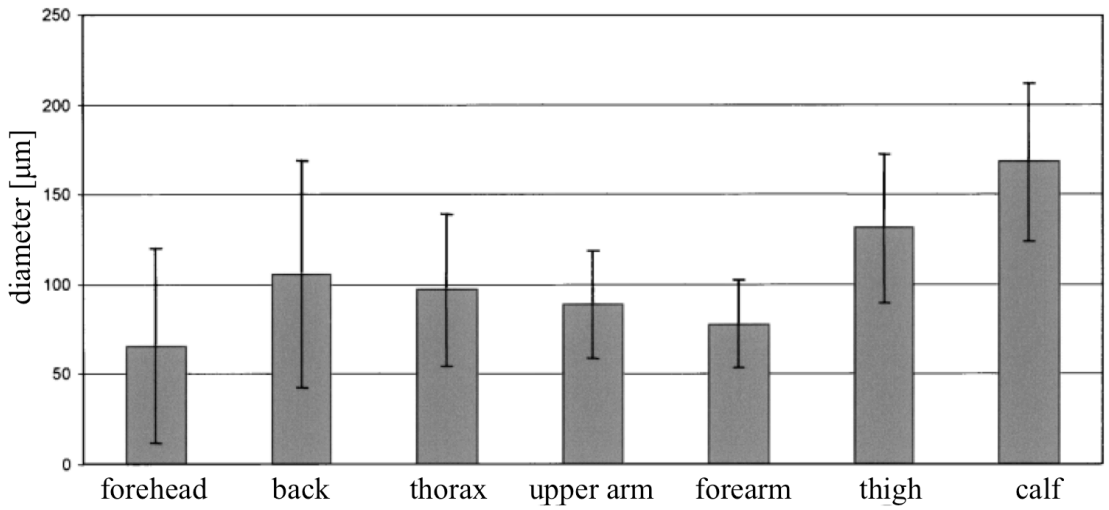

Figure 2.1. Diameter of hair follicle orifices on seven body sites.[18]

From Table 2.1 the method used by Drai and Guillot was the closest one to the size requirement of <40 nm to penetrate the epidermis, and this was achieved using planetary ball milling.[13] The first three examples from Table 2.1 had their samples prepared by the Center for Technology Transfer in Ceramics in France. Their product size range is much larger than the size range of the aragonite tablets (product size : 50 – 150 μm vs nacre tablet: 5 – 15 μm). The fourth study produced nacre particles that were either much smaller or larger than aragonite tablets, whilst the final study listed is a very fine powder. There is no universally accepted protocol to produce nacre aragonite tablet that allows direct comparison to other research. Therefore, a systematic study was undertaken to produce aragonite tablets of an appropriate size range for use on skin and wound healing and with minimal contamination for use in safety and efficacy studies of nacre.

2.3. Contamination

Heavy metals are a non-degradable pollutant in many types of environment, such as aquatic[19], agricultural soil[20] and air.[21] There are many activities that could contribute to heavy metal pollution in seawater, such as offshore mining[22], industrial discharges[23] or accidental spillage of gasoline.[24] Marine organisms ingest heavy metals and bioaccumulate them.[25] Oyster beds are naturally vulnerable to this contamination.[23] Additionally, oysters that are grown in polluted environments might accumulate heavy metals,[26] such as lead and cadmium, in their shells.[26,27] Oysters obtain the raw inorganic materials for their developing shells from their surrounding water, which might include heavy metals. Heavy metal levels in oyster shells could become a pollution indicator of their environment.[28] Indeed, Thompson et al. have reported that heavy metals affect the functionality of oyster proteins.[29] Besides the above mentioned sources of pollution, heavy metals could also be introduced into marine products during canning processes.[30]

In the present study, heavy metals could also be introduced from the wear of the grinding balls or the grinding bowl. Of the five examples given in Table 2.1 only Chen et al. claims that their nacre preparations were free from heavy metals (As, Pb, Cd and Hg) based on atomic absorption spectrometry (Model Analyst 600, PerkinElmer, Washington, D.C., U.S.A.).[12] In the present study, inductively coupled plasma mass spectrometry and atomic emission spectrometry (ICP MS-AES) were used to detect and quantify the presence of heavy metals.

We have recently published a protocol describing a planetary ball-milling technique that was developed for producing nacre preparations of a consistent size and with minimal contamination, as part of this thesis.[31] The planetary ball milling technique was chosen because it was used to generate the finest powder as summarized in Table 2.1. In this Chapter, additional details of the ball milling technique, optimization of the process and the properties of the nacre preparation, which complement the paper, are described.

2.4. Planetary Ball-Milling

In 1907, Ricketts used a porcelain ball-mill to crush blood cells.[32] In 1933, Krueger introduced a new type of ball-mill that operates under aseptic conditions to macerate bacteria (see Fig. 2.2).[33] Furnstal introduced a portable ball mill 2 years later[34], which was later built and commercialized by Quill (see Fig. 2.3).[35]

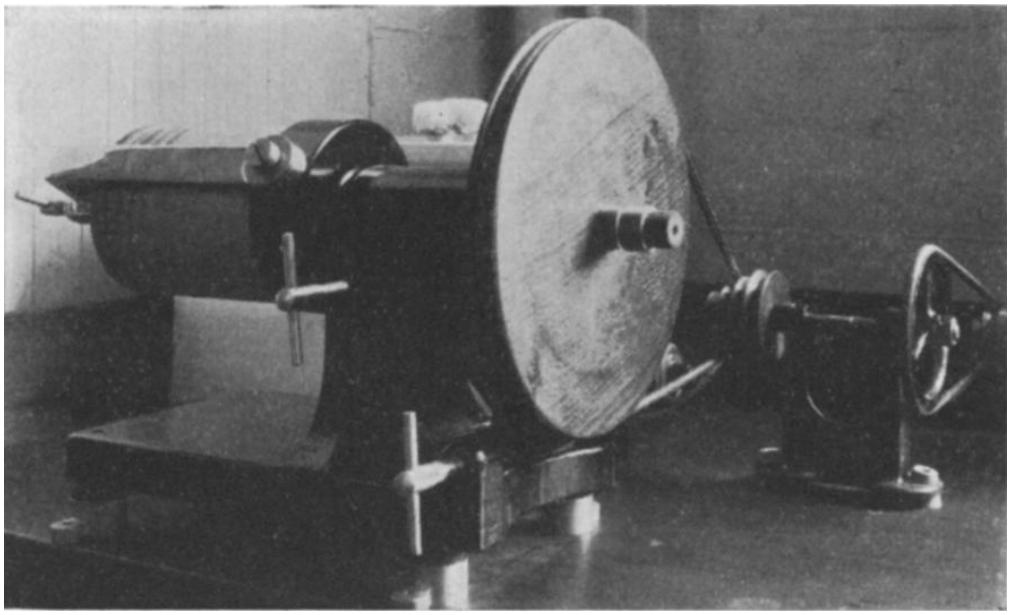

Figure 2.2. Apparatus with the grinding unit rotated to the horizontal position locked in place.[33]

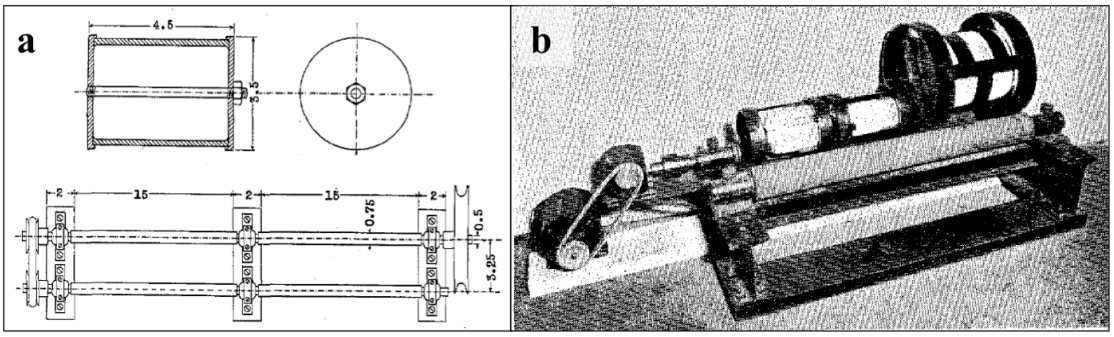

Figure 2.3. Ball milling. a) Diagram by Furnstal. Upper left, cross section of container. Upper right, end view of container. Lower, top view of rotating shaft assembly.[34] b) Ball mill built by Quill according to the diagram.[35]

Ball milling relies on the balls imparting force on the subject particles. The name "planetary' was derived because the equipment construction resembles a planetary gear. The grinding jar rotates on its own axis but at the same time also revolves around an axis (see Fig. 2.4).[36] In order to minimize denaturation of proteins, which is common in ball-milling[37,38], a number of factors need to be taken into consideration in developing and optimizing the ball-milling process. The rationale for the choice of ball-milling materials is described below in section 2.5 while the adjustment of milling parameters is described in section 2.6.

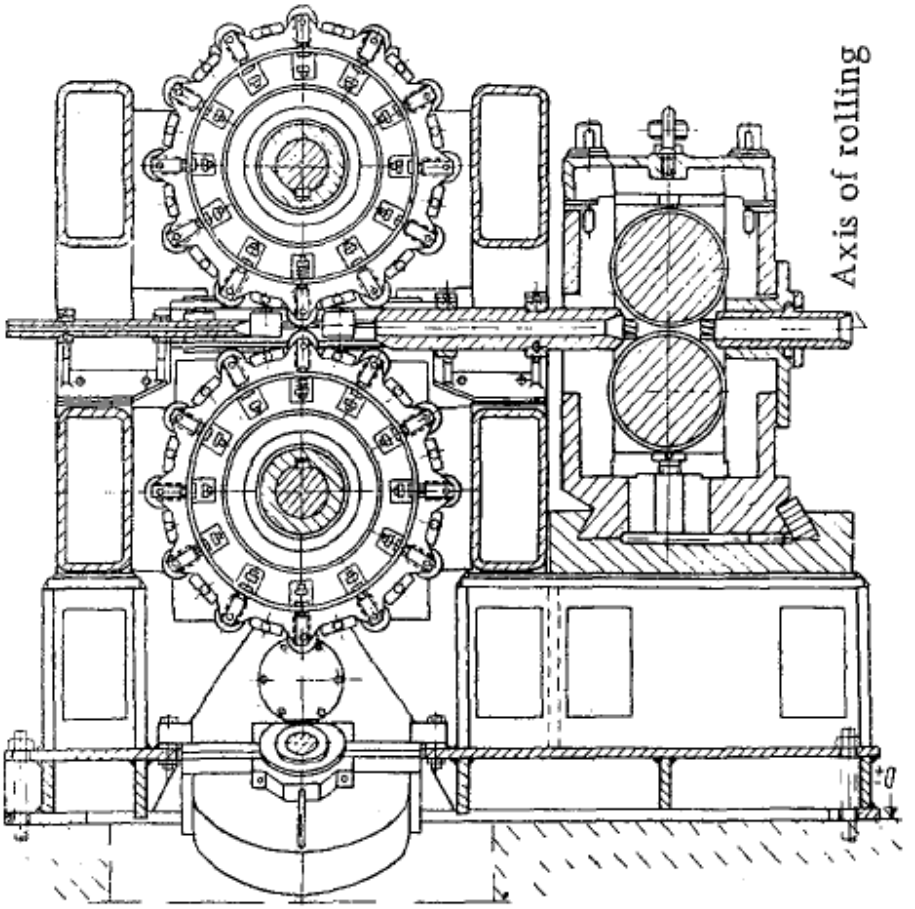

Figure 2.4. Diagram of planetary ball milling.[36]

2.5. Choice of materials for ball milling

There are seven types of material available from Fritsch GmbH to choose for the milling bowl and balls, namely agate (SiO_2), sintered corundum (99.7% Al_2O_3), silicon nitride (Si_3N_4), zirconium oxide (ZrO_2), stainless steel (Fe-Cr-Ni), tempered steel (Fe-Cr), and tungsten carbide (WC). A number of properties need to be considered when choosing the type of material for the bowl and milling balls, namely abrasion resistance, suitability for samples with different degrees of hardness, brittleness and fibrosity, as well as cost and availability (Table 2.2). In addition, to minimize contamination, the material used for the bowl must be the same as that used for the balls. As a general principle, materials for the bowl need to be harder than the sample to be ground.[39]

Table 2.2 Type of material for planetary ball milling. Adapted from www.fritsch-milling.com[39]

No	Material (Mineral hardness)	Abrasion Resistance	Physical properties of samples
1	Stainless Steel – Fe-Cr-Ni (5.5 – 6.3 Mohs[40])	Fairly Good	Medium-Hard, Brittle
2	Sintered Corundum 99.7% Al_2O_3 (9 Mohs[41])	Fairly Good	Medium-Hard, Fibrous
3	Agate – SiO_2 (6.5 – 7 Mohs[42])	Good	Soft to Medium-Hard
4	Tempered Steel – Fe-Cr (7.8 – 8.5 Mohs[40])	Good	Hard, Brittle
5	Zirconium Oxide – ZrO_2 (11 Mohs[43])	Very Good	Fibrous, Abrasive
6	Tungsten Carbide – WC (9 – 9.5 Mohs[44])	Very Good	Abrasive
7	Silicon Nitride – Si_3N_4 (8.5 Mohs[44])	Excellent	Abrasive, Metal Free Grinding

Materials with high abrasion resistance are required to prevent sample contamination. Once worn, the bowl and/or the ball need to be replaced and the cost of replacement can be substantial. For example, in 2011, the quote for a stainless steel grinding bowl for this project was $2110. Additionally, different materials have different prices for the same item. For example, the stainless steel grinding balls were quoted at $4 each for 5 mm balls and $23 each for 20 mm balls. In contrast, for the same ball sizes, zirconium oxide grinding balls were quoted at $6 and $183 respectively. For the current study on milling nacre, which is a relatively hard material[45], agate (SiO_2), sintered corundum (99.7% Al_2O_3), stainless steel (Fe-Cr-Ni) and tempered steel (Fe-Cr) balls were eliminated because their abrasion resistances are not sufficient to crush nacre. Silicon nitride (Si_3N_4) balls have the best abrasion resistance. They have the advantage of metal free leftover, as the material does not contain any metal. This means that even if the balls are worn, the wear-off does not contain any metal. Tungsten carbide (WC) and zirconium oxide (ZrO_2) balls have similar abrasion resistance and are both suitable for abrasive samples such as nacre. However, the prices for Si_3N_4 and WC are almost double that of ZrO_2 and their use

would reduce the ability to give added value to oyster shell that is treated as waste by the pearling industry. Nevertheless, an advantage of ZrO_2 is that it is readily available in-house. It was therefore decided to use ZrO_2 in this study. The next step was to optimize a number of parameters to ensure the consistent production of nacre particles. Our findings can be directly compared with those of Drai and Guillot (see Table 2.1) who also used ZrO_2 in their work on the processing of shell nacre.[13]

2.6. Optimization of milling parameters

All ball-milling parameters, namely volume of excipient, sample size, grinding ball size, number of balls, speed and duration were assessed systematically. The aim of optimization is to maximize yield, ensure a uniform particle size distribution and minimize contamination and cost of processing. These six parameters were thus varied systematically (one at a time) to gain insight into the particular effect of each individual parameter on the milling process. The unit and variance for each parameter is tabulated in Table 2.3.

Table 2.3. Milling parameters

No	Parameter	Unit	Variance
1	Volume of excipient	mL	5 to 30
2	Sample size	Gram	0.1, 5, 10, 15 and 20
3	Grinding ball size	mm	5 and 20
4	Number of balls	--	2 to 4 for 5 mm and 200 for 20 mm
5	Speed	Rpm	200, to 1000
6	Duration	Minute	1 to 1440

2.6.1. Volume of excipient

The first parameter that will be discussed is the volume of excipient (Milli Q water). The grinding bowl volume used is 80 mL, and thus the total volume of sample, grinding balls and excipient should not exceed this volume. Grinding balls 5 mm in diameter have a volume of 0.065 mL, so 200 would occupy about 13.0 mL of the space. Each 20

mm grinding ball has a volume of 4.19 mL. So, use of 2, 3 or 4 of 20 mm balls would take 8.38, 12.57 or 16.76 mL respectively.

Table 2.4. The effect of changing volume of excipient to yield. * indicates yield is definitely contaminated.

Ball Size (mm)	Number of Balls	Speed (rpm)	Duration (min)	Excipient (mL)	Sample Size (g)	Yield
20	4	400	120	5	5	82%
20	4	400	120	15	5	96%
20	4	400	120	30	5	98%
20	4	600	120	5	5	94%
20	4	600	120	15	5	112%*
20	4	600	120	30	5	117%*

Table 2.4 shows the effect of increasing volume of excipient relative to yield of the product. There are two groups of data, the first three rows were milled at 400 rpm and the second three rows were milled at 600 rpm. There is an increasing trend of yield for both groups, which can be considered as a positive outcome. Yields of greater than 100% (* in Table 2.4) raised the question of the origin of the extra yield. The most parsimonious explanation is that it was derived as a result of contamination in the form of degraded ZrO_2 balls (see Fig. 2.5). Such contamination was confirmed by X-Ray Diffraction (XRD) analyses, with asterisked samples contaminated with zirconium, in the form of zirconia. The XRD analyses of the fifth and sixth experiment in Table 2.4 are depicted in Figs 2.5a and b respectively. It is possible that excess amounts of excipient created more space for nacre and the grinding ball to move around. Consequently, the chance for a collision between the grinding ball and nacre is lowered. Conversely, the chance to have collision of grinding balls with each other is increased. In order to provide a pivotal point for other experiments, the volume of excipient is suggested to be in 1:1 proportion with the sample size.[31] It is assumed that the density of nacre is 1 g/mL. For example, the volume of excipient for 5 and 15 g sample sizes are 5 and 15 mL respectively.

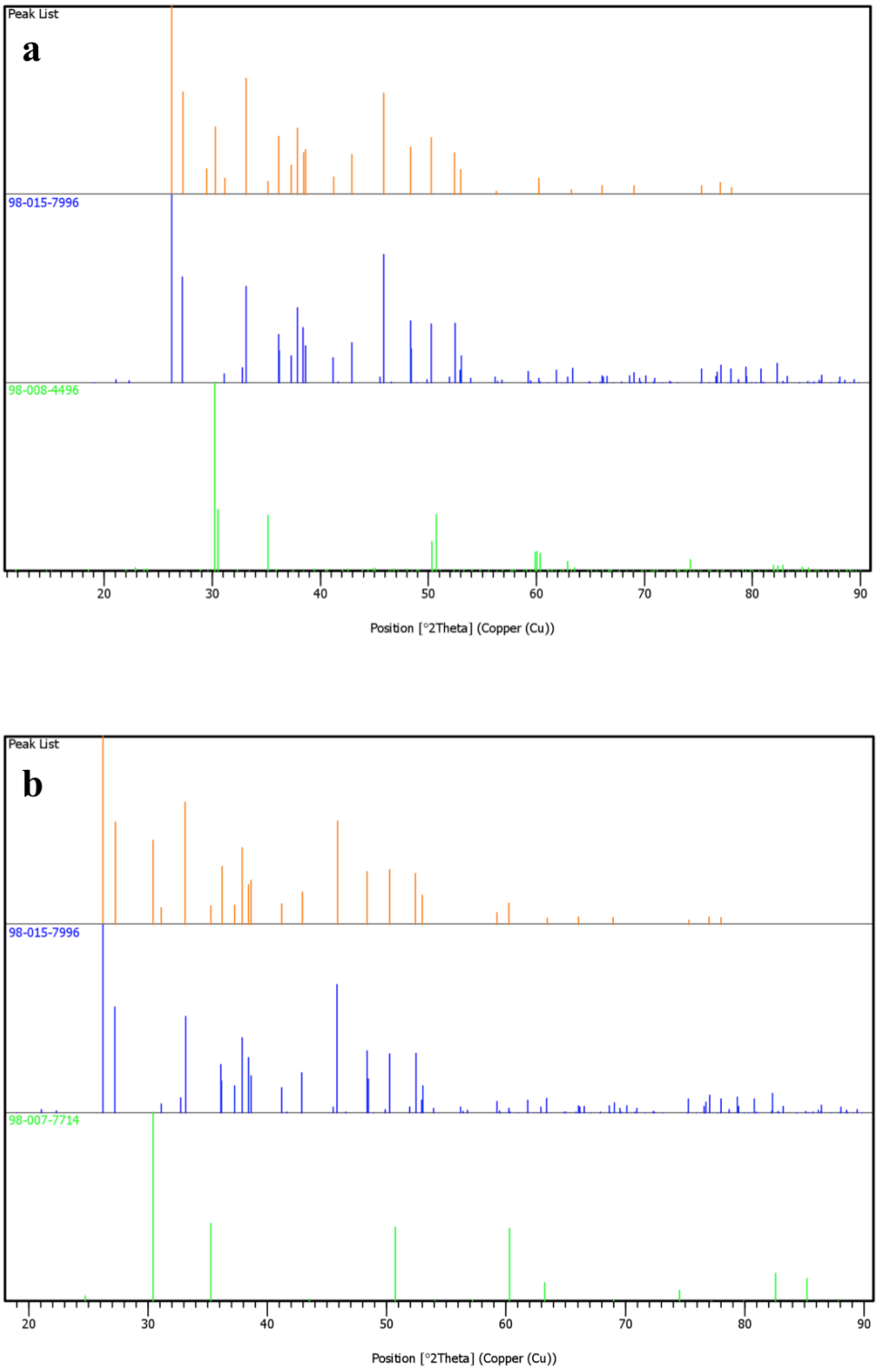

Figure 2.5. XRD analysis confirms zirconium contamination on both fifth (a) and sixth (b) samples. Orange peaks indicate the total peaks; Blue peaks indicate aragonite peaks; Green peaks indicate zirconium peaks. Heights of the peaks correspond to peak intensities.

2.6.2. Sample size

The first sets of ball milling experiments were performed using a sample size of 0.1 g of crushed nacre. At the time of starting these experiments, there was no published literature on which to base the protocols. A post-doctoral fellow in the group was using 0.1 g of crushed nacre for an ionic liquid experiment.[5] Since this weight had already proven suitable in an ionic liquid extraction process, it was initially selected for experimentation in the ball milling process. It was noticed that experiments with speeds greater than 500 rpm resulted in a yield of powder that was greater than 0.1 g, i.e. the initial weight of the nacre sample. This fact indicated that the material from the grinding balls had been worn off, adding to the final product weight. Proof of this contamination was obtained when the size of the balls that were used for experiments were compared with unused balls by measuring diameter with a vernier calliper. The balls size reduced dramatically from 5 mm to 3 mm diameter (40% reduction) presumably due to numerous collisions with each other rather than crushing shell nacre between them, to reduce the likelihood of fragmenting the balls.

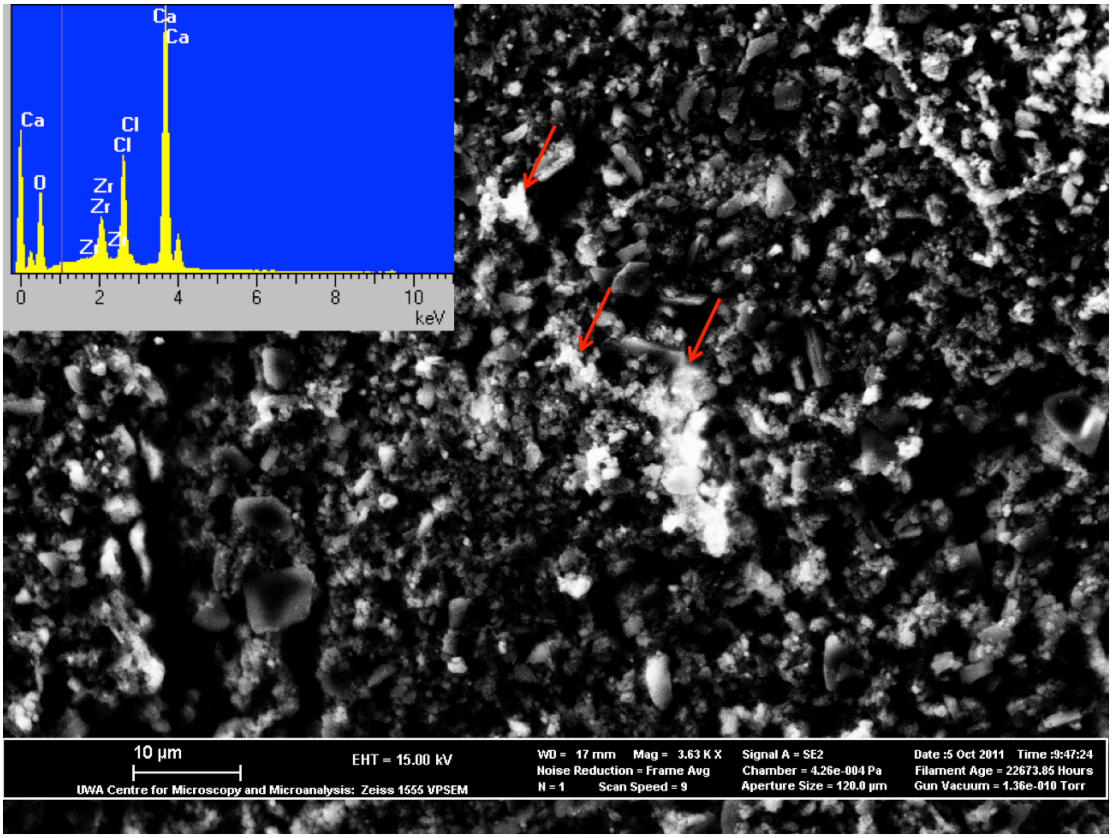

Figure 2.6. SEM image of milled nacre contaminated with ZrO_2. Insert at top left shows elemental analysis of the scan. Parameters: 100 mg of nacre, 200 of 5 mm balls, 500 rpm, 2 hour and 20 mL of Milli Q water.

Both milled nacre powder itself and zirconium oxide that was worn off the balls during grinding are white in colour and it is not possible to distinguish the nacre from the zirconium oxide by visual inspection. However, one practical protocol developed was to stir the powders in water. In the presence of zirconium oxide powder, the appearance of the suspension changes from colourless to milky white and indeed this change was observed in these experiments and clearly indicated the presence of zirconium oxide. However, more accurate qualitative and quantitative analyses were needed. Fig. 2.6 shows a scanning electron microscope (SEM) image of milled nacre that was contaminated by zirconium oxide from the grinding balls. The red arrows in the image are pointing to white areas, which were suspected to be the contaminant (ZrO_2). Energy dispersive x-ray spectroscopy (EDS) that was coupled to the SEM provided elemental analysis that confirmed the presence of Zr. See insert of Fig. 2.6.

The presence of chlorine can be explained since the shells were grown in a saline environment.

After establishing that 0.1 g was too small a sample size, which led to a highly contaminated product, the sample size was increased dramatically. Increasing the sample size will increase the ball-to-nacre collision and therefore reduce the ball-to-ball collision. Lower wear from the grinding balls should thus lower contamination. In addition, increasing the sample size should itself result in a higher yield of nacre powder. In order to use the space in the grinding bowl efficiently, the sample size must be increased as much as possible. The grinding bowl volume is 80 mL. It has been mentioned in section 2.6.1 that 200 balls with 5 mm diameter would occupy 13 mL of space, while 2 to 4 balls with 20 mm diameter would occupy space roughly between 8 – 17 mL. In order to simplify the calculation, 20 mL of space was allocated for the balls, with 60 mL available for shell nacre and movement of the balls. Half of it was allocated for air and the other half, 30 mL was allocated for the sample size and the volume of excipient. As it was suggested to use a ratio of 1:1 between the volume of excipient and sample size[31], therefore it was decided to use 15 g nacre and 15 mL of Milli Q water for all subsequent experiments.

2.6.3. Grinding ball size

There are two sizes of grinding balls that were used in the experiments, namely 5 and 20 mm. There are a number of factors that need to be considered before selecting the grinding ball size which are summarized in Table 2.5.

Table 2.5. Comparison between 5 mm and 20 mm grinding balls.

	5 mm	20 mm
Number	200	2, 3 or 4
Individual Price	$6	$183
Total Price	$ 1,200	$366, $549 or $732
Maintenance	Take longer time to clean	Take shorter time to clean
Impact on collision	Small	Large

There were 200 balls used for experiments using 5 mm balls, while only 2 – 4 balls were used for the similar experiments with 20 mm balls. As mentioned above, for ZrO_2 balls the price for 5 mm ball in 2011 was $6 each and for 20 mm ball $183 each with the latter being 30 times more expensive. However, many more balls are needed when using the smaller balls. The procurement of 200 balls of the 5 mm ones would cost $1,200, whereas 3 and 4 balls of the 20 mm ones would only cost $549 and $732 respectively. In brief, it is more economical to use 20 mm balls. As a reminder, the nacre used in this study was provided free of charge from Pearl Technology Pty Ltd, as it was an industrial waste. This study has the potential to add an economical value to this industrial waste with minimum expense. Therefore, an expensive processing step should be avoided.

Once the milling process had been completed, the product was a paste. However, the balls were embedded in the paste and needed to be recovered, washed and then dried for re-use. Loss of nacre was minimized by removing the balls from the bowl one-by-one and washing them individually, making sure that they did not carry any milled nacre with them. This was time consuming, each ball taking ~15 seconds, a total of at least 50 minutes for 200 balls. The same process with 2-4 large balls took substantially less time. Unless, this process could be automated in an industrial setting and the yield is directly proportional to the number of balls used, then the use of fewer numbers of balls should be encouraged. It was therefore important to compare the yield derived from using the small versus the large balls and select the most effective and

efficient process. Table 2.6 compares the yields between similar experiments with different numbers and sizes of grinding balls. From this table we can see that 2 x 20 mm balls produced very low yield. Interestingly, addition of one extra 20 mm ball gave a yield that was higher than 200 x 5 mm balls. Further addition of another 20 mm ball did not improve the yield greatly. The conclusion was that 20 mm balls are preferred to maximize the yield as well as the efficiency in terms of reducing the time taken to wash nacre from individual balls.

Table 2.6. Comparison of yield between similar experiments using 5 and 20 mm balls.

Ball Size (mm)	Number of Balls	Speed (rpm)	Duration (min)	Excipient (mL)	Sample Size (g)	Yield
5	200	400	120	15	15	70%
20	2	400	120	15	15	39%
20	3	400	120	15	15	77%
20	4	400	120	15	15	83%

2.6.4. Number of balls

There are strengths and weaknesses in using more balls. For each experiment, all balls were coated with a small amount of nacre paste, which needed to be washed off during the recovery process. Washing the nacre paste off the ball inevitably resulted in some reduction of yield each time a ball was recovered. Thus, using more balls means there will be more nacre paste being lost in the recovery process. However, as shown by Table 2.6 above having more balls does not necessarily lower yield. The yield increased from 39% to 77% then to 83%, when the number of balls used was added from 2 to 3 then to 4. The function of the grinding ball is to crush the nacre with force. Consequently, more balls should give higher yield.

Table 2.7. Zirconium level contamination obtained through ICP MS-AES. The unit is given in ppm. Yield percentage is given in the bracket.

Parameters				Number of 20 mm ball	
Size	Speed	Duration	Volume	3	4
15 g	400 rpm	2 hours	15 mL	**25.1 (77%)**	**1600 (83%)**
15 g	600 rpm	2 hours	15 mL	**2110 (79%)**	**5420 (87%)**

From section 2.6.1 it is concluded that there is a relationship between sample size and the number of balls present. If the sample size is too small then the grinding balls collide and wear each other down instead of crushing the nacre. When this occurs, the milled nacre becomes contaminated with fragments of the balls. Table 2.7 gives the contamination level of zirconium for 2 examples where the use of three rather than four 20 mm balls results in lower Zr contamination. Zirconium levels were obtained using inductively coupled plasma mass spectrometry and atomic emission spectrometry (ICP MS-AES). In the first example, the zirconium level was increased enormously from 25.1 to 1600 ppm just by adding 1 extra grinding ball but the yield was only increased a little from 77 to 83%. In the second example, zirconium level was more than doubled from 2110 to 5420 ppm and the yield but again the yield was only increased a little from 79 to 87%. There was thus substantial increment in zirconium contamination due to 1 additional ball.

The data in Tables 2.6 and 2.7 provide evidence for the advantages and disadvantages of using more balls. Table 2.6 shows that increasing number of balls increases the yield substantially, as in the case from two to three 20 mm balls. It can also decrease the yield, as in the case from three to four 20 mm balls. Table 2.7 shows that having more balls results in the presence of more contamination from degradation of the balls. Hence, unless there was a large difference in yield between two and three 20 mm balls, which was almost doubled (see table 2.6), attention needs to be paid to the drawbacks discussed above when introducing additional grinding ball(s) to the system.

Two further options were therefore considered with the aim of balancing the need for increased yield with decreased contamination. The first was to increase the yield by using 4 balls but with the risk of higher contamination. The second was to use 3 balls to reduce the contamination of the shell nacre, but with a lower yield. In this study, the latter option was chosen since the supply of nacre is abundant relative to the amount required for potential therapeutic purposes.

2.6.5. Speed

Five speed levels were used in this study, namely 200 rpm, 400 rpm, 600 rpm, 800 rpm and 1000 rpm. Initial experiments showed that a low speed of 200 rpm was ineffective in breaking down the nacre despite long duration and varying other parameters. The percentage yield was only 33% when milling was undertaken at 200 rpm for 18 hours using 200 x 5 mm balls, 15 g sample and 15 mL of excipient (Milli Q water). A similarly low yield was obtained when 4 x 20 mm balls were used for 2 hours and maintaining the sample size and excipient volume as above. Milling at higher speeds of 800 or 1000 rpm gave the advantage of shorter durations. For example, using the same parameters as for the experiment at 200 rpm above, the times required for similar yields at 800 and 1000 rpm were 10 and 5 minutes respectively. In spite of this advantage, milling at high speeds causes the temperature to dramatically rise inside the bowl. This high temperature has the potential to damage the material that is being processed. Fortunately, the ball-milling machine has a built-in program to introduce a pause time that can be automated. As suggested by the operating manual, the length of pause time depends on the speed used, and it is expected that higher speeds will heat up the bowl and increase the pressure inside the bowl more quickly, and therefore a longer pause time is required.[42] In addition, it should be noted that the time needed to cool down the system is longer than that needed to heat it up. For example, the temperature after

milling at 800 rpm for 30 minutes reached 72 °C. The milling was performed as 3 cycles of 10 minutes each with 30 minutes pause in between the cycles. Similarly, temperatures after milling at 1000 rpm for 20 minutes reached 93 °C. The milling was performed as 2 cycles of 10 minutes with 30 minutes pause. It is clear that to achieve the same temperature (i.e. 72 °C) for milling at 1000 rpm, a pause time longer than 30 minutes would be required.

Table 2.8. Reference values for speed limit.[42]

Ball diameter (mm)	Speed (rpm) for agate	Speed (rpm) for other materials
<5	1100	1100
5	900	1000
10	750	850
>10	600	700*

Table 2.8 shows the speed limit for ball milling depending on the material and the diameter of the ball. The maximum speed for the machine is 1100 rpm. There are 7 types of material available as described in Table 2.2, namely, agate, stainless steel, sintered corundum, tempered steel, zirconium oxide (ZrO_2), tungsten carbide and silicon nitride. Except agate, the other 6 materials belong to the column for "other materials". As ZrO_2 belongs to this "other materials" group, thus the speed limit for ZrO_2 balls with diameter greater than 10 mm should not exceed 700 rpm (See Table 2.8). In order not to exceed the speed limit, the highest speed limit used for experiments using 20 mm balls was chosen to be 600 rpm. A speed of 200 rpm was removed from consideration due to low yields and 800 or 1000 rpm could not be used for 20 mm balls due to speed restrictions for the device from the manufacturer.[42] Speeds of 400 rpm and 600 rpm were therefore investigated further.

Increasing speeds while maintaining the other parameters results in higher contamination with ZrO_2. Referring back to table 2.7 above, the zirconium level is

higher at 600 rpm than at 400 rpm for both 3 and 4 x 20 mm grinding balls. When three 20 mm grinding balls were used at 600 rpm, the product is more than 80 times more contaminated compared to the product at 400 rpm. Likewise, the product of four 20 mm grinding balls at 600 rpm was at least 3 times more contaminated compared to the product at 400 rpm.

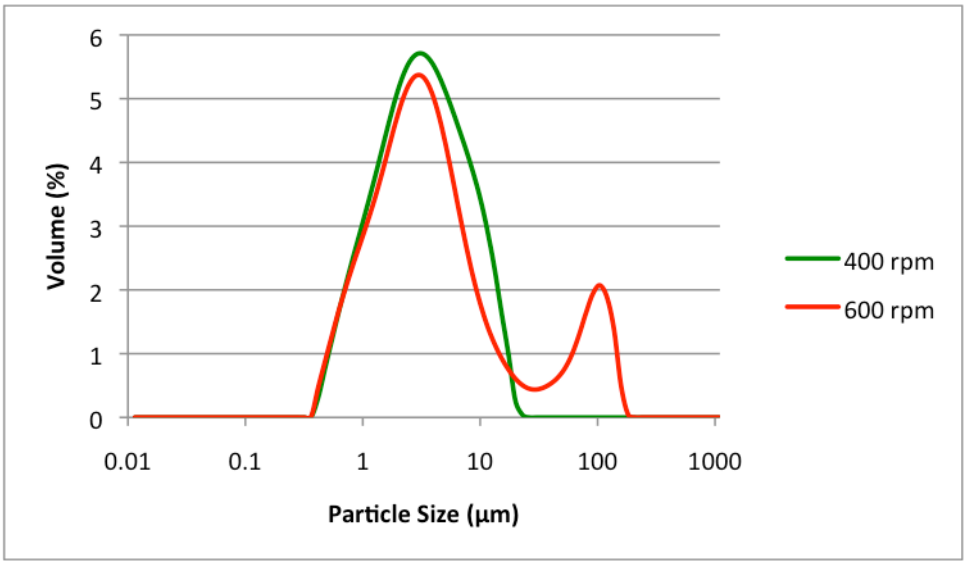

Figure 2.7. Particle size distribution of the milling results at 400 rpm (green) and 600 rpm (red). Other parameters: 15 g, 2 hours, three 20 mm grinding balls and 15 mL Milli Q water as excipient.

One of the criteria for optimal processing is uniform size distribution of the nacre. Fig. 2.7 shows that unimodal particle size distribution was obtained at 400 rpm but not at 600 rpm. The analysis was undertaken using a Mastersizer Hydro S2000 from Malvern Instrument. Details of the analysis are described in the attached publication.[31] It is evident that changing the speed also changes the particle size distribution. The additional peak at 600 rpm curve in Fig. 2.7 is most likely caused by the aggregation of particles.

2.6.6. Duration

Every production cycle must be time-efficient. Certainly, there is a minimum duration for the milling process to be completed using any of the given parameters. At the same time, the duration should be within reasonable limits. For example, it has been mentioned above in section 2.6.5 that after 18 hours of milling at 200 rpm, the yield was only about 33% from 15 g of nacre. Assuming a linear relationship between time and yield, then after 54 hours of milling the yield might reach 99%. Nonetheless, it is neither time- nor cost-efficient to run a milling machine for 54 hours only to generate about 14.85 g of nacre powder. Thus, it was not tested because there is little chance that it could be applied in industry.

The longer the duration, the more heat will be generated. In section 2.6.5, it has been mentioned that milling at 1000 rpm for 20 minutes was performed as 2 cycles of 10 minutes with 30 minutes pause time to cool down the system. The temperature of the ball milling bowl recorded at the end of the second cycle was 93 °C. Unfortunately, when another cycle of 10 minutes was added, the system exploded. This explosion was due to the high temperatures in a closed compartment, which created high pressure. It can damage the equipment as well as potentially the surroundings. The pause time was then doubled to 60 minutes i.e. 3 cycles of 10 minutes with 60 minutes pause time. Unfortunately, the system exploded again. It was only successful when a pause time of 75 minutes was introduced. Pause time is not included in the total duration. Thus, if the experiment involved milling for 30 minutes at 1000 rpm, the experiment was actually performed as 3 cycles of 10 minutes with 75 minutes pause time in between the cycles. Thus, the total amount of time needed was 3 hours. Without pause time it is not possible to mill nacre in a short time. The only speed that did not require a pause time was 200 rpm. However, as mentioned above, to mill 15 g of nacre at 200 rpm will require at least

36 hours of constant milling. Finding sufficient pause time so as to avoid explosions was a trial and error process.

One way to prevent an explosion due to high temperatures is to use a special grinding bowl that is attached to a pressure gauge. In brief, the pressure gauge measures and displays the pressure within the bowl. When the pressure is reaching the pressure limit of the bowl (i.e. 400 kPa), the milling process will be paused. Thus, it prevents excessive pressure, which leads to explosion (Personal Communication with Ronald Cheong from John Morris Scientific). However, such a device is expensive, quoted at $15,000.00 (Fritsch GmBH, Western Australia) and was not possible for the current study. Another possibility is to use a ventilation device to release the pressure during the milling process.[13] However, this was not considered further because such a device would allow leakage of both small particles of nacre generated as milling progressed as well as of the excipient (Milli Q water) used during the process.

An alternative way of controlling temperature and therefore avoiding high pressures is to undertake ball milling at low temperatures. This has been accomplished in a patent application by Drai and Guillot[13] in which temperatures were kept below 40 °C. However, the process was complicated involving freezing the grinding bowl, the nacre and/or the grinding balls to a temperature as low as -30 °C for a period of time ranging from 1 minute to 48 hours and was therefore considered impractical for the purpose of designing a methodology that might be suitable for scale-up and manufacture for cosmetic of therapeutic use. Accordingly the pause time approach was considered more practical, as well as being more economical for potential scale up of any processing for down stream applications.

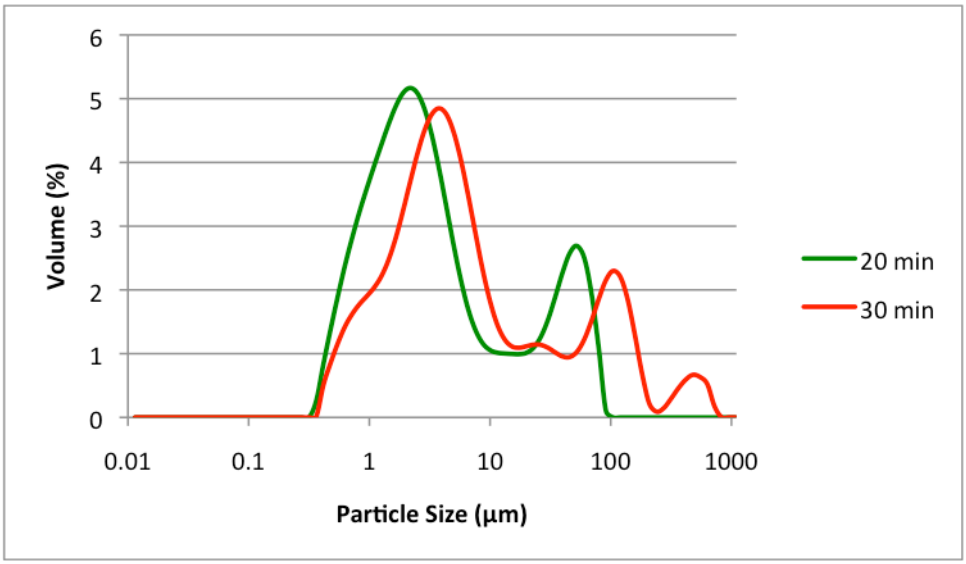

Figure 2.8. Particle size distribution changes with different duration. Parameters: 15 g, 200 of 5 mm balls, 15 mL Milli Q water and 1000 rpm.

Changing the duration of milling might change the particle size distribution. Fig. 2.8 shows the particle size distribution for two similar experiments with the duration being varied from 20 minutes to 30 minutes. Compared to 20 minutes, at 30 minutes, the first two peaks are shifted to larger particles and another larger peak appeared. Nacre tablets have a tendency to aggregate with each other thus generating larger pieces.[46,47] However, increasing the duration might also result in higher contamination of the product with ZrO_2 given that as the size of nacre particles become smaller as the grinding proceeds, there will be more collisions between the grinding balls.

2.7. Preface to the publication

The publication that follows describes the ball-milling process that gave the best preparation based on the aforementioned criteria, namely, high percentage of yield, minimum contamination and uniform size distribution. Yield was straightforward to assess by weighing the dry milled nacre powder and comparing to the original sample size. The presence of contamination was assessed using two techniques, namely, elemental analysis with EDS and differential scanning calorimetry (DSC). XRD

provided a semi-quantitative analysis of the amount of contamination, while ICP MS-AES provided an accurate concentration of the contamination. Particle size distribution was obtained through Mastersizer Hydro 2000s, Malvern Instrument.

In addition, other analytical techniques were used to analyze and further characterize the ball milling products. Scanning Electron Microscopy (SEM) and Transmission Electron Microscopy (TEM) were used to give 3D and 2D images respectively. Additional analytical techniques that were used in conjunction with microscopy include electron diffraction and high resolution TEM. The discussion in the publication emphasizes that nacre is made of aragonite tablets and the end-product of the milled nacre was still aragonite. This is important because ball milling generates heat which can transform aragonite to calcite.[48] As a result, the author questions whether the ball milling process has facilitated the transformation of aragonite tablets to calcite. This question was addressed through XRD, SEM, TEM and DSC as described in the publication. The data from all experiments confirmed that the heat generated from the ball-milling process did not transform aragonite tablets to calcite.

2.8. Publication

See Appendix 1

2.9. Subsequent Studies

This ball milling study provided a thorough investigation of the different parameters required for the preparation of high yields of consistently sized nacre preparations with low levels of contamination. The principles used in this study to adjust the parameters could also be applied to other studies utilizing the ball milling process, such as production of $Cu_2(Zn,Fe)SnS_4$ powders for thin film solar cell[49], preparation of

nanostructure cathode materials[50] and production of graphene nanosheets.[51] The current study provides insight into the potential production of standardized nacre preparations for commercial production and for other research, including therapeutic testing.

In the ensuing chapters, the effects of the least and most contaminated samples generated by the ball milling process are investigated using *in vitro* models of wound repair.. There are two major areas that will be investigated, namely toxicity and efficacy of milled nacre. Chapter 3 will discuss further investigation and experimentation of toxicity of nacre on skin cells. The highly contaminated sample will be assessed as to whether it is more noxious to the skin cells compared to the sample with low contamination. Additionally, Chapter 4 will test these nacre preparations for their efficacy using *in vitro* models of wound healing. The potential of the milled nacre to enhance cell migration in a scratch assay will be explored to mimic potential effects of nacre on the re-epithelialisation phase of wound healing. Additionally, the effect of milled nacre on collagen secretion by fibroblasts will also be analysed to assess potential effects on the remodelling/granulation tissue deposition phases of wound repair.

There will be a number of common issues that will be discussed in Chapter 3 and 4. First, there has been much attention given in this study to make sure that aragonite tablets were obtained, with little or no transformation to calcite. Therefore, calcite will be used as one of the controls. Any observed effects from the milled nacre will be assessed whether they are specific to aragonite or whether they could be generated by other polymorphs of calcium carbonate, i.e. calcite. If calcite does not produce similar effects as the nacre then this study will be the first scientific evidence for the benefit of the aragonite structure on skin cells. Second, as has been previously

mentioned, the water soluble matrix of nacre could promote wound healing.[3] Therefore, the organic component of nacre will also be used to determine whether both the inorganic and organic components of nacre are needed to produce an effect or whether either one of them is sufficient. The extraction of the organic component will be discussed later in the Materials and Methods section in Chapter 3. In conclusion, this will be the first study using fully characterized nacre extract prepared using an optimized methodology to assess potential effects of nacre on skin cells in vitro.

2.10. References

1 Haws, M. in *Publication No. 127* (ed Center for Tropical and Subtropical Aquaculture) (University of Hawaii at Hilo, Hawaii, 2002).

2 Li, Y.-C., Chen, C.-R. & Young, T.-H. Pearl extract enhances the migratory ability of fibroblasts in a wound healing model. *Pharmaceutical Biology* **51**, 289-297, doi:10.3109/13880209.2012.721130 (2013).

3 Lee, K. *et al.* Nacre-driven water-soluble factors promote wound healing of the deep burn porcine skin by recovering angiogenesis and fibroblast function. *Mol Biol Rep* **39**, 3211-3218, doi:10.1007/s11033-011-1088-4 (2012).

4 Sun, J. & Bhushan, B. Hierarchical structure and mechanical properties of nacre: a review. *RSC Advances* **2**, 7617-7632, doi:10.1039/c2ra20218b (2012).

5 Boulos, R. A. *et al.* Unzipping oyster shell. *RSC Advances* **3**, 3284-3290, doi:10.1039/c2ra21763e (2013).

6 Sudo, S. *et al.* Structures of mollusc shell framework proteins. *Nature* **387**, 563 - 564 (1997).

7 Farre, B. *et al.* Shell layers of the black-lip pearl oyster Pinctada margaritifera: Matching microstructure and composition. *Comparative Biochemistry and Physiology Part B: Biochemistry and Molecular Biology* **159**, 131-139, doi:http://dx.doi.org/10.1016/j.cbpb.2011.03.001 (2011).

8 Bédouet, L. *et al.* Proteomics Analysis of the Nacre Soluble and Insoluble Proteins from the Oyster Pinctada margaritifera. *Mar Biotechnol* **9**, 638-649, doi:10.1007/s10126-007-9017-1 (2007).

9 Lamghari, M. *et al.* Stimulation of bone marrow cells and bone formation by nacre: in vivo and in vitro studies. *Bone* **25**, 91S-94S (1999).

10 Lopez, E., Faou, A. L., Borzeix, S. & Berland, S. Stimulation of rat cutaneous fibroblasts and their synthetic activity by implants of powdered nacre (mother of pearl). *Tissue and Cell* **32**, 95-101, doi:10.1054/tice.1999.0091 (2000).

11 Rousseau, M. *et al.* Restoration of stratum corneum with nacre lipids. *Comparative Biochemistry and Physiology Part B: Biochemistry and Molecular Biology* **145**, 1-9, doi:10.1016/j.cbpb.2006.06.012 (2006).

12 Chen, H. S., Chang, J. H. & Wu, J. S. B. Calcium Bioavailability of Nanonized Pearl Powder for Adults. *Journal of Food Science* **73**, H246-H251, doi:10.1111/j.1750-3841.2008.00965.x (2008).

13 Drai, J. & Guillot, J. Process for the preparation of nacre mechano-structured by mechanosynthesis, mechano-structured nacre thus obtained and uses thereof. United States patent (2011).

14 Nudelman, F. Forming nacreous layer of the shells of the bivalves Atrina rigida and Pinctada margaritifera: an environmental- and cryo-scanning electron microscopy study. *J Struct Biol* **162**, 290 - 300 (2008).

15 Vogt, A. *et al.* 40[thinsp]nm, but not 750 or 1,500[thinsp]nm, Nanoparticles Enter Epidermal CD1a+ Cells after Transcutaneous Application on Human Skin. *J Invest Dermatol* **126**, 1316-1322 (2006).

16 Bos, J. D. & Meinardi, M. M. H. M. The 500 Dalton rule for the skin penetration of chemical compounds and drugs. *Experimental Dermatology* **9**, 165-169, doi:10.1034/j.1600-0625.2000.009003165.x (2000).

17 Schneider, M., Stracke, F., Hansen, S. & Schaefer, U. F. Nanoparticles and their interactions with the dermal barrier. *Dermato-Endocrinology* **1**, 197-296, doi:10.4161/derm.1.4.9501 (2009).

18 Otberg, N. *et al.* Variations of Hair Follicle Size and Distribution in Different Body Sites. *J Investig Dermatol* **122**, 14-19 (2004).

19 Pan, K. & Wang, W.-X. Trace metal contamination in estuarine and coastal environments in China. *Science of The Total Environment* **421,Äì422**, 3-16, doi:http://dx.doi.org/10.1016/j.scitotenv.2011.03.013 (2012).
20 Dong, X. *et al.* A novel approach for soil contamination assessment from heavy metal pollution: A linkage between discharge and adsorption. *Journal of Hazardous Materials* **175**, 1022-1030, doi:http://dx.doi.org/10.1016/j.jhazmat.2009.10.112 (2010).
21 Lee, B.-K. & Park, G.-H. Characteristics of heavy metals in airborne particulate matter on misty and clear days. *Journal of Hazardous Materials* **184**, 406-416, doi:http://dx.doi.org/10.1016/j.jhazmat.2010.08.050 (2010).
22 Riba, I., Blasco, J., Jiménez-Tenorio, N. & DelValls, T. Á. Heavy metal bioavailability and effects: I. Bioaccumulation caused by mining activities in the Gulf of Cádiz (SW, Spain). *Chemosphere* **58**, 659-669, doi:http://dx.doi.org/10.1016/j.chemosphere.2004.02.015 (2005).
23 Mishra, S. *et al.* Trace metals and organometals in selected marine species and preliminary risk assessment to human beings in Thane Creek area, Mumbai. *Chemosphere* **69**, 972-978, doi:http://dx.doi.org/10.1016/j.chemosphere.2007.05.013 (2007).
24 Freije, A. M. Heavy metal, trace element and petroleum hydrocarbon pollution in the Arabian Gulf: Review. *Journal of the Association of Arab Universities for Basic & Applied Sciences* **17**, 90-100, doi:10.1016/j.jaubas.2014.02.001 (2015).
25 Bryan, G. W., Waldichuk, M., Pentreath, R. J. & Darracott, A. *Bioaccumulation of Marine Pollutants [and Discussion]*. Vol. 286 (1979).
26 Huanxin, W., Lejun, Z. & Presley, B. J. Bioaccumulation of heavy metals in oyster (Crassostrea virginica) tissue and shell. *Environmental Geology* **39**, 1216-1226, doi:10.1007/s002540000110 (2000).
27 Gregory, P. Calcium Salts. *Prescriber's Letter* **Document 1603013** (2000).
28 Pourang, N., Richardson, C. A., Chenery, S. R. N. & Nasrollahzedeh, H. Assessment of trace elements in the shell layers and soft tissues of the pearl oyster Pinctada radiata using multivariate analyses: a potential proxy for temporal and spatial variations of trace elements. *Environ Monit Assess* **186**, 2465-2485, doi:10.1007/s10661-013-3553-0 (2014).
29 Thompson, E. L. *et al.* A proteomic analysis of the effects of metal contamination on Sydney Rock Oyster (Saccostrea glomerata) haemolymph. *Aquatic Toxicology* **103**, 241-249, doi:http://dx.doi.org/10.1016/j.aquatox.2011.03.004 (2011).
30 Mol, S. Levels of selected trace metals in canned tuna fish produced in Turkey. *Journal of Food Composition and Analysis* **24**, 66-69, doi:http://dx.doi.org/10.1016/j.jfca.2010.04.009 (2011).
31 Tjandra, E. S., Boulos, R. A., Duncan, P. C. & Raston, C. L. Unfastening pearl nacre nanostructures under shear. *CrystEngComm* **15**, 6896-6900, doi:10.1039/c3ce40760h (2013).
32 Ricketts, H. T. Observations on the Virus and Means of Transmission of Rocky Mountain Spotted Fever. *The Journal of Infectious Diseases* **4**, 141-153, doi:10.2307/30101875 (1907).
33 Krueger, A. P. New Type of Ball Mill for Maceration of Tissues and Bacteria under Aseptic Conditions. *The Journal of Infectious Diseases* **53**, 185-186, doi:10.2307/30088514 (1933).
34 Furnstal, A. H. A Simple Rotating Ball Mill. *Industrial & Engineering Chemistry Analytical Edition* **7**, 342-343, doi:10.1021/ac50097a021 (1935).
35 Quill, L. L. An inexpensive ball mill. *Industrial & Engineering Chemistry Analytical Edition* **8**, 27-27, doi:10.1021/ac50099a010 (1936).

36 Verderevskii, V. A. & Merzlyakov, V. D. The rolling of sections on a planetary mill. *Metallurgist* **8**, 187-190, doi:10.1007/bf00734306 (1964).
37 Monder, C. & Ramstad, P. E. The effect of ball-milling upon certain properties of proteins. *Archives of Biochemistry and Biophysics* **46**, 376-384, doi:http://dx.doi.org/10.1016/0003-9861(53)90209-4 (1953).
38 D'Appolonia, B. L. & Gilles, K. A. Protein Alteration in Flour Dmaged by Ball-Milling and Roller-Milling. *Cereal Chemistry* **44**, 324-332 (1967).
39 Fritsch. *Planetary Micro Mill PULVERISETTE 7 premium line*, <http://www.fritsch-milling.com/products/milling/planetary-mills/pulverisette-7-premium-line/accessories/> (2014).
40 Roseville Rock Rollers Inc. *Mohs Hardness Scale*, <http://www.rockrollers.com/features/hardness.html> (2016).
41 John Morris Scientific. *Mortar, sintered corundum*, <http://www.johnmorris.com.au/Mortar-sintered-corundum.aspx?pd=9671> (2016).
42 Fritsch GmbH. *Operating instructions Planetary Micro Mill PULVERISETTE 7 premium line*. (Fritsch GmbH, 2012).
43 Merriam-Webster. *Mohs' scale*, <http://www.merriam-webster.com/dictionary/Mohs'%20scale> (2016).
44 Larson Jewellers. *Tungsten, Cobalt, and More on Mohs Scale of Mineral Hardness*, <https://www.larsonjewelers.com/Tungsten-Cobalt-and-More-on-Mohs-Scale-of-Mineral-Hardness.aspx> (2016).
45 Finnemore, A. *et al.* Biomimetic layer-by-layer assembly of artificial nacre. *Nat Commun* **3**, 966, doi:http://www.nature.com/ncomms/journal/v3/n7/suppinfo/ncomms1970_S1.html (2012).
46 Checa, A. G. *et al.* Crystallographic control on the substructure of nacre tablets. *Journal of Structural Biology* **183**, 368-376, doi:http://dx.doi.org/10.1016/j.jsb.2013.07.014 (2013).
47 Zuykov, M. *et al.* In vitro growth of calcium carbonate crystals on bivalve shells: Application of two methods of synthesis. *Materials Science and Engineering: C* **32**, 1158-1163, doi:http://dx.doi.org/10.1016/j.msec.2012.03.002 (2012).
48 Yoshioka, S. & Kitano, Y. Transformation of aragonite to calcite through heating. *Geochemical Journal* **19**, 245-249 (1985).
49 Azanza Ricardo, C. L., Su'ait, M. S., Müller, M. & Scardi, P. Production of Cu2(Zn,Fe)SnS4 powders for thin film solar cell by high energy ball milling. *Journal of Power Sources* **230**, 70-75, doi:http://dx.doi.org/10.1016/j.jpowsour.2012.12.045 (2013).
50 Kim, S.-B., Kim, S.-J., Kim, C.-H., Kim, W.-S. & Park, K.-W. Nanostructure cathode materials prepared by high-energy ball milling method. *Materials Letters* **65**, 3313-3316, doi:http://dx.doi.org/10.1016/j.matlet.2011.07.023 (2011).
51 Jeon, I.-Y. *et al.* Edge-carboxylated graphene nanosheets via ball milling. *Proceedings of the National Academy of Sciences of the United States of America* **109**, 5588-5593, doi:10.1073/pnas.1116897109 (2012).

Chapter 3

Chapter 3: Toxicity of Ball-Milled Pearl Nacre on Skin Cells

3.1. Introduction

As discussed in Chapter 1, nacre has been used for cosmetics since ancient times.[1,2] Therefore, it is presumed that there should be no adverse effects of nacre on the skin. Indeed, Rousseau et al. have tested nacre lipids on artificially dehydrated skin explants.[3] In other organs, it has been shown that nacre is able to initiate bone mineralization in the presence of osteoblasts *in vitro*[4] and induce osteogenesis in sheep vertebrae[5,6] without any observed adverse effects.[7] In spite of this evidence for bones, there is limited scientific data to support the safe use of nacre on skin.[8]

In recent years, there has been a growing interest from the cosmetic industry to use nacre as a key ingredient.[9] However, as discussed in Chapter 2, there are many modern human activities that could introduce heavy metals, pesticides, detergents and other waste into marine environments[10] which could result in uptake by oysters and possible contamination of their nacre. As expected, it has also been shown that the type and concentration of pollutant varies in different marine environments.[11] For example, Lerebours et al. investigated the presence of pollutants in 165 flatfish dab (*Limanda limanda*) from six sites in the North Sea and English Channel.[12] The investigation showed that the liver of fish sampled from North Dogger was highly intoxicated by Cd (406 $\pm$ 122 µg/kg liver tissue), whereas the liver of fish sampled from Rye Bay contained high amounts of organic chemicals from the polychlorinated biphenyl (PCB) family.[12] As mentioned in Chapter 2, oysters obtain inorganic elements for building their shells from the surrounding environment and therefore might be susceptible to incorporation of heavy metals within the nacre. However two studies[13,14], as well as the results presented in Chapter 2, have shown that heavy metals appear not to accumulate

in oyster shells suggesting that heavy metals existing in the environment will not be incorporated into the nacre, and are therefore unlikely to be a source of contamination. Indeed, a number of studies have shown that heavy metals are accumulated in the soft tissue and not the shell[15-18] and therefore would not impact on the content of the nacre.

It was established that ball-milling results in substantial contamination of the nacre by Zr and Cd which are constituents of the balls themselves.[19] It therefore appears that contamination from processing rather than environmental pollution is more likely to be the major contributor to the presence of heavy metals in processed nacre. Thus, systematic studies are required to examine the safety of nacre processed by ball milling.

The studies on bone describe above used nacre from *Pinctada maxima* [4-6] while the current work used nacre from *Pinctada margaritifera*. It is unknown whether nacre from the two species has the same chemical composition. However, a phylogenetic study using Bayesian Inference (BI) analysis of partial sequence data of the mitochondrial *cox1* gene has shown that these two species are closely related.[20] It is therefore likely that the chemical composition of the nacre of the two species is similar and thus that nacre preparations from both *P. maxima* and *P. margaritifera* could be used interchangeably.

Herein the toxicity of nacre on skin cells prepared from *P. margaritifera* has been investigated using two different samples of nacre prepared as described in Chapter 2. Sample 8 was selected because it is the least contaminated and sample 11 because it is the most contaminated. By choosing samples that were the least contaminated versus the most and including a calcium carbonate control in calcite form, the aim was to

determine whether the contamination with Zr and Cd from the ball milling system influenced toxicity and was therefore an important consideration in nacre preparation.

The presence of heavy metals is an important issue for cosmetics as they can cause local adverse effects on skin including irritation, sensitization or photoreactions.[21] Unlike Zr, Cd is a common heavy metal found in cosmetics.[22,23] There are no strict regulations that govern the level of contamination that is acceptable in cosmetic products globally. Nevertheless in Nigeria the presence of Cd in any amount in cosmetics is prohibited.[24] Additionally, the Food and Agricultural Organization made a joint statement with the World Health Organization that there should be no Cd in any food additives but allows a provisional tolerable weekly intake of 7 μg/kg body weight, i.e. 7 ppb.[25] However, cosmetic industries usually use the US Food and Drug Administration permissible lead (Pb) concentration for candy (0.1 μg/g ≈ 0.1ppm) as the acceptable limit for Cd in lipsticks or other cosmetics.[26] However, it has been shown that many cosmetics in the market have Cd levels beyond this limit.[22,24,27] The amount of Cd in Sample 11 according to ICP MS-AES analysis is 111 ppm, which is far beyond the acceptable limit. The amount of Cd in Sample 8 was recorded as less than 0.1 ppm. According to Nordberg, long-term exposure to Cd is detrimental to the renal, pulmonary, hepatic and reproductive systems.[28] McMurray and Tainer reported in 2003 that Cd is possibly responsible for increasing the incidence of certain forms of cancer by direct inhibition of DNA mismatch repair.[29] Cd also has been reported to cause kidney damage and bone degradation by affecting calcium metabolism.[30] Therefore, it is crucial to assess the presence of heavy metal in nacre samples before using it for aesthetic or therapeutic purposes. Whilst sample 11 is unlikely to be suitable for human use, it is interesting to compare the effects of this most contaminated sample with the least in terms of its effects on skin cells.

It is important to test the cytotoxicity of a compound on both keratinocytes and fibroblasts, in order to assess its biocompatibility with skin. As has been mentioned in Chapter 1, keratinocytes and fibroblasts are the predominant cells of the epidermis and dermis respectively. Any compound applied to skin comes into contact with the epidermal layer and therefore keratinocytes first. If it can permeate the epidermis then it is likely to diffuse within the dermis and come into contact with the fibroblast cells. When the skin is ulcerated the compound comes into contact directly with the dermal layer and therefore, for potential wound healing use, the impact of the compounds on fibroblasts is even more likely to be important.[31] Whilst testing with both cell types is important, evidence suggests toxicity profiles of compounds are similar across the two cell types. For example, Nadim et al. found a similar cytotoxicity pattern between immortalized human keratinocytes (HaCaT) and in v-myc transfected human fibroblast cells MSU 1.1[32] for caffeic acid (CA), epigallocatechin-3-gallate (EGCG) and their glucosylated forms, alpha-*O*-D-glucopyranosyl caffeic acid (Glc-CA) and alpha-*O*-D-glucopyranosyl epigallocatechin gallate (Glc-EGCG).[33] Further, in a study of wound healing properties of jojoba (*Simmondsia chinensis*) liquid wax, it was found that the wax has similar low toxicity on both human fibroblasts[34] and HaCaT cells.[35]

However in other studies, cytotoxicity assays of the same compound using keratinocytes and fibroblasts gave conflicting results. For example, Chen et al. tested the cytotoxic effects of three denture adhesives, namely, Polident® cream, Protefix® cream and Protefix® powder on three cell lines, namely primary human oral keratincoytes (HOKs), primary human oral fibroblasts (HOFs) and permanent mouse fibroblasts cell lines from the China Centre for Type Culture Collection (L929).[31] Their results showed that the three adhesives were cytotoxic for HOKs and HOFs but not for L929.[31] Similarly, evaluation of the photo-toxic effects of chlorpromazine showed that

human epidermal keratinocytes were sensitive to phototoxicity while human fibroblasts were insensitive.[36] Likewise, nacre might not be toxic to epidermal skin cells (keratinocytes), which are represented by HaCaT cells. However, it may still be toxic for the lower dermal layer, represented by NIH/3T3 cells (fibroblasts) and *vice versa*. Therefore, in the work reported here, immortalized human keratinocytes (HaCaT) and immortalized mouse fibroblasts (NIH/3T3) were used to investigate potential toxicity of the two nacre preparations. Table 3.1 provides a summary of the two cell lines. These two immortalized cell lines were used as they are readily available, and convenient compared to primary cell lines that would have to be obtained from tissue biopsies.

Table 3.1. Cell lines' profile summary.

Cell Line	Mortality	Species	Cell Type	Skin Layer
HaCaT	Immortalized	Mouse	Keratinocyte	Epidermis
NIH/3T3	Immortalized	Human	Fibroblast	Dermis

HaCaT and NIH/3T3 are two common cell lines that are used for wound healing and cytotoxicity studies for skin products. For example, Wiegand et al. used HaCaT cells to assess the effects of superabsorbent polymer (SAP) containing wound dressings in the treatment of non-healing wounds.[37] HaCaT cells were also used by Boonkaew et al. to examine the cytotoxicity of wound dressings containing silver particles, and HaCat cells are widely accepted to be a good model for epidermal cells despite the potential for some differences to primary keratinocytes.[38] Sarkar et al. used both 3T3 fibroblasts and HaCaT keratinocytes to evaluate the biocompatibility of a chitosan-collagen scaffold with nano/microfibrous architecture for skin tissue engineering.[39] Similarly, Radu et al. tested the biocompatibility of poly (3-hydroxybutyrate-co-3-hydroxyvalerate) (PHBV) nanofibers for skin tissue engineering applications using HaCaT cells.[40] Likewise, toxicity evaluation of yttria-alumina-silica spray-dried microspheres was performed *in vitro* on HaCaT cells.[41] In a publication not related with

this thesis, this author has also tested toxicity of a novel antibiotic compound using both HaCaT and NIH/3T3 cells.[42] The toxicity of many other compounds such as zinc oxide[43,44], titanium dioxide[45], modified graphene oxide[46], antituberculosis drugs (thiazolyhydrazone derivatives)[47] and antifungal agents (2-hydroxyphenacyl azole and 2-hydroxyphenacyl azolium)[48] have also been tested on NIH/3T3 fibroblasts.

As described in the Introduction to Chapter 2 and the associated paper, three different processes can be used to prepare the nacre, i.e. grinding, ball milling and ionic liquid processing. Ground nacre contains both inorganic and organic components. Ball-milled nacre also contains both components, but as described in Chapter 2, some of the organic components might have been lost during the process. Finally, ionic liquid processed nacre only contains the inorganic component.[49] Inclusion of pure nacre prepared using ionic liquid allowed investigation regarding which component of nacre is responsible for any observed effects. If the samples prepared in Chapter 2, i.e. samples 8 and 11, produced similar results compared to ionic liquid processed nacre, then it might be concluded that any effects were due to the inorganic component of nacre rather than any organic components in the matrix.

There are three questions that were investigated in this Chapter:

1. Is nacre toxic to skin cells?
2. Does heavy metal contamination from the ball milling decrease cell viability?
3. Do different nacre preparations result in different viability?

The first question will be addressed by comparing the results between the cells treated with nacre prepared in different ways and the two controls. The first control was a negative control where there was no treatment at all. The second control was a positive

control where the cells were treated with $CaCO_3$ or its corresponding conditioned media. Further, the second question will be addressed by comparing the results of Sample 8 and Sample 11. The last question will be addressed by comparing the results from nacre prepared in the three different ways (grinding, ball milling and ionic liquid extraction).

3.2. Materials and Methods

3.2.1. Materials

3.2.1.1. Ground Nacre

Nacre from *P. margaritifera* shell was ground using a mortar and pestle. The dimension of the ground nacre is approximately less than 5 mm. The Ground nacre is referred to hereafter as **Nacre G**.

3.2.1.2. Milled Nacre

Milled nacre was obtained as described in Chapter 2. As described in the publication[19], sample 8 has the lowest contamination of Zr (referred to hereafter as **Nacre M8**) and sample 11 has the highest contamination (referred to hereafter as **Nacre M11**). These two samples were used in the studies in this chapter.

3.2.1.3. Ionic Liquid Processed Nacre

Ionic liquid processed nacre uses *n*-butyl-3-methylimidazolium hexafluorophosphate [BMIM][PF_6], to extract nacre tablets.[49] The ionic liquid in the extraction process results in the production of pure aragonite nacre without organic materials and therefore allowed testing of the effect of the inorganic component alone. Boulos et al. described this nacre preparation in their paper to obtain exclusively the inorganic component of nacre, i.e. the aragonite tablets.[49] This nacre is referred hereafter as **Nacre I**.

3.2.1.4. Commercial $CaCO_3$

As a control, this study used commercially available $CaCO_3$ from Sigma Aldrich (Catalogue number 239216). It is referred hereafter as **$CaCO_3$**.

3.2.1.5. Cell lines

Two cell lines were used for the *in vitro* studies in this chapter, namely HaCaT and NIH/3T3 lines. HaCaT is an immortalized human keratinocytes cell line[50,51], while NIH/3T3 is an immortalized mouse fibroblast cell line.[52] These two cell lines were maintained in culture media as follows: Dulbecco's Modified Eagle's Medium/F-12+GlutaMAX from Gibco (Mulgrave, Vic, Australia) with 10% (v/v) Foetal Bovine Serum (FBS, JRH Biosciences), 2mM Penicillin (Gibco) and 2mM Streptomycin (Gibco). This mix is referred hereafter as **media**. The cell lines were split at 80% confluency and housed in an incubator at 37 °C with 5% CO_2.

3.2.1.6. Conditioned Media

Conditioned media was prepared by mixing **media** with one of the nacre preparations or the **$CaCO_3$** control and left to stand overnight. This was expected to solubilise the organic component of the nacre so that the effects of the organic components could be assessed in isolation. The protein amount was quantified in section 3.2.2.1.

Either 100 mg of nacre preparations or 100 mg of the **$CaCO_3$** control was dispersed in 1 mL of **media**. The dispersion was shaken gently to avoid the formation of bubbles at room temperature. After 3 hours shaking, the dispersion was kept overnight at 4 °C. It was then centrifuged gently at 100 rpm for 3 minutes. The supernatant was transferred into a new sterile tube and later sterilized through 0.2 μm pore size membrane filtration.

3.2.2. Methods

Table 3.2 summarizes the workflow of the toxicity testing. The first assay was an MTS Viability Assay that was performed using HaCaT cells. Two different controls were used for all experiments. The first control is a negative control, which involved cells with no added nacre. The second control is a false positive control using $CaCO_3$ from Sigma Aldrich (see section 3.2.1.4). It is in calcite form, the stable polymorph.[53] If the cells treated with milled nacre produce similar results compared to the false positive control, any effects cannot be attributed specifically to aragonite or organic components of the nacre.

Table 3.2. Toxicity tests. The cells marked with "+" sign indicates that the treatment was added for that particular assay.

In Vitro Assays	Outcome Measure	Treatments				
HaCaT Keratinocytes		**Nacre M8**	**Nacre M11**	**Nacre G**	**Nacre I**	**$CaCO_3$**
MTS Viability Assay	Viability	+	+	N/A	+	+
Dose/Response	Viability	+	N/A	N/A	N/A	+
Live/Dead Assay (P)	Live Cell Count	+	N/A	+	N/A	+
Live/Dead Assay (C)	Live Cell Count	+	N/A	+	N/A	+
ROS Assay (P)	Stress Level	+	N/A	+	N/A	+
ROS Assay (C)	Stress Level	+	N/A	+	N/A	+
NIH/3T3 Fibroblasts						
Dose/Response	Viability	+	N/A	N/A	N/A	+
Live/Dead Assay (P)	Live Cell Count	+	N/A	+	N/A	+
Live/Dead Assay (C)	Live Cell Count	+	N/A	+	N/A	+
ROS Assay (P)	Stress Level	+	N/A	+	N/A	+
ROS Assay (C)	Stress Level	+	N/A	+	N/A	+

The second assay was a dose-response assay performed with varying concentrations to identify whether there was a level at which nacre might be toxic to HaCaT and NIH/3T3 cells. Finally, live/dead and reactive oxygen species assays were conducted. In these last two experiments, there were two modifications introduced. First, Nacre G was used. Second, the experiments were performed using conditioned

media of the corresponding nacre or control particle in addition to the nacre samples. Addition of Nacre G and conditioned media in these experiments allowed for assessment of whether any effects observed were due to the inorganic component alone, organic component alone or both. Only Nacre G contains both inorganic and the complete matrix of organic components.

3.2.2.1. Quantification of Protein Amount in Conditioned Media

In order to determine whether the conditioned media prepared in section 3.2.1.6 has additional organic matter derived from the samples, protein quantification was carried out using Pierce™ BCA Protein Assay Kit as per manufacturer's instructions (Life Technologies, catalog number: 23225). **Media** was used as diluent for this quantification assay. Thus, the concentration of proteins in the conditioned media in the results section (see section 3.3.2 below) is the additional proteins on top of the proteins that originated from the addition of 10% (v/v) of FBS above. Conditioned media of Nacre M8, Nacre G and $CaCO_3$ were prepared for the live/dead and ROS assays.

3.2.2.2. MTS Viability Assay: Pilot Study

The study was performed using CellTiter 96® AQ_{ueous} One Solution Cell Proliferation Assay from Promega. It employs a novel tetrazolium compound [3-(4,5-dimethylthiazol-2-yl)-5-(3-carboxymethoxyphenyl)-2-(4-sulfophenyl)-2H-tetrazolium, inner salt; MTS] and an electron-coupling reagent (phenazine ethosulfate; PES). The assay was prepared as follows:

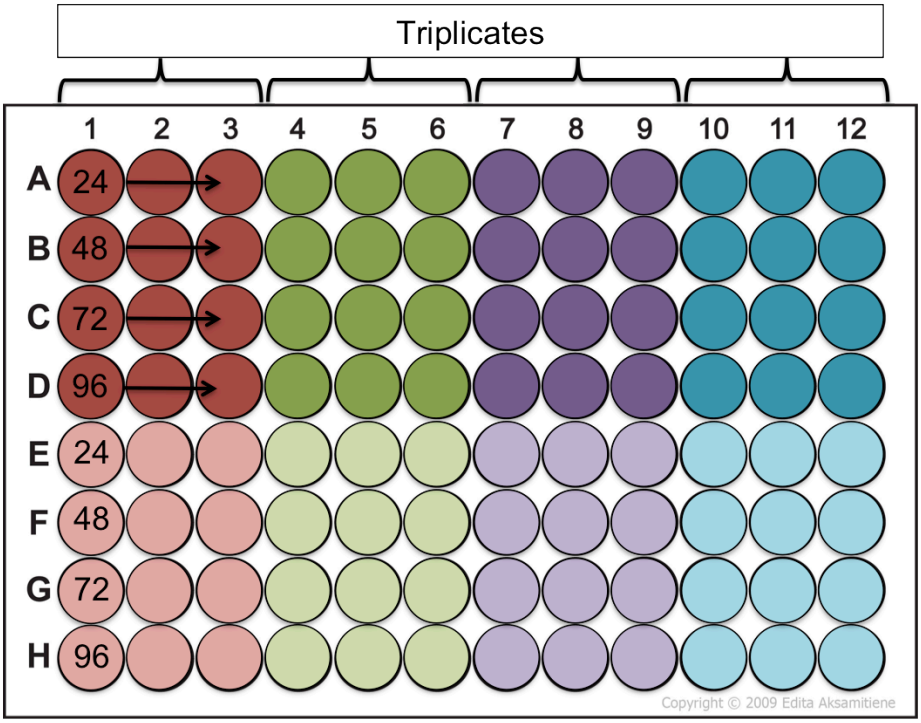

Figure 3.1. Arrangement of MTS Viability Assay. Each colour represents control or different treatments. The experiments for each time point were performed in different line. The arrangement of transfer plate for absorbance reading should follow the original plate. Up to 8 treatment and/or controls can be set up.

1.5×10^3 HaCaT cells were seeded for each well on 96 well plates in 50 µL of media. Cells were incubated for 2h at 37 °C with 5% CO_2 to allow cell attachment to the plate surface. Four treatments were used in this study: **Nacre M8**, **Nacre M11**, **Nacre I and $CaCO_3$**. For each type of treatment 0.2 mg of particles was dispersed in 100 µL of media. Then 50 µL of the dispersion was added to the cells giving a final concentration of the treatment of 0.1 mg/mL. Time 0 started after the addition of treatment. For each treatment and the control, the experiment was done in triplicate for four (4) time points: 24, 48, 72 and 96 hours. The plate is as depicted in Fig. 3.2. The plates were then incubated at 37 °C with 5% CO_2 overnight. At each time point, 60 µL MTS solution was added to each well. The plates were then incubated for 3 hours at 37 °C with 5% CO_2. Then, 60 µL from each well was transferred to a new plate for absorbance reading at 490 nm using an EnSpire 2300 Multimode Plate Reader. The relative cell viability is proportional to the absorbance and was calculated using Equation 1:

Equation 1:

$$\text{Relative cell viability (\%)} = \frac{\text{Mean of } A_{490nm} \text{ of sample}}{\text{Mean of } A_{490nm} \text{ of control}} \times 100$$

3.2.2.3. MTS Viability Assay : Dose/Response Studies

This experiment was conducted as described above (see section 3.2.2.2). Instead of using a single final concentration of 0.1 mg/mL, two additional concentrations were introduced: 1 and 10 mg/mL. These studies were performed on both HaCaT and NIH/3T3 cell lines. For each cell line only two treatments were used in addition to controls: **Nacre M8** and **$CaCO_3$**. Each concentration was performed in separate 96 well plates, however the three plates were prepared concurrently. See Table 3.2 for the summary of the toxicity studies.

3.2.2.4. Live/Dead Assays with Nacre Preparations

Nacre G was used in this assay to identify whether there were any toxic organic components that were lost during the preparation of the milled nacre. This section used both HaCaT and NIH/3T3 cell lines. See Table 3.2 for the summary of the toxicity studies. The treatments used were **Nacre G**, **Nacre M8** and **$CaCO_3$**. 2.0 x 10^4 cells were seeded on each well in 24 well plates in 250 μL media. Treatment particles were added at the following concentrations: 0.2, 2 and 20 mg/mL in media giving final volume of 500 μL and final concentrations of 0.1, 1 and 10 mg/mL respectively. Each treatment and control was made in triplicate in two different plates. The first plate was incubated for 24 hours at 37 °C with 5% CO_2. The second one was incubated for 72 hours. At the stipulated time point, each well was washed with Phosphate Buffered Saline (PBS) three times. Cells were then stained with 100 μL of 1 μM Calcein and 100 μL of 2 μM Ethidium Bromide (EtBr). The plate was then wrapped with aluminium foil and incubated for 30 minutes at 37 °C with 5% CO_2. The fluorescence was measured

using an Olympus IX71 inverted microscope with 20x objective and fixed exposure time. The live and dead cells were counted using Cell Counter plug-in from ImageJ[54]. The total number of cells is the sum of live and dead cells. Percentage of viable cells for each experiment was calculated as Equation 2.

Equation 2:

$$\text{Live Cells (\%)} = \frac{\text{Number of Living Cells}}{\text{(Number of Live Cells+Number of Dead Cells)}} \times 100$$

3.2.2.5. Live/Dead Assays with Conditioned Media

This experiment is similar to section 3.2.2.4 with some modifications. Instead of adding the treatment particles of **Nacre G**, **Nacre M8** and **$CaCO_3$**, the corresponding conditioned media were added. Individual conditioned media was prepared as described in section 3.2.1.6. The percentage of viable for each experiment was calculated as Equation 2 above. See Table 3.2 for the summary of the toxicity studies.

3.2.2.6. Reactive Oxygen Species with Nacre Preparations

This experiment used both HaCaT and NIH/3T3 cell lines. The treatments used were **Nacre G**, **Nacre M8** and **$CaCO_3$**. See Table 3.2 for the summary of the toxicity studies. 6.0×10^3 cells were seeded in a 96 well plate for each treatment in triplicate. The plate was incubated at 37 °C with 5% CO_2. After 24 hours incubation, the cells were washed three times with PBS. 100 µL of 2',7' – dichlorodihydrofluorescin diacetate (DCFH-DA) 0.1x solution was added to each well. This solution is light sensitive, so plates were wrapped in foil to keep in the dark. After this addition, the plate was incubated for 1 hour at 37 °C with 5% CO_2. The DCFH-DA solution was then removed and the wells washed three times with PBS. Then 100 µL of the particles at 0.1, 1, and 10 mg/mL were added and incubated for 24 hours. On the next day, the cells were washed again three times with PBS. 200 µL of 1x Lysis Buffer was added and the plate was incubated

at room temperature for 15 minutes while wrapped in foil. Then 100 μL of each well was transferred into a new plate and read at 480 nm excitation and 530 nm emission using an EnSpire 2300 Multimode Plate Reader.

3.2.2.7. Reactive Oxygen Species with Conditioned Media

This experiment is the same as described above (see section 3.2.2.6) with some modifications. Instead of adding the treatment particles of **Nacre G**, **Nacre M8** and **$CaCO_3$** corresponding conditioned medias were added. Individual conditioned media was prepared as described in section 3.2.1.6. See Table 3.2 for the summary of the toxicity studies.

3.2.2.8. Statistical Analysis

Each experiment was performed in triplicate. All results were analysed statistically using GraphPad Prism 6.0d for Macintosh (GraphPad Software, Inc. La Jolla, California, USA). Two-Way ANOVA was performed to determine whether the treatments had an effect ($p < 0.05$ as significant). The two factors are concentration and time. The reactive oxygen species (ROS) assay was analyzed using one-way ANOVA ($p < 0.05$ as significant).

3.3. Results

3.3.1. Summary of Toxicity Studies

Table 3.3. Summary of toxicity studies result for Chapter 3. If there was no significant difference for the particular experiments then it is labelled with "No. Sig. Diff". If there were one or more concentrations with significant results then it is labeled with Significant ($p<0.05$). Refer to the text for related studies below for further detail regarding which concentration(s) showed significant effects.

In Vitro Assays	**Outcome Measure**	**Treatment**				
HaCaT Keratinocytes		**Nacre M8**	**Nacre M11**	**Nacre G**	**Nacre I**	**$CaCO_3$**
MTS Viability Assay	Viability	No. Sig. Diff	No. Sig. Diff	N/A	No. Sig. Diff	No. Sig. Diff
Dose/Response	Viability	**Significant**	N/A	N/A	N/A	No. Sig. Diff
Live/Dead Assay (P)	Live Cell Count	**Significant**	N/A	**Significant**	N/A	**Significant**
Live/Dead Assay (C)	Live Cell Count	No. Sig. Diff	N/A	No. Sig. Diff	N/A	No. Sig. Diff
ROS Assay (P)	Stress Level	No. Sig. Diff	N/A	No. Sig. Diff	N/A	No. Sig. Diff
ROS Assay (C)	Stress Level	No. Sig. Diff	N/A	No. Sig. Diff	N/A	No. Sig. Diff
NIH/3T3 Fibroblasts						
Dose/Response	Viability	**Significant**	N/A	N/A	N/A	**Significant**
Live/Dead Assay (P)	Live Cell Count	**Significant**	N/A	**Significant**	N/A	**Significant**
Live/Dead Assay (C)	Live Cell Count	No. Sig. Diff	N/A	No. Sig. Diff	N/A	No. Sig. Diff
ROS Assay (P)	Stress Level	No. Sig.Diff	N/A	No. Sig.Diff	N/A	No. Sig.Diff
ROS Assay (C)	Stress Level	No. Sig.Diff	N/A	No. Sig. Diff	N/A	No. Sig. Diff

3.3.2. Quantification of Protein in Conditioned Media

The amount of protein in conditioned media of **Nacre M8**, **Nacre G** and **$CaCO_3$** were determined at 58.2 ± 2.7, 25.7 ± 0.8 and 2.1 ± 0.8 µg/mL respectively. They were significantly different to each other (one way ANOVA, $p<0.05$).

3.3.3 MTS Viability Assay

The results are summarized in Fig. 3.2. There was no significant difference in viability of cell treated with **Nacre M8**, **Nacre M11, Nacre I** and **$CaCO_3$** at any time-point (two-way ANOVA; $p > 0.05$).

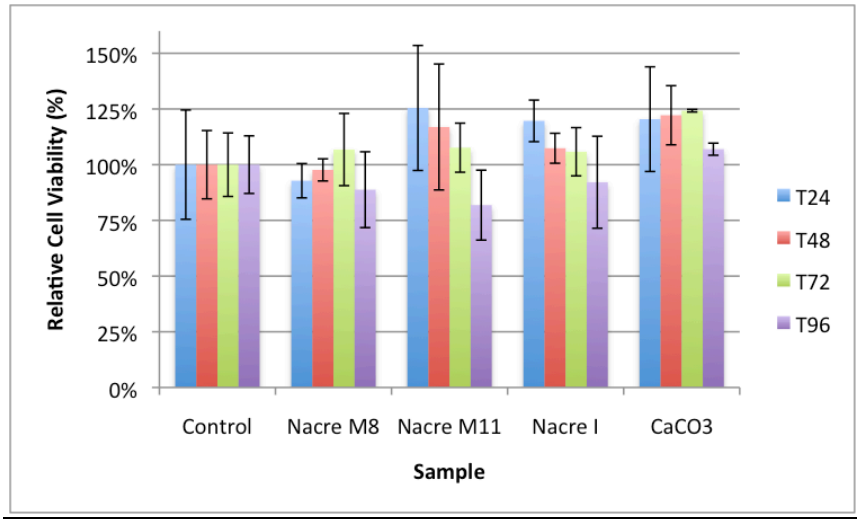

Figure 3.2. Relative cell viability (%) of HaCaT cells treated with Nacre M8, Nacre M11, Nacre I and $CaCO_3$. Error bars show standard deviation. There was no significant difference observed.

3.3.4. Dose-Response Studies

Fig. 3.3 summarizes the results for the dose response assay in HaCaT keratinocytes. There was no significant difference for cells treated with **$CaCO_3$** at any concentration ($p > 0.05$). **Nacre M8** was shown to significantly lower cell viability at 1 mg/mL from 48 hours after incubation (at 72-hours: **Nacre M8,** 75 $\pm$ 17 % vs Control, 100 $\pm$ 12%; at 96-hours: **Nacre M8,** 66 $\pm$ 15 % vs Control, 100 $\pm$ 7%, $p < 0.05$), whereas at 10 mg/mL it significantly reduced cell viability from 48 hours post incubation (at 48-hours: **Nacre M8,** 75 $\pm$ 22 % vs Control, 100 $\pm$ 6 %; at 72-hours: **Nacre M8,** 44 $\pm$ 8 % vs Control, 100 $\pm$ 12 %; at 96-hours: **Nacre M8,** 39 $\pm$ 12 % vs Control, 100 $\pm$ 7 %, $p < 0.05$).

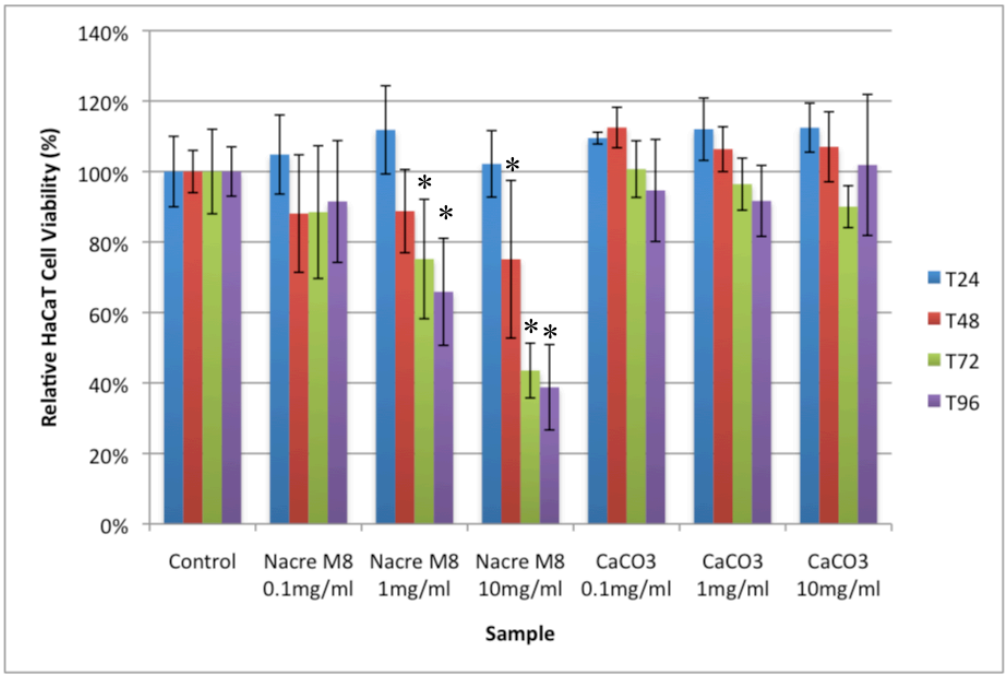

Figure 3.3. **Relative cell viability (%) of HaCaT keratinocytes treated with Nacre M8 and $CaCO_3$ at 0.1, 1 and 10 mg/mL.** Error bars show standard deviation. Significance was set at * $p < 0.05$.

Fig. 3.4 summarizes the results for the dose response assay in NIH/3T3 fibroblasts. The results are similar to those with HaCaT cells (see Fig. 3.3), but not identical. **Nacre M8** at 1 mg/mL did not lower cell viability significantly at any time point ($p > 0.05$). However, at 10 mg/mL Nacre **M8** had lowered the cell viability significantly from the beginning to the end of experiment (at 24-hours: **Nacre M8,** 82 $\pm$ 15 % vs Control, 100 $\pm$ 9 %; at 48-hours: **Nacre M8,** 77 $\pm$ 11 % vs Control, 100 $\pm$ 4 %; at 72-hours: **Nacre M8,** 70 $\pm$ 18 % vs Control, 100 $\pm$ 14 %; at 96-hours: **Nacre M8,** 60 $\pm$ 12 % vs Control, 100 $\pm$ 12 %, $p < 0.05$). Moreover, **$CaCO_3$** at 0.1 mg/mL significantly increased cell viability at the end of the experiment (at 96-hours: **$CaCO_3$,** 89 $\pm$ 5 % vs Control, 100 $\pm$ 11 %, $p < 0.05$).

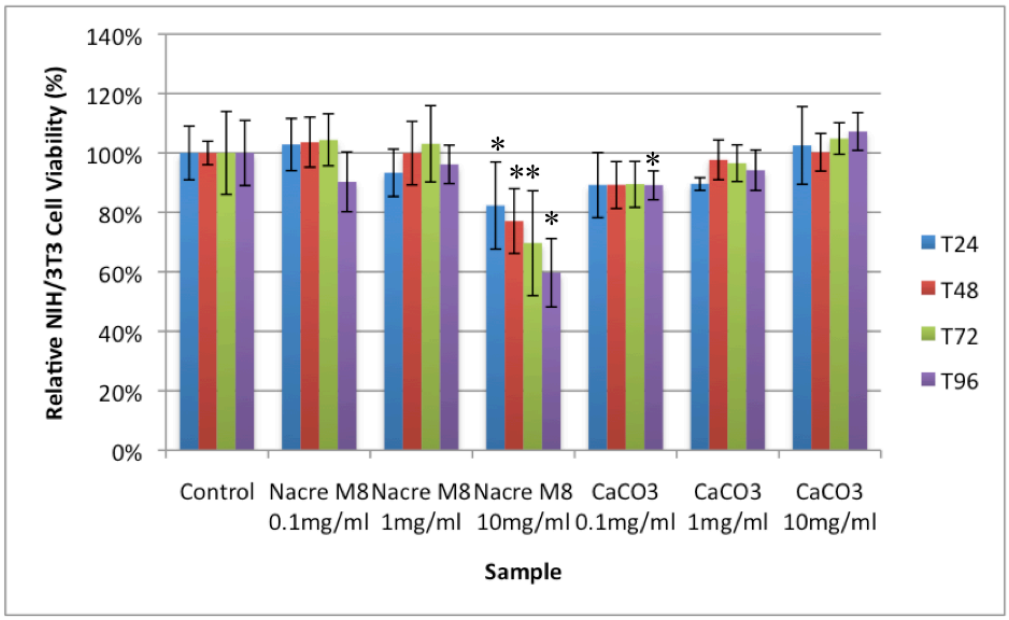

Figure 3.4. Relative cell viability (%) of NIH/3T3 fibroblasts treated with Nacre M8 and $CaCO_3$ at 0.1, 1 and 10mg/mL. Error bars show standard deviation. Significance was set at * $p < 0.05$.

3.3.5. Live/Dead Assays with Nacre Preparations

The results for HaCaT cells are summarized in Fig. 3.5. There was no significant difference in living cell percentage for **$CaCO_3$** at any concentration or incubation time, except at 0.1 mg/mL at 24-hour post incubation where the percentage of living cells was significantly lower compared to control (**$CaCO_3$,** 91.1 $\pm$ 1.3 % vs Control, 97.1 $\pm$ 1.8 %, $p < 0.05$). When the HaCaT cells were treated with **Nacre M8**, there were significant differences at all concentrations for the 24 H incubation (**Nacre M8:** at 0.1 mg/mL, 89.9 $\pm$ 2.3 %; at 1 mg/mL, 77.0 $\pm$ 1.6 %; at 10 mg/mL, 74.9 $\pm$ 4.0 % vs Control: 97.1 $\pm$ 1.8 %, $p < 0.05$). However, when the HaCaT cells with the same treatment were incubated for 72 H, the significant differences were only observed for 1 and 10 mg/mL (**Nacre M8:** at 1 mg/mL, 77.9 $\pm$ 1.2 %; at 10 mg/mL, 76.4 $\pm$ 4.2 % vs Control: 99.7 $\pm$ 0.0 %, $p < 0.05$). HaCaT cells treated with **Nacre G** showed significant differences at 10 mg/mL for both incubation times (at 24-hours: **Nacre G,** 72.6 $\pm$ 8.8 % vs Control, 97.1 $\pm$ 1.8 %; at 72-hours: **Nacre G,** 84.9 $\pm$ 1.7 % vs Control, 99.7 $\pm$ 0.0 %, $p < 0.05$).

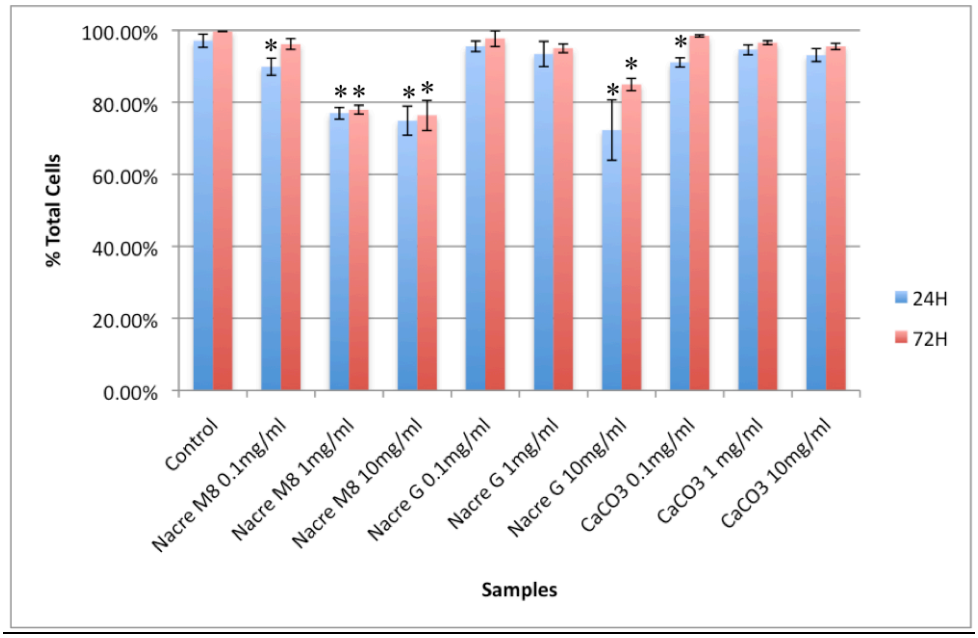

Figure 3.5. Live/Dead assays showing percentage of live cells in the HaCaT culture post incubation with Nacre M8, Nacre G and $CaCO_3$ at 0.1, 1 and 10mg/mL. Data presented as average ± SD. Significance was set at * $p < 0.05$.

Fig. 3.6 summarizes the results for NIH/3T3 cells. Cell viability with **Nacre M8** added was significantly reduced at a concentration of 0.1 mg/mL at both 24 and 72 hours post incubation (at 24 hours: **Nacre M8,** 73.4 ± 16.4 % vs Control, 100 ± 0.0 %; at 72-hours: **Nacre M8,** 51.7 ± 10.3 % vs Control, 93.3 ± 3.5 %, $p < 0.05$). Meanwhile, viability of the cells treated with 0.1 mg/mL of **Nacre G** or **$CaCO_3$** did not show any significant change at any time point ($p > 0.05$).

At a concentration of 1 mg/mL, cell viability with **Nacre M8** extract added was significantly reduced at 24-hours post incubation (**Nacre M8,** 72.5 ± 37.3 % vs Control, 100 ± 0.0 %, $p < 0.05$). This significant reduction was no longer observed at 72-hours post incubation ($p > 0.05$). Inversely, at 1 mg/mL cell viability with **Nacre G** added was not significantly reduced at 24-hours, but at 72-hours post incubation (**Nacre G,** 53.5 ± 4.6 % vs Control, 93.3 ± 3.5 %, $p < 0.05$). Cells treated with 0.1 mg/mL of **$CaCO_3$** did not show any significant change in viability at any time point ($p > 0.05$).

At 10 mg/mL the viability was significantly reduced at both 24 and 72 -hours for **Nacre M8** and **$CaCO_3$** (at 24-hours: **Nacre M8,** 0.0 ± 0.0 % and **$CaCO_3$,** 0.0 ± 0.0 % vs Control, 100 ± 0.0 %; at 72-hours: **Nacre M8,** 68.0 ± 0.0 % and **$CaCO_3$,** 67.4 ± 7.6 % vs Control, 93.3 ± 3.5 %, $p < 0.05$). Cell viability treated with 10 mg/mL of **Nacre G** was only significantly reduced at 72-hours (**Nacre G,** 52.2 + 20.8 % vs Control, 93.3 ± 3.5 %, $p < 0.05$).

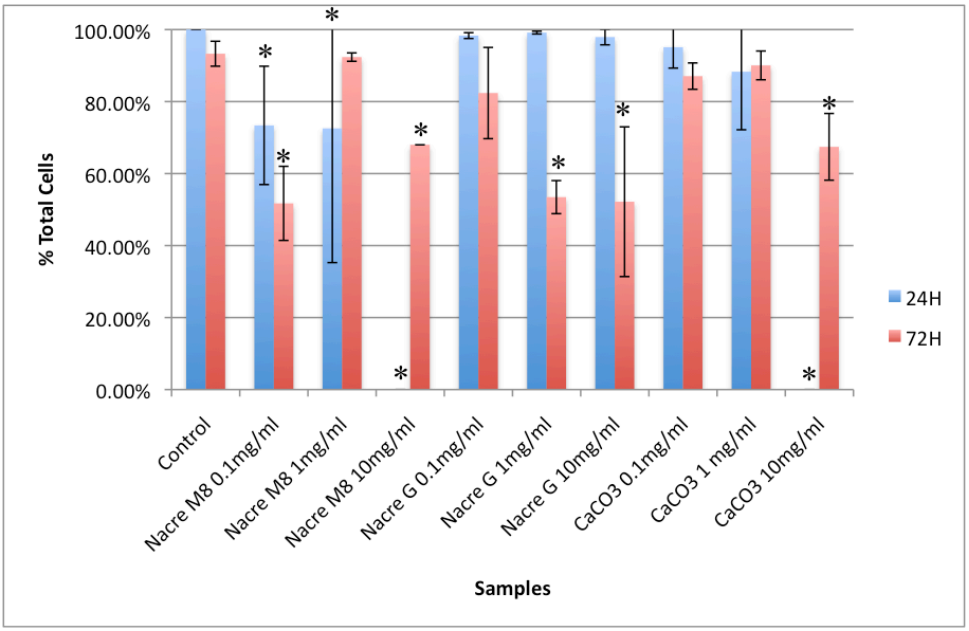

Figure 3.6. Live/Dead assays showing percentage of live cells in the NIH/3T3 culture post incubation with Nacre M8, Nacre G and $CaCO_3$ at 0.1, 1 and 10mg/mL. Data presented as average ± SD. Significance was set at * $p < 0.05$.

3.3.6. Live/Dead Assays with Conditioned Media

There was no significant difference for both HaCaT and NIH/3T3 cells with any treatment and any incubation time ($p > 0.05$). See Figs 3.7 and 3.8 respectively.

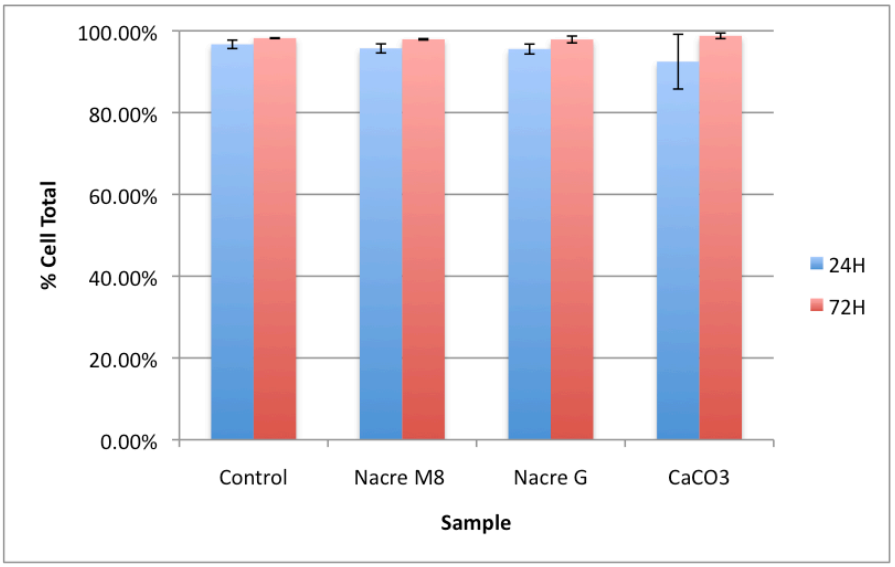

Figure 3.7. Live/Dead assays showing percentage of live cells in the HaCaT culture post incubation with conditioned media of Nacre M8, Nacre G and $CaCO_3$. Data presented as average ± SD. Significance was set at * $p < 0.05$.

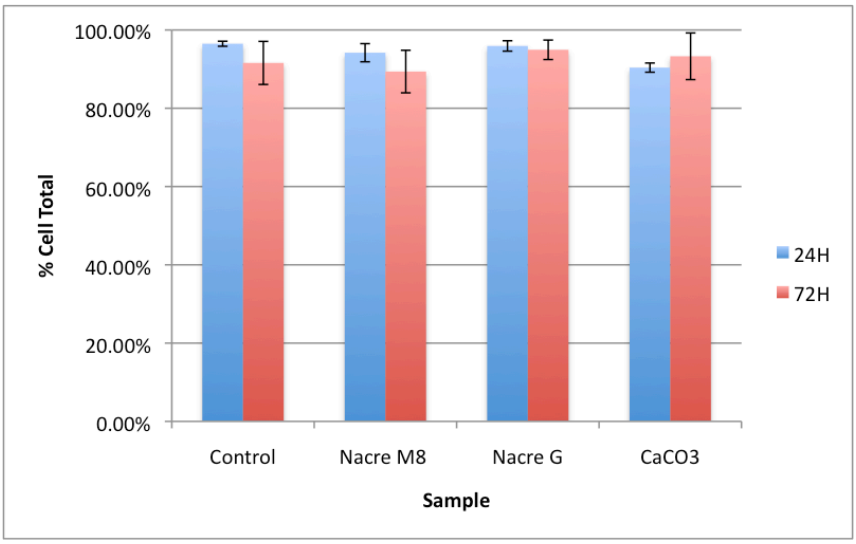

Figure 3.8. Live/Dead assays showing percentage of live cells in the NIH/3T3 culture post incubation with conditioned media of Nacre M8, Nacre G and $CaCO_3$. Data presented as average ± SD. Significance was set at * $p < 0.05$.

3.3.7. Reactive Oxygen Species Assay with Nacre Preparations

There was no significant difference for NIH/3T3 and HaCaT cells with any treatment and at any concentration (one-way ANOVA; $p > 0.05$). See Fig. 3.9.

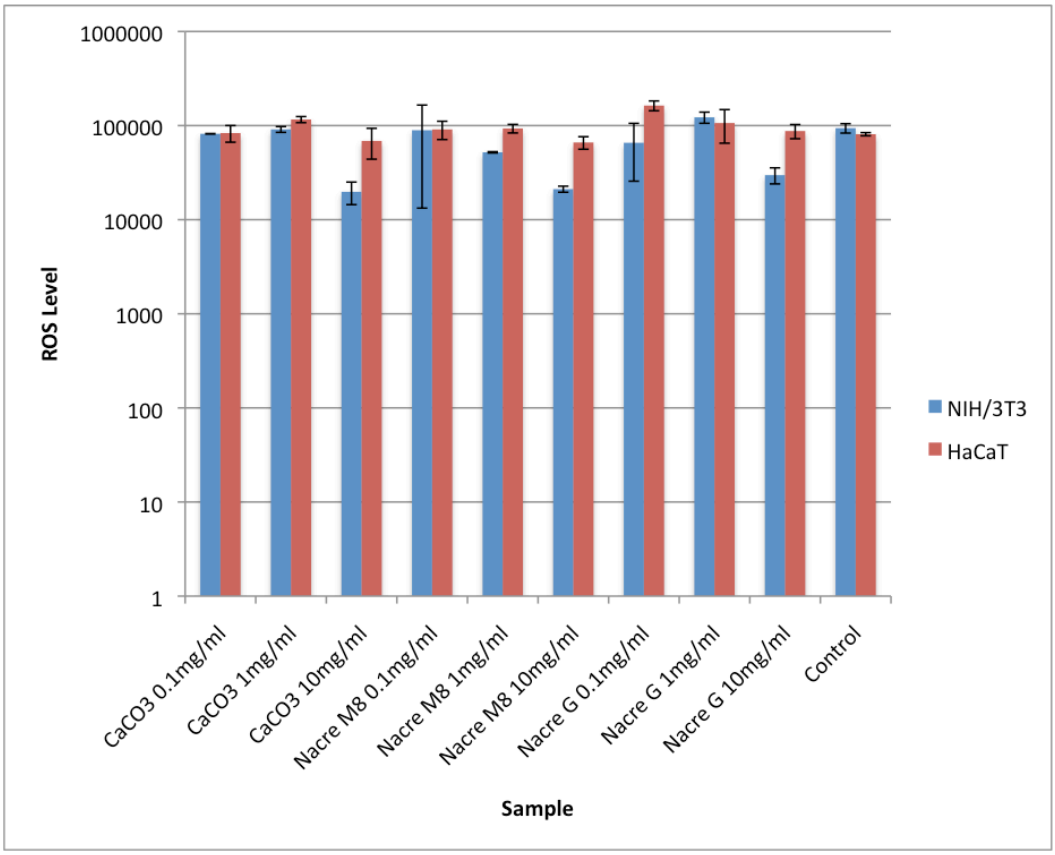

Figure 3.9. Reactive oxygen species (ROS) assay showing ROS levels in NIH/3T3 and HaCaT cells stressed with $CaCO_3$, Nacre M8 and Nacre G at 0.1, 1 and 10mg/mL for 24 hours.

3.3.8. Reactive Oxygen Species Assay with Conditioned Media

There was no significant difference for HaCaT and NIH/3T3 cells with any treatment (one-way ANOVA; $p > 0.05$). See Fig. 3.10.

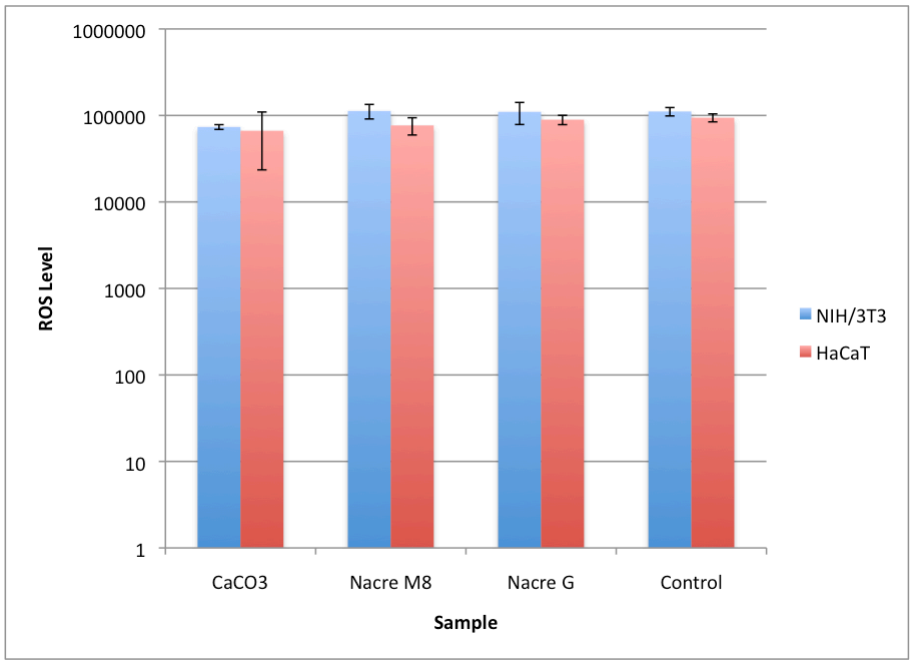

Figure 3.10. Reactive oxygen species (ROS) assay showing ROS levels in NIH/3T3 and HaCaT cells stressed with conditioned media of $CaCO_3$, Nacre M8 and Nacre G for 24 hours.

3.4. Discussion

The key findings from this toxicity study can be summarized as follows:

1. Nacre is safe for skin cells in vitro at concentrations up to 1 mg/mL

2. Heavy metal contamination in milled nacre did not result in significantly lower cell viability

3. Nacre prepared using different techniques did not produce significant differences in the toxicity results

3.4.1 Safe concentrations of nacre

At a concentration of 0.1 mg/mL **Nacre M11**, **Nacre G** and **Nacre I** did not show any significant differences from untreated control samples. Interestingly, at 0.1 mg/mL **Nacre M8** and **$CaCO_3$** reduced HaCaT cell count significantly in the live/dead assay at 24-hours post incubation, but this reduction in viable cell count was no longer observed at 72-hours post incubation. This situation has also been observed in another study.[8] The cells might have broken down the calcium carbonate salt and utilized the calcium ions. Cells can absorb Ca^{+2} through the cell membrane and use it for cell communication and many other cellular and enzymatic functions.[55] A set of different results was observed with NIH/3T3 cell lines in the live/dead assay, 0.1 mg/ml of **Nacre M8** reduced the cell count significantly for both 24-hours and 72-hours time points but **$CaCO_3$** did not. A low concentration of 0.09 mM calcium has been shown to be not toxic and even induce mesenchymal cell-like phenotype in normal human epidermal keratinocytes.[56] 0.1 mg/mL calcium carbonate is equivalent to 1.0 mM calcium, which is much higher than 0.09 mM. Therefore, this concentration of 0.1 mg/mL might be toxic to cells.

Nacre G at 1 mg/mL did not alter the viable cell number in the live/dead assay significantly nor affect the ROS level in HaCaT cells. However, NIH/3T3 cells were significantly affected with reduced viable cell counts at 72-hours post incubation in the live/dead assay (see Fig. 3.7). **Nacre M8** at 1 mg/mL gave contradicting results, where it significantly lowered cell viability in the dose-response assay (see Fig. 3.4) and viable cell count in live/dead assay (see Fig. 3.6) of HaCaT cells but had much less damaging effect on NIH/3T3 cells in both assays (see Figs 3.5 and 3.7). In brief, it seems that NIH/3T3 is more robust towards nacre. Furthermore, these results contradict previous finding that has shown that calcium concentration up to 25 mM is safe for

keratinocytes.[57] Nacre concentration of 1 mg/ml is equivalent to 10 mM, which should be still within the safe limit. Indeed, a dispersion of **$CaCO_3$** at 1 mg/mL did not affect cell viability in the dose-response assay, the live/dead assay or ROS levels in either cell types.

At 10 mg/mL, **Nacre M8** appeared to be toxic to both HaCaT and NIH/3T3 cells. The same finding was observed for cells treated with **Nacre G**. The MTS viability assay in dose/response study results showed much lower relative viability and live/dead assay results showed fewer living cells compared to controls. At 10 mg/mL, **$CaCO_3$** only appeared to be toxic for NIH/3T3 cells. These changes in viability do not appear to be related to increases in ROS level, since there were no significant differences in reactive oxygen species in any cells treated with the highest concentration of **Nacre M8**, **Nacre G** or **$CaCO_3$**. This suggests that the cause of the toxicity may not be a biochemical response of the cells to the nacre preparations. This argument was corroborated by Lopez et al in an animal study where they implanted a mix of 50 mg nacre or $CaCO_3$ with 150 µl blood (concentration: ~333 mg/mL) on the ventral surface of rats and observed no sign of toxicity.[58] Their concentration of 333 mg/mL is higher than 10 mg/mL, which was used in the current work. Although it is important to underline that their work was performed *in vivo*, so there are many factors that justify the necessity for much higher concentration such as size of animal, first pass metabolism effect, liver metabolism and renal secretion. An alternative explanation may be that the significant reduction in cell viability and living cell count was due to physical competition for surface area. Both HaCaT and NIH/3T3 must attach to a surface before they can divide.[50,52] On the other hand, calcium carbonate is known to be insoluble in water, its solubility was determined at 12 ppm at 22 °C and 14 ppm at 37.5 °C.[59] Therefore, in samples treated with the highest concentration of **Nacre M8**, **Nacre**

G or **$CaCO_3$** there was substantial sedimentation of particulate material on the surface area to which the cells need to attach. This could therefore limit the area for cells attachment and proliferation.[60] This problem could probably be overcome by using plates with fewer wells, so the surface area for each well is larger. For example, 24-well plates could be used instead of using 96-well plates. In this way, the cells would have ample space to attach and proliferate despite of the nacre sediment.

3.4.2. Heavy metal contamination from the ball-milling process is not toxic to skin cells

Nacre M11, the highly contaminated sample, did not show any significant differences in toxicity (as assessed by viability) when compared to control or to its low contamination counterpart, **Nacre M8**. According to Wood et al., Cd and Zr are classified as moderate to high toxicity heavy metals.[61] Therefore, this is an unexpected result considering the very high concentrations of Cd and Zr in the **Nacre M11** sample. As discussed above, it is known that that heavy metals can cause many detrimental effects locally on skin or systemically when absorbed in the body. These detrimental effects require the heavy metal to be in contact with or more commonly taken up by the cells.[62]

A plausible explanation is that these immortalized cells are not as sensitive as normal cells towards contamination. There are many studies that have obtained different results from normal and immortalized cells. For example, in a study of an antitumor agent, Cidofovir, the difference in responses to the same subject by different kind of keratinocytes (normal, immortalized and transformed) have been demonstrated.[63] Further, Gérard and Goldbeter argued that the cell cycle and circadian clock are coupled in normal cells but are disconnected in immortalized cells.[64] Docosahexaenoic acid, a

type of polyunsaturated fatty acids, has been demonstrated to trigger a concentration-dependent death of the immortalized H9c2 cardiac cells but not in primary neonatal cardiomiocytes.[65] Moreover, suppressor p53 and Ras oncoproteins were shown to be abundant in the nucleus and perinucleus of immortalized mouse embryonic fibroblasts (MEF), whereas these two proteins were barely detected in the perinucleus of primary MEF cells.[66] Finally, Sherwood et al. found that immortalized human bronchial epithelial cells (16HBE14o-) had an ability which was not possessed by the primary cells that is to recover most of their ATP and wound-induced Ca^{2+} signalling when cultured in the absence of arsenic for 7 days.[67] Thus, due to biological differences between primary and immortalized cell lines it is advisable to repeat these experiments in the future using primary cells. Then the results from primary and immortalized cell lines can be analysed to get a better understanding of the potential heavy metal toxicity. Furthermore, the heavy metal contained in nacre might not be toxic to skin cells as tested in this study, however when it is used in cosmetics or skin care products then it might be absorbed through skin and entering the blood circulation system. From here, heavy metal might be accumulated in several organs such as heart, brain, kidneys or liver and compromises their functions.[68] Hence, at this stage, this current finding could not be used as justification for allowing the presence of heavy metal in cosmetics or skin care products.

3.4.3. Method of nacre preparation does not appear to affect toxicity

No significant differences were observed in the MTS Viability assay between the ball-milled nacre samples **M8** and **M11** and the ionic liquid processed nacre – **Nacre I** (see Fig. 3.3). The difference between the two ball-milled preparations and **Nacre I** was in the presence of organic component, which was only present in ball-milled preparations whereas the **Nacre I** was pure inorganic aragonite tablets.[49] These initial results suggest

that the organic component of nacre is not toxic. Furthermore, this argument was also supported by the results from the live/dead assay and ROS assay of the conditioned media from **Nacre M8** and **Nacre G** that showed no significant differences with the controls (see Figs. 3.8, 3.9 and 3.11). It was unexpected that the protein amount in the conditioned media from **Nacre M8** was more than twice the protein amount in the conditioned media from **Nacre G** (58.2 ± 2.7 vs 25.7 ± 0.8 μg/mL). Theoretically, the water soluble protein concentration of nacre should range from 0.3 to 5 mg/ml.[69] The low protein amount of the conditioned media from **Nacre G** was possibly because most of the proteins were still trapped in the brick and mortar structure. The nacre could be decalcified with weak acid (pH 4) to obtain the soluble proteins.[70]

The results of the investigations above so far show that neither the inorganic component nor the organic component of the prepared nacre samples appear to be toxic to skin cells *in vitro*. There were no clear trends or consistent findings between different tests that might provide evidence of toxicity and therefore provide concern for the application of nacre on the skin. This is in line with a previous finding which claimed that nacre is biocompatible with human skin.[8] These positive initial results should be further supported with similar evidence using multiple primary cells from different patients as there are genetic variation from person to person that might exhibit contradicting results.[71]

To produce the same amount of aragonite tablets, the **Nacre I** technique takes a much longer time compared to Nacre **M8** or Nacre **M11**. Boulos et al. required 2 hours to process 10 mg of nacre into **Nacre I**[49], whereas 15 g of nacre could be milled in 2 hours to produce Nacre **M8** or Nacre **M11.**[19] Even with the pause time considered for the milling process, both Nacre **M8** and Nacre **M11** productions only entail 3 hours

time. Additionally, it is important to note that Boulos et al. did not specify the percentage of nacre that was processed into **Nacre I** from the 10 mg starting material. Further, ball milling is as reproducible as the ionic liquid process and both of them have a similar problem. As discussed earlier in Chapter 2, in the ball milling process ball-to-ball collision is inevitable and the ball is worn gradually. Similarly, the anion PF_6^- decomposition from the ionic liquid [BMIM][PF_6] is inevitable and increases the level of F^- in the sample.[49] The procurement cost of the ball milling apparatus is certainly much higher compared to ionic liquid. However, in the long run ionic liquid will require more capital investment. Boulos et al. required 20 ml of ionic liquid for 10 mg of nacre.[49] The density of [BMIM][PF_6] is 1.38 g/ml at 20 °C.[72] So, the ionic liquid required for one experiment is 27.6 g. The price for 50 g of [BMIM][PF_6] is A$338 for 97% purity or A$1910 for 98.5% purity.[72,73] Therefore, for a continuous research or production, ball-milling is a favoured technique to use because with additional 50% time (from 2 hours to 3 hours), one can get 1500 times more aragonite tablets (from 10 mg to 15 g).

3.4.4. Preferred component of nacre for further study

In spite of the above findings, it is still challenging to ascertain which component or preparation of nacre would be the most beneficial in studies of efficacy. Each component has its own advantages and disadvantages. For example, the aragonite tablets as in **Nacre M8**, **Nacre M11**, **Nacre G** and **Nacre I** is easy to use, quantify and control. Aragonite or calcium carbonate in general is known for its slow decay and low toxicity.[74,75] However, as discussed above at high concentration this inorganic component may have been competing for surface at the bottom of the wells because they are highly insoluble at physiological conditions (pH = 7.4).[76] Despite of this disadvantage, nacre powder has been shown to promote bone development *in vitro*.[4,7,77]

It is important to note the nacre powder used in the bone studies might still contain the organic components. Thus, although nacre powder was shown to be beneficial for bone development, the effects might not originate from the inorganic component of nacre i.e. aragonite. These studies, unfortunately, did not use other sources of aragonite, such as coral[78], crystal from hill[79] or hot spring travertine.[80] Inclusion of aragonite from other sources other than from nacre could provide insight as to whether aragonite from different sources could produce the beneficial effect. Synthetic aragonite described by Carteret et al. should be used as one of the controls.[81] If proven, then this may provide opportunities for developing different therapies for repairing bone.

As has been mentioned in Chapter 1, the organic component of nacre only makes up 5% of the whole nacre[82] and amounts to less than 2% when dry.[83] This organic matrix is composed of numerous proteins, glycoproteins and polysaccharides.[84] These organic molecules might be insoluble or soluble in water.[85] At least 13 proteins that are associated with nacre biomineralization have been identified from the *P. margaritifera* shell.[86] It has always been a challenge to recover all of the proteins from the matrix[87], as some of them are low molecular weight.[88] It is therefore inevitable that some organic components would be lost in the nacre preparation process. Due to their small sizes and low densities, these proteins do not separate well and are poorly stained in gel electrophoresis.[89] Additionally Bédouet et al. have identified peptides and low molecular metabolites with molecular sizes range between 100 and 700 Da from the water soluble matrix.[88] Conchiolin and chitin are among molecules from the matrix, which are insoluble in water and acid.[90,91] The water soluble molecules from this matrix has been shown to have therapeutic effects not only in bone development[92] but also in a wound healing study.[93] Therefore, it is possible that the organic component with its rich variety of molecules could offer promise for wound healing.

3.5. Conclusion

The inorganic component of nacre appeared to be not toxic up to 0.1 mg/ml on HaCaT regardless of method of preparations. However, at the same concentration it appeared to be toxic to NIH/3T3 in the live/dead assay although the other two assays did not agree with this finding. Furthermore, the water-soluble organic component of nacre did not show any toxic effect in all assays. Therefore, the organic component of **Nacre M8** and **Nacre G** were chosen for functional assessment in the next chapter.

3.6. References

1 Xu, H., Huang, K., Gao, Q., Gao, Z. & Han, X. A study on the prevention and treatment of myopia with nacre on chicks. *Pharmacological Research* **44**, 1-6, doi:10.1006/phrs.2000.0780 (2001).

2 Pal, D., Sahu, C. K. & Haldar, A. Bhasma : The ancient Indian nanomedicine. *Journal of Advanced Pharmaceutical Technology & Research* **5**, 4-12, doi:10.4103/2231-4040.126980 (2014).

3 Rousseau, M. *et al.* Restoration of stratum corneum with nacre lipids. *Comparative Biochemistry and Physiology Part B: Biochemistry and Molecular Biology* **145**, 1-9, doi:10.1016/j.cbpb.2006.06.012 (2006).

4 Silve, C. *et al.* Nacre initiates biomineralization by human osteoblasts maintained In Vitro. *Calcif Tissue Int* **51**, 363-369, doi:10.1007/bf00316881 (1992).

5 Lamghari, M. *et al.* Stimulation of bone marrow cells and bone formation by nacre: in vivo and in vitro studies. *Bone* **25**, 91S-94S (1999).

6 Lamghari, M., Berland, S., Laurent, A., Huet, H. & Lopez, E. Bone reactions to nacre injected percutaneously into the vertebrae of sheep. *Biomaterials* **22**, 555-562, doi:10.1016/s0142-9612(00)00213-1 (2001).

7 Lopez, E. *et al.* Demonstration of the capacity of nacre to induce bone formation by human osteoblasts maintained in vitro. *Tissue and Cell* **24**, 667-679, doi:http://dx.doi.org/10.1016/0040-8166(92)90037-8 (1992).

8 Agarwal, V. *et al.* Evaluating the effects of nacre on human skin and scar cells in culture. *Toxicology Research* **3**, 223-227, doi:10.1039/c4tx00004h (2014).

9 in *Global Cosmetic Industry* Vol. 171 17 (2003).

10 Sea Pollution. *The Journal of the Royal Society for the Promotion of Health* **89**, 115-116, doi:10.1177/146642406908900301 (1969).

11 Van Cauwenberghe, L., Vanreusel, A., Mees, J. & Janssen, C. R. Microplastic pollution in deep-sea sediments. *Environmental Pollution* **182**, 495-499, doi:http://dx.doi.org/10.1016/j.envpol.2013.08.013 (2013).

12 Lerebours, A. l. Ø. *et al.* Genetic Alterations and Cancer Formation in a European Flatfish at Sites of Different Contaminant Burdens. *Environmental Science & Technology* **48**, 10448-10455, doi:10.1021/es502591p (2014).

13 Chen, H. S., Chang, J. H. & Wu, J. S. B. Calcium Bioavailability of Nanonized Pearl Powder for Adults. *Journal of Food Science* **73**, H246-H251, doi:10.1111/j.1750-3841.2008.00965.x (2008).

14 Chang, F., Li, G., Haws, M. & Niu, T. Element concentrations in shell of Pinctada margaritifera from French Polynesia and evaluation for using as a food supplement. *Food Chemistry* **104**, 1171-1176, doi:http://dx.doi.org/10.1016/j.foodchem.2007.01.032 (2007).

15 Bu-Olayan, A. H. & Subrahmanyam, M. N. V. Accumulation of copper, nickel, lead and zinc by snail, Lunella coronatus and pearl oyster, Pinctada radiata from the Kuwait coast before and after the gulf war oil spill. *Science of The Total Environment* **197**, 161-165, doi:http://dx.doi.org/10.1016/S0048-9697(97)05428-4 (1997).

16 Shiber, J. G. Trace metals with seasonal considerations in coastal algae and molluscs from Beirut, Lebanon. *Hydrobiologia* **69**, 147-162, doi:10.1007/bf00016544 (1980).

17 Lim, P.-E., Lee, C.-K. & Din, Z. Accumulation of heavy metals by cultured oysters from Merbok Estuary, Malaysia. *Marine Pollution Bulletin* **31**, 420-423, doi:http://dx.doi.org/10.1016/0025-326X(95)00144-C (1995).

18 Orton, J. H. Summary of an Account of Invstigations into the Cause or Causes of the Unusual Mortality among Oysters in English Oyster Beds during 1920 and 1921. *Journal of the Marine Biological Association of the United Kingdom* **13**, 1-23 (1923).
19 Tjandra, E. S., Boulos, R. A., Duncan, P. C. & Raston, C. L. Unfastening pearl nacre nanostructures under shear. *CrystEngComm* **15**, 6896-6900, doi:10.1039/c3ce40760h (2013).
20 Cunha, R., Blanc, F., Bonhomme, F. & Arnaud-Haond, S. Evolutionary Patterns in Pearl Oysters of the Genus *Pinctada* (Bivalvia: Pteriidae). *Mar Biotechnol* **13**, 181-192, doi:10.1007/s10126-010-9278-y (2011).
21 Nohynek, G. J., Antignac, E., Re, T. & Toutain, H. Safety assessment of personal care products/cosmetics and their ingredients. *Toxicology and Applied Pharmacology* **243**, 239-259, doi:http://dx.doi.org/10.1016/j.taap.2009.12.001 (2010).
22 Al-Qutob, M. A., Alatrash, H. M. & Abol-Ola, S. Determination of different heavy metals concentrations in cosmetics purchased from the Palestinian markets by ICP/MS. *Advances in Environmental Sciences* **5**, 287-293 (2013).
23 Lee, S. M., Jeong, H. J. & Chang, I. S. Simultaneous determination of heavy metals in cosmetic products. *International Journal of Cosmetic Science* **31**, 401-401, doi:10.1111/j.1468-2494.2009.00517_5.x (2009).
24 Ayenimo, J. G., Yusuf, A. M., Adekunle, A. S. & Makinde, O. W. Heavy Metal Exposure from Personal Care Products. *Bull Environ Contam Toxicol* **84**, 8-14, doi:10.1007/s00128-009-9867-5 (2010).
25 FAO/WHO. Evaluation of certain food additives and contaminatns : sixty-first report of the Joint FAO/WHO Expert Committee on Food Additives. (Food and Agricultural Organization of the United Nations and World Health Organization, Rome, Italy, 2003).
26 USFDA. (ed US Department of Health and Human Services. Food and Drug Administration.) (2006).
27 Nourmoradi, H., Foroghi, M., Farhadkhani, M. & Vahid Dastjerdi, M. Assessment of Lead and Cadmium Levels in Frequently Used Cosmetic Products in Iran. *Journal of Environmental and Public Health* **2013**, 5, doi:10.1155/2013/962727 (2013).
28 Nordberg, G. Cadmium and human health: A perspective based on recent studies in China. *The Journal of Trace Elements in Experimental Medicine* **16**, 307-319, doi:10.1002/jtra.10039 (2003).
29 McMurray, C. T. & Tainer, J. A. Cancer, cadmium and genome integrity. *Nat Genet* **34**, 239-241 (2003).
30 Waalkes, M. Cadmium and human health. *Health and Environmental Digest* **5**, 1-3 (1991).
31 Chen, F., Wu, T. & Cheng, X. Cytotoxic effects of denture adhesives on primary human oral keratinocytes, fibroblasts and permanent L929 cell lines. *Gerodontology* **31**, 4-10, doi:10.1111/j.1741-2358.2012.00681.x (2014).
32 Hurlin, P. J., Maher, V. M. & McCormick, J. J. Malignant Transformation of Human Fibroblasts Caused by Expression of a Transfected T24 HRAS Oncogene. *Proceedings of the National Academy of Sciences of the United States of America* **86**, 187-191, doi:10.2307/33083 (1989).
33 Nadim, M. *et al.* Improvement of polyphenol properties upon glucosylation in a UV-induced skin cell ageing model. *International Journal of Cosmetic Science* **36**, 579-587, doi:10.1111/ics.12159 (2014).
34 Ranzato, E., Mazzucco, L., Patrone, M. & Burlando, B. Platelet lysate promotes in vitro wound scratch closure of human dermal fibroblasts: different roles of

cell calcium, P38, ERK and PI3K/AKT. *Journal of Cellular and Molecular Medicine* **13**, 2030-2038, doi:10.1111/j.1582-4934.2008.00467.x (2009).

35 Ranzato, E., Martinotti, S. & Burlando, B. Wound healing properties of jojoba liquid wax: An in vitro study. *Journal of Ethnopharmacology* **134**, 443-449, doi:http://dx.doi.org/10.1016/j.jep.2010.12.042 (2011).

36 Rai, V., Dayan, N. & Michniak-Kohn, B. A comparative evaluation of photo-toxic effect of fractionated melanin and chlorpromazine hydrochloride on human (dermal fibroblasts and epidermal keratinocytes) and mouse cell line/s (fibroblast Balb/c 3T3). *Toxicology in Vitro* **25**, 538-544, doi:http://dx.doi.org/10.1016/j.tiv.2010.11.017 (2011).

37 Wiegand, C., Abel, M., Ruth, P. & Hipler, U. C. Superabsorbent polymer-containing wound dressings have a beneficial effect on wound healing by reducing PMN elastase concentration and inhibiting microbial growth. *J Mater Sci: Mater Med* **22**, 2583-2590, doi:10.1007/s10856-011-4423-3 (2011).

38 Boonkaew, B., Kempf, M., Kimble, R. & Cuttle, L. Cytotoxicity testing of silver-containing burn treatments using primary and immortal skin cells. *Burns*, doi:http://dx.doi.org/10.1016/j.burns.2014.02.009 (2014).

39 Sarkar, S. D., Farrugia, B. L., Dargaville, T. R. & Dhara, S. Chitosan–collagen scaffolds with nano/microfibrous architecture for skin tissue engineering. *Journal of Biomedical Materials Research Part A* **101**, 3482-3492, doi:10.1002/jbm.a.34660 (2013).

40 Sundaramurthi, D., Krishnan, U. M. & Sethuraman, S. Biocompatibility of Poly(3-hydroxybutyrate-co-3-hydroxyvalerate) (PHBV) Nanofibers for Skin Tissue Engineering. *Journal of Biomedical Nanotechnology* **9**, 1383-1392, doi:10.1166/jbn.2013.1618 (2013).

41 Radu, T., Chiriac, M. T., Popescu, O., Simon, V. & Simon, S. In vitro evaluation of the effects of yttria–alumina–silica microspheres on human keratinocyte cells. *Journal of Biomedical Materials Research Part A* **101A**, 472-477, doi:10.1002/jbm.a.34320 (2013).

42 Iscla, I. *et al.* A new antibiotic with potent activity targets MscL. *J Antibiot*, doi:10.1038/ja.2015.4 (2015).

43 Demir, E. *et al.* Zinc oxide nanoparticles: Genotoxicity, interactions with UV-light and cell-transforming potential. *Journal of Hazardous Materials* **264**, 420-429, doi:http://dx.doi.org/10.1016/j.jhazmat.2013.11.043 (2014).

44 Everett, W. N. *et al.* Phosphate-enhanced cytotoxicity of zinc oxide nanoparticles and agglomerates. *Toxicology Letters* **225**, 177-184, doi:http://dx.doi.org/10.1016/j.toxlet.2013.12.005 (2014).

45 Demir, E. *et al.* Genotoxic and cell-transforming effects of titanium dioxide nanoparticles. *Environmental Research* **136**, 300-308, doi:http://dx.doi.org/10.1016/j.envres.2014.10.032 (2015).

46 Datta, K. K. R. *et al.* Quaternized carbon dot-modified graphene oxide for selective cell labelling - controlled nucleus and cytoplasm imaging. *Chemical Communications* **50**, 10782-10785, doi:10.1039/c4cc02637c (2014).

47 Turan-Zitouni, G. *et al.* Synthesis and antituberculosis activity of new thiazolylhydrazone derivatives. *European Journal of Medicinal Chemistry* **43**, 981-985, doi:http://dx.doi.org/10.1016/j.ejmech.2007.07.001 (2008).

48 Emami, S. *et al.* 2-Hydroxyphenacyl azoles and related azolium derivatives as antifungal agents. *Bioorganic & Medicinal Chemistry Letters* **18**, 141-146, doi:http://dx.doi.org/10.1016/j.bmcl.2007.10.111 (2008).

49 Boulos, R. A. *et al.* Unzipping oyster shell. *RSC Advances* **3**, 3284-3290, doi:10.1039/c2ra21763e (2013).

50 Boukamp, P. *et al.* Normal keratinization in a spontaneously immortalized aneuploid human keratinocyte cell line. *The Journal of Cell Biology* **106**, 761-771 (1988).
51 Fusenig, N. E. & Boukamp, P. Multiple stages and genetic alterations in immortalization, malignant transformation, and tumor progression of human skin keratinocytes. *Molecular Carcinogenesis* **23**, 144-158, doi:10.1002/(sici)1098-2744(199811)23:3<144::aid-mc3>3.0.co;2-u (1998).
52 Jainchill, J. L., Aaronson, S. A. & Todaro, G. J. Murine Sarcoma and Leukemia Viruses: Assay Using Clonal Lines of Contact-Inhibited Mouse Cells. *Journal of Virology* **4**, 549-553 (1969).
53 Gebauer, D., Völkel, A. & Cölfen, H. Stable Prenucleation Calcium Carbonate Clusters. *Science* **322**, 1819-1822, doi:10.1126/science.1164271 (2008).
54 Abramoff, M. D., Magalhaes, P. J. & Ram, S. J. Image processing with image-j. *Biophotonics International* **11**, 36-42 (2004).
55 Rasmussen, H. Cell Communication, Calcium Ion, and Cyclic Adenosine Monophosphate. *Science* **170**, 404-412, doi:10.2307/1729413 (1970).
56 Takagi, R., Yamato, M., Murakami, D., Sugiyama, H. & Okano, T. Low calcium culture condition induces mesenchymal cell-like phenotype in normal human epidermal keratinocytes. *Biochemical and Biophysical Research Communications* **412**, 226-231, doi:http://dx.doi.org/10.1016/j.bbrc.2011.07.069 (2011).
57 Law, J., Chowdhury, S., Aminuddin, B. & Ruszymah, B. Effect of calcium concentration on keratinocyte differentiation in 2-d culture and 3d-construct. *Regenerative Research* **4**, 22-29 (2015).
58 Lopez, E., Faou, A. L., Borzeix, S. & Berland, S. Stimulation of rat cutaneous fibroblasts and their synthetic activity by implants of powdered nacre (mother of pearl). *Tissue and Cell* **32**, 95-101, doi:10.1054/tice.1999.0091 (2000).
59 Whipple, G. C. & Jr, A. M. The Solubility of Calcium Carbonate and of Magnesium Hydroxide and the Precipitation of These Salts with Lime Water. *The Journal of Infectious Diseases* **3**, 151-165, doi:10.2307/30071685 (1906).
60 Di Battista, J. *et al.* Proliferation and differentiation of human adipose-derived mesenchymal stem cells (ASCs) into osteoblastic lineage are passage dependent. *Inflamm. Res.* **63**, 907-917, doi:10.1007/s00011-014-0764-y (2014).
61 Wood, J. M. Biological Cycles for Toxic Elements in the Environment. *Science* **183**, 1049-1052, doi:10.1126/science.183.4129.1049 (1974).
62 Qu, C.-S. *et al.* Human Exposure Pathways of Heavy Metals in a Lead-Zinc Mining Area, Jiangsu Province, China. *PLoS ONE* **7**, e46793, doi:10.1371/journal.pone.0046793 (2012).
63 Andrei, G., Topalis, D., De Schutter, T. & Snoeck, R. Insights into the mechanism of action of cidofovir and other acyclic nucleoside phosphonates against polyoma- and papillomaviruses and non-viral induced neoplasia. *Antiviral Research* **114**, 21-46, doi:http://dx.doi.org/10.1016/j.antiviral.2014.10.012 (2015).
64 Gérard, C. & Goldbeter, A. Entrainment of the Mammalian Cell Cycle by the Circadian Clock: Modeling Two Coupled Cellular Rhythms. *PLoS Computational Biology* **8**, e1002516, doi:10.1371/journal.pcbi.1002516 (2012).
65 Qadhi, R. *et al.* Differential responses to docosahexaenoic acid in primary and immortalized cardiac cells. *Toxicology Letters* **219**, 288-297, doi:http://dx.doi.org/10.1016/j.toxlet.2013.03.010 (2013).
66 Shaiken, T. E. & Opekun, A. R. Dissecting the cell to nucleus, perinucleus and cytosol. *Scientific Reports* **4**, 4923, doi:10.1038/srep04923 (2014).

67 Sherwood, C. L., Lantz, R. C. & Boitano, S. Chronic Arsenic Exposure in Nanomolar Concentrations Compromises Wound Response and Intercellular Signaling in Airway Epithelial Cells. *Toxicological Sciences* **132**, 222-234, doi:10.1093/toxsci/kfs331 (2013).
68 Singh, R., Gautam, N., Mishra, A. & Gupta, R. Heavy metals and living systems: An overview. *Indian Journal of Pharmacology* **43**, 246-253, doi:10.4103/0253-7613.81505 (2011).
69 Marin, F., Luquet, G., Marie, B., Medakovic, D. & Gerald, P. Molluscan Shell Proteins: Primary Structure, Origin, and Evolution. *Current Topics in Developmental Biology* **80**, 209 - 276 (2007).
70 Dauphin, Y. Soluble Organic Matrices of the Calcitic Prismatic Shell Layers of Two Pteriomorphid Bivalves. *Journal of Biological Chemistry* **278**, 15168-15177, doi:10.1074/jbc.M204375200 (2003).
71 Replogle, R. A. *Natural genetic variation affecting calcium homeostasis* Ph.D. thesis, Purdue University, (2013).
72 Sigma-Aldrich. *1-butyl-3-methylimidazolium hexafluorophosphate for catalysis, ≥98.5% (T)* <http://www.sigmaaldrich.com/catalog/product/sial/18122?lang=en&region=AU> (2016).
73 Sigma-Aldrich. *1-butyl-3-methylimidazolium hexafluorophosphate ≥97.0% (HPLC)* <http://www.sigmaaldrich.com/catalog/product/aldrich/70956?lang=en&region=AU> (2016).
74 Haruta, S., Hanafusa, T., Fukase, H., Miyajima, H. & Oki, T. An Effective Absorption Behavior of Insulin for Diabetic Treatment Following Intranasal Delivery Using Porous Spherical Calcium Carbonate in Monkeys and Healthy Human Volunteers. *Diabetes Technology & Therapeutics* **5**, 1-9, doi:10.1089/152091503763816409 (2003).
75 Huang, S., Chen, J. C., Hsu, C. W. & Chang, W. H. Effects of nano calcium carbonate and nano calcium citrate on toxicity in ICR mice and on bone mineral density in an ovariectomized mice model. *Nanotechnology* **20**, 375102-375108, doi:doi:10.1088/0957-4484/20/37/375102 (2009).
76 Qiu, N. *et al.* Calcium carbonate microspheres as carriers for the anticancer drug camptothecin. *Materials Science and Engineering: C* **32**, 2634-2640, doi:http://dx.doi.org/10.1016/j.msec.2012.08.026 (2012).
77 Shen, Y., Zhu, J., Zhang, H. & Zhao, F. In vitro osteogenetic activity of pearl. *Biomaterials* **27**, 281-287, doi:http://dx.doi.org/10.1016/j.biomaterials.2005.05.088 (2006).
78 Sinha, S. & Rez, P. Distortions of the calcite and aragonite atomic structures from interstitial water. *Materials Chemistry and Physics* **157**, 56-62, doi:http://dx.doi.org/10.1016/j.matchemphys.2015.03.013 (2015).
79 Filippi, M. & Hyrsl, J. Aragonite from Cicov hill in the Czech Republic. *Mineralogical Record* **35**, 137-142 (2004).
80 Greer, H., Zhou, W. & Guo, L. Phase transformation of Mg-calcite to aragonite in active-forming hot spring travertines. *Miner Petrol*, 1-10, doi:10.1007/s00710-015-0367-5 (2015).
81 Carteret, C. *et al.* Polymorphism Studied by Lattice Phonon Raman Spectroscopy and Statistical Mixture Analysis Method. Application to Calcium Carbonate Polymorphs during Batch Crystallization. *Crystal Growth & Design* **9**, 807-812, doi:10.1021/cg800368u (2009).

82 Song, F., Zhang, X. H. & Bai, Y. L. Microstructure and Characteristics in the Organic Matrix Layers of Nacre. *Journal of Materials Research* **17**, 1567-1570, doi:doi:10.1557/JMR.2002.0233 (2002).
83 Weiner, S. Organization of extracellularly mineralized tissues: a comparative study of biological crystal growth. *CRC Crit Rev Biochem* **20**, 365 - 408 (1986).
84 Albeck, S., Addadi, L. & Weiner, S. Regulation of Calcite Crystal Morphology by Intracrystalline Acidic Proteins and Glycoproteins. *Connective Tissue Research* **35**, 365-370, doi:doi:10.3109/03008209609029213 (1996).
85 Wang, X., Liu, S., Xie, L., Zhang, R. & Wang, Z. Pinctada fucata mantle gene 3 (PFMG3) promotes differentiation in mouse osteoblasts (MC3T3-E1). *Comparative Biochemistry and Physiology Part B: Biochemistry and Molecular Biology* **158**, 173-180, doi:http://dx.doi.org/10.1016/j.cbpb.2010.11.004 (2011).
86 Joubert, C. *et al.* Transcriptome and proteome analysis of Pinctada margaritifera calcifying mantle and shell: focus on biomineralization. *BMC Genomics* **11**, 613 (2010).
87 Michenfelder, M. *et al.* Erratum: "Characterization of two molluscan crystal-modulating biomineralization proteins and identification of putative mineral binding domains", vol. 70, no. 4, pp. 522–533 (2003). *Biopolymers* **73**, 291-291, doi:10.1002/bip.20020 (2004).
88 Bédouet, L. *et al.* Identification of low molecular weight molecules as new components of the nacre organic matrix. *Comparative Biochemistry and Physiology Part B: Biochemistry and Molecular Biology* **144**, 532-543, doi:10.1016/j.cbpb.2006.05.012 (2006).
89 Gotliv, B.-A., Addadi, L. & Weiner, S. Mollusk Shell Acidic Proteins: In Search of Individual Functions. *ChemBioChem* **4**, 522-529, doi:10.1002/cbic.200200548 (2003).
90 Bédouet, L. *et al.* Proteomics Analysis of the Nacre Soluble and Insoluble Proteins from the Oyster Pinctada margaritifera. *Mar Biotechnol* **9**, 638-649, doi:10.1007/s10126-007-9017-1 (2007).
91 Schonitzer, V. & Weiss, I. The structure of mollusc larval shells formed in the presence of the chitin synthase inhibitor Nikkomycin Z. *BMC Structural Biology* **7**, 71 (2007).
92 Chaturvedi, R., Singha, P. K. & Dey, S. Water Soluble Bioactives of Nacre Mediate Antioxidant Activity and Osteoblast Differentiation. *PLoS ONE* **8**, 1-1, doi:10.1371/journal.pone.0084584 (2013).
93 Lee, K. *et al.* Nacre-driven water-soluble factors promote wound healing of the deep burn porcine skin by recovering angiogenesis and fibroblast function. *Mol Biol Rep* **39**, 3211-3218, doi:10.1007/s11033-011-1088-4 (2012).

Chapter 4

Chapter 4: Assessment of the Potential Effects of Pearl Nacre on Wound Healing Using *in vitro* Assays.

4.1. Introduction

Wound healing is a complex process and the resulting scars often cause both physical and psychological impacts. In recent years, two of the major areas of wound healing research have focused on decreasing time to heal and on reconstructive/regenerative strategies to improve scar appearance.

The key factor underpinning the poor appearance of a scar is the dermal collagen matrix. In normal skin, this is loosely packed and fibres are oriented in a random 'basket weave' pattern.[1] By contrast, in scars collagen bundles are larger, running parallel to the epithelial surface and are more densely packed.[1] Previously, ball milled nacre that was described in Chapter 2 has been shown to be safe for use on both NIH/3T3 fibroblasts and HaCaT keratinocytes (see section 3.4.1). Here, the ball milled nacre preparation, **Nacre M8**, was further studied to explore its effect on the migration rate of keratinocytes and fibroblasts to determine if the nacre preparation might enhance wound-healing rates using *in vitro* models. **Nacre M8** was chosen for this study due to its low contamination. The **Nacre M8** preparation was then investigated for its effect on collagen deposition by primary human dermal fibroblasts to determine if the preparation could impact on the matrix produced by the fibroblasts.

The organic component of nacre consists of different macromolecules which have different solubility in water.[2] The water-soluble fractions are usually called water-soluble matrix (WSM) and have been investigated in the context of the potential to accelerate wound healing. Jian-Ping et al. demonstrated that the water soluble matrix

(WSM) from a freshwater pearl oyster, *Hyriopsis cumingii* Lea (Unionidae), could promote wound healing by stimulating fibroblast mitosis, collagen deposition and tissue inhibitor of metalloproteinase-1 (TIMP-1) production.[3] Similarly, Li et al. claimed that WSM from the same oyster increased the number of migratory fibroblasts (Hs68 cells and human foreskin fibroblasts) three times more than the control in a scratch assay study.[4] Furthermore, in a study of wound healing in porcine skin with deep second-degree burns, the WSM from pearl oyster, *Pteria martensii*, accelerated the wound healing process by rapidly restoring angiogenesis and fibroblast activity.[5] A similar study using WSM from the scallop *Pecten maximus* on human primary fibroblasts showed that there was no effect on proliferation and an insignificant effect on cell migration.[6] Therefore the organic components of nacre from pearl oyster appear to be promising to accelerate wound-healing although there is conflicting evidence.

After the initial inflammatory stage in the wound healing process, the second stage is re-epithelialisation and granulation tissue formation. At this stage, fibroblasts and keratinocytes interact and cooperate to restore the epidermal barrier.[7] Dermal fibroblasts migrate and contribute to the secretion of granulation tissue.[8] Then, keratinocytes migrate and proliferate over this granulation tissue to restore epithelial integrity.[9] Formation of new epidermis is critical to prevent bacterial infection[10] and to start the re-modelling process.[7] Consequently, accelerating the closure of the wound gap is still a clinical challenge and the search for compounds that can promote closure is important.[11,12] In Chapter 3, it was shown that **Nacre M8** was not toxic to skin cells but at the same time did not significantly alter the proliferation rate of keratinocytes. Furthermore, several studies have claimed that the organic component of nacre is beneficial for wound healing.[3-5] Two of these studies have studied the efficacy of organic component of nacre on fibroblasts in increasing migration rate using a scratch

assay and produced conflicting results.[4,5] In addition, no research to date has assessed the effect of nacre preparations on keratinocyte migration. Therefore, in this Chapter the organic component of **Nacre M8** will be investigated for its efficacy in increasing the migration rate of fibroblasts and keratinocytes using a scratch migration assay.

The scratch migration assay is a simple assay that has been used to study a number of compounds that may alter the migration rate of fibroblasts and keratinocytes *in vitro*. For example, Hostanska et al. studied the efficacy of a homeopathic remedy (mixture of *Arnica montana*, *Calendula officinalis*, *Hypericum perforatum* and *Symphytum officinale*) in closing the wound using NIH/3T3 fibroblasts in a scratch assay.[13] Their results showed that 1:100 dilutions of the remedy significantly increased the migration rate of the fibroblasts ($p<0.001$).[13] In a similar study, Fronza et al. determined that 10μg/mL of *Calendula officinalis* extracts significantly increased the migration rate of Swiss 3T3 albino mouse fibroblasts by 70.53% $\pm$ 2.64 ($p<0.05$).[14] Furthermore, the influence of mesenchymal stem cell secreted factors in the wound healing process was also investigated using *in vitro* scratch assays on single cells or co-cultures of L929 fibroblasts and HaCaT keratinocytes.[15] For studies of individual cell types, fibroblast wound closure was faster than keratinocytes.[15] Additionally, for the co-culture study, it was revealed that fibroblasts lead the way in closing the artificial wound.[15]

The scratch assay has also been used to assess keratinocyte migration and the effects of compounds on this process. Loo et al. investigated the efficacy of five concentrations of hydrogen peroxide-H_2O_2 (100, 250, 500, 750 and 1000 μM) in inducing keratinocyte migration using a scratch migration assay.[16] The investigation found that low levels of H_2O_2 of up to 500 μM might be beneficial for the re-

epithelialisation process.[16] Similarly, a DNA binding protein, high-mobility group box-1 (HMGb-1), was applied exogenously to HaCaT cells (an immortalized keratinocyte cell line) using a scratch migration assay.[17] The experiment with HaCaT cells treated with HMGb-1 had significantly faster wound closure ($p<0.01$).[17] Lastly, HaCaT cells treated with 20% non-toxic platelet lysate had a significant increase in wound closure rate ($p<0.01$).[18] Therefore, the use of the *in vitro* scratch assay has been widely validated for measuring the potential efficacy of compounds and mixtures on migration rates of skin cells. Here, the scratch assay has been used to assess migration rates of both cell types after exposure to ball milled nacre extract.

The final stage of wound healing is re-modelling of the skin structure, which includes scar formation. Scars are formed due to excessive deposition of predominantly collagen I by fibroblasts.[19] Collagen is a generic name for a super family of proteins, which have three α polypeptide chains.[20] One or several α polypeptide chains can form homo- or heterotrimers of collagen.[21] There are 29 distinct collagens. They can be loosely classified into several groups, namely fibrillar collagens (I, II, III, V, XI, XXIV and XXVII); collagens forming networks (IV, VIII and X); collagens associated with large fibrils (IX, XII, XIV, XVI, XIX, XX, XXI and XXII) and collagens forming thread-like fibrils (VI, XXVI, XXVIII and XXIX).[22] Collagen types I and III are the most important in the wound healing process, with collagen III deposited early in the healing process but replaced over time by excessive collagen I deposition that is the basis of scar matrix.[23] Friedman et al. showed that excessive deposition of collagen type I can cause derangement of the fibre structure followed by hypertrophic scar formation.[24] In scar tissue, collagen bundles have a parallel orientation to the epidermis rather than a random and basket-weave formation observed in normal skin.[25] Interestingly, WSM from the nacre of *Pinctada fucata* was reported to increase the

transcription of the COL-1A2 gene that is one of the collagen type I subunits.[26] This finding was supported by a similar study that used WSM from the shell of a scallop, *Pecten maximus*.[6]

In this chapter, the effects of **Nacre M8** on the amount of collagen type I deposition by primary dermal fibroblasts were investigated using a Scar-in-a-Jar assay. Chen et al. recently developed this assay in 2009 to enable analysis and quantification of collagen deposition in a single well.[27] Since then many compounds that might affect fibrosis have been studied using the Scar-in-a-Jar assay. Additionally, in this study the assay has been modified to include measures of the orientation of the collagen type I deposited by the fibroblasts. This allows more complete assessment of the effects of the compounds on collagen deposition, providing a measure of 'quality' as well as quantity.

There are three questions that were investigated in this chapter:

1. Does the organic component of **Nacre M8** increase the migration rate of fibroblasts and keratinocytes?
2. Does the organic component of **Nacre M8** increase the amount of collagen type I deposited by fibroblasts?
3. Does the organic component of **Nacre M8** increase the randomness of collagen type I orientation deposited by fibroblasts thereby yielding a more 'normal' structure?

The first question will be addressed through scratch migration assay and the result is relevant for wound healing. The second and last questions will be addressed through scar-in-a-jar assay and their results are relevant not only for wound healing but also for the use of nacre in cosmetics or skin care products.

4.2. Material and Methods

4.2.1. Materials

4.2.1.1. Cell lines

HaCaT[28,29] and NIH/3T3[30] cell lines were used to model keratinocyte and fibroblast cell types respectively for the *in vitro* scratch migration assays. Primary human dermal fibroblasts were grown from explant cultures from three-millimetre punch biopsies. Fibroblasts between P2 and P4 were used for the Scar-in-a-Jar assays.

4.2.1.2. Nacre Preparation and Conditioned Media

Table 4.1 below summarizes the samples that were analyzed for both scratch migration and Scar-in-a-Jar assays. Media conditioned with **Nacre M8**, **$CaCO_3$** and **Nacre G** were prepared as described in section 3.2.1.6. In spite of the results from protein quantification that the protein content of media conditioned with **Nacre G** is only half that of media conditioned with **Nacre M8** (see section 3.3.2), media conditioned with **Nacre G** might contain organic molecules that were lost during **Nacre M8** preparation. Therefore, media conditioned with **Nacre G** was used in the Scratch Migration Assay. However, it was not used in Scar-in-a-Jar assays due to no significantly different results between samples treated with **Nacre M8** and **Nacre G** conditioned media (see section 4.3.1 below). Conditioned media of **$CaCO_3$** served as a positive control.

Table 4.1. Experiment samples

Scratch Migration Assay	**Scar-in-a-Jar**
Nacre M8 Conditioned Media	**Nacre M8** Conditioned Media
$CaCO_3$ Conditioned Media	**$CaCO_3$** Conditioned Media
Nacre G Conditioned Media	

4.2.2. Methods

4.2.2.1. Scratch Migration Assay

The scratch migration assay was adapted from the method described by Liang et al.[31] 2.0 x 10^5 cells were seeded into each well of a 12-well plate. The plate was incubated at 37 °C with 5% CO_2 until a confluent monolayer was formed. The scratch was then performed using a yellow p200 pipette tip. In order to smooth the edges of the cell free area, after the scratch was made the wells were washed twice with 1 mL of phosphate buffer saline (PBS). The cells were then suspended in 1 mL of normal **media** or conditioned media of **Nacre G**, **Nacre M8** and **$CaCO_3$**. Each experiment was made in triplicate (see Fig. 4.1).

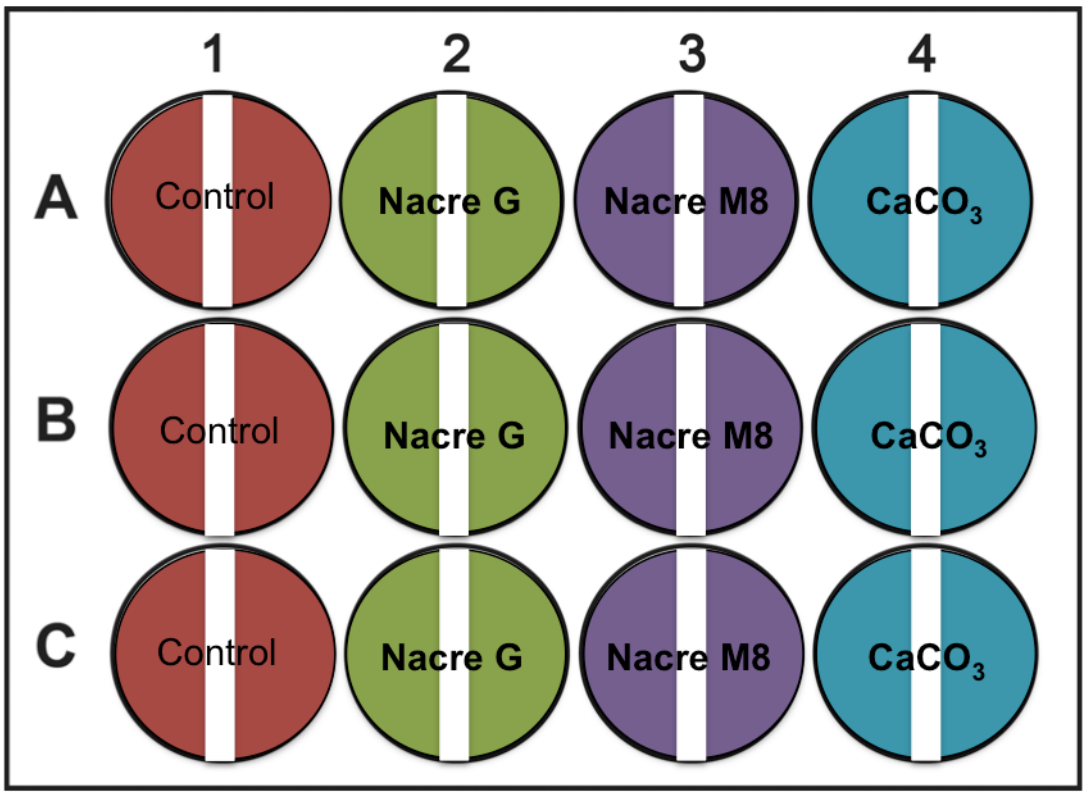

Figure 4.1. Arrangement of scratch migration assay. The white gap in the centre of the wells represents the scratch, which is cell free.

The scratches were imaged at 0, 5, 18 and 24 hours using a light microscope (Olympus 1x51; final objective 4x). In between the imaging times, the well plate was incubated at 37 °C with 5% CO_2. The cover plate was inked to ensure the same

imaging areas were photographed. The cell free area was first marked using the Free Hand tool and then calculated using the Measure function using ImageJ.[32] The percentage of scratch closure at 5, 8 and 24 hours was calculated as Equation 3.

Equation 3:

$$\text{Gap Closure at time T (\%)} = \frac{\text{Cell free area at time T}}{\text{Cell free area at time 0}} \times 100$$

4.2.2.2. Scar-in-a-Jar Assay

The Scar-in-a-Jar assay was adapted from the method described by Chen et al.[27] 50000 low passage primary human fibroblast cells[33] were seeded into each well of a 24-well plate in normal media. After 16 hours of incubation at 37 °C with 5% CO_2, cells were cultured in one of the conditions as described in Table 4.2 In all conditions the media contains 0.5% foetal bovine serum (FBS, JRH Biosciences, Lenexa, KS), 1% penicillin (Gibco) and 1% streptomycin (Gibco, Carsbad, CA).

Table 4.2. Culture media contents

Condition	**Additional media content**
Crowded	100 μM L-ascorbic acid 2-phosphate, 37.5 mg/mL Ficoll 70, 25 mg/mL Ficoll 400 and 5ng/mL TGFβ1
Negative Control	100 μM L-ascorbic acid 2-phosphate
Nacre M8 Conditioned Media	100 μM L-ascorbic acid 2-phosphate, 37.5 mg/mL Ficoll 70, 25 mg/mL Ficoll 400, 5ng/mL TGFβ1 and **Nacre M8** Conditioned Media
Positive Control	100 μM L-ascorbic acid 2-phosphate, 37.5 mg/mL Ficoll 70, 25 mg/mL Ficoll 400, 5ng/mL TGFβ1 and **$CaCO_3$** Conditioned Media

After 6 days incubation at 37 °C with 5% CO_2, the media was removed and the wells washed once with PBS. The cells were blocked with 3% bovine serum albumin (BSA) in PBS for 10 minutes at room temperature. The cells were then incubated with primary antibody (monoclonal mouse anti collagen type 1, Sigma Aldrich, Catalogue No. 2546 in 3% BSA in PBS) for 90 minutes at 37 °C with 5% CO_2 followed by

washing three times with PBS. The cells were then fixed with 2% paraformaldehyde for 10 minutes at room temperature and followed by washing three times with PBS. The cells were blocked again with 3% BSA in PBS for 10 minutes as above. Afterward, the cells were incubated with secondary antibody (Goat anti-mouse Alexa Fluor® 488, Life Technologies, Catalogue No. A11001 in PBS) for 30 minutes at 37 °C with 5% CO_2. After the incubation, the secondary antibody was discarded and the cells were washed three times with PBS. In order to permeabilise the cells, 500 µl of 100% methanol was added into each well and then incubated at 4 °C for 20 minutes. Methanol was then removed and the cells were washed three times with PBS. 500 µl of Hoechst stain 33258 (Invitrogen, Catalogue No. 3569) diluted 1 in 1000 with PBS was added into each well and incubated at room temperature for 20 minutes. The cells were washed with PBS for the last time and the plate was later covered in aluminium foil prior to imaging

4.2.2.3. Imaging and Analysis

Each well was imaged twice with a Nikon TE300 camera. The exposure time for nuclei (blue image) was set at 300 ms and for collagen (green image) at 1 ms. Both images were analysed using NIS-elements software (Nikon, Japan). First, the region of interest (ROI) of the blue image was determined to make sure that it covered the whole well. The position of the ROI was recorded to produce a green image with identical ROI. The threshold was then adjusted to provide optimum reading of nuclei. This was followed by using the 'measure' function, which provides object count and binary area. The binary area of the green image was divided by the object count from the blue image to give the value of collagen per cell.

The orientation of collagen was analysed from the green image. The image was divided into 6 smaller ROIs. Empty spaces, where there was scarce or no collagen, were not selected. The selection of each ROI was blinded to prevent bias in site selection. The coherency of the collagen was measured using OrientationJ Measure plug-in in imageJ.[34] This function essentially draws an ellipse for each ROI based on the orientation of the collagen fibres in the ROI being measured. When coherency is closer to 0, it means the collagen is more randomly oriented i.e. similar to the structure found in normal skin dermal matrix. When coherency is closer to 1, it means the collagen has lost its randomness and is elongated with parallel fibres predominating. This is more similar to scar dermal matrix. The values were exported onto a spreadsheet for statistical analysis.

4.2.2.4. Statistical Analyses

Scratch migration and Scar-in-a-Jar assays were performed in triplicate and quadruplicate respectively. All results were analysed statistically using GraphPad Prism 6.0d for Macintosh (GraphPad Software, Inc. La Jolla, California, USA). One-Way ANOVA was performed for the Scratch Migration Assay and Scar-in-a-Jar to determine whether the treatments had an effect and presented as means $\pm$ SD ($p<0.05$ as significant with 95% confidence). For the orientation of the collagen, the median of the coherency values were analysed using Mann-Whitney U-test ($p<0.05$ as significant with 95% confidence).

4.3. Results

4.3.1. Scratch Migration Assay

4.3.1.1. NIH/3T3 Scratch Migration Assay

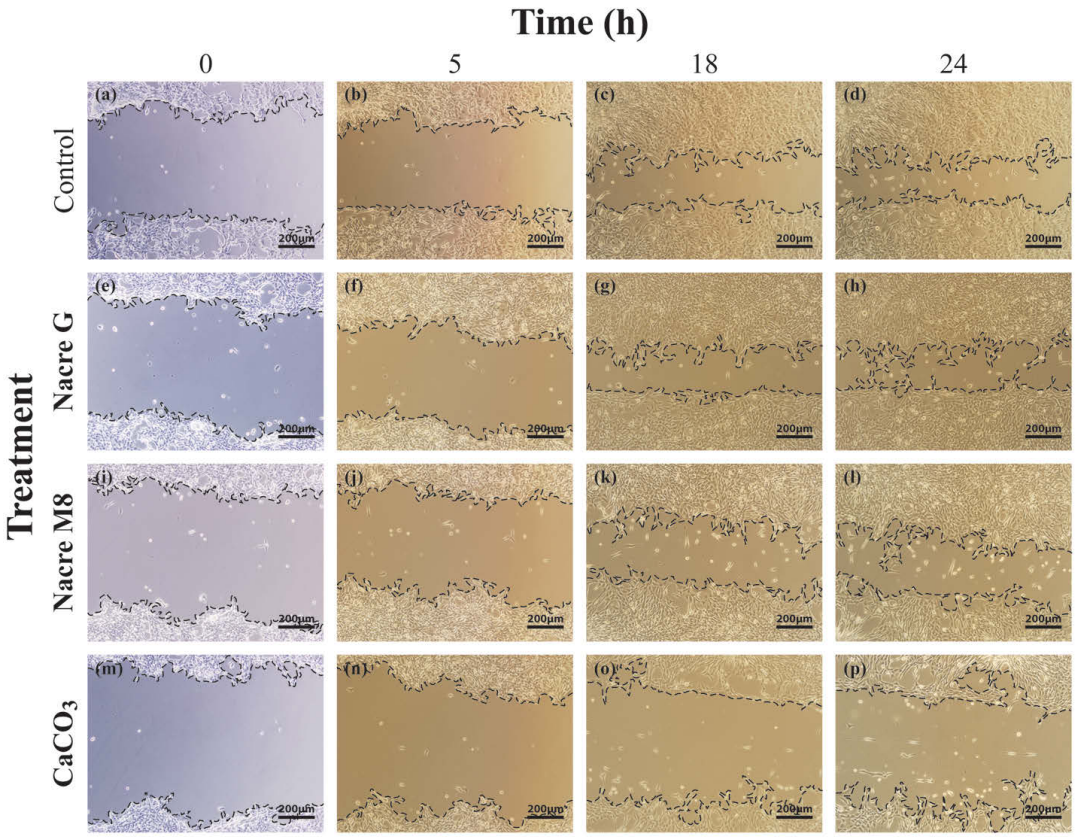

Figure 4.2. Representative images of scratch area on NIH/3T3 cells at 0, 5, 18 and 24 hours. Dashed lines were made to better illustrate the artificial wound bed area, which was cell free. The cells at the wound margin from the top and bottom were proliferating and invading the wound bed area. The cell free area was measured at each time point and the area at time 0 was set as the 100% wound area.

Fig. 4.2 shows representative images of wound closure over the 24-hour post incubation period for a NIH/3T3 scratch migration assay. Additionally, the wound closure rates of the triplicates are presented as mean ± SD in Fig. 4.3. The only significant difference observed was between **Nacre G** and **$CaCO_3$** at 24-hour post incubation (**Nacre G**, 69.41 ± 2.16 % vs **$CaCO_3$**, 48.34 + 23.80 %, $p<0.05$).

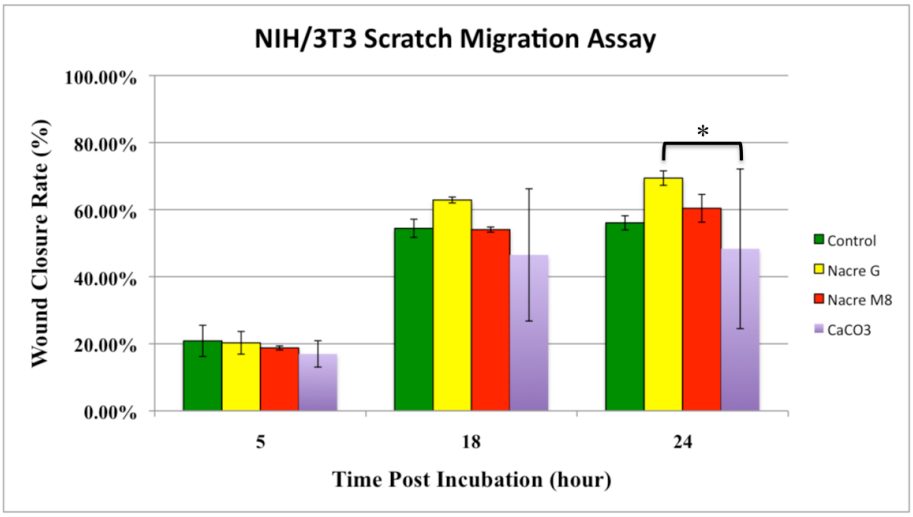

Figure 4.3. Wound closure rate of NIH/3T3 fibroblasts treated with Nacre G, Nacre M8 and $CaCO_3$ in 24 hours post incubation. Error bars show standard deviation. Significance was set at * $p<0.05$

4.3.1.2. HaCaT Scratch Migration Assay

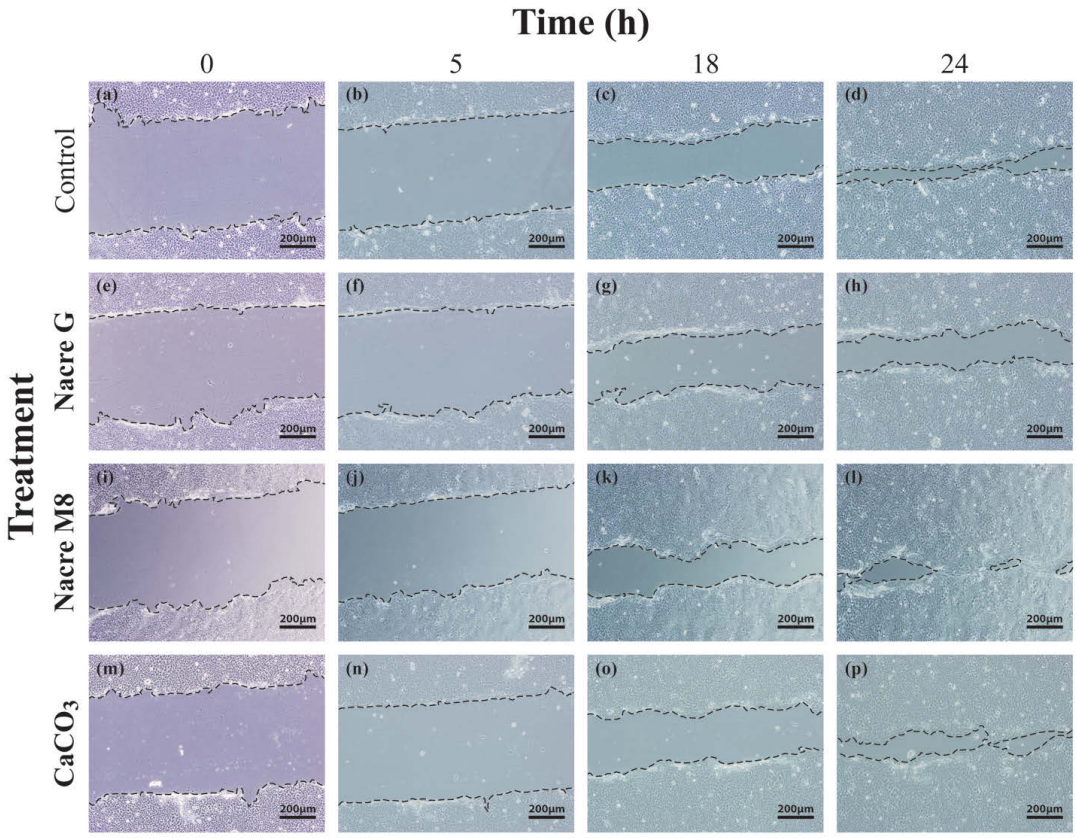

Figure 4.4. Representative images of scratch area on HaCaT cells at 0, 5, 18 and 24 hours. Dashed lines were made to better illustrate the artificial wound bed area, which was cell free. The cells at the wound margin from the top and bottom were proliferating and invading the wound bed area. The cell free area was measured at each time point and the area at time 0 was set as the 100% wound area.

Fig. 4.4 shows representative images of wound closure over the 24-hour post incubation period for a HaCaT scratch migration assay. Additionally, the wound closure rates of the triplicates are presented as mean ± SD in Fig. 4.5. There was no significant difference in HaCaT migration rate when the cells were treated with **Nacre G**, **Nacre M8** and **$CaCO_3$** at any time-point (two-way ANOVA; $p>0.05$)

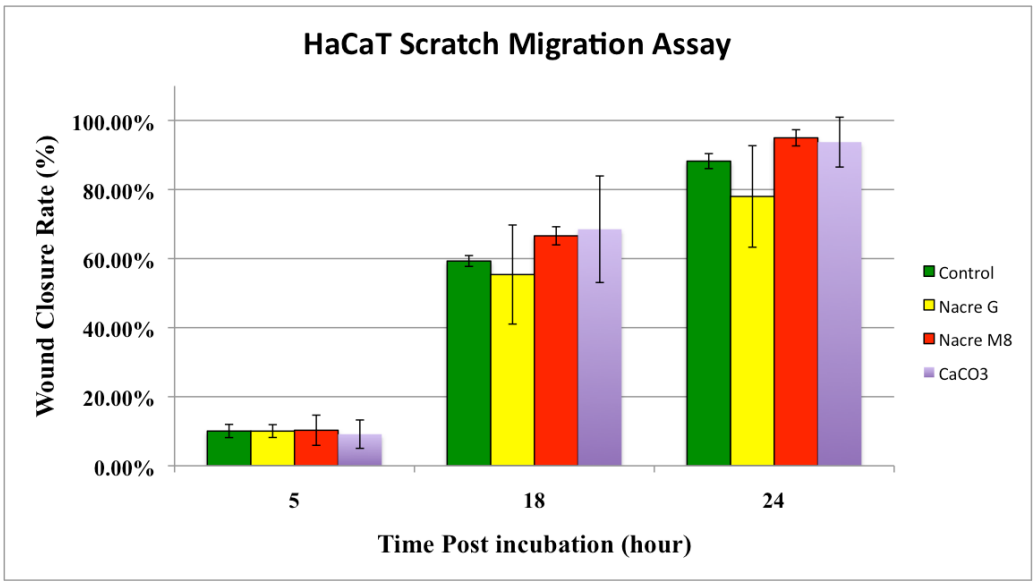

Figure 4.5. Wound closure rate of HaCaT keratinocytes treated with Nacre G, Nacre M8 and $CaCO_3$ in 24 hours post incubation. Error bars show standard deviation. Significance was set at * $p<0.05$

4.3.2. Scar-in-a-Jar Assay

Fig. 4.6 shows representative photographs of (a) collagen type I and (b) nuclei from Scar-in-a-Jar assay. The number of nuclei corresponds to the number of cells. Fig. 4.6a was then divided into 6 ROI and the orientation of the collagen in each ROI was evaluated using the OrientationJ Measure as shown by Fig. 4.7. The ellipse drawn in each ROI indicates the coherency of the collagen.

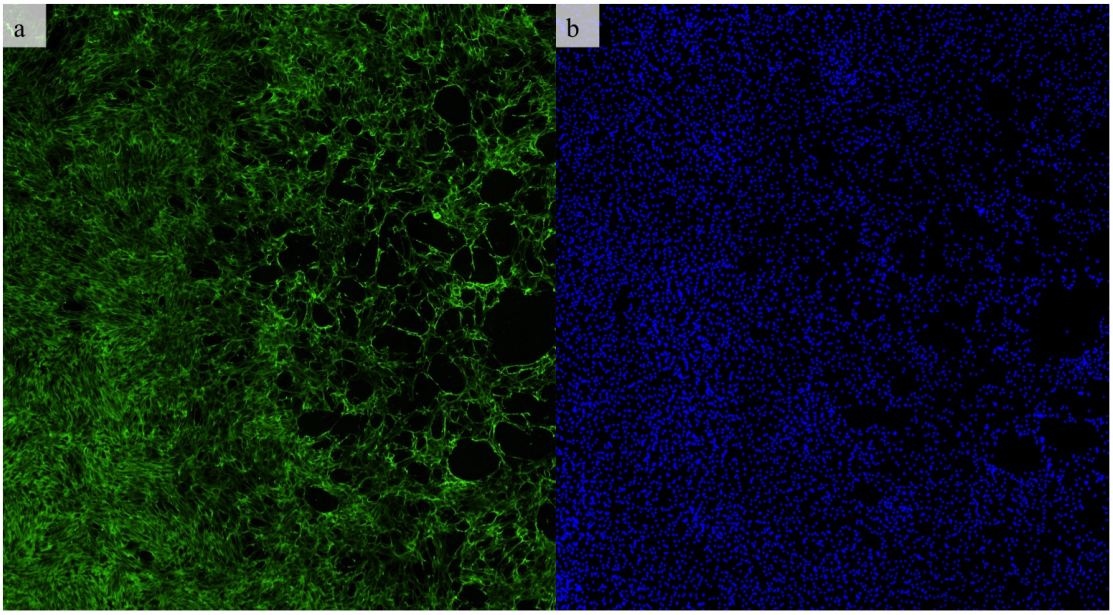

Figure 4.6. Representative images of (a) collagen type I and (b) nucleus.

Fig. 4.8 summarizes the amount of collagen per cell from the Scar-in-a-Jar assay. There was no significant different between Ficoll (the control under 'crowded' condition) and the normal Control. However, the amount of collagen/cell was significantly higher compared to Ficoll and Control when the cells were treated with the conditioned media of **Nacre M8** or **$CaCO_3$** (**Nacre M8**, 2083 $\pm$ 142 collagen/cell or **$CaCO_3$**, 2713 $\pm$ 386 collagen/cell vs Ficoll, 1125 $\pm$ 270 collagen/cell or Control, 951 + 335 collagen/cell, $p<0.05$). The amount of collagen/cell of the cells treated with the conditioned media of **$CaCO_3$** was also significantly higher than the ones treated with the conditioned media of **Nacre M8** (**$CaCO_3$**, 2713 $\pm$ 386 collagen/cell vs **Nacre M8**, 2083 $\pm$ 142 collagen/cell, $p<0.05$).

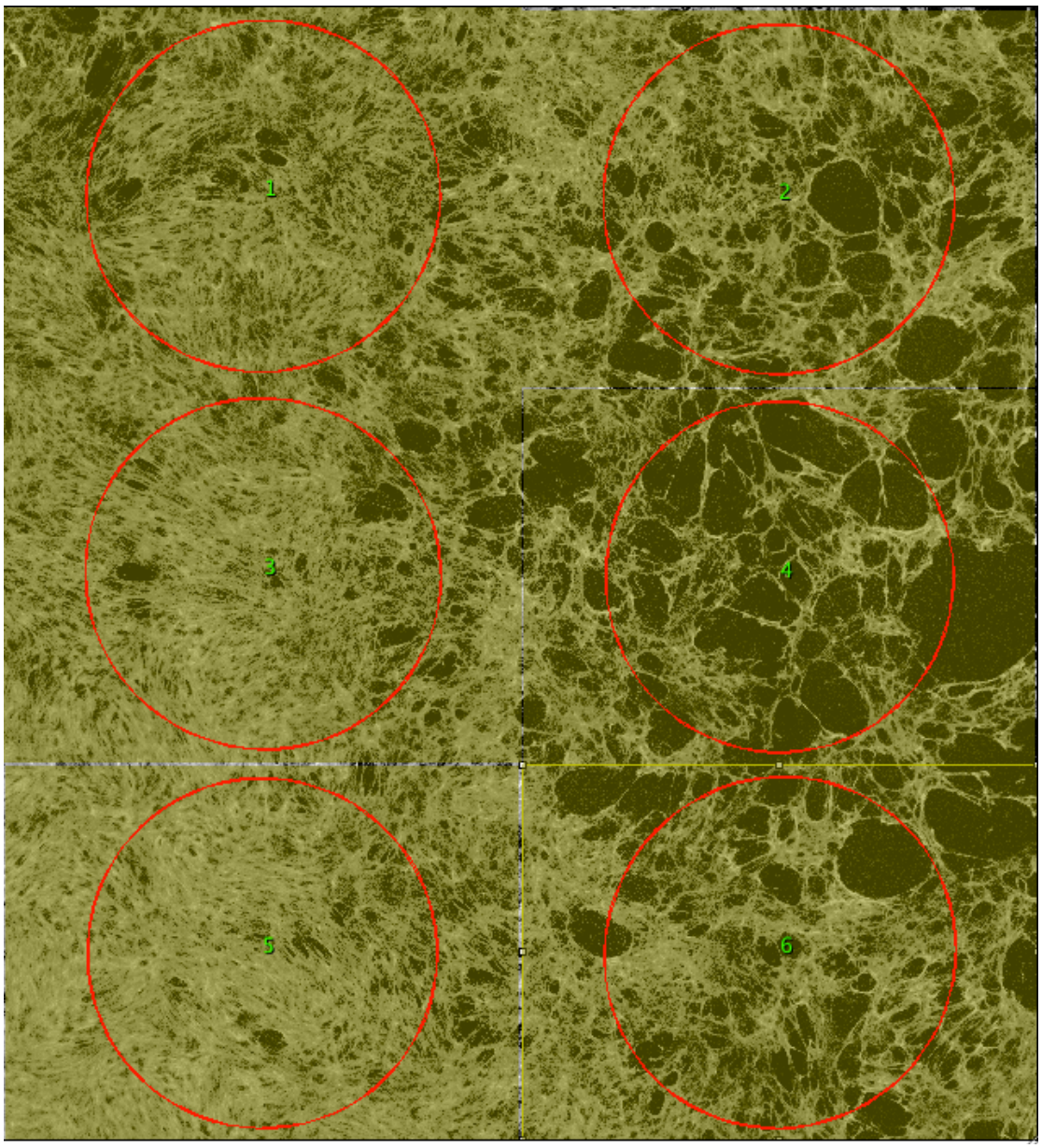

Figure 4.7. A representative image of the 6 smaller ROIs. The red ellipses indicate the coherency of the collagen in that particular ROI. The more circular the red ellipses, the better.

The coherency values are shown in Fig. 4.9. The collagen type I produced from the Ficoll crowded group and conditioned media of **$CaCO_3$** were significantly less coherent (less aligned) compared to the Control (p-value 0.0286, significance was set at $p<0.05$). Finally, Fig. 4.10 shows the overlay image from collagen image and nucleus image from a representative of each group.

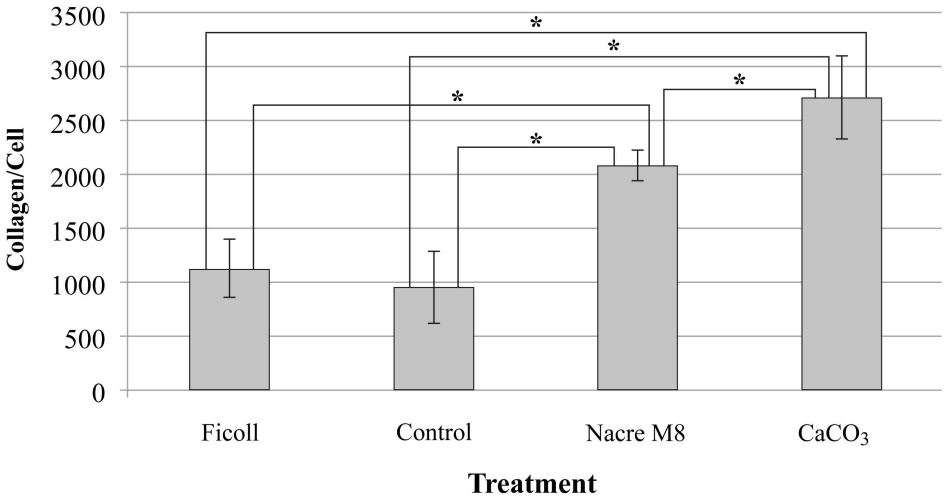

Figure 4.8. Amount of collagen per cell from scar-in-a-jar assay. Data is presented as mean ± SD. Significance was set at *p<0.05.

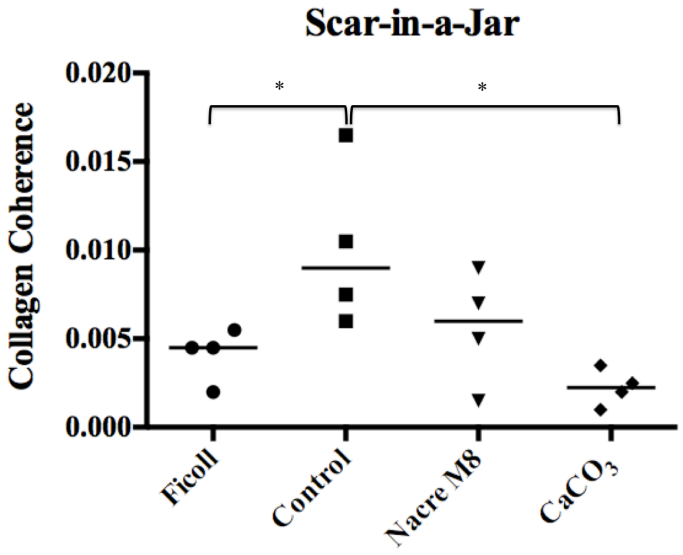

Figure 4.9. Coherence of collagen with different treatments. Data points represent replicates. Significance was set at * p<0.05. The lower the coherence value means that the architecture of the collagen is more random as in normal skin.

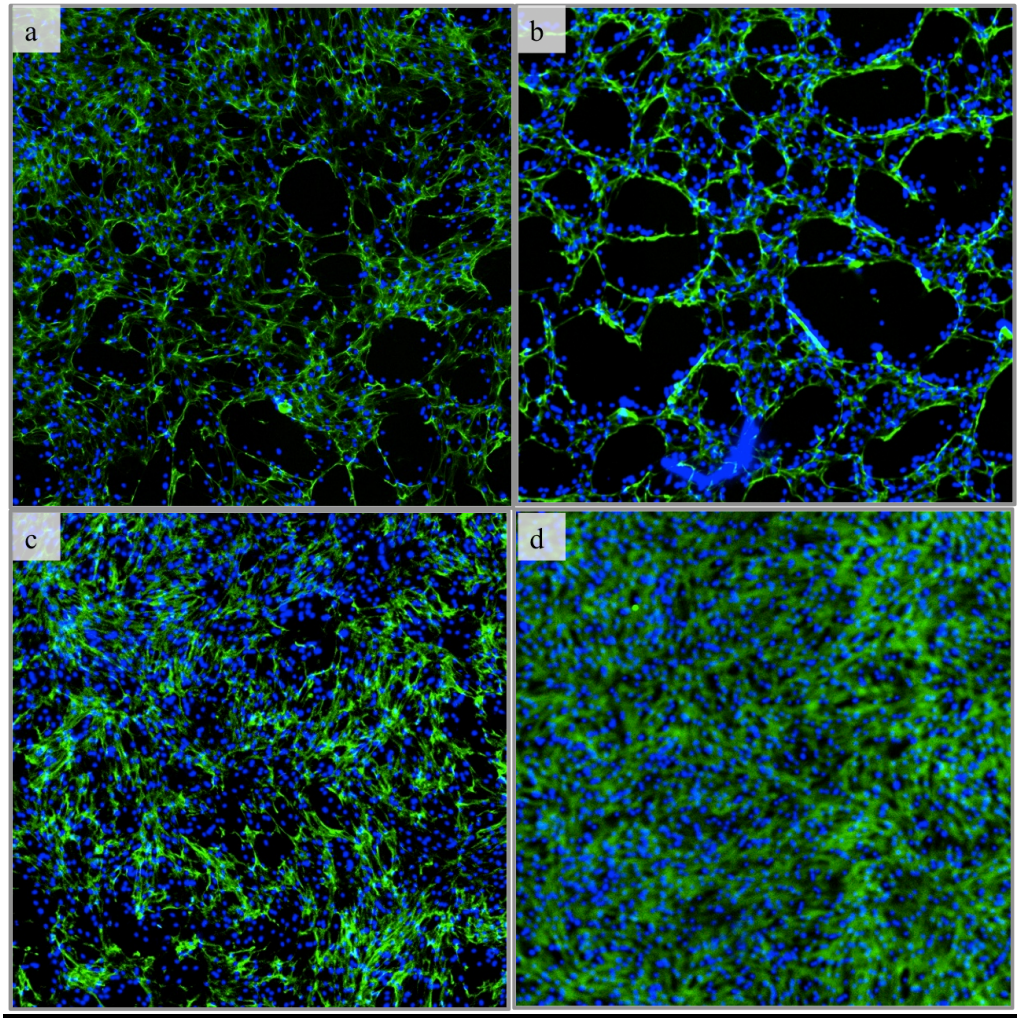

Figure 4.10. Overlay of nuclei and collagen images. a) Ficoll; b) Control; c) **Nacre M8** and d) **CaCO3**

4.4. Discussion

The key findings from the above studies can be summarized as follows:

1. The organic component of **Nacre M8** and **Nacre G** did not significantly increase the migration rate of either NIH/3T3 fibroblasts or HaCaT keratinocytes.

2. The organic component of **Nacre M8** as well as the conditioned media of **$CaCO_3$** significantly increased the amount of collagen type I deposited by primary dermal fibroblasts.

3. The conditioned media of **$CaCO_3$** reduced the collagen coherence significantly, but organic component of Nacre M8 failed to follow suit.

4.4.1. Nacre M8 and Nacre G do not affect skin cell migration rates

Despite prior evidence that the organic component of pearl nacre could improve the migration rate of human newborn foreskin fibroblasts (Hs68)[4], the results above (see section 4.3.1.1) showed that the prepared organic component in this study had no effect on migration. These findings are in line with the results from Lee et al. who showed that pearl extract did not affect NIH/3T3 fibroblast migration rates.[5] These conflicting outcomes might be due to the difference in the cell lines used in the studies. Hs68 fibroblasts are primary cells while NIH/3T3 fibroblasts are immortalized cells. The plausible explanation regarding different responses between primary and immortalized cells have been discussed earlier in section 3.4.2. Additionally, newborn foreskin fibroblasts and adult skin fibroblasts commonly produce different responses.[35] Adult skin fibroblasts, for example, grow at a slower rate than newborn foreskin fibroblasts.[36] Protein Kinase C-α that is known for its function in regulating cell proliferation also has higher activity in adult fibroblasts compared to foreskin fibroblasts.[37] Further, telomerase activity in newborn fibroblasts has been reported to be 16-fold higher than in adult fibroblasts ($p<0.05$).[38] Therefore, newborn fibroblasts may have an intrinsic potential to respond to external stimuli that is absent in adult fibroblasts. Since the purpose of this study is to assess possible therapeutic or cosmetic benefits of nacre the use of adult cells is more appropriate. Whilst WSM of nacre might exert an effect on newborn fibroblasts this is not relevant to the purposes of this study, as exemplified by the average age of a patient with a wound reported by the US Wound Registry which is 61.7 years.[39]

Besides the different types of fibroblasts used in the previous studies, the source of the pearl nacre could also attribute to these conflicting results. The pearl nacre used in the newborn foreskin fibroblasts was originated from a freshwater pearl oyster,

Hyriopsis cumingii Lea (Unionidae family).[4] Meanwhile, the study that was performed by Lee et al. and had similar results to the current study used pearl nacre from a saltwater pearl oyster *Pteria martensii*.[5] Both Pteria and Pinctada belong to the Pteriidae family. Additionally, Unionidae and Pteriidae families belong to Bivalvia class. Therefore, the oyster used in Lee et al. study is closer to the oyster used in the current study, *Pinctada margaritifera*. This habitat difference could result in chemical composition difference in the oyster shell, which in turn could dictate the effect of their organic components in the fibroblasts migration study. Gutmannsbauer and Hänni claimed that there is little chemical difference between saltwater and freshwater oyster, one of them is manganese (Mn).[40] Mn occurs in the shell of freshwater oyster, *Hyriopsis schlegelii*, as $MnCO_3$ and its oxides, but in the shell of saltwater oyster, *Pteria martensii*, it occurs as atomic Mn.[41]

Overall, after 24-hours post incubation, none of the fibroblast samples showed closure of more than 80% (see Fig. 4.3). In contrast, all of the keratinocyte groups except for those treated with **Nacre G** had mean closure at 24 hours of >80%. This is inconsistent with previous findings which claimed fibroblasts have a faster scratch closure rate than keratinocytes.[15] In these other studies, Walter et al. used L929 fibroblasts and HaCaT keratinocytes[15], while the current study used NIH/3T3 fibroblasts and HaCaT keratinocytes. Thus, the contradictory findings might be due to the different biochemical responses of L929 and NIH/3T3 fibroblasts. A comparative study of the two fibroblast cell lines would be a simple way to resolve this issue. In a pharmacological study, Clenbuterol, a long-acting β2-adrenoceptor agonist, induced significant increase of nerve growth factor (NGF) mRNA in 3T3 cells but not in L929 cells.[42] In addition Hardilová et al. have reported a stress response to silver by NIH/3T3 fibroblasts which was absent in L929 fibroblasts.[43] Therefore it is clear these two cell

lines have different phenotypes and this is therefore the most likely explanation for the difference in scratch closure rates in comparison to HaCaT cells observed.

There were no significant differences between Control and treated groups (**Nacre G**, **Nacre M8** and **$CaCO_3$** at any time point ($p>0.05$) for both NIH/3T3 fibroblasts and HaCaT keratinocytes as summarized in Figs 4.3 and 4.5 respectively. These results were supported with the findings in Chapter 3 (see Figs 3.7 and 3.8) that the treated groups did not have significantly higher number of living cells. It was then natural that the treated groups did not have significantly higher wound closure rate.

4.4.2. Calcium is important to stimulate collagen type I deposition

The cell culture 'crowded' with Ficoll did not deposit more collagen type I than the Control as expected (see Fig. 4.8). Meanwhile, the primary cells treated with the conditioned media of **Nacre M8** and **$CaCO_3$** produced significantly more collagen than both Ficoll and the Control (see Fig. 4.8).

Higher collagen production is potentially beneficial in the early stage of the wound healing process to accelerate extracellular matrix formation.[44] More rapid deposition of granulation tissue could enhance re-epithelialisation and lead to faster wound closure.[45] Figs 4.6 and 4.7 show the collagen production after 6 days post-stimulation. It is possible that the organic component of nacre contained in the conditioned media of **Nacre M8** stimulated expression of collagen. Thus, organic component of nacre from **Nacre M8** might be beneficial for wound healing.

In order to avoid scarring, collagen production at a later stage of wound healing should be balanced by up-regulation of collagenase expression to degrade any

excess.[46,47] If the high production of collagen (see Fig. 4.7) continued in the remodelling phase of wound healing, then scarring might be exacerbated. However, it is possible that the organic component of nacre could also stimulate collagen degradation or turnover *in vivo*. Therefore the effects of organic component of nacre on collagen turnover should be measured using other assays. For example, the level of collagen type I could also be measured using enzyme-linked immunosorbent assay (ELISA) through specific antibodies as described by De Scheerder et al.[48] Alternatively, the degradation products from collagen type I could be measured by Serum CrossLaps One Step ELISA.[49] An *in vivo* study is essential to get a holistic understanding of the effects of organic component of nacre on collagen metabolism.

It was surprising that the primary cells treated with the conditioned media of **$CaCO_3$** had significantly higher collagen production than those treated with the conditioned media of **Nacre M8** (see Fig. 4.8). Additionally, the conditioned media of **Nacre M8** was not decalcified so there was still some calcium in this media. The solubility product constant (Ksp) for calcite (**$CaCO_3$**) is $10^{-8.480}$ and for aragonite (**Nacre M8**) is $10^{-8.336}$.[50] Therefore, the data here suggests that calcium alone better stimulates collagen production than soluble nacre extract. Ca^{2+} is an important secondary messenger in wound healing.[51] The regulatory effect of Ca^{2+} and collagen synthesis has been well established[52], yet the specific pathway still needs to be elucidated.[53] Calcium alginate was reported to accelerate wound healing by up-regulating collagen type I synthesis and the ratio between collagen type I and type III in diabetic rats.[54] A study using chondrocytes revealed that increased extracellular Ca^{2+} induces collagen type X synthesis but not type II.[55] Furthermore, chondrocytes favour the synthesis of collagen type I rather than type II when Ca^{2+} from $CaCl_2$ is present at a concentration as low as 0.1 mM.[56] Dstomat et al. suggests that higher pH due to the

introduction of Ca^{2+} is favourable for TGF-β activation, which stimulates collagen synthesis.[53] Although Lee et al. have reported that calcium alone can facilitate collagen gene expression the same study also reported that WSM of nacre stimulated more production of collagen than calcium alone.[5] This finding contradicts the current finding (see Fig. 4.8). Lee et al. suggested that the superior stimulation by WSM is due to the synergistic effect between the calcium and other molecules contained in it that have not been characterized.[5] In Author's opinion, this suggestion should be nullified. Similar to the current study, Lee et al. used calcite as a positive control and as mentioned above Ksp of aragonite is higher compare to calcite.[5] Therefore at the same initial concentration, aragonite would have higher concentration of Ca^{2+} compare to calcite, which acted as a positive control. The level of Ca^{2+} in the media may therefore solely determine the beneficial effect of nacre extract.

These contradictory findings could also be attributed to the different species of oyster used in the studies, which results in the variation of the organic molecules. Lee et al. used *Pteria martensii*[5], while the current study used *Pinctada margaritifera*. According to the World Register of Marine Species, *Pteria martensii* is actually an obsolete name of *Pinctada imbricata*.[57] Temkin provides an extensive explanation regarding the divergence pattern between *P. margaritifera* and *P. imbricata* using ribosomal DNA sequences.[58] Nevertheless, there is no research to date that has examined the content of WSM from *P. imbricata* so no comparison could be made with the content of WSM from *P. margaritifera*. A future study could use the organic component of nacre from both species to investigate whether they produce similar results.

4.4.3. Calcium is important in maintaining the 'normal' architecture of collagen.

The scar-in-a-jar assay has shown that collagen type I production was significantly higher when the primary dermal fibroblasts were treated with the conditioned media of **Nacre M8** and **$CaCO_3$** (see Fig. 4.8). It has been reported previously that nacre could induce collagen production.[59] Moreover, it has been discussed in section 4.4.2 that when an increased rate of collagen production is not balanced with increased collagen degradation, there is an accumulation of collagen in the dermis.[46] This can be important in hypertrophic (poor) scar formation.[60] The arrangement of these newly synthesized collagen bundles determines the likelihood of scar formation. Collagen bundles in normal skin tissue have random orientation, whereas in scar tissue the orientation is parallel with each other.[61] The quantification of the orientation of the collagen bundles in the current study is summarized in Fig. 4.9. The chance of forming a scar increases with a coherence value higher than the control. From the data in Figs 4.9, it is apparent that the conditioned media of **Nacre M8** and **$CaCO_3$** are very unlikely to increase the likelihood of scar formation. The most striking result from the data is that the conditioned media of **$CaCO_3$** significantly decreased the coherence value. The coherency value of Ficoll was also significantly lower than the control group (see Fig. 4.9), but the collagen produced was not significantly higher than the control group (see Fig. 4.8). Additionally, as discussed above in section 4.4.2 both the conditioned media of **Nacre M8** and **$CaCO_3$** contains Ca^{2+}. Therefore, it seems that Ca^{2+} plays an important role in maintaining 'normal' collagen architecture.

It has been mentioned several times in Chapter 1 that pearl nacre has been claimed to possess anti aging effect by researcher or skin care companies.[62-66] One of the notable sign of aging is wrinkle and appearance of wrinkle is directly related with decreased amount of collagen.[67] Therefore, the findings of this study suggest that pearl

nacre is acceptable to be used as an ingredient for skin care or cosmetics as it significantly increased the amount of collagen produced. However, the same data also revealed that other form of calcium carbonate could deliver a better result than pearl nacre.

The data from Fig. 4.9 also suggests that calcite (**$CaCO_3$**) is a better choice than aragonite (**Nacre M8**) for wound healing application. **Nacre M8** increased the amount of collagen significantly and at the same time did not increase the chance of scar formation. Meanwhile, **$CaCO_3$** also increased the amount of collagen significantly and concurrently significantly decreased the chance of scar formation. The current results contradict previous finding by Lopez et al. that claimed the opposite.[59] Lopez et al. used nacre from *Pinctada maxima*, which is a close relative to *Pinctada margaritifera* that was used in the current study. Due to their genetic resemblance[68], the chance that their organic component contributes to these contradicting findings is low and hence not considered. A more plausible explanation is that Lopez et al. did the experiment *in vivo*, while the current study was performed *in vitro*. As *in vivo* study is one step closer for medical application to real patient, it is therefore important to follow up the current study in *in vivo* setting. Thus, the claim made by Lopez et al. might later be reconfirmed or negated.

4.5. Conclusion

The water-soluble matrix contained in the conditioned media of **Nacre M8** did not promote faster migration rate of either NIH/3T3 fibroblasts or HaCaT keratinocytes. Additionally, the data suggested that conditioned media of **$CaCO_3$** was a better candidate for wound healing than conditioned media of **Nacre M8** with its superior effect on collagen production and at the same time managing to lower the coherency of collagen. However, a follow up *in vivo* study is needed to validate the current finding.

4.6. References

1 Ferguson, M. W. J. & Sharon, O. K. Scar-Free Healing: From Embryonic Mechanisms to Adult Therapeutic Intervention. *Philosophical Transactions: Biological Sciences* **359**, 839-850, doi:10.2307/4142114 (2004).

2 Bédouet, L. et al. Proteomics Analysis of the Nacre Soluble and Insoluble Proteins from the Oyster Pinctada margaritifera. *Mar Biotechnol* **9**, 638-649, doi:10.1007/s10126-007-9017-1 (2007).

3 Jian-Ping, D. et al. Effects of pearl powder extract and its fractions on fibroblast function relevant to wound repair. *Pharmaceutical Biology* **48**, 122-127 (2010).

4 Li, Y.-C., Chen, C.-R. & Young, T.-H. Pearl extract enhances the migratory ability of fibroblasts in a wound healing model. *Pharmaceutical Biology* **51**, 289-297, doi:10.3109/13880209.2012.721130 (2013).

5 Lee, K. et al. Nacre-driven water-soluble factors promote wound healing of the deep burn porcine skin by recovering angiogenesis and fibroblast function. *Mol Biol Rep* **39**, 3211-3218, doi:10.1007/s11033-011-1088-4 (2012).

6 Latire, T. et al. Shell Extracts from the Marine Bivalve Pecten maximus Regulate the Synthesis of Extracellular Matrix in Primary Cultured Human Skin Fibroblasts. *PLoS ONE* **9**, 1-12, doi:10.1371/journal.pone.0099931 (2014).

7 Werner, S., Krieg, T. & Smola, H. Keratinocyte-Fibroblast Interactions in Wound Healing. *J Invest Dermatol* **127**, 998-1008 (2007).

8 Ehrlich, H. P. & Diez, T. Role for gap junctional intercellular communications in wound repair. *Wound Repair & Regeneration* **11**, 481, doi:10.1046/j.1524-475X.2003.11616.x (200

9 Kehe, K., Abend, M., Ridi, R., Peter, R. U. & van Beuningen, D. Tissue engineering with HaCaT cells and a fibroblast cell line. *Arch Dermatol Res* **291**, 600-605, doi:10.1007/s004030050461 (1999).

10 Lai, Y. et al. Activation of TLR2 by a Small Molecule Produced by Staphylococcus epidermidis Increases Antimicrobial Defense against Bacterial Skin Infections. *J Invest Dermatol* **130**, 2211-2221 (2010).

11 Squarize, C. H., Castilho, R. M., Bugge, T. H. & Gutkind, J. S. Accelerated Wound Healing by mTOR Activation in Genetically Defined Mouse Models. *PLoS ONE* **5**, e10643, doi:10.1371/journal.pone.0010643 (2010).

12 Ching, Y.-H., Sutton, T. L., Pierpont, Y. N., Robson, M. C. & Payne, W. G. The Use of Growth Factors and Other Humoral Agents to Accelerate and Enhance Burn Wound Healing. *Eplasty* **11**, e41 (2011).

13 Hostanska, K., Rostock, M., Melzer, J., Baumgartner, S. & Saller, R. A homeopathic remedy from arnica, marigold, St. John‚Äôs wort and comfrey accelerates in vitro wound scratch closure of NIH 3T3 fibroblasts. *BMC Complementary and Alternative Medicine* **12**, 100-100, doi:10.1186/1472-6882-12-100 (2012).

14 Fronza, M., Heinzmann, B., Hamburger, M., Laufer, S. & Merfort, I. Determination of the wound healing effect of Calendula extracts using the scratch assay with 3T3 fibroblasts. *Journal of Ethnopharmacology* **126**, 463-467, doi:http://dx.doi.org/10.1016/j.jep.2009.09.014 (2009).

15 Walter, M. N. M., Wright, K. T., Fuller, H. R., MacNeil, S. & Johnson, W. E. B. Mesenchymal stem cell-conditioned medium accelerates skin wound healing: An in vitro study of fibroblast and keratinocyte scratch assays. *Experimental Cell Research* **316**, 1271-1281, doi:http://dx.doi.org/10.1016/j.yexcr.2010.02.026 (2010).

16 Loo, A. E. K., Ho, R. & Halliwell, B. Mechanism of hydrogen peroxide-induced keratinocyte migration in a scratch-wound model. *Free Radical Biology and*

Medicine **51**, 884-892, doi:http://dx.doi.org/10.1016/j.freeradbiomed.2011.06.001 (2011).

17 Ranzato, E., Patrone, M., Pedrazzi, M. & Burlando, B. HMGb1 promotes scratch wound closure of HaCaT keratinocytes via ERK1/2 activation. *Mol Cell Biochem* **332**, 199-205, doi:10.1007/s11010-009-0192-4 (2009).

18 Ranzato, E., Patrone, M., Mazzucco, L. & Burlando, B. Platelet lysate stimulates wound repair of HaCaT keratinocytes. *British Journal of Dermatology* **159**, 537-545, doi:10.1111/j.1365-2133.2008.08699.x (2008).

19 Phan, T.-T., Sun, L., Bay, B.-H., Chan, S.-Y. & Lee, S.-T. Dietary Compounds Inhibit Proliferation and Contraction of Keloid and Hypertrophic Scar-Derived Fibroblasts In Vitro: Therapeutic Implication for Excessive Scarring. *The Journal of Trauma: Injury, Infection, and Critical Care* **54**, 1212-1224, doi:10.1097/01.TA.0000030630.72836.32 (2003).

20 Gelse, K., Pöschl, E. & Aigner, T. Collagens--structure, function, and biosynthesis. *Advanced Drug Delivery Reviews* **55**, 1531-1546, doi:http://dx.doi.org/10.1016/j.addr.2003.08.002 (2003).

21 Hubert, T., Grimal, S., Carroll, P. & Fichard-Carroll, A. Collagens in the developing and diseased nervous system. *Cell. Mol. Life Sci.* **66**, 1223-1238, doi:10.1007/s00018-008-8561-9 (2009).

22 Ivanova, V. P. & Krivchenko, A. I. A current viewpoint on structure and evolution of collagens. I. Fibrillar collagens. *J Evol Biochem Phys* **48**, 127-139, doi:10.1134/s0022093012020016 (2012).

23 Ross, R. & Benditt, E. P. Wound Healing and Collagen Formation. I. Sequential Changes in Components of Guinea Pig Skin Wounds Observed in the Electron Microscope. *The Journal of Biophysical and Biochemical Cytology* **11**, 677-700, doi:10.2307/1603837 (1961).

24 Friedman, D. W. et al. Regulation of Collagen Gene Expression in Keloids and Hypertrophic Scars. *Journal of Surgical Research* **55**, 214-222, doi:http://dx.doi.org/10.1006/jsre.1993.1132 (1993).

25 van Zuijlen, P. P. M. et al. Collagen morphology in human skin and scar tissue: no adaptations in response to mechanical loading at joints. *Burns* **29**, 423-431, doi:10.1016/s0305-4179(03)00052-4 (2003).

26 Chaturvedi, R., Singha, P. K. & Dey, S. Water Soluble Bioactives of Nacre Mediate Antioxidant Activity and Osteoblast Differentiation. *PLoS ONE* **8**, 1-1, doi:10.1371/journal.pone.0084584 (2013).

27 Chen, C. Z. C. et al. The Scar-in-a-Jar: studying potential antifibrotic compounds from the epigenetic to extracellular level in a single well. *British Journal of Pharmacology* **158**, 1196-1209, doi:10.1111/j.1476-5381.2009.00387.x (2009).

28 Boukamp, P. et al. Normal keratinization in a spontaneously immortalized aneuploid human keratinocyte cell line. *The Journal of Cell Biology* **106**, 761-771 (1988).

29 Fusenig, N. E. & Boukamp, P. Multiple stages and genetic alterations in immortalization, malignant transformation, and tumor progression of human skin keratinocytes. *Molecular Carcinogenesis* **23**, 144-158, doi:10.1002/(sici)1098-2744(199811)23:3<144::aid-mc3>3.0.co;2-u (1998).

30 Jainchill, J. L., Aaronson, S. A. & Todaro, G. J. Murine Sarcoma and Leukemia Viruses: Assay Using Clonal Lines of Contact-Inhibited Mouse Cells. *Journal of Virology* **4**, 549-553 (1969).

31 Liang, C.-c., Park, A. Y. & Guan, J.-l. In vitro scratch assay: a convenient and inexpensive method for analysis of cell migration in vitro. *Nature Protocols* **2**, 329-333, doi:http://dx.doi.org/10.1038/nprot.2007.30 (2007).

32 Abramoff, M. D., Magalhaes, P. J. & Ram, S. J. Image processing with image-j. *Biophotonics International* **11**, 36-42 (2004).
33 Lareu, R. R., Arsianti, I., Harve Karthik, S., Peng, Y. & Raghunath, M. In Vitro Enhancement of Collagen Matrix Formation and Crosslinking for Applications in Tissue Engineering: A Preliminary Study. *Tissue Engineering* **13**, 385-391, doi:http://dx.doi.org/10.1089/ten.2006.0224 (2007).
34 Rezakhaniha, R. et al. Experimental investigation of collagen waviness and orientation in the arterial adventitia using confocal laser scanning microscopy. *Biomech Model Mechanobiol* **11**, 461-473, doi:10.1007/s10237-011-0325-z (2012).
35 Igarashi, A., Takehara, K., Soma, Y., Kikuchi, K. & Ishibashi, Y. Mitogenic activities for skin fibroblasts in the sera from untreated scleroderma patients at the early stage. *Arch Dermatol Res* **281**, 383-386, doi:10.1007/bf00455321 (1989).
36 Praeger, B. In-vitro studies of aging. *Dermatologic Clinics* **4**, 359-369 (1986).
37 Woo Choi, S., Park, H.-Y., Rubeiz, N. G., Sachs, D. & Gilchrest, B. A. Protein kinase C-α levels are inversely associated with growth rate in cultured human dermal fibroblasts. *Journal of Dermatological Science* **18**, 54-63, doi:http://dx.doi.org/10.1016/S0923-1811(98)00025-5 (1998).
38 Betts, D. H. et al. Reprogramming of telomerase activity and rebuilding of telomere length in cloned cattle. *Proceedings of the National Academy of Sciences of the United States of America* **98**, 1077-1082 (2001).
39 Fife, C. E., Carter, M. J., Walker, D. & Thomson, B. Wound Care Outcomes and Associated Cost Among Patients Treated in US Outpatient Wound Centres. *Wounds* **24**, 10-17 (2012).
40 Gutmannsbauer, W. & Hänni, H. Structural and chemical investigations on shells and pearls of naacre forming salt- and fresh-water bivalve molluscs. *Journal of Gemmology* **24**, 241-252 (1994).
41 Horiguchi, Y. Biochemical studies on Pteria (Pintada) martensii (Dunker) and Hyriopsis schlegelii (v. Martens) -X. on the chemical states of Mn in shell. *Bulletin of the Japanese Society of Scientific Fisheris* **25**, 675-679 (1959).
42 Samina Riaz, S. & Tomlinson, D. R. Pharmacological modulation of nerve growth factor synthesis: a mechanistic comparison of vitamin D receptor and beta(2)-adrenoceptor agonists. *Molecular Brain Research* **85**, 179-188, doi:http://dx.doi.org/10.1016/S0169-328X(00)00254-0 (2000).
43 Hardilová, Š., Havrdová, M., Panáček, A., Kvítek, L. & Zbořil, R. Hsp70 as an indicator of stress in the cells after contact with nanoparticles. *Journal of Physics: Conference Series* **617**, doi:10.1088/1742-6596/617/1/012023 (2015).
44 Schäfer, M. & Werner, S. Transcriptional Control of Wound Repair. *Annual Review of Cell and Developmental Biology* **23**, 69-92, doi:doi:10.1146/annurev.cellbio.23.090506.123609 (2007).
45 Li, W. et al. The p38-MAPK/SAPK Pathway is Required for Human Keratinocyte Migration on Dermal Collagen. *J Investig Dermatol* **117**, 1601-1611, doi:10.1046/j.0022-202x.2001.01608.x (2001).
46 Linares, H. A. From wound to scar. *Burns* **22**, 339-352, doi:http://dx.doi.org/10.1016/0305-4179(95)00164-6 (1996).
47 Renò, F. et al. In vitro mechanical compression induces apoptosis and regulates cytokines release in hypertrophic scars. *Wound Repair and Regeneration* **11**, 331-336, doi:10.1046/j.1524-475X.2003.11504.x (2003).
48 De Scheerder, I., De Buyzere, M., Delanghe, J., Robbrecht, J. & Clement, D. L. New ELISA methods for the determination of antibodies against collagen type I, III and IV. *Z. Anal. Chem.* **330**, 349-349, doi:10.1007/bf00469271 (1988).

49 Rosenquist, C. et al. Serum CrossLaps One Step ELISA. First application of monoclonal antibodies for measurement in serum of bone-related degradation products from C-terminal telopeptides of type I collagen. *Clinical Chemistry* **44**, 2281-2289 (1998).

50 Plummer, L. N. & Busenberg, E. The solubilities of calcite, aragonite and vaterite in CO2-H2O solutions between 0 and 90¬∞C, and an evaluation of the aqueous model for the system $CaCO_3$-CO2-H2O. *Geochimica et Cosmochimica Acta* **46**, 1011-1040, doi:http://dx.doi.org/10.1016/0016-7037(82)90056-4 (1982).

51 Lansdown, A. B. G. Calcium: a potential central regulator in wound healing in the skin. *Wound Repair and Regeneration* **10**, 271-285, doi:10.1046/j.1524-475X.2002.10502.x (2002).

52 Dietrich, J. W. & Duffield, R. Effects of the Calcium Antagonist Verapamil on *in Vitro* Synthesis of Skeletal Collagen and Noncollagen Protein. *Endocrynology* **105**, 1168-1172, doi:http://dx.doi.org.ezproxy.library.uwa.edu.au/10.1210/endo-105-5-1168 (1979).

53 Dstomat, A. J., Gutmann, J. L., Witherspoon, D. E. & Harper, R. P. Effects of Calcium Hydroxide and Tumor Growth Factor-β on Collagen Synthesis in Subcultures I and V of Osteoblasts. *Journal of Endodontics* **26**, 494-499, doi:http://dx.doi.org/10.1097/00004770-200009000-00002 (2000).

54 Wang, T. et al. Calcium alginate enhances wound healing by up-regulating the ratio of collagen types I/III in diabetic rats. *International Journal of Clinical and Experimental Pathology* **8**, 6636-6645 (2015).

55 Bonen, D. K. & Scmid, T. M. Elevated extracellular calcium concentrations induce type X collagen synthesis in chondrocyte cultures. *The Journal of Cell Biology* **115**, 1171-1178 (1991).

56 Deshmukh, K. & Sawyer, B. D. Synthesis of collagen by chondrocytes in suspension culture: modulation by calcium, 3':5'-Cyclic AMP, and Prostaglandins. *Proceedings of the National Academy of Sciences of the United States of America* **74**, 3864-3868 (1977).

57 WoRMS. *Pinctada Röding, 1798* <http://www.marinespecies.org/aphia.php?p=taxdetails&id=138396> (2015).

58 Temkin, I. Molecular phylogeny of pearl oysters and their relatives (Mollusca, Bivalvia, Pterioidea). *BMC Evolutionary Biology* **10**, 342 (2010).

59 Lopez, E., Faou, A. L., Borzeix, S. & Berland, S. Stimulation of rat cutaneous fibroblasts and their synthetic activity by implants of powdered nacre (mother of pearl). *Tissue and Cell* **32**, 95-101, doi:10.1054/tice.1999.0091 (2000).

60 Anitha, B., Ragunatha, S. & Inamadar, A. Scars in dermatology: Clinical significance. *Indian Journal of Dermatology, Venereology and Leprology* **74**, 420-423 (2008).

61 Garner, W. L. et al. Hypertrophic scar fibroblasts accelerate collagen gel contraction. *Wound Repair and Regeneration* **3**, 185-191, doi:10.1046/j.1524-475X.1995.30210.x (1995).

62 Cao, G., Xu, Z., Wei, H., Yao, S. & Liu, Y. Pearl and mother-of-pearl powder in health-care. *Chin Pharm J* **21**, 635-638 (1996).

63 Lorac. *Lorac Couture Shine Liquid Lipstick*, 2015).

64 HydroPeptide. *Eye Authority: Dark Circles, Puffines, Fine Lines* <http://shop.hydropeptide.com/eye-authority#.Vh5qqChJUfz> (2015).

65 Oriflame. *Giordani Gold Bronzing Pearls*, <http://in.oriflame.com/products/product?code=21632> (2015).

66 SIRCUIT®. *SWELL Ocean Cooling Mask*, <http://sircuitskin.com/inc/sdetail/32524/45981> (2015).

67 Takema, Y., Hattori, M. & Aizawa, K. The relationship between quantitative changes in collagen and formation of wrinkles on hairless mouse skin after chronic UV irradiation. *Journal of Dermatological Science* **12**, 56-63, doi:http://dx.doi.org/10.1016/0923-1811(95)00467-X (1996).

68 Cunha, R., Blanc, F., Bonhomme, F. & Arnaud-Haond, S. Evolutionary Patterns in Pearl Oysters of the Genus *Pinctada* (Bivalvia: Pteriidae). *Mar Biotechnol* **13**, 181-192, doi:10.1007/s10126-010-9278-y (2011).

Chapter 5

Chapter 5: General Discussion

5.1. Overview of research

Skin is the largest organ in the body.[1] Restoring wounded skin to its original state is a major challenge because adult skin does not have the capability to regenerate but heals by a reparative process resulting in scars.[2-4] Therefore, an exogenous intervention is required to improve repair and reduce scar formation. Additionally, wrinkled skin is a visible sign of aging which is caused by collagen deficiency.[5] There are many claims made by the cosmetics or skin care industry that their products could delay or even reverse this aging process.[6-8] However, these companies rarely provide scientific evidence that can support their claims. There are also many procedures offered by medical clinics to combat aging but the efficacy is arguable.[9]

Nacre or mother-of-pearl has been under scrutiny in the last decade for its efficacy for anti aging and wound healing. This study hypothesised that nacre contains organic and/or inorganic elements that are beneficial either for cosmetic use or to enhance wound healing. Despite the wide use of nacre in research there is no protocol to prepare nacre that is universally accepted. Additionally, there is no study to date that address the safety of nacre for skin. Therefore, Chapter 2 established a standardised protocol to prepare nacre using ball milling. The toxicity of nacre produced through ball milling was tested on HaCaT and NIH/3T3 cell lines and addressed in Chapter 3. Prepared nacre was further tested for its efficacy using two functional assays in Chapter 4, namely, scratch migration and scar-in-a-jar assays.

5.1.1. Summary of results

In this study, a paper describing a standardised protocol to generate nacre powder with a unimodal particle size distribution has been published.[10] The nacre powder does not inhibit the growth of HaCaT or NIH/3T3 cells. The powder also does not elevate the level of reactive oxygen species in the cell cultures. Therefore, nacre prepared using the ball milling protocol does not appear to be toxic and is likely to be safe when applied to skin. The organic component of nacre did not increase the migration rate of HaCaT or NIH/3T3 cells. The data from scar-in-a-jar assay suggested that Ca^{2+} increased collagen production significantly and at the same time maintain a more "normal" architecture. This may be beneficial in wound healing and/or cosmetic applications.

5.2. Limitations and Strengths of this Study

5.2.1. Limitations

The current study considers nacre tablets as pure aragonite[10,11], instead of as a composite of nano-grains of aragonite and organic matrix.[12,13] This limitation might have implications for the interpretation of the results in Chapter 3 which involved **Nacre I that** was assumed to be pure aragonite. Consequently, the only difference between **Nacre I** and **Nacre G**, **Nacre M8** or **Nacre M11** was the concentration of organic component.

5.2.1.1. Nacre Preparations

There are three limitations in this study that might directly or indirectly affect the results in the subsequent chapters. The first limiting factor is the high temperature of the ball milling process. Heat is one of the common causes of protein denaturation. Many proteins will denature at 41 °C.[14] The temperature of the grinding bowl could reach 93 °C at the end of the ball milling process. Considering that the temperature of the habitat

of *Pinctada margaritifera* that ranges between 23 – 26 °C[15] it seems unlikely that the proteins could survive the heat generated during the ball milling process. However, Bourrat et al. claimed that nacre is stable up to 230 °C and degradation of the organic component did not occur until the temperature reached at least 250 °C.[16] The ball milling apparatus used in this study was not equipped with internal thermometer to measure the temperature during the ball milling process. Despite the stability of nacre, the Author of this thesis suggests that the ball milling process be carried out at low temperatures to prevent explosion hazards.

Another limitation is that organic components from the matrix may also have been washed away during the recovery process. This may explain the low protein content of the conditioned media of **Nacre M8** which is only about 58.2 μg/mL (see section 3.3.2), while another study showed that the organic component contained up to 1 mg/mL.[17] This loss could have been prevented if the milling was performed under dry conditions. However, dry milling was not recommended due to the unknown health hazard of airborne nanoparticles.[18-20] The incomplete organic matrix might then limit the potential of **Nacre M8** water-soluble matrix in wound healing if prepared using this method. **Nacre M8** is the least contaminated preparation through ball milling (see section 3.2.1.2). Therefore other methods of preparation for the organic matrix, such as decalcification with weak acid or adding EDTA[21], will need to be further investigated.

5.2.1.2. Toxicity Testing

The main limiting factor for the toxicity study was the use of immortalized cell lines rather than primary cells. It would have provided important additional data to use primary keratinocytes and primary fibroblasts in the study as they might give different

responses. The differences between primary cells and these cells line have been discussed in more detail in section 3.4.2.

Another limiting factor was the lack of identification of active compound in the conditioned media. The preparation of the conditioned media could also be improved with a concentration step by centrifugation. The possibility of bacterial and fungal contamination was not considered in the current study. The prepared nacre powder was not disinfected prior to use in experiments. Green et al. described a simple disinfection method using antibiotic and anti-mycotic solution.[22] This should be applied for the toxicity testing as well as the functional assays.

Change of pH was not considered an important factor in the current study due to low solubility of calcium carbonate in general as dictated by the solubility product constant (Ksp) of calcite ($10^{-8.480}$) and aragonite ($10^{-8.336}$).[23]

5.2.1.3. Functional Assays

The major limiting factor for scratch migration and scar-in-a-jar assays is the lost fraction of organic components during the nacre preparation process (discussed above in section 5.1.2.1). This lost fraction might also underpin the conflicting results between the current study and the previous published study discussed in section 4.4.2. Lee et al. claimed that WSM of nacre promotes higher production of collagen than calcium alone[24], whereas the data in section 4.3.2 found otherwise. Using only one oyster species as the source of nacre is another limitation since differences between species, particularly in the organic components of the matrix, may make findings species specific rather than widely applicable. Another limitation is that there was only one culture of primary dermal fibroblasts used in the study. Using multiple primary cell

cultures is necessary to give a more accurate indication of individual variation, which is common and an important aspect of patient responses to any treatment.[25,26] As there is significant genetic variability between humans it is critical to test multiple primary cells from different individuals to determine the frequency of the response to treatment. Furthermore, in the scar-in-a-jar assay lower amount of collagen might have higher coherence value which actually only reflects collagen deficiency rather than increased parallelism of the collagen bundles.

5.2.2. Strengths

5.2.2.1. Nacre Preparations

As discussed in Chapter 2, the potential effect of modulating each parameter (volume of excipient, sample size, grinding ball size, number of balls, speed and duration) related to the ball milling process was systematically investigated in this study. This is a significant strength of the research presented here and will facilitate future studies on nacre processing with the impact on preparation of the many parameters now described. Finally, this study has also shown that varying the ball milling operating parameters can generate a product with minimal contamination of heavy metals.

5.2.2.2. Toxicity Testing

The major strength of this study is the agreement between the different tests used that demonstrate nacre is safe for skin. Following systematic literature reviews, to my knowledge no previous study has investigated the potential toxicity of nacre. Therefore, the findings from this study provide important preliminary data for further research and for the use of nacre in cosmetics or therapeutics.

5.2.2.3. Functional Assays

The main strength of this study is that this is the first to investigate the effects of nacre WSM on collagen deposition and the architecture of deposited collagen. The data from this study suggest that the Ca^{2+} is the key to the potential effects of nacre on collagen deposition. This finding suggests that the actual benefits of using nacre may be limited and that the use of cheaper alternatives as the source of Ca^{2+} may be feasible. Further studies using more patients are required to validate this claim.

5.3. Significance of these findings and relevance to the field

5.3.1. Principles defined in Chapter 2 could be used as a template for upscaling to industrial production

There are many cosmetics in the market that contain nacre powder as mentioned in section 1.2.4. In the United States, nacre is listed as mother-of-pearl (MOP) in the International Nomenclature Cosmetic Ingredient (INCI) of the Personal Care Products Council (previously known as Cosmetic, Toiletry and Fragrance Association-CTFA). It could be assumed that safety studies on nacre are required for the purpose of obtaining INCI accreditation. However, the study is not published and access to it requires an annual fee of between $995 and $8,750.[27] Meanwhile, there have been many attempts to use nacre for therapeutic purposes either for skin or bone related issues.[24,28-33] The safety study performed to obtain INCI accreditation is probably only for cosmetics and not medical purposes. Additionally, there are also very few regulations that dictate the permissible amount of heavy metals in cosmetics (see section 3.1).

The current study is the first to investigate the quality of nacre powder produced by ball milling. It has been discussed in Chapter 2 that using pearl oyster from pristine water could solve the concerns regarding heavy metal contamination due to

environmental pollution. At the same time, a more prominent source of heavy metal contamination is potentially the ball milling process. The principles described in Chapter 2 regarding the effects of modulating each parameter on product contamination and particle distribution could be applied by the cosmetics industry to deliver uncontaminated nacre powder for use in cosmetics.

5.3.2. Isolation of the organic component of nacre in its native state.

The ball milling process has been proven to be effective to generate nacre powder.[10] However, this was at the expense of denatured proteins due to the high temperature during the process. Fractions of the organic component of nacre have been shown to be an important biological factor for osteogenesis both *in vitro* and *in vivo*.[34] Unfortunately, there was no mention regarding what were the controls in their studies. Chaturvedi et al. only used untreated cells as control when they made a claim that organic component of nacre mediates antioxidant activity and osteoblast differentiation.[29] Therefore, there is a chance that other source of calcium could also deliver the same result or even better as in the current scar-in-a-jar assay. Moreover, in their wound healing study Lee et al. claimed that the calcium control by itself could catalyze fibroblast proliferation and type I collagen synthesis but it could be significantly increased when combined with the organic components of nacre.[24] Therefore, it is deemed necessary to isolate the organic component of nacre in its native state.[35] This may also help to explain the morphological differences and the phylogenetic relationships between different oyster species.[35] The active compound that is responsible for producing the beneficial effects in bone or skin could then later be identified from this pool of organic molecules.

The simplest way to extract the organic component of nacre is with water.[36] As the name suggests the macromolecules extracted through this method are restricted to the water-soluble components of the matrix. However, some proteins that are still trapped in the 'brick and mortar' structure cannot be extracted through this method, as well as any water insoluble factors. The most common method to isolate the organic components of nacre is through decalcification using EDTA, acetic acid or another weak acid.[36] However, this acidic environment might also denature some proteins or break the quaternary structure of certain proteins. Zhang et al. has introduced an undecalcification extraction process of nacre protein using phosphate buffer (pH 7.0).[37] A matrix protein, p10, was extracted through this process and later crystallised.[37] The limitation of this method is similar with the first two methods, namely, only the water-soluble molecules are extracted. Rousseau et al. investigated the effect of nacre lipids on stratum corneum and for their study nacre lipids were extracted using a mixture of chloroform/ethanol (2:1) at a concentration of 500 mg/mL for nacre powder.[33] This method could fill in the gap to extract the water insoluble molecules. In order to simplify the extraction process, Boulos et al. developed an extraction method using an ionic liquid, *n*-butyl-3-methylimidazolium hexafluorophosphate [BMIM][PF_6].[11] The ionic liquid dissolves the organic matrix of nacre at room temperature and then the aragonite nacre tablets can be recovered leaving the complete organic matrix in the ionic liquid.[11] The remaining challenge is how to separate the ionic liquid from the organic matrix. If the ionic liquid could be recovered, the theoretical leftover is a complete organic matrix. Then, an active compound could be identified from this pool of organic matrix.

5.3.3. Optimizing the use of ball-milled nacre for cosmetics purposes.

As mentioned in Chapter 1, the general public is led to believe that the pearl nacre contained in the cosmetics will make their skin glow as the pearl is iridescent. The lustre from pearl nacre is a result of the 'brick and mortar' structure of the inorganic aragonite tablets and organic matrix.[38] The incoming light to the 'brick and mortar' structure is diffracted and this diffraction creates the iridescence colour.[39] Furthermore, the strength of the iridescence colour is determined by the smoothness of the surface and the width of the groove.[39] A rough surface will produce less diffraction and the smaller width will produce stronger diffraction.[39] The outer surface of the shell has grooves with smaller width compare to the inner layer, thus it produces stronger diffraction.[39] If this outer surface is polished, the diffraction produced will be even better.[39] Therefore, if the 'brick and mortar' structure is broken down, as in the case of nacre powder, the lustre will no longer be evident.

Direct observation during preparation of nacre found that nacre from the shell still retained its lustre after being ground with mortar and pestle, i.e. **Nacre G**. However, nacre lost its lustre after being ball milled. Using the knowledge gained from Chapter 2, it will be possible to adjust the parameters for ball milling to obtain nacre powder within the desirable size range that is still lustrous. As mentioned in Chapter 2, the size of nacre tablets ranges from 5 – 15 μm.[40] It has also been reported that if the width of the groove exceeds 11.5 μm, then no iridescence colour will be produced.[39] In this case, the width of the groove can be interpreted as the size of aragonite tablet. So, in order to simplify the calculation the size of the nacre tablet is limited to 10 μm. The thickness of the tablet ranges between 0.3 – 0.5 μm dependent on species.[41] If it is assumed that the minimum criteria are 3 tablets and 2 layers to allow diffraction to occur, the desirable size range of nacre particles is between 15 – 30 μm with a thickness

less than 1 μm. The parameters setting to prepare **Nacre M8** could be used with speed reduction to 350 or 300 rpm. Nacre M8 was prepared at 400 rpm, so speeds higher than 400 rpm is more likely to produce a finer particle than 5 – 15 μm, whereas speeds of up to 200 rpm were proven to require a much longer time to obtain high yield.

If adapting the ball milling process is successful, there will be no further need to add mica and/or other silica compounds into cosmetic products to provide the same effect as the nacre particles used will retain their natural lustre. This will improve the products and reduce the risk involved in using relatively untested compounds such as mica and/or other silica compounds in cosmetics on the skin. Other work has indicated that continuous exposure to mica dust could result in pneumoconiosis.[42] Furthermore, a study of the effect of mica on cultured mouse macrophage cells (RAW264.7) revealed that 100 μg/mL of mica is a potent inducer of cell death.[43] Heppleston has reviewed the toxicity of silica on the pulmonary system and described possible biochemical pathways of silica in inducing pulmonary fibrosis and carcinogenesis.[44] Therefore the use of these compounds in cosmetics in not without risk, particularly with prolonged exposure. There are only 6 products in Table 1.2 that contain pearl nacre without mica and/or other silica compounds. Beside silica compounds, bismuth is another common ingredient in cosmetics that claim to have nacre in their products. As mentioned in section 1.2.4, bismuth is used due to its similar physical appearance to pearl powder. There are 5 products in Table 1.2 that listed bismuth in their ingredients. There are some claims that bismuth can render human skin yellow and leather-like, and long term use may induce paralysis of the minute blood vessels.[45,46] However, Brinton and Napheys rejected these claims as they did not find those effects on their patients following internal and external administration for months.[47] Given the conflicting and in some cases concerning data regarding the safety of other components in cosmetics, further

development of nacre powders that retain lustre and eventual replacement of other compounds with this nacre will likely be beneficial to the cosmetic industry.

5.3.4. A number of cosmetics ingredients could be made redundant with the advancement of pearl nacre preparation.

The manufacturers of the 21 products listed in Table 1.2 have tried to associate their products with pearl or properties of pearl directly or indirectly. There are 11 products that use the word "pearl" in their product name. However, only 6 products actually contain pearl. Further, only 2 out of 6 products do not have mica and/ or other silica compounds in their ingredients. These 2 products are Pearl of Youth Pearl Powder and Pond's White Beauty Pearl Cleansing Gel. The other five products do not contain pearl, but mica and/ or other silica compounds instead. These 5 products are L'Oreal Infallible® 24Hr Eye Shadow Endless Pearl, Avon Rare Pearls Body Powder, Clarins White Plus Pearl-to-Cream Brightening Cleanser, Neutrogena Instant Nail Enhancer – Pearl Sheen and Oriflame Giordani Gold Bronzing Pearls. As discussed above in section 5.2.3, the cosmetic industry still relies heavily on added substances such as mica to produce the lustre effect or to lead customers to believe that it is pearl that delivered the described effect.

Cosmetics have many other ingredients, which are added to promote skin rejuvenation. Hyaluronic acid (HA) is one of them. There are at least 3 products from Table 1.2 that added HA as one of the ingredients in addition to pearl and mica. One of them is a lipstick from Lorac Cosmetics, which claim that the pearl nacre contained in it can keep lips soft, smooth, supple and naturally rejuvenated.[6] It was also claimed that the HA could fill in the fine lines on lips.[6] HA is a polysaccharide made of *D*-glucuronic acid and *N*-acetyl glucosamine.[48] HA is mainly found in skin and is

important in all three stages of wound healing.[49] The appearance of skin including lips is related to the amount and architecture of collagen.[50,51] Toward the end of wound healing, HA is broken down and replaced by collagenous scar.[49] Introduction of exogenous HA causes down regulation of fibroblast proliferation[52], which subsequently results in lower collagen synthesis.[53] For this reason, the remodelling is improved as reported by a study that introduced exogenous HA on a mouse limb organ culture, which stimulated scarless repair.[54] In brief, exogenous HA decreases collagen synthesis and improves remodelling. Meanwhile, as discussed in Chapter 4 conditioned media of Nacre M8 increased collagen synthesis and maintain 'normal' architecture of collagen. Additionally, collagen provides strength and structure to skin. Therefore, substance that could promote higher amount of collagen on skin is preferred for cosmetics. For this particular reason, there are cosmetics that include procollagen peptide/s to stimulate collagen production. For example, Pearl Professional Anti-Wrinkle Mist from Starmaker (#17 in Table 1.2) added Matrixyl™ in their ingredients in addition to pearl powder and mica. Matrixyl™ is palmitotyl pentapeptide-3 and contains the sequence Lys-Thr-Thr-Lys-Ser.[55] Matrixyl™ is a fragment of procollagen type I and traded by a cosmetic company Sederma from France.[56] This peptide stimulates synthesis of collagen types I and II and also fibronectin.[57]

In summary, with advances in pearl nacre preparation and given the positive effects of nacre on collagen production shown in this thesis, it is feasible that nacre may be effective in replacing many of the collagen peptide or HA based products currently used to promote collagen production.

5.4. Future work

5.4.1. Improvements to experimental design

In order to limit the possibility of protein denaturation, the ball milling could be performed in a temperature-controlled environment as described by Drai and Guillot.[58] It has been discussed in Chapter 2 that the ball milling apparatus has a higher chance to introduce heavy metals compared to environmental pollution. Therefore, it is recommended to use a ball milling apparatus made of tungsten carbide (WC) or silicon nitride (Si_3N_4) that are more resistant to degradation. The effects of nacre from different shell species could be examined to determine if some species have better effects than other. Oyster shell from other members of the *Pinctada* family such as *Pinctada fucata* or *Pinctada maxima* could be used. Even other species like the abalones (*Haliotis sp*), scallops (*Pecten sp*) or mussels (*Mytilus sp*) could become alternative sources of nacre as well. Although these different species might have some homologous nacre matrix proteins with *P. margaritifera*[36], but each species has different sets of organic matrix components. It is possible that one of these components is toxic to skin cells. The use of these other species might validate the current finding to be widely acceptable rather than species specific to *P. margaritifera*.

5.4.2. Future work for nacre preparation

The principles discussed in Chapter 2 should be retested with nacre from other sources proposed above in section 5.3.1 to investigate whether the outcomes are reproducible among species. Furthermore, it would be very valuable for the cosmetics industry if the proposed work to break down nacre to a size range where the products still retain its lustre could be realised. Additionally, this different kind of nacre could also be prepared using ionic liquid as described by Boulos et al.[11] The products of these two nacre preparations can be analysed for purity using inductively coupled plasma mass

spectrometry and atomic emission spectrometry (ICP MS-AES), thermo gravimetric analysis (TGA), x-ray diffraction (XRD) and fourier transform infrared spectroscopy (FTIR).

5.4.3. Future work for toxicity testing

The current results should be further validated using at least another keratinocyte and fibroblast cell line available before being tested on multiple primary cells and ultimately *in vivo* using an animal model. The current findings on the safety of nacre and increased collagen synthesis provides support for *in vivo* studies. The toxicity testing could also be enhanced with repeated dose in addition to the current single dose testing. The 50% lethal dose (LD_{50}) for each preparation should be determined by testing several concentrations.

The current toxicity study has excluded the damaging effect of heavy metal contamination from the ball milling process. Additional control treatments that are treated with Zr and Cd could further validate this claim. Preparation of conditioned media could be improved by using EDTA to extract soluble proteins as described by Liu et al.[21] The EDTA preparation may contain proteins not included in the current preparation, or with components at a higher concentration than obtained in this study. This may explain discrepancies in data obtained using soluble components of the nacre between the study presented here and those of others. Therefore the use of additional protein extraction method is required to determine whether there are soluble components that can influence wound healing.

5.4.4. Future work for functional assays

Future work should include analysis of the effects of nacre on elastin and TGF- β in addition to collagen. Elastin is also produced by fibroblasts.[59] Furthermore, as mentioned in Chapter 1, elastin works together with collagen to provide resilience and suppleness to skin.[60] TGF- β is also a critical regulator of the dermal matrix and wound healing process.[2] Therefore, it will be important to investigate the effects of nacre components, either organic or inorganic, on elastin and TGF- β homeostasis. Other calcium salts such as $Ca(OH)_2$, $CaCl_2$ or $Ca(NO_3)_2$ and other calcium carbonate polymorphs could also be used as controls. Additionally, since cosmetics usually have substances other than nacre, then it is recommendable to do the assays with different kind of mixtures rather than with nacre alone.

5.5. Conclusion

Despite the superior results produced by the calcium control, this study was the first to provide scientific evidence to suggest the use of nacre in cosmetics and wound healing regime is safe and has the potential to influence skin characteristics, including collagen amount. The work also provides a standardised methodology for nacre preparation that can be adapted for future preparations. These findings add valuable knowledge to understanding the mechanism of action of nacre not only for skin related studies but also for bone related studies. Further work to investigate the possibility of Ca^{2+} from different salts other than calcium carbonate to provide similar result is required to validate the current finding and to determine whether the use of nacre in cosmetic products and wound healing could be justified.

5.6. References

1 Hänel, K. H., Cornelissen, C., Lüscher, B. & Baron, J. M. Cytokines and the Skin Barrier. *International Journal of Molecular Sciences* **14**, 6720-6745, doi:10.3390/ijms14046720 (2013).

2 Linares, H. A. From wound to scar. *Burns* **22**, 339-352, doi:http://dx.doi.org/10.1016/0305-4179(95)00164-6 (1996).

3 Martin, P. Wound Healing--Aiming for Perfect Skin Regeneration. *Science* **276**, 75-81, doi:10.1126/science.276.5309.75 (1997).

4 Coolen, N. A., Schouten, K. C. W. M., Boekema, B. K. H. L., Middelkoop, E. & Ulrich, M. M. W. Wound healing in a fetal, adult, and scar tissue model: A comparative study. *Wound Repair and Regeneration* **18**, 291-301, doi:10.1111/j.1524-475X.2010.00585.x (2010).

5 Jenkins, G. Molecular mechanisms of skin ageing. *Mechanisms of Ageing and Development* **123**, 801-810, doi:http://dx.doi.org/10.1016/S0047-6374(01)00425-0 (2002).

6 Lorac. *Lorac Couture Shine Liquid Lipstick*, 2015).

7 Oriflame. *Giordani Gold Bronzing Pearls*, <http://in.oriflame.com/products/product?code=21632> (2015).

8 SIRCUIT®. *SWELL Ocean Cooling Mask*, <http://sircuitskin.com/inc/sdetail/32524/45981> (2015).

9 Zouboulis, C. C. & Makrantonaki, E. Clinical aspects and molecular diagnostics of skin aging. *Clinics in Dermatology* **29**, 3-14, doi:http://dx.doi.org/10.1016/j.clindermatol.2010.07.001 (2011).

10 Tjandra, E. S., Boulos, R. A., Duncan, P. C. & Raston, C. L. Unfastening pearl nacre nanostructures under shear. *CrystEngComm* **15**, 6896-6900, doi:10.1039/c3ce40760h (2013).

11 Boulos, R. A. *et al.* Unzipping oyster shell. *RSC Advances* **3**, 3284-3290, doi:10.1039/c2ra21763e (2013).

12 Rousseau, M. *et al.* Sheet nacre growth mechanism: a Voronoi model. *Journal of Structural Biology* **149**, 149-157, doi:10.1016/j.jsb.2004.09.005 (2005).

13 Hovden, R. *et al.* Nanoscale assembly processes revealed in the nacroprismatic transition zone of Pinna nobilis mollusc shells. *Nat Commun* **6**, doi:10.1038/ncomms10097 (2015).

14 Holme, T. A. *Denaturation*, <http://www.chemistryexplained.com/Co-Di/Denaturation.html> (2015).

15 van Dyk, M. *Pinctada margaritifera*, <http://www.gbri.org.au/Species/Pinctadamargaritifera.aspx?moid=465> (2011).

16 Bourrat, X. *et al.* Nacre biocrystal thermal behaviour. *CrystEngComm* **9**, 1205-1208, doi:10.1039/b709388h (2007).

17 Pereira Mouriès, L., Almeida, M.-J., Milet, C., Berland, S. & Lopez, E. Bioactivity of nacre water-soluble organic matrix from the bivalve mollusk Pinctada maxima in three mammalian cell types: fibroblasts, bone marrow stromal cells and osteoblasts. *Comparative Biochemistry and Physiology Part B: Biochemistry and Molecular Biology* **132**, 217-229, doi:http://dx.doi.org/10.1016/S1096-4959(01)00524-3 (2002).

18 Airborne nanoparticles are bad news. *Filtration & Separation* **39**, 20, doi:http://dx.doi.org/10.1016/S0015-1882(02)80039-8 (2002).

19 Myojo, T. *et al.* Risk assessment of airborne fine particles and nanoparticles. *Advanced Powder Technology* **21**, 507-512, doi:http://dx.doi.org/10.1016/j.apt.2010.05.004 (2010).

20 Kuhlbusch, T. A. J., Asbach, C., Fissan, H., Göhler, D. & Stintz, M. Nanoparticle exposure at nanotechnology workplaces: A review. *Particle and Fibre Toxicology* **8**, 22-22, doi:10.1186/1743-8977-8-22 (2011).

21 Liu, C. *et al.* In-depth proteomic analysis of shell matrix proteins of Pinctada fucata. *Scientific Reports* **5**, 17269, doi:10.1038/srep17269 http://www.nature.com/articles/srep17269#supplementary-information (2015).

22 Green, D. W., Kwon, H.-J. & Jung, H.-S. Osteogenic Potency of Nacre on Human Mesenchymal Stem Cells. *Molecules and Cells* **38**, 267-272, doi:10.14348/molcells.2015.2315 (2015).

23 Plummer, L. N. & Busenberg, E. The solubilities of calcite, aragonite and vaterite in CO2-H2O solutions between 0 and 90¬∞C, and an evaluation of the aqueous model for the system CaCO3-CO2-H2O. *Geochimica et Cosmochimica Acta* **46**, 1011-1040, doi:http://dx.doi.org/10.1016/0016-7037(82)90056-4 (1982).

24 Lee, K. *et al.* Nacre-driven water-soluble factors promote wound healing of the deep burn porcine skin by recovering angiogenesis and fibroblast function. *Mol Biol Rep* **39**, 3211-3218, doi:10.1007/s11033-011-1088-4 (2012).

25 Thornton, A. & Lukas, D. Individual variation in cognitive performance: developmental and evolutionary perspectives. *Philosophical Transactions of the Royal Society B: Biological Sciences* **367**, 2773-2783, doi:10.1098/rstb.2012.0214 (2012).

26 Lundeberg, T. & Lund, I. Treatment recommendations should take account of individual patient variation not just group responses. *Acupuncture in Medicine* **27**, 31-32 (2009).

27 Personal Care Products Council. *On-Line INFOBASE*, <http://www.personalcarecouncil.org/science-safety/line-infobase> (2016).

28 Agarwal, V. *et al.* Evaluating the effects of nacre on human skin and scar cells in culture. *Toxicology Research* **3**, 223-227, doi:10.1039/c4tx00004h (2014).

29 Chaturvedi, R., Singha, P. K. & Dey, S. Water Soluble Bioactives of Nacre Mediate Antioxidant Activity and Osteoblast Differentiation. *PLoS ONE* **8**, 1-1, doi:10.1371/journal.pone.0084584 (2013).

30 Li, Y.-C., Chen, C.-R. & Young, T.-H. Pearl extract enhances the migratory ability of fibroblasts in a wound healing model. *Pharmaceutical Biology* **51**, 289-297, doi:10.3109/13880209.2012.721130 (2013).

31 Lopez, E., Faou, A. L., Borzeix, S. & Berland, S. Stimulation of rat cutaneous fibroblasts and their synthetic activity by implants of powdered nacre (mother of pearl). *Tissue and Cell* **32**, 95-101, doi:10.1054/tice.1999.0091 (2000).

32 Shen, Y., Zhu, J., Zhang, H. & Zhao, F. In vitro osteogenetic activity of pearl. *Biomaterials* **27**, 281-287, doi:http://dx.doi.org/10.1016/j.biomaterials.2005.05.088 (2006).

33 Rousseau, M. *et al.* Restoration of stratum corneum with nacre lipids. *Comparative Biochemistry and Physiology Part B: Biochemistry and Molecular Biology* **145**, 1-9, doi:10.1016/j.cbpb.2006.06.012 (2006).

34 Lamghari, M. *et al.* Stimulation of bone marrow cells and bone formation by nacre: in vivo and in vitro studies. *Bone* **25**, 91S-94S (1999).

35 Marin, F. Molluscan shell proteins: primary structure, origin, and evolution. *Curr Top Dev Biol* **80**, 209 - 276 (2008).

36 Bédouet, L. *et al.* Proteomics Analysis of the Nacre Soluble and Insoluble Proteins from the Oyster Pinctada margaritifera. *Mar Biotechnol* **9**, 638-649, doi:10.1007/s10126-007-9017-1 (2007).

37 Zhang, C., Li, S., Ma, Z., Xie, L. & Zhang, R. A Novel Matrix Protein p10 from the Nacre of Pearl Oyster (*Pinctada fucata*) and Its Effects on Both CaCO3

Crystal Formation and Mineralogenic Cells. *Mar Biotechnol* **8**, 624-633, doi:10.1007/s10126-006-6037-1 (2006).
38 Levi-Kalisman, Y. Structure of the nacreous organic matrix of a bivalve mollusk shell examined in the hydrated state using cryo-TEM. *J Struct Biol* **135**, 8 - 17 (2001).
39 Liu, Y., Shigley, J. & Hurwit, K. Iridescence color of a shell of the mollusk *Pinctada Margaritifera* caused by diffraction. *Opt. Express* **4**, 177-182 (1999).
40 Nudelman, F. Forming nacreous layer of the shells of the bivalves Atrina rigida and Pinctada margaritifera: an environmental- and cryo-scanning electron microscopy study. *J Struct Biol* **162**, 290 - 300 (2008).
41 Meyers, M. A., Chen, P.-Y., Lin, A. Y.-M. & Seki, Y. Biological materials: Structure and mechanical properties. *Progress in Materials Science* **53**, 1-206, doi:http://dx.doi.org/10.1016/j.pmatsci.2007.05.002 (2008).
42 Skulberg, K. R., Gylseth, B., Skaug, V. & Hanoa, R. Mica pneumoconiosis -- A literature review. *Scandinavian Journal of Work, Environment & Health* **11**, 65-74 (1985).
43 Holopainen, M., Hirvonen, M.-R., Komulainen, H. & Klockars, M. Effect of the shape of mica particles on the production of tumor necrosis factor alpha in mouse macrophages. *Scandinavian Journal of Work, Environment & Health* **30**, 91-98 (2004).
44 Heppleston, A. G. Pulmonary Toxicology of Silica, Coal and Asbestos. *Environmental Health Perspectives* **55**, 111-127, doi:10.2307/3429696 (1984).
45 Cooley, A. J. *The toilet in ancient and modern times : with a review of the different theories of beauty and copious allied information, social, hygienic, and medical*. 432 (B. Franklin, 1970).
46 *Modern etiquette in public and private*. 167 (Frederick Warne and Co., 1887).
47 Brinton, D. G. & Napheys, G. H. *Personal Beauty: How to Cultivate and Preserve it in Accordance with the Laws of Health*. 208 (W. J. Holland, 1870).
48 Price, R. D., Myers, S., Leigh, I. M. & Navsaria, H. A. The Role of Hyaluronic Acid in Wound Healing: Assessment of Clinical Evidence. *American Journal of Clinical Dermatology* **6**, 393-402 (2005).
49 Frenkel, J. S. The role of hyaluronan in wound healing. *International Wound Journal* **11**, 159-163, doi:10.1111/j.1742-481X.2012.01057.x (2014).
50 Kim, S.-Y. *et al.* Protective Effects of Dietary Soy Isoflavones against UV-Induced Skin-Aging in Hairless Mouse Model. *Journal of the American College of Nutrition* **23**, 157-162, doi:10.1080/07315724.2004.10719356 (2004).
.51 Aust, M. C. *et al.* Percutaneous collagen induction. Scarless skin rejuvenation: fact or fiction? *Clinical and Experimental Dermatology* **35**, 437-439, doi:10.1111/j.1365-2230.2010.03779.x (2010).
52 Mesa, F. L. A., J ; Cabrera, A ; Bravo, M ; Caballero, T ; Revelles, F ; Del Moral, R G ; O'Valle, F. Antiproliferative effect of topic hyaluronic acid gel. Study in gingival biopsies of patients with periodontal disease. *Histology and Histopathology* **17**, 747-753 (2002).
53 Croce, M. A. *et al.* Hyaluronan affects protein and collagen synthesis by in vitro human skin fibroblasts. *Tissue and Cell* **33**, 326-331, doi:http://dx.doi.org/10.1054/tice.2001.0180 (2001).
54 Iocono, J. A., Ehrlich, H. P., Keefer, K. A. & Krummel, T. M. Hyaluronan induces scarless repair in mouse limb organ culture. *Journal of Pediatric Surgery* **33**, 564-567, doi:http://dx.doi.org/10.1016/S0022-3468(98)90317-7 (1998).

55 Amer, M. & Maged, M. Cosmeceuticals versus pharmaceuticals. *Clinics in Dermatology* **27**, 428-430, doi:http://dx.doi.org/10.1016/j.clindermatol.2009.05.004 (2009).
56 Reszko, A. E., Berson, D. & Lupo, M. P. Cosmeceuticals: Practical Applications. *Obstetrics and Gynecology Clinics* **37**, 547-569 (2010).
57 Katayama, K. A.-B., J ; Raghow, R ; Kang, A H ; Seyer, J M. A pentapeptide from type I procollagen promotes extracellular matrix production. *The Journal of Biological Chemistry* **268**, 9941-9944 (1993).
58 Drai, J. & Guillot, J. Process for the preparation of nacre mechano-structured by mechanosynthesis, mechano-structured nacre thus obtained and uses thereof. United States patent (2011).
59 Sephel, G. C. & Davidson, J. M. Elastin Production in Human Skin Fibroblast Cultures and Its Decline with Age. *J Investig Dermatol* **86**, 279-285 (1986).
60 Nasrollahi, S. A., Fouladdel, S., Taghibiglou, C., Azizi, E. & Farboud, E. S. A peptide carrier for the delivery of elastin into fibroblast cells. *International Journal of Dermatology* **51**, 923-929, doi:10.1111/j.1365-4632.2011.05214.x (2012).

Appendix 1

Paper published from the data in Chapter 2

CrystEngComm

RSC Publishing

COMMUNICATION

View Article Online
View Journal

Unfastening pearl nacre nanostructures under shear†

Edwin S. Tjandra,[a] Ramiz A. Boulos,[b] Peter C. Duncan[c] and Colin L. Raston*[b]

Cite this: DOI: 10.1039/c3ce40760h

Received 30th April 2013,
Accepted 9th July 2013

DOI: 10.1039/c3ce40760h

www.rsc.org/crystengcomm

Planetary ball milling of nacre is effective in unfastening the aragonite tablets in high yield with minimal damage, with some of the organic mortar remaining intact on the tablets. The milling process provides a means for transforming a waste material, nacre, which was harvested from pristine waters, into an uncontaminated powder form of the biogenic material with a unimodal particle size distribution for bio-applications or for providing accessible amounts of $CaCO_3$.

Oyster shells are biogenic barriers that separate and protect the animal from the elements and are primarily made of a stronger inner nacreous layer and an outer prismatic layer. Nacre is arranged in a brick and mortar like structure with the bricks composed mainly of aragonite which is one of the three polymorphs of $CaCO_3$, and the mortar is composed of organic material, mostly proteins and polysaccharides.[1] The mechanism of formation of nacre was first proposed by Rousseau *et al.*, as the so called Voronoi model, whereby the organic inter-lamellar sheets deposit first to form organic compartments followed by aragonite growing through the mineral bridges to fill the gaps between the sheets.[2] In addition, the bottom up hierarchical construction of nacre has been described by Cartwright and Checa,[3] starting from the fabrication of the polysaccharide chitin upon which aragonite eventually grows.

Typically nacre has an exceptionally high elastic modulus relative to bulk $CaCO_3$ in the calcite phase.[2] Such mechanical property, in addition to its ability to prevent and treat myopia on chicks,[4] induce osteogenesis *in vitro*[5] and in the vertebrae of sheep,[6] and induce cutaneous fibroblast growth in rats,[7] has attracted interest in being able to replicate the structure of nacre.[8,9] Indeed artificial nacre has previously been reported,[10,11] as have similarly structured material based on sheets of clay.[12,13]

Controlling the formation of the different phases of $CaCO_3$ represents a major challenge.[14] In contrast, molluscs specifically build aragonite in the inner part of the shell and calcite in the outer part. This selectively raises questions on how the animal forms both polymorphs, whether the polymorphs are formed under similar conditions, and what role the macromolecules in the shell play in polymorph selectivity.[15] Recent studies support the existence of stable nanoclusters of amorphous calcium carbonate (ACC) which are then transformed into the different polymorphs.[16] Furthermore a layer of amorphous $CaCO_3$ has been identified around aragonite tablets from the abalone *Haliotis laevigata*,[17] as has the formation of two amorphous calcium carbonates en route to crystallisation of the material.[18]

In further understanding the structure of the nacre, and for ultimately gaining insight into additional applications, we have undertaken a systematic study on its breakdown under shear using planetary ball milling utilizing nacre from the oyster *Pinctada margaritifera* (Fig. 1). A related study is the basis of a patent application.[19] We find that the nacre can be unfastened or disassembled with respect to the tablets, with high conversion, and with minimal damage to the smaller tablets, being able to generate large quantities of individual tablets with most of the mortar attached to the bricks.

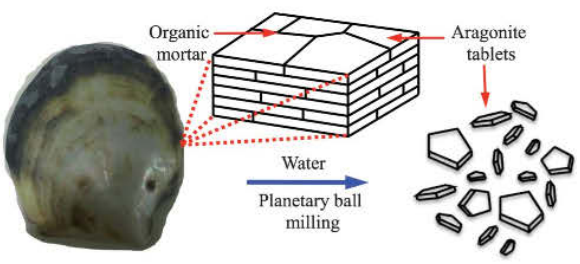

Fig. 1 Schematics of the planetary ball milling processing of nacre.

[a]*Centre for Strategic Nano-Fabrication, School of Chemistry and Biochemistry, The University of Western Australia, 35 Stirling Hwy, Crawley, W. A. 6009, Australia*
[b]*School of Chemical and Physical Sciences, Flinders University, Bedford Park, S. A. 5042, Australia. E-mail: colin.raston@flinders.edu.au; Tel: +61 82017958*
[c]*Centre for Microscopy, Characterisation and Analysis, The University of Western Australia, 35 Stirling Hwy, Crawley, W. A. 6009, Australia*

† Electronic supplementary information (ESI) available. See DOI: 10.1039/c3ce40760h

The oysters in the present study were farmed in the pristine waters of the Abrolhos Islands, Western Australia, and were sacrificed *in situ* with the relatively soft conchiolin outer layer of the shell removed by wet sandblasting. The shell was then crushed in a porcelain mortar and pestle before being wet milled with Milli Q water as a liquid excipient. The presence of the water facilitates the processing and addresses safety concerns for dry milling where there is the potential for airborne nano-particulates. A Planetary Micro Mill PULVERISETTE 7 premium line (Fritsch GmbH) with an 80 mL zirconium oxide (ZrO_2) interior bowl was used for the milling process. Several processing parameters were varied systematically, namely; speed, time, grinding bead size, number of balls, sample size, and volume of excipient. All milling processes were done in Milli Q water so that any contaminants arise exclusively from the milling balls and chamber. Ground shell prior to ball milling was analysed as a control using inductively coupled plasma mass spectrometry and atomic emission spectrometry (ICP MS-AES). Large concentrations of Ca (from the shell), Na and S were detected, with low levels of the heavy toxic metals Cd, Pb, and Hg, which is consistent with the nacre being formed in pristine water.

There are three factors that determine the quality of the product; (i) the percentage yield, (ii) the level of contamination from the milling process, and (iii) the uniformity of the sample size distribution. The percentage yield of conversion of the shell using the planetary ball mill, into material dispersible in water, are summarised in Fig. 2. The results show that the higher speeds compensate for the need for longer milling times, whereas the longer milling times do not compensate for lower milling speeds. For example, changing the time of milling from 4 hours to 24 hours and reducing the speed from 400 rpm to 200 rpm resulted in <10% yield. The volume of the excipient (water) is also important with an excess decreasing the distribution of the shell within a confined space and thus reducing the probability of effective collisions resulting in a lower yield. The other extreme of no excipient would result in the aforementioned dry powder.

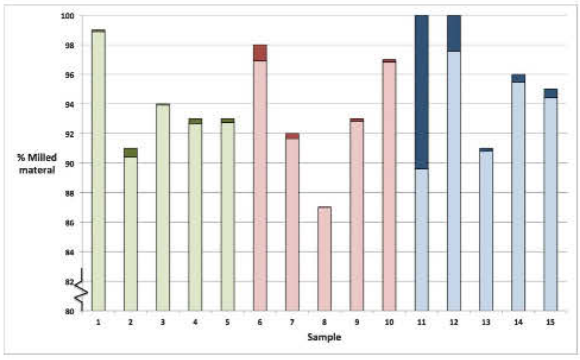

Fig. 2 Percent milled material using 5 mm zirconia balls and 15 g shell dispersed in 15 mL of water (green bars) operating at 400 rpm for 4 h (1), 600 rpm for 2 h (2), 800 rpm for 30 min (3), 1000 rpm for 20 min (4), and 1000 rpm for 30 min (5); 20 mm zirconia balls operating at 400 rpm for 2 h (red bars) using 5 g shell and 30 mL of water and 4 balls (6), 10 g shell and 15 mL of water and 4 balls (7), 15 g shell and 15 mL of water and 3 balls (8), 15 g shell and 15 mL of water and 4 balls (9), and 20 g shell and 15 mL of water and 4 balls (10); samples 11–15 (blue bars) had same conditions as samples 5–10 respectively but milled at 600 rpm for 2 h. The top section of the bars show any contamination. Further details of the milling conditions are given in Table S1, ESI.†

For the most part, the percentage yield and the level of contamination are co-dependent on the milling speed, the number of balls and the sample size. Milling at lower speeds results in lower yield but leads to less wear of the milling balls and casing and thus less contamination (Table S4, ESI†). More balls need a larger sample size to create a cushioning effect and reduce the collision of the balls with each other and with the casing, thereby reducing the likelihood of contamination. The results establish that when a small amount of nacre is processed, in particular when the mass ratio between sample and balls is $\leqslant 1:1$ for high rotational speed, there is significant ZrO_2 contamination from the balls and milling container. Using 20 mm zirconia balls rather than 5 mm zirconia balls results in a similar level of contamination, however the use of larger balls is preferable in reducing the time required to prepare and clean the balls between milling samples, and this is important in cost effective scaling up of the process for down stream applications. In addition to Zr from the zirconia balls, other contaminants from the milling process that were detected by ICP MS-AES include Hf and Cd. These results contradict the claim by Drai and Guillot that contamination from the balls does not occur.[19] Our findings show that optimal conditions for the milling of nacre are a sample loading size of 15 g shell dispersed in 15 mL of Milli Q water with a milling speed of 400 rpm for 2 hours using 3 zirconia balls (20 mm). These conditions were high yielding and have the lowest level of contamination, as established using ICP MS-AES.

The sedimentation property of the milled nacre precluded determining particle size distribution using dynamic light scattering (DLS). A meaningful particle size was however possible using a Mastersizer Hydro 2000S, Malvern Instruments, which involves stirring the solution during particle size analysis. The sample using our optimal milling conditions showed a single peak suggesting uniformity of particle size in the sample. Further details of the size distribution are in Table S2 and Fig. S2, ESI.† The particle size distribution by volume shows that the largest peak, hereafter called the prime peak, corresponds to a particle size of 5 μm which is consistent with the size of aragonite tablets.[1] The particle size distribution also show two other peaks greater than 50 μm suggesting incomplete milling of the crushed nacre in some samples.

X-Ray diffraction (XRD) studies performed using a Panalytical Empyrean instrument, showed that the milled nacre is composed mainly of aragonite with a small amount of calcite (Table S2, ESI†). There was no evidence of aragonite to calcite transformation from the intense shear associated with the milling process, unlike previous studies showing vaterite to calcite transformation under ball milling conditions.[20] This is significant given that the difference in enthalpies (ΔH) between aragonite and the thermodynamically stable polymorph, calcite, is small[21] and the lack of phase transition under those conditions could be due to organic-matter stabilization of aragonite. In sample 11, an additional peak corresponding to ZrO_2 was present, which is a contamination from the milling process (Table S3, ESI†).

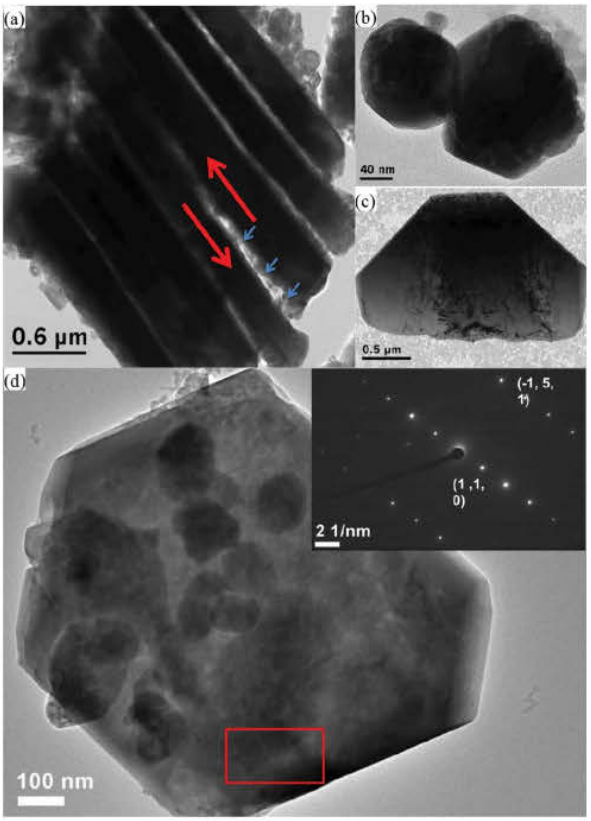

Fig. 3 (a) An array of aragonite tablets showing partial disassembly arising from shearing in the direction of the red arrows, and the associated distortion of the organic mortar, highlighted by the blue arrows. (b) Irregular tablets with curved and straight edges, and (c) a polygonal tablet. (d) Aragonite tablet with its electron diffraction in the inset from the red box area. Images were taken from the powder of sample 9.

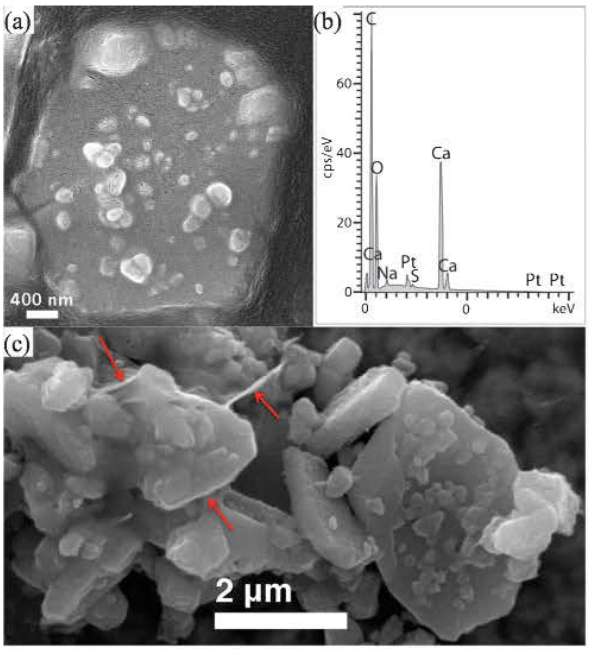

Fig. 4 SEM images of a nacre tablet (a) with its elemental analyses (b), and clusters of nacre tablets, (c), showing the organic mortar (red arrows). Images were taken from the powder of sample 9.

Transmission electron microscopy (TEM) images were used to gain insight into the nature of the particles, and also the mechanism of unfastening of the tablets. The planetary milling breaks apart tablets with an intermediate structure captured in Fig. 3a, which shows a fragment of the nacre as a collection of stacked tablets. The image captures a slippage between tablets arising from the milling process, indicated by red arrows, with some of the affected organic material forced into small nodules (blue arrows). This lateral shearing is a consequence of the planetary action of the ball milling, as opposed to classical high intensity ball milling where high energy impact between the balls shatters the material sandwiched between them. Espinosa *et al.*, have explained in length the deformation mechanism on a theoretical basis,[22] which we now substantiate experimentally.

Fig. 3b shows two tablets with different morphologies, a cylindrical structure on the left and a polygonal structure on the right. Additionally, another individual polygonal tablet is shown in Fig. 3c. These different morphologies agree with findings by Rousseau *et al.* where aragonite tablets extend cylindrically first and acquire their polygonal shape later when they make contact with each other.[2] Fig. 3d shows an aragonite tablet from milled nacre with its corresponding electron diffraction pattern (inset), which has been indexed to the [1, −1, 6] zone-axis.[23]

SEM image of the processed material were obtained using scanning electron microscope ZEISS 1555 VP-FESEM along with energy dispersive X-ray spectroscopy (EDS) to identify the elemental composition of the material. Multiple layers of aragonite tablets from crushed (*i.e.* pre-milling) nacre with the elemental analysis consistent with $CaCO_3$ and additional images of the milled nacre obtained by SEM Phillips XL30 are shown in Fig. S3 and S4 respectively, ESI.†

SEM images of individual tablets establishes that their surfaces are rough, as expected due to the presence of nanoasperites[24] of calcium carbonate, Fig. 4a. Fig. 4b presents the elemental analysis of the tablet showing Ca, C and O peaks. The high reading of carbon is caused by the combination of the organic matter from the nacre and the carbon tape that was used on the stage. Sodium is present which arises from shell growth in a marine environment, and trace levels of sulfur are evident in the organic component of the nacre. The tendency of the milled nacre to cluster is probably caused by the organic mortar that glues them together. In Fig. 4c this organic mortar material is marked with red arrows. Fourier Transform Infrared Spectroscopy (FTIR) of the sample, Fig. S7, ESI,† shows the presence of $CaCO_3$ but was insensitive to the presence of the organic mortar which is ~5% of the material.[25] The bricks sizes in the Fig. 4c range from submicron to several micron, with the thickness of the tablets close to 0.5 μm, which is consistent with the thickness established for tablets from the same species, which were generated from

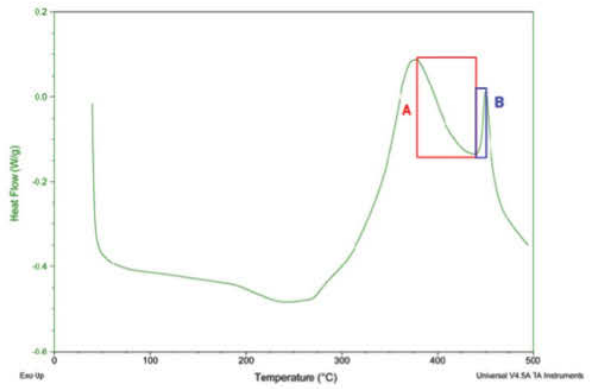

Fig. 5 DSC graph of processed material (sample 11) showing the polymorph transformation, aragonite to calcite (A) and the exotherm for zirconia (B). Graphs of all samples are available in Fig. S4, ESI.†

disassembly of the tablets using an ionic liquid, as opposed to intense shear in the present study.[26]

The transformation of aragonite to calcite was examined using differential scanning calorimetry (DSC) TA Q10. Samples were heated from 40 °C to 500 °C with temperature increment of 20 °C min^{-1}. The conversion of aragonite to calcite occurred in between 382–439 °C as the exotherm in Fig. 5 area A. Area B in the same figure corresponds to the exotherm for zirconia at 443 °C,[27] which is a result of the high level of contamination in the sample. XRD on the post DSC treated material reconfirmed the transformation (see Fig. S5, ESI†).

We recently established an alternative method to break down the nacre using an ionic liquid, which results in dissolution of all the organic mortar, as a soft energy process, and with minimal damage to the tablets, albeit with longer processing times rather than hours or minutes in the present study.[26] The high energy shearing processes herein leaves much of the organic material on the tablets, seemingly with minimal damage to them. The two processes are therefore complementary in disassembling the pearl nacre, but with different distribution of the organic material, either in the ionic liquid and potentially undamaged, or mainly attached to the tablets with potential damage from the shear and localised high temperatures associated with the planetary milling.

In summary, the shear associated with planetary milling is effective in breaking down nacre into individual tablets, without damage, unlike conventional grinding. In addition, insight into the effect of shear on pearl nacre in unfastening nacre under shear has been established. The results provide a means for transforming a waste material, nacre, grown in pristine waters, into an uncontaminated powder form of the biogenic material with a unimodal particle size distribution. The smaller particle size of the nacre resulting from the process favours absorption and degradation of the biomineral in biological systems, although the extent to which it is harmful for clinical use is a subject for further study. Contaminations from the system, yield and particle size distribution can be controlled by the choice of parameters, with the least contaminated samples currently being investigated for their healing effect in a burn injury model study. Moreover, the milled nacre can also be treated with an ionic liquid to provide accessible amounts of pure $CaCO_3$ with a range of applications in industry.

Financial support by the Australian Research Council and Pearl Technology Pty Ltd is gratefully acknowledged, as is access to TEM, SEM and XRD facilities in the Centre for Microscopy, Characterisation and Analysis, The University of Western Australia.

Notes and references

1 M. Rousseau, A. Meibom, M. Gèze, X. Bourrat, M. Angellier and E. Lopez, *J. Struct. Biol.*, 2009, **165**, 190–195.
2 M. Rousseau, E. Lopez, A. Couté, G. Mascarel, D. C. Smith, R. Naslain and X. Bourrat, *J. Struct. Biol.*, 2005, **149**, 149–157.
3 J. H. E. Cartwright and A. G. Checa, *J. R. Soc. Interface*, 2007, **4**, 491–504.
4 H. Xu, K. Huang, Q. Gao, Z. Gao and X. Han, *Pharm. Res.*, 2001, **44**, 1–6.
5 M. Lamghari, M. J. Almeida, S. Berland, H. Huet, A. Laurent, C. Milet and E. Lopez, *Bone*, 1999, **25**, 91S–94S.
6 M. Lamghari, S. Berland, A. Laurent, H. Huet and E. Lopez, *Biomaterials*, 2001, **22**, 555–562.
7 E. Lopez, A. L. Faou, S. Borzeix and S. Berland, *Tissue Cell*, 2000, **32**, 95–101.
8 E. Munch, M. E. Launey, D. H. Alsem, E. Saiz, A. P. Tomsia and R. O. Ritchie, *Science*, 2008, **322**, 1516–1520.
9 B. Bhushan, *Philos. Trans. R. Soc. London, Ser. A*, 2009, **367**, 1445–1486.
10 N. Gehrke, N. Nassif, N. Pinna, M. Antonietti, H. S. Gupta and H. Cölfen, *Chem. Mater.*, 2005, **17**, 6514–6516.
11 A. Finnemore, P. Cunha, T. Shean, S. Vignolini, S. Guldin, M. Oyen and U. Steiner, *Nat. Commun.*, 2012, **3**, 966.
12 P. Podsiadlo, A. K. Kaushik, E. M. Arruda, A. M. Waas, B. S. Shim, J. Xu, H. Nandivada, B. G. Pumplin, J. Lahann, A. Ramamoorthy and N. A. Kotov, *Science*, 2007, **318**, 80–83.
13 A. Walther, I. Bjurhager, J.-M. Malho, J. Pere, J. Ruokolainen, L. A. Berglund and O. Ikkala, *Nano Lett.*, 2010, **10**, 2742–2748.
14 J. E. Parker, S. P. Thompson, A. R. Lennie, J. Potter and C. C. Tang, *CrystEngComm*, 2010, **12**, 1590–1599.
15 G. Falini, S. Albeck, S. Weiner and L. Addadi, *Science*, 1996, **271**, 67–69.
16 D. Gebauer, A. Völkel and H. Cölfen, *Science*, 2008, **322**, 1819–1822.
17 N. Nassif, N. Pinna, N. Gehrke, M. Antonietti, C. Jäger and H. Cölfen, *Proc. Natl. Acad. Sci. U. S. A.*, 2005, **102**, 12653–12655.
18 D. Gebauer, P. N. Gunawidjaja, J. Y. P. Ko, Z. Bacsik, B. Aziz, L. Liu, Y. Hu, L. Bergström, C.-W. Tai, T.-K. Sham, M. Edén and N. Hedin, *Angew. Chem., Int. Ed.*, 2010, **49**, 8889–8891.
19 J. Drai and J. Guillot, US Patent US20110004218 A1, 2011.
20 D. O. Northwood and D. Lewis, *Am. Mineral.*, 1968, **53**, 2089–2092.
21 G. Wolf, J. Lerchner, H. Schmidt, H. Gamsjäger, E. Königsberger and P. Schmidt, *J. Therm. Anal. Calorim.*, 1996, **46**, 353–359.
22 H. D. Espinosa, J. E. Rim, F. Barthelat and M. J. Buehler, *Prog. Mater. Sci.*, 2009, **54**, 1059–1100.
23 J. Villiers, *Am. Mineral.*, 1971, **56**, 758–767.
24 B. Bruet, H. Qi, M. Boyce, R. Panas, K. Tai, L. Frick and C. Ortiz, *J. Mater. Res.*, 2005, **20**, 2400–2419.

25 A. P. Jackson, J. F. V. Vincent and R. M. Turner, *Proc. R. Soc. London, Ser. B*, 1988, **234**, 415–440.
26 R. Boulos, C. Harnagea, X. Duan, R. Lamb, F. Rosei and C. Raston, *RSC Adv.*, 2013, **3**, 3284–3290.
27 P. D. L. Mercera, J. G. Van Ommen, E. B. M. Doesburg, A. J. Burggraaf and J. R. H. Ross, *Appl. Catal.*, 1990, **57**, 127–148.

Supporting Information

Unfastening pearl nacre nanostructures under shear

Edwin Setiawan Tjandra,[a] Ramiz A Boulos,[a] Peter Duncan[b] and Colin L Raston*[a]

Planetary Ball Milling

The shell nacre was milled according to the parameters in table 1. Other conditions tested but not listed in the table, include shorter durations (1, 5 and 10 minutes), lower speed (200rpm), less balls (100 5mm-balls and 2 20mm-balls), and/or smaller sample size (100mg). However, those conditions did not give optimum yield and introduced a lot of contamination as discussed in the paper.

Table S1. Ball milling conditions of each sample

Sample #	Sample Size (g)	Ball Size	No of Balls	Excipient Milli Q	Speed (rpm)	Duration
1	15	5mm	200	15ml	400	4 hrs
2	15	5mm	200	15ml	600	2 hrs
3	15	5mm	200	15ml	800	30 mins
4	15	5mm	200	15ml	1000	20 mins
5	15	5mm	200	15ml	1000	30 mins
6	5	20mm	4	30ml	400	2 hrs
7	10	20mm	4	15ml	400	2 hrs
8	15	20mm	3	15ml	400	2 hrs
9	15	20mm	4	15ml	400	2 hrs
10	20	20mm	4	15ml	400	2 hrs
11	5	20mm	4	30ml	600	2 hrs
12	10	20mm	4	15ml	600	2 hrs
13	15	20mm	3	15ml	600	2 hrs
14	15	20mm	4	15ml	600	2 hrs
15	20	20mm	4	15ml	600	2 hrs

Following the milling process the samples were suspended in 100 ml of Milli Q water and the suspension was immediately decanted into a clean container leaving the partially milled nacre behind, which was dried and weighed. The suspension was filtered using filter paper with a pore size of 2.5 μm. The residue was redispersed in 100 ml Milli Q water and centrifuged at 3220 x g for 15 minutes. The supernatant was transferred and kept, while the pellet was redispersed in 100 ml Milli Q water and centrifuged as above. The residue was dried, weighed, and kept for analyses.

Conventional Ball Milling

As a comparison of the effectiveness of the planetary mill, a one-off experiment using a SPEX SamplePrep 8000D Dual Mixer/Mill® was carried out using a sample size of 15g, 12 3/8" stainless steel ball and double distilled water as an excipient. The milling time was set to 2 hours at a speed of 875 cycles/min. Figure S1 shows TEM images of damaged aragonite tablets as a result of the milling process.

TEM Images of Damaged Tablets

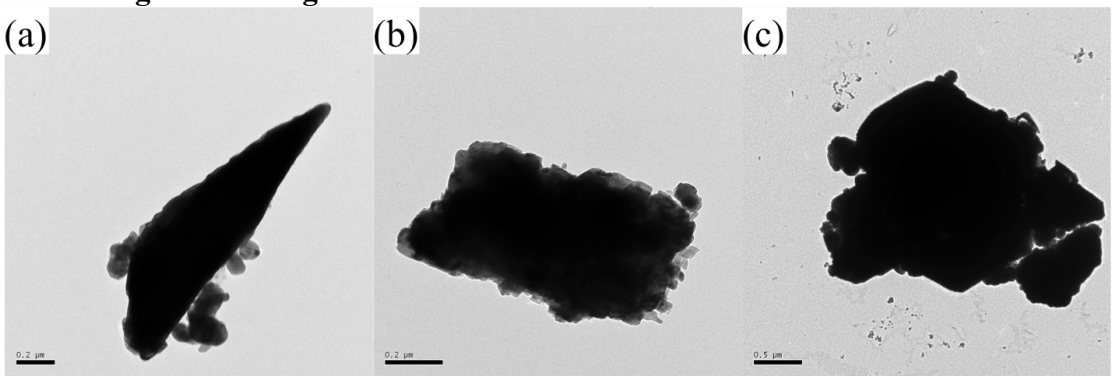

Figure S1. Damaged aragonite tablets. (a) The tablet does not look like a polygonal aragonite tablet. (b) The rough edges of the tablet are due to the shear force of conventional milling. (c) The damaged tablet almost being cracked into two pieces. The bar sizes are 0.2µm (a-b) and 0.5µm (c).

Particle Size Distribution (Mastersizer Hydro 2000S)

Table S2. Particle Size Distribution.

Sample #	d (0.1)	d (0.5)	d (0.8)	d (0.9)	Max
1	0.688	3	48.164	141.798	724.436
2	0.597	1.822	22.07	102.793	316.228
3	0.747	2.284	5.611	16.336	120.226
4	0.737	2.546	17.313	41.89	91.201
5	0.003	4.522	45.022	103.635	724.436
6	0.456	14.852	327.987	450.803	831.764
7	0.012	6.667	366.765	499.038	954.993
8	0.888	2.949	6.554	9.309	22.909
9	0.928	3.279	8.744	16.381	91.201
10	0.861	2.809	6.696	10.404	26.303
11	0.777	2.634	6.958	11.704	26.303
12	0.799	2.669	9.806	51.585	138.038
13	0.883	3.172	10.347	65.436	181.97
14	0.802	2.495	5.805	12.241	91.201
15	0.84	3.185	304.735	470.047	954.993

d(0.1) value indicates 10% of the samples are below that size, d(0.5) value means 50% of the samples are below that size, d(0.8) value means 80% of the samples are below that size, d(0.9) value means 90% of the samples are below that size, Max value indicates the largest possible size of that sample. All values are in micrometer.

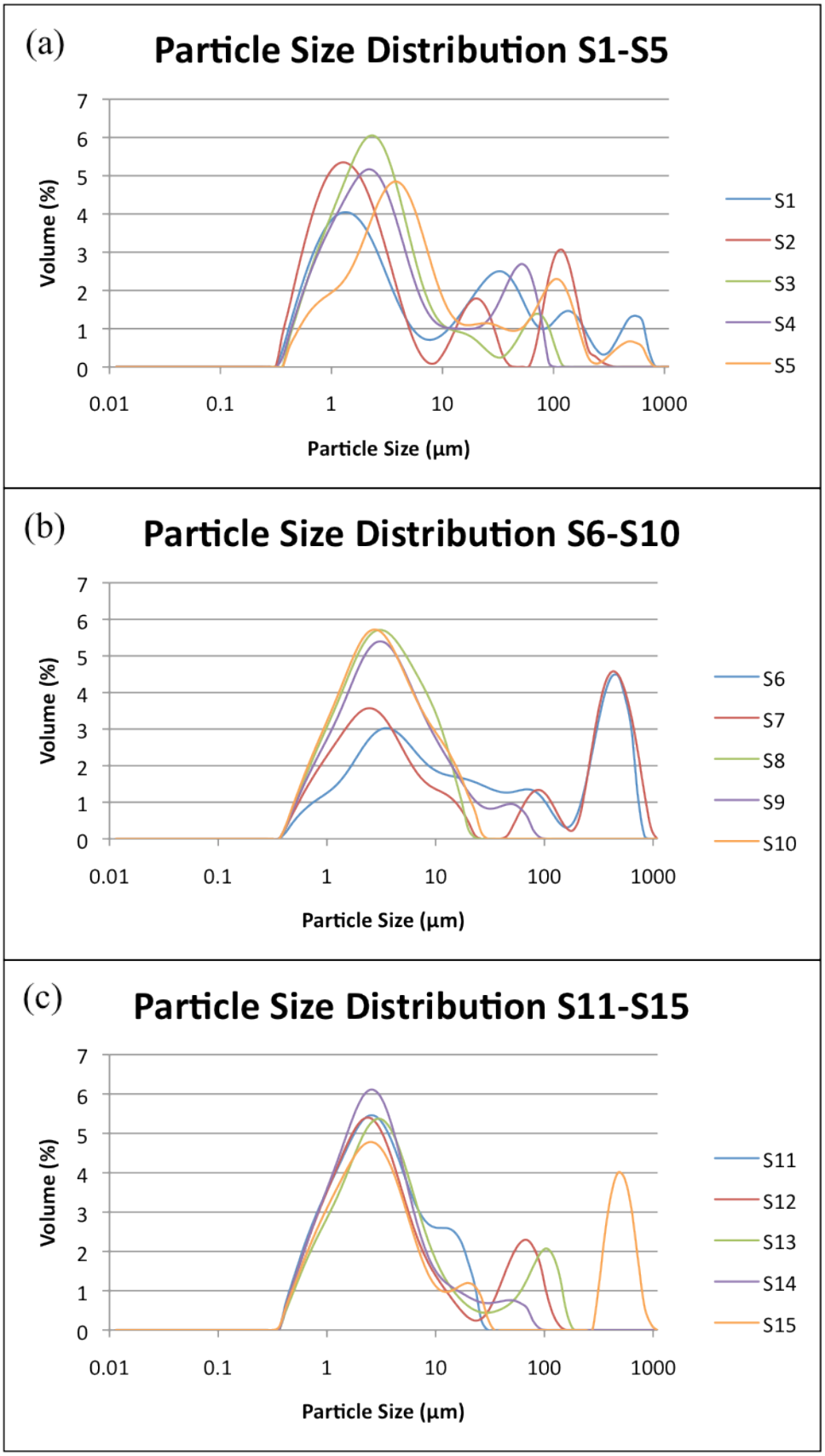

Figure S2. Particle size distribution of samples 1-5(a), 6-10(b) and 11-15(c).

Scanning Electron Microscopy (SEM)
Samples were embedded on carbon tape and layered with 3nm Platina (Pt).

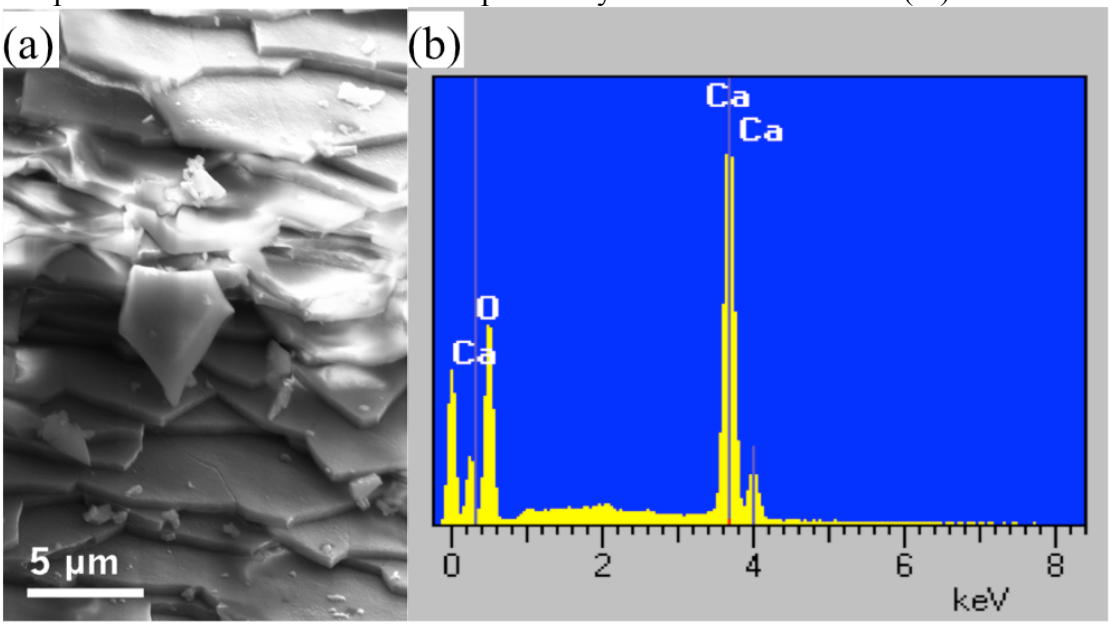

Figure S3. Crushed nacre. (a) Multiple layers of aragonite tablets from crushed nacre and (b) its elemental analysis

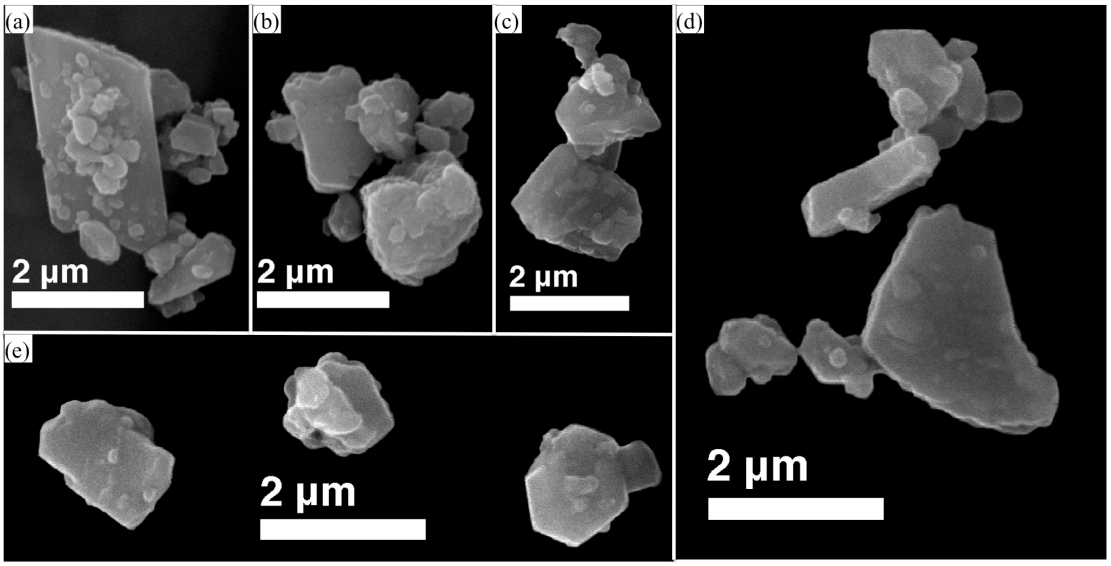

Figure S4. Milled nacre with various sizes and shapes.

X-Ray Diffraction (XRD)

Ground and milled nacre were subjected to X-Ray powder diffraction analysis. Ground nacre was analysed as a control to determine the effect of heat and shear forces from milling processes on the phase transformation of aragonite. The percentage compositions are summarized in table S3. It is worthy to note that this analysis was meant for qualitative instead of quantitative analysis. So, the number below is a guide only as the margin of error from the software could be as high as 20%.

Table S3. Percentage compositions analysis from XRD.

Sample	Aragonite	Calcite	Other
Ground	79%	21%	
1	100%	0%	
2	75%	25%	
3	62%	38%	
4	66%	34%	
5	84%	16%	
6	100%	0%	
7	100%	0%	
8	89%	11%	
9	91%	9%	
10	93%	7%	
11*	95%	0%	5% ZrO_2
12	100%	0%	
13	100%	0%	
14	100%	0%	
15	89%	11%	
Conventional	86%	14%	

XRD analysis of sample 9 before and after DSC treatment shows that aragonite transformed to calcite after treatment (see Fig. S5 below).

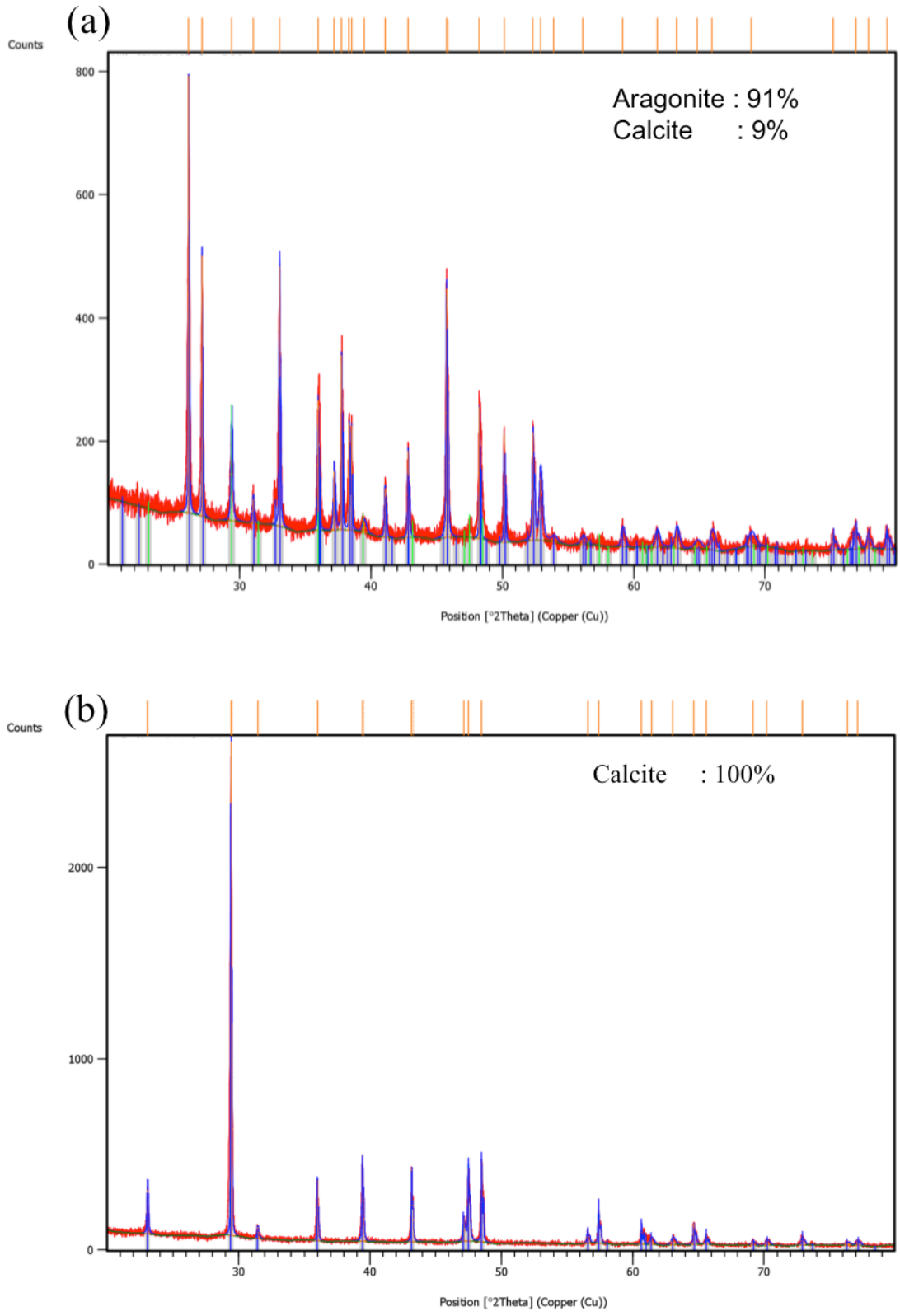

Figure S5. XRD spectrum of sample 9 before (a) and after (b) DSC treatment showing that it only contains calcite.

Differential Scanning Calorimetry (DSC)

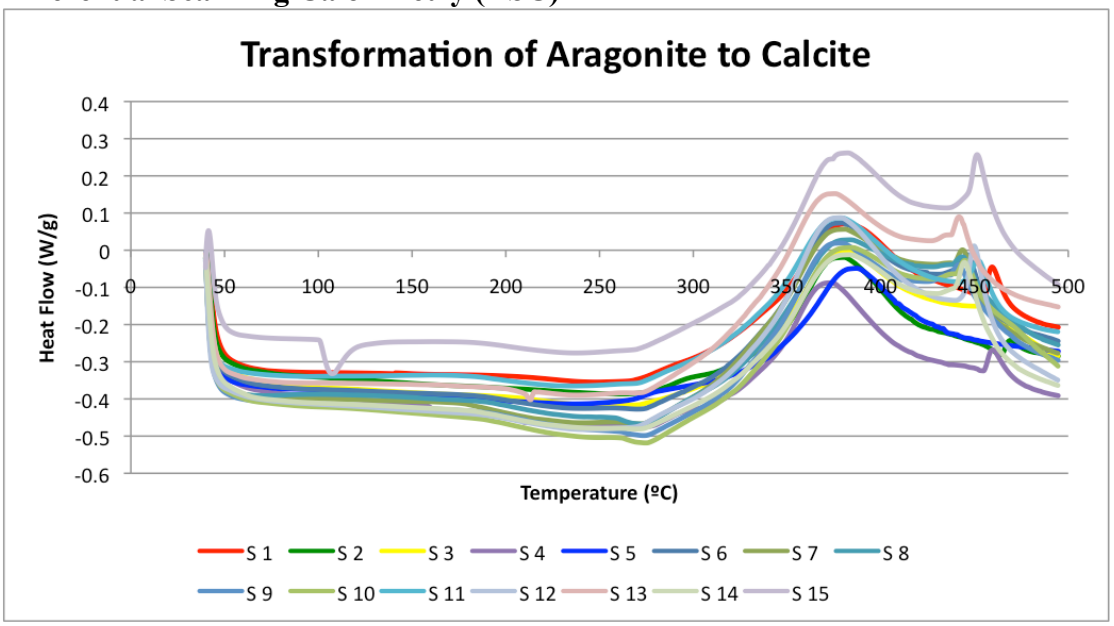

Figure S6. DSC graph of the 15 samples.

Fourier Transform Infrared Spectroscopy (FTIR)

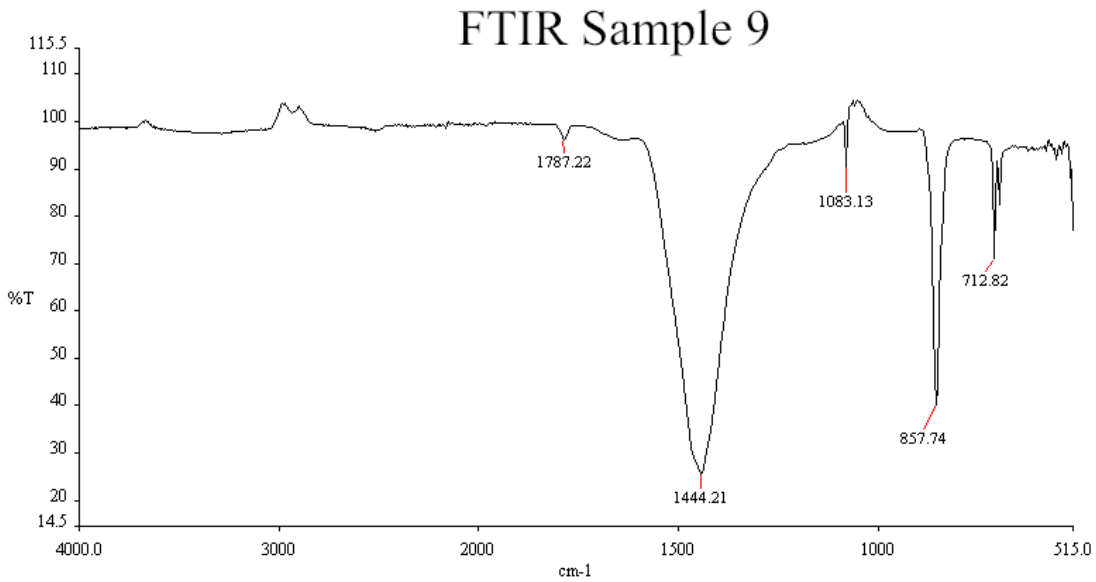

Figure S7. FTIR of Sample 9 corresponds to aragonite.

Inductively Coupled Plasma Mass Spectrometry and Atomic Emission Spectrometry (ICP MS – AES)

Full analysis results of the ground nacre and the planetary milled nacre were given in Table S4.

Table S4. ICP MS – AES data

Sample\Atom	Na	Mg	Al	P	S	K	Ca	Fe	Sr	Zr	Li
Ground	4810	1050	20.2	8.4	184	79.3	356000	32.2	1090	9.3	0.5
S 1	2420	1600	14.3	7.0	169	24.6	363000	6.0	1220	1100	0.4
S 2	1790	1990	30	2.7	164	15.3	364000	14.8	1180	5970	0.4
S 3	2100	4040	6.3	8.3	169	20.3	382000	10.3	1150	828	0.4
S 4	2190	1670	29.3	6.0	168	12.3	373000	7.1	1050	3140	0.5
S 5	951	1690	13.6	4.3	166	6.81	376000	9.1	1150	2730	0.6
S 6	3340	2400	47.7	1.1	161	38.3	366000	10.8	1090	10800	0.5
S 7	3500	1270	108	2.5	166	36.4	361000	5.9	1090	3520	0.5
S 8	3530	2650	0.2	5.3	178	38	370000	7.13	1210	25.1	0.6
S 9	3510	2070	4.59	7.2	174	34.4	366000	8.9	1180	1600	0.5
S 10	3430	1760	8.6	8.1	175	32	363000	6.8	1150	1640	0.6
S 11	3280	9750	416	9.7	134	28.8	315000	25	909	104000	0.3
S 12	3010	3440	94.4	8.3	169	31	361000	15.7	1070	24200	0.5
S 13	3350	1970	12.1	6.1	167	40.5	366000	3.1	1170	2110	0.5
S 14	3180	1770	21.5	4.7	168	34.2	370000	4.3	1070	5420	0.5
S 15	3160	3140	26.7	8.9	171	34.8	360000	8.7	1110	5880	0.6

Sample\Atom	As	Se	Rb	Y	Nb	Mo	Pd	Ag	Cd	In
Ground	< 0.1	< 0.1	< 0.1	0.2	0.2	0.3	< 0.1	< 0.1	< 0.1	< 0.1
S 1	< 0.1	< 0.1	< 0.1	51.1	0.4	0.2	< 0.1	0.2	1.2	< 0.1
S 2	< 0.1	< 0.1	< 0.1	408	0.6	0.6	< 0.1	0.2	6.0	< 0.1
S 3	< 0.1	< 0.1	< 0.1	61.1	0.61	0.2	< 0.1	< 0.1	0.9	< 0.1
S 4	< 0.1	< 0.1	< 0.1	179	0.6	0.4	< 0.1	< 0.1	3.2	< 0.1
S 5	< 0.1	< 0.1	< 0.1	185	3.1	0.4	< 0.1	0.1	3.2	< 0.1
S 6	< 0.1	< 0.1	< 0.1	21.9	1.3	1.1	< 0.1	0.4	10.9	< 0.1
S 7	< 0.1	< 0.1	< 0.1	5.2	1.33	0.5	< 0.1	0.2	4.0	< 0.1
S 8	< 0.1	< 0.1	< 0.1	0.2	0.2	0.2	< 0.1	< 0.1	< 0.1	< 0.1
S 9	< 0.1	< 0.1	< 0.1	1.8	0.4	0.3	< 0.1	< 0.1	1.6	< 0.1
S 10	< 0.1	< 0.1	< 0.1	2.0	0.5	0.3	< 0.1	< 0.1	1.9	< 0.1
S 11	< 0.1	< 0.1	< 0.1	119	4.7	8.6	< 0.1	4.2	111	< 0.1
S 12	< 0.1	< 0.1	< 0.1	26.4	1.0	1.9	< 0.1	0.8	21.8	< 0.1
S 13	< 0.1	< 0.1	< 0.1	2.6	0.6	0.3	< 0.1	< 0.1	2.2	< 0.1
S 14	< 0.1	< 0.1	< 0.1	7.23	0.6	0.6	< 0.1	0.2	5.8	< 0.1
S 15	< 0.1	< 0.1	< 0.1	7.5	0.7	0.6	< 0.1	0.2	6.2	< 0.1

Sample\Atom	Dy	Ho	Er	Tm	Yb	Lu	Hf	Ta	W	Hg
Ground	< 0.1	< 0.1	< 0.1	< 0.1	< 0.1	< 0.1	< 0.1	< 0.1	< 0.1	< 0.1
S 1	< 0.1	< 0.1	< 0.1	< 0.1	0.3	< 0.1	6.3	< 0.1	< 0.1	< 0.1
S 2	< 0.1	< 0.1	< 0.1	< 0.1	0.8	< 0.1	36.2	< 0.1	< 0.1	< 0.1
S 3	< 0.1	< 0.1	< 0.1	< 0.1	0.2	< 0.1	5.9	< 0.1	< 0.1	< 0.1
S 4	< 0.1	< 0.1	< 0.1	< 0.1	0.4	< 0.1	17.1	< 0.1	< 0.1	< 0.1

S 5	< 0.1	< 0.1	< 0.1	< 0.1	0.4	< 0.1	16.8	0.2	< 0.1	< 0.1
S 6	1.61	0.8	2.1	0.8	5.3	1.5	58.7	0.1	< 0.1	< 0.1
S 7	0.5	0.3	0.7	0.3	1.7	0.5	20.2	< 0.1	< 0.1	< 0.1
S 8	< 0.1	< 0.1	< 0.1	< 0.1	< 0.1	< 0.1	0.2	< 0.1	< 0.1	< 0.1
S 9	0.2	< 0.1	0.2	< 0.1	0.6	0.2	7.8	< 0.1	< 0.1	< 0.1
S 10	0.2	< 0.1	0.3	< 0.1	0.7	0.2	9.4	< 0.1	< 0.1	< 0.1
S 11	10.9	5.3	14.5	5.7	39.1	10.8	489	0.4	0.3	< 0.1
S 12	2.7	1.3	3.5	1.4	9.4	2.6	112	< 0.1	< 0.1	< 0.1
S 13	0.3	0.1	0.4	0.1	0.9	0.3	11.3	< 0.1	< 0.1	< 0.1
S 14	0.7	0.4	0.9	0.4	2.4	0.7	29.4	< 0.1	< 0.1	< 0.1
S 15	0.8	0.4	1.0	0.4	2.6	0.7	31.7	< 0.1	< 0.1	< 0.1

Sample\Atom	Be	Sc	Ti	V	Cr	Mn	Co	Ni	Cu	Zn
Ground	< 0.1	0.2	44.3	1.2	2.5	2.7	0.2	0.9	1.6	2.5
S 1	< 0.1	0.2	6.9	2.0	1.0	8.3	0.2	0.7	2.2	2.6
S 2	< 0.1	0.8	5.1	2.2	1.0	7.3	0.2	0.4	0.7	2.6
S 3	< 0.1	0.2	58.1	1.0	0.4	7.5	0.1	0.5	0.5	8.8
S 4	< 0.1	0.5	9.1	2.2	0.8	9.7	0.2	0.4	0.4	3.4
S 5	< 0.1	0.5	7.2	2.3	0.8	8.5	0.2	0.4	0.8	1.1
S 6	< 0.1	1.5	15	1.9	0.9	11.5	0.2	0.7	1.0	2.1
S 7	< 0.1	0.7	12.1	2.5	0.8	11.8	0.2	0.5	1.0	2.1
S 8	< 0.1	0.2	7.0	1.5	0.9	8	0.2	0.5	0.8	1.6
S 9	< 0.1	0.4	9.4	1.7	1.0	8.3	0.2	0.5	1.5	0.2
S 10	< 0.1	0.4	10.9	1.9	0.9	9.4	0.2	0.4	0.6	1.6
S 11	< 0.1	10.7	61.6	1.2	1.9	10.5	0.2	2.2	0.4	0.3
S 12	< 0.1	2.5	23.5	2.2	1.3	9.8	0.2	0.9	0.9	4.4
S 13	< 0.1	0.5	11.4	1.6	0.8	8.9	0.2	0.4	0.5	1.7
S 14	< 0.1	0.9	15.2	2.2	0.8	9.0	0.2	0.6	0.9	0.5
S 15	< 0.1	0.9	16.1	2.0	0.8	10.3	0.2	0.5	0.5	0.9

Sample\Atom	Sn	Sb	Te	Cs	Ba	La	Ce	Pr	Nd	Eu
Ground	0.8	< 0.1	< 0.1	< 0.1	0.8	< 0.1	< 0.1	< 0.1	< 0.1	< 0.1
S 1	1.3	< 0.1	< 0.1	< 0.1	0.8	< 0.1	0.9	< 0.1	< 0.1	< 0.1
S 2	1.9	< 0.1	< 0.1	< 0.1	0.5	< 0.1	0.8	< 0.1	< 0.1	< 0.1
S 3	1.3	< 0.1	< 0.1	< 0.1	0.5	< 0.1	0.7	< 0.1	< 0.1	< 0.1
S 4	0.5	< 0.1	< 0.1	< 0.1	0.4	< 0.1	1.6	< 0.1	< 0.1	< 0.1
S 5	1.1	< 0.1	< 0.1	< 0.1	0.8	< 0.1	1.1	< 0.1	< 0.1	< 0.1
S 6	0.9	< 0.1	< 0.1	< 0.1	1.6	0.4	1.2	< 0.1	0.4	< 0.1
S 7	0.9	< 0.1	< 0.1	< 0.1	1.0	0.2	0.7	< 0.1	0.2	< 0.1
S 8	0.7	< 0.1	< 0.1	< 0.1	0.6	< 0.1	0.3	< 0.1	< 0.1	< 0.1
S 9	0.5	< 0.1	< 0.1	< 0.1	0.6	< 0.1	0.3	< 0.1	< 0.1	< 0.1
S 10	0.1	< 0.1	< 0.1	< 0.1	0.7	< 0.1	0.4	< 0.1	< 0.1	< 0.1
S 11	1.4	< 0.1	0.3	< 0.1	7.4	2	7.8	0.6	2.8	0.2
S 12	0.4	< 0.1	< 0.1	< 0.1	2.3	0.5	2.3	< 0.1	0.7	< 0.1
S 13	0.8	< 0.1	< 0.1	< 0.1	0.8	0.2	0.7	< 0.1	< 0.1	< 0.1
S 14	0.7	< 0.1	< 0.1	< 0.1	0.9	0.2	0.7	< 0.1	0.2	< 0.1
S 15	0.3	< 0.1	< 0.1	< 0.1	1.1	0.2	0.8	< 0.1	0.2	< 0.1

Sample\Atom	Tl	Pb	Bi	Th	U	Ga	Ge	Gd	Tb	Sm

Ground	< 0.1	0.2	< 0.1	< 0.1	< 0.1	< 0.1	< 0.1	< 0.1	< 0.1	< 0.1
S 1	< 0.1	0.4	< 0.1	< 0.1	0.1	< 0.1	< 0.1	< 0.1	< 0.1	< 0.1
S 2	< 0.1	0.3	< 0.1	< 0.1	0.1	< 0.1	< 0.1	< 0.1	< 0.1	< 0.1
S 3	< 0.1	0.2	< 0.1	< 0.1	< 0.1	< 0.1	< 0.1	< 0.1	< 0.1	< 0.1
S 4	< 0.1	0.1	< 0.1	< 0.1	< 0.1	< 0.1	< 0.1	< 0.1	< 0.1	< 0.1
S 5	< 0.1	0.1	< 0.1	< 0.1	0.2	< 0.1	< 0.1	< 0.1	< 0.1	< 0.1
S 6	< 0.1	0.2	< 0.1	2.2	4.6	< 0.1	< 0.1	< 0.1	< 0.1	< 0.1
S 7	< 0.1	0.2	< 0.1	0.7	1.5	< 0.1	< 0.1	< 0.1	< 0.1	< 0.1
S 8	< 0.1	0.2	< 0.1	< 0.1	< 0.1	< 0.1	< 0.1	< 0.1	< 0.1	< 0.1
S 9	< 0.1	< 0.1	< 0.1	0.2	0.5	< 0.1	< 0.1	< 0.1	< 0.1	< 0.1
S 10	< 0.1	0.2	< 0.1	0.3	0.6	< 0.1	< 0.1	< 0.1	< 0.1	< 0.1
S 11	< 0.1	< 0.1	< 0.1	15.6	31.5	0.131	< 0.1	3.5	0.9	< 0.1
S 12	< 0.1	0.2	< 0.1	3.8	8.0	< 0.1	< 0.1	< 0.1	< 0.1	< 0.1
S 13	< 0.1	0.1	< 0.1	0.4	0.7	< 0.1	< 0.1	< 0.1	< 0.1	< 0.1
S 14	< 0.1	< 0.1	< 0.1	1.0	2.1	< 0.1	< 0.1	< 0.1	< 0.1	< 0.1
S 15	< 0.1	0.1	< 0.1	1.05	2.1	< 0.1	< 0.1	< 0.1	< 0.1	< 0.1

Appendix 2

Other papers published during the course of the thesis

SCIENTIFIC REPORTS

OPEN

SUBJECT AREAS:
PROCESS CHEMISTRY
SOLID-STATE CHEMISTRY

Received
21 October 2013

Accepted
5 December 2013

Published
22 January 2014

Correspondence and requests for materials should be addressed to C.L.R. (colin.raston@flinders.edu.au)

Spinning up the polymorphs of calcium carbonate

Ramiz A. Boulos[1], Fei Zhang[1,2], Edwin S. Tjandra[3], Adam D. Martin[4], Dino Spagnoli[3] & Colin L. Raston[1]

[1]Centre for NanoScale Science and Technology, School of Chemical and Physical Sciences, Flinders University, Bedford Park, SA 5042 Australia, [2]Department of Polymer Science and Engineering, School of Chemistry and Chemical Engineering, Shanghai Jiao Tong University, Shanghai 200240, China, [3]School of Chemistry and Biochemistry, The University of Western Australia, 35 Stirling Hwy, Crawley, WA 6009, Australia, [4]Department of Chemistry, The University of New South Wales, High St, Kensington, NSW 2052.

Controlling the growth of the polymorphs of calcium carbonate is important in understanding the changing environmental conditions in the oceans. Aragonite is the main polymorph in the inner shells of marine organisms, and can be readily converted to calcite, which is the most stable polymorph of calcium carbonate. Both of these polymorphs are significantly more stable than vaterite, which is the other naturally occurring polymorph of calcium carbonate, and this is reflected in its limited distribution in nature. We have investigated the effect of high shear forces on the phase behaviour of calcium carbonate using a vortex fluidic device (VFD), with experimental parameters varied to explore calcium carbonate mineralisation. Variation of tilt angle, rotation speed and temperature allow for control over the size, shape and phase of the resulting calcium carbonate.

Carbon dioxide fixation from the atmosphere by marine organisms as large deposits of calcium carbonate is important in the carbon cycle. The rising concentration of carbon dioxide in the atmosphere, estimated to be 40% higher than preindustrial levels and higher than at any point in the last 800,000 years[1], has led to a shift in the equilibrium of dissolved CO_2 in seawater. This has lowered the pH of seawater and along with increasing temperatures, has greatly affected the optimum conditions for calcium carbonate ($CaCO_3$) mineralisation[2,3]. Deposition of $CaCO_3$ by marine organisms, in the form of aragonite in the nacreous layer or inner shell[4–6], is therefore likely to be tested by the climate change[7,8] in the Anthrapocene era[9]. Controlling the formation of $CaCO_3$ polymorphs is important in understanding the mineralisation process with such changing environmental conditions, and for this purpose we used the recently developed, continuous flow processing, vortex fluidic device (VFD)[10–13]. While the conditions here are much more extreme and different to those likely to be encountered in the environment in the future, the results highlight the conditions required for selective preparation of different polymorphs of calcium carbonate. The vortex fluidic device (VFD), is capable of producing thin films in which high shear forces provide a mechanical energy which is effective in manipulating the growth of a range of diverse materials, including the synthesis of mesoporous silica[11], decorating carbon nano-onions with palladium nanoparticles[12], exfoliation of laminar material[10], forming composite material with live algal cells and controlling organic reactions[13].

Calcite is the most stable polymorph of $CaCO_3$ and is the least soluble in water as opposed to vaterite, which is the least stable polymorph and most soluble in water. These stability differences arise from the way the calcium and carbonate ions are assembled in the extended solid-state structures, Fig. 1a[14–17]. Aragonite and calcite have similar structures with the inter-planar carbonate ions in a staggered arrangement relative to each other, minimising electrostatic repulsion, while in the less dense vaterite they are almost eclipsed relative to each other. The structures have been further explored in the present study using the recently developed Hirshfeld surface analysis[18], in gaining further insight into the interplay of the ions in the solid state. Transformation from vaterite to aragonite and calcite is possible at 0–30°C and 60–80°C respectively[19,20]. In addition, aragonite is readily converted to calcite in nature at temperatures higher than 380°C[21]. The nucleation and growth of the three different polymorphs can be manipulated through the addition of crystal modifiers, including bio-polymers, inorganic salts, and macromolecules[22,23]. Developing protocols for gaining access to the different polymorphs of calcium carbonate is central to mimicking processes in nature, for example in generating synthetic aragonite, which has only recently been developed using polymer-mediated mineral growth, in addition to layer-by-layer deposition of a porous organic material[24]. Also important is gaining control over the interconversion of the different polymorphs of calcium carbonate where particular applications demand the presence of one phase of

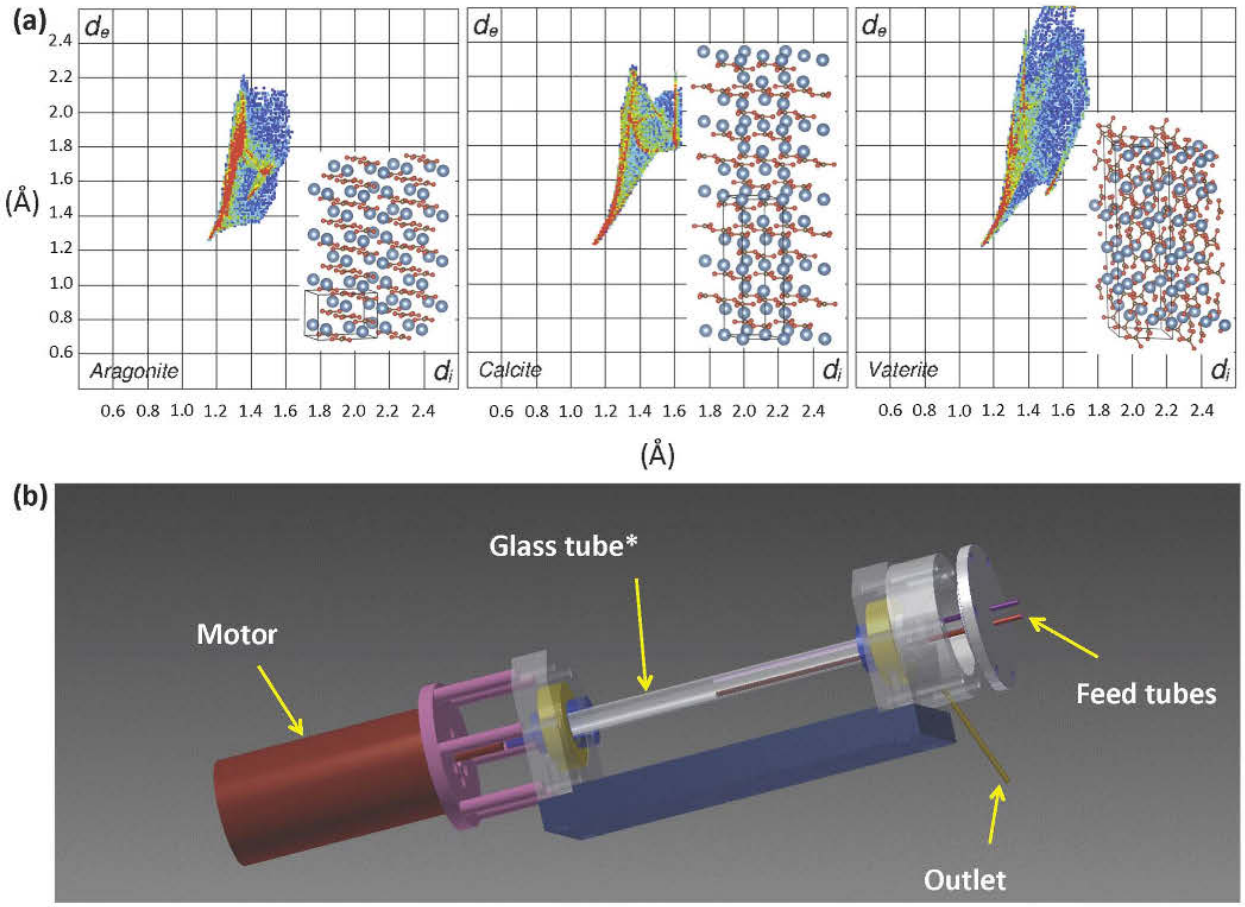

Figure 1 | (a) Hirshfeld surfaces of the calcium carbonate polymorphs, and (b) schematic of the vortex fluidic device (VFD). *Standard 10 mm NMR tube. 1(b) reproduced with permission from Bob Northeast.

specific particle size and morphology (e.g. paper coating)[25] while another application may require the *in situ* conversion of $CaCO_3$ from one phase to another, such as in drug delivery[26].

Results

The VFD used herein has a 10 mm tube with the capacity for high rotational speeds and variation in the tilt angle, θ, relative to the horizontal position, Fig. 1b. The latter can dramatically affect the shear forces present within the dynamic thin films[13], which include solutions of Milli-Q water, seawater, and a mixture of ethanol and Milli-Q water, noting that ethanol is effective in $CaCO_3$ polymorph control under conventional batch processing[27]. Milli-Q water spiked with NaCl matching the activity of salt in seawater and Milli-Q water spiked with 1% and 2% of Mg^{2+} also features in the study, noting that the presence of Mg^{2+} ions attenuates the growth of calcite with no effect on aragonite formation[28,29]. Aqueous solutions of $NaHCO_3$ as the source of carbonate ions and aqueous solutions of $CaCl_2$ as the source of calcium ions were fed into the VFD at a flow rate of 1 mL/min, in parallel with classical batch processing in a round bottom flask as control experiments. The effect of varying the ratios of HCO_3^-: Ca^{2+} on $CaCO_3$ polymorph formation was investigated with relevance to the changing atmospheric and seawater concentration of CO_2 (see experimental).

For batch processing at room temperature, 71% of the samples produced calcite quantitatively, as established using X-ray diffraction (XRD) data, Fig. 2a. A 2 : 1 ratio of HCO_3^- and Ca^{2+} results in a mixture of calcite (66.8%) and vaterite (33.2%), and decreasing or increasing the ratio of HCO_3^-: Ca^{2+} increased the percentage of calcite in the product at the expense of forming vaterite. For batch processing at 80°C there was little control in the formation of the $CaCO_3$ polymorphs, with XRD data revealing a mixture of aragonite, calcite and vaterite in all but one sample. Nevertheless, as the ratio of HCO_3^- to Ca^{2+} increases, the percentage of vaterite increases and to a lesser extent the percentage of aragonite increases, whereas the percentage of calcite decreases, Fig. 2a.

At room temperature, operating the VFD at 500 rpm at a tilt angle of 45° afforded a mixture of calcite and vaterite in 57% of the samples, while at 80°C the percentage of samples with both polymorphs dropped to 29%, Fig. 2b. Operating the VFD at 4500 rpm at a tilt angle of 45° gave no difference in the outcome for the continuous flow processing at room temperature and 80°C, with calcite being exclusively formed. The choice of 45° tilt relates to the angle that provides the greatest shear below 60° tilt. This has been judged by extensive optimisation of exfoliation of graphene and simple Diels Alder reactions[13]. Vaterite formation at 80°C was favoured at 1 : 10 and 10 : 1 ratios of HCO_3^- to Ca^{2+}. Reducing the angle of rotation of the VFD from 45° to 0° at 500 rpm also selectively afforded pure calcite for all ratios, irrespective of the temperature of the reaction.

We have shown that the VFD is effective in forming calcite or vaterite at high or low shear in aqueous systems with no evidence of the formation of aragonite despite its presence in nature in molluscan shells. Substituting Milli-Q water for seawater in the VFD and also in batch processing afforded vaterite quantitatively, Fig. 2c. Optimum conditions for obtaining vaterite in the VFD are low shear

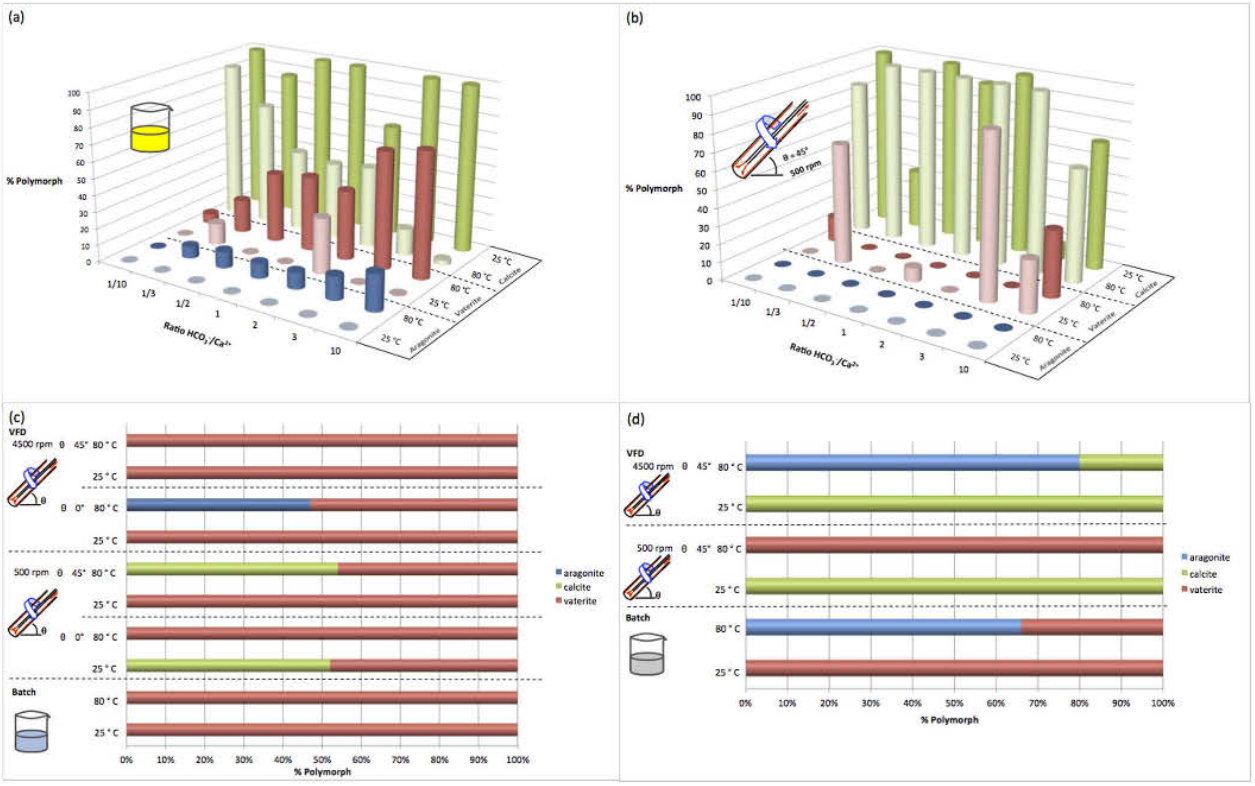

Figure 2 | Effect of HCO_3^-/Ca^{2+} ratio, shear, and medium on polymorph synthesis. 3D plots for the ratio of HCO_3^-/Ca^{2+} at room temperature and 80°C for (a) batch processing and (b) VFD processing at 500 rpm, $\theta = 45°$, against percent of the polymorph. 2D plots for $CaCO_3$ polymorphs produced in seawater (c) and in 20% ethanol with Milli-Q water (d). VFD synthesis of $CaCO_3$ at 4500 rpm, and 500 rpm at a tilt angle of $\theta = 0°$, affording calcite exclusively. (VFD jet feed flow rates 1.0 mL/min). For clarity reasons, the order of temperature for calcite in (a) and (b) has been reversed.

at 45° tilt angle (500 rpm), high shear at 45° tilt angle (4500 rpm) or 0° tilt angle, all at room temperature. Aragonite was produced in 45% yield at 80°C using the VFD at a rotation speed of 4500 rpm and 0° tilt angle. These results may reflect the presence of Mg^{2+} ions present in seawater inducing the formation of aragonite[30]. This was corroborated by XRD data for material prepared in the presence of Mg^{2+} ions, with 1% and 2% Mg^{2+} in Milli-Q water which resulted in 1% aragonite (99% calcite) in the VFD at operating at 500 rpm and 5000 rpm, at 45° tilt at room temperature. For the same conditions in the absence of added Mg^{2+}, the product was exclusively calcite, and batch processing in the presence of 1% and 2% Mg^{2+} resulted in 1% aragonite (99% calcite) and 10% aragonite (90% calcite) respectively, in contrast to forming vaterite and calcite in the absence of Mg^{2+}. The presence of carbonate and calcium ions in seawater made it inherently difficult to measure the concentration of the prepared $NaHCO_3$ and $CaCl_2$ solutions. Rather saturated solutions were prepared by the addition of excess $CaCl_2$ and $NaHCO_3$ to seawater followed by filtration. ICP-AES established that the seawater had 12500 ppm Na, 1237 ppm Mg, 891 ppm S, 389 ppm K, 400 ppm Ca, 8.9 ppm Sr and 1.35 ppm Si. (The Na and Si concentrations are higher than the global mean concentration in seawater of 10561 ppm and 0.03 ppm respectively, while that of Sr is lower than the average at 13 ppm.) Matching the activity of salt in seawater had no effect on aragonite formation with both batch and VFD processing resulting in 100% calcite.

Addition of ethanol induces aragonite formation[27] and in the present study the effect of the presence of ethanol was studied for a 20% volume mixture of ethanol in Milli-Q water, using the VFD and also in batch mode as a control. For a stoichiometric ratio of HCO_3^- to Ca^{2+} at 2 : 1, at room temperature, the VFD resulted in the formation of calcite regardless of the speed and tilt angle, Fig. 2d. In contrast, using the batch mode at room temperature, pure vaterite was obtained, while at 80°C a mixture of 64% aragonite and 34% calcite resulted. At higher temperatures and low shear stress using the VFD, vaterite was the exclusive product, while at a higher shear stress a mixture of aragonite and vaterite resulted. This is consistent with ethanol stabilising vaterite at higher temperatures by inhibiting its dissolution. Interestingly placing vaterite powder, which was prepared using the VFD operating in continuous flow mode, in water devoid of ethanol and now operating the VFD in the confined mode at a tilt angle of 45° and room temperature resulted in vaterite to calcite conversion. (The confined mode is for a finite volume of liquid processed in the VFD, where there can be intense shear at high speed in the absence of the viscous drag shear associated with continuous flow operation of the device[13].) Replacing the water with hexane in the VFD operating under confined mode gave no such phase change and this is consistent with the phase change in Milli-Q water arising from the dissolution of vaterite and the precipitation of the calcium carbonate as calcite.

The effect of tilt angle and speed on calcium carbonate synthesis in the VFD was studied for the ethanol/water system where reactant concentrations can be predetermined unlike in seawater, and where all three polymorphs can be produced, Fig. 2d. The effect of tilt angles at 4500 rpm and 80°C on the percentage of polymorph shows that for tilt angles below 45°, vaterite and aragonite dominate while at > 45°, calcite and aragonite dominate, Fig. 3b. Optimal conditions for aragonite synthesis occur at 45° with a yield of 80%. A plot of percentage of polymorph versus rotational speed at a tilt angle of 45° established that at 500 rpm vaterite is exclusively formed, and as the speed increases, the percentage of vaterite decreases to 0% at just under 4000 rpm, Fig. 3c. At 6000 rpm, aragonite and calcite are

present in 80% and 20% respectively, a polymorph mixture that is not uncommon in molluscan shells[31]. Above 6000 rpm the percentage of aragonite decreases and that of calcite increases.

Hirshfeld surface analysis, as a recently developed tool for understanding the interplay of molecules and ions in the solid state[18], highlights differences in the three polymorphs of $CaCO_3$. This includes a variation in the percentage of O···Ca and O···O interactions in the Hirshfeld surfaces, at 63.8 and 20.4%, 63.9 and 25%, and 53.7 and 34.8%, respectively for vaterite, calcite and aragonite, Fig. 1a[18]. C···C interactions are absent in the Hirshfeld surfaces of vaterite and calcite, whereas there is a small component in that of aragonite (5.4%). More significantly, vaterite is distinctly different in having a significant component of C···O interactions between carbonate ions, making up 9.1% of the Hirshfeld surface for the polymorph, which appears as a spike in the bottom right hand side of the fingerprint plot[18], Fig. 1a.

As well as controlling the polymorphs of $CaCO_3$, the use of the VFD is also effective in controlling the size and morphology of the

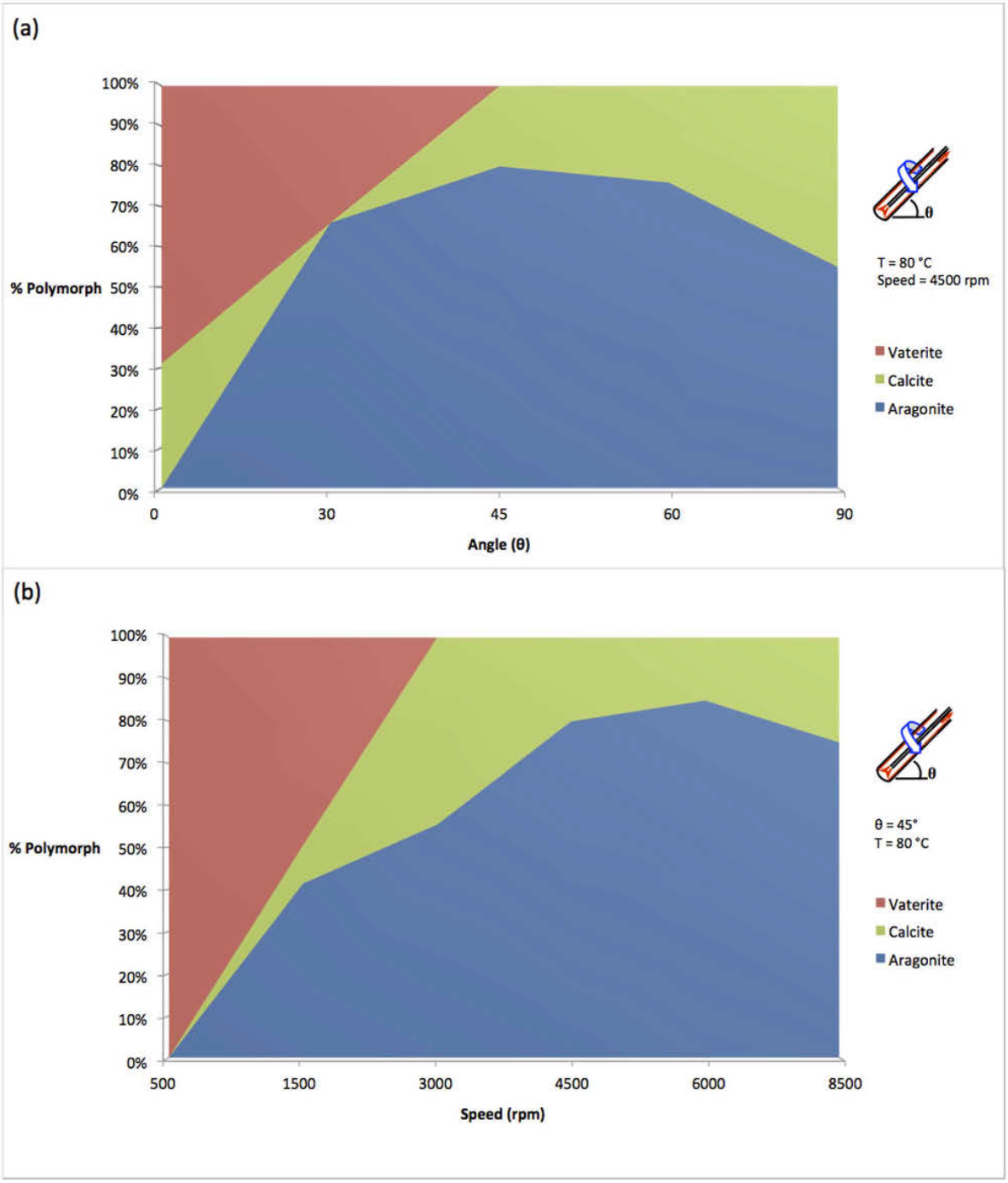

Figure 3 | Rotational speed and tilt angle control on calcium carbonate polymorph formation. Varying the tilt angle (a) and speed (b) in 20% ethanol under continuous flow conditions, for flow rates of 1.0 mL/min.

particles. A comparison between the morphology using TEM and SEM for samples processed at 45° tilt angle and room temperature using the VFD establishes the ability to also control the shape and size of the calcite crystals, with an average size of approximately 1 μm, Fig. 4a–h. This is in contrast to little control in shape and size for calcite crystals produced using batch processing, Fig. 4i–p.

Discussion

The results establish that at high temperature and high shear (4500 rpm) in Milli-Q water in the VFD results in the selective formation of the most stable polymorph, namely calcite. In contrast, operating the VFD at room temperature and low shear (500 rpm) favours exclusively vaterite, and this is consistent with previous experiments where $CaCO_3$ produced in a spinning disc processor (SDP) at 500 rpm consists of the vaterite polymorph[32]. (The SDP relates to the VFD in providing a dynamic thin film, but on a disc rather than in a tube.) The high shear forces in the VFD resulting in the formation of calcite are akin to the mechanical energy associated with milling which is capable of inducing a vaterite to calcite transformation[33].

Replacing the Milli-Q water with seawater in the VFD, however, results in the quantitative formation of vaterite at high shear (4500 rpm), at room temperature and 80°C. Presumably this arises from the high ionic activity of metal ions and carbonate ions in seawater preferentially precipitating $CaCO_3$ and circumventing the dissolution of vaterite, Eq. 1.

$$CaCO_{3(s)} \rightleftharpoons Ca^{2+}_{(aq)} + CO^{2-}_{3\ (aq)} \quad (1)$$

The ability to generate a mixture of aragonite and calcite at high shear (4500 rpm) and in 20% ethanol in the VFD, highlights the delicate balance between the these polymorphs, which is consistent with a relatively small energy difference between their formation energies[34,35]. This relates to similar crystal structures, which are distinctly different to that of vaterite, and this is further highlighted in the Hirshfeld surface analysis.

We have demonstrated the differential formation of crystalline $CaCO_3$ polymorphs under shear using a vortex fluidic device (VFD), unlike in batch processing. The ratio of Ca^{2+} to HCO_3^- is important in controlling the polymorph(s) using batch processing while using the VFD, calcite is obtained selectively at high shear, regardless of the tilt angle and temperature. Selective formation of vaterite using seawater under batch conditions occurs at room temperature and 80°C, and in the VFD at 45° and high shear. In the VFD up to 45% aragonite is accessible in seawater and up to 80% (and 20% calcite) in a mixture of ethanol and water, which is similar to the ratio of the polymorph in molluscan shells. Overall, the variation in shear and temperature in controlling the polymorphs of calcium carbonate has implications in understanding how marine organisms create their shells as conditions in the oceans change. The ability to control the size, shape and morphology of polymorphs of calcium carbonate is also significant, for a range of applications, from paper coatings to catalysis, to drug delivery, to templates for carbonaceous materials. Moreover, such control establishes a precedent for using the device to control the crystallisation outcome of a raft of materials.

Methods

The VFD consists of a 10 mm NMR tube as the reaction chamber with reactants fed into the chamber with controlled flow rates using a peristaltic pump, Fig. 1b. The tilt angle of the VFD can be varied from 0° to 90° and the rotational speed can be varied from 500 rpm to 7000 rpm. A heat jacket equipped with a heat gun can be used to operate reactions above room temperature.

The $CaCO_3$ was prepared by the reaction of sodium hydrogen carbonate ($NaHCO_3$) and calcium chloride ($CaCl_2$) to give calcium hydrogen carbonate (Eq. 2) which then decomposes to $CaCO_3$, H_2O and CO_2 (Eq. 3). $NaHCO_3$ was purchased from Optigen Scientific Pty. Ltd. and was of Optigrade™, and $CaCl_2$ was purchased from Chem-Supply Pty. Ltd. and was of laboratory reagent quality.

$$2HCO^-_{3\,(aq)} + Ca^{2+}_{(aq)} \longrightarrow Ca(HCO_3)_{2(aq)} \quad (2)$$

$$Ca(HCO_3)_2 \longrightarrow CaCO_{3(s)} + H_2O_{(l)} + CO_{2\,(g)} \quad (3)$$

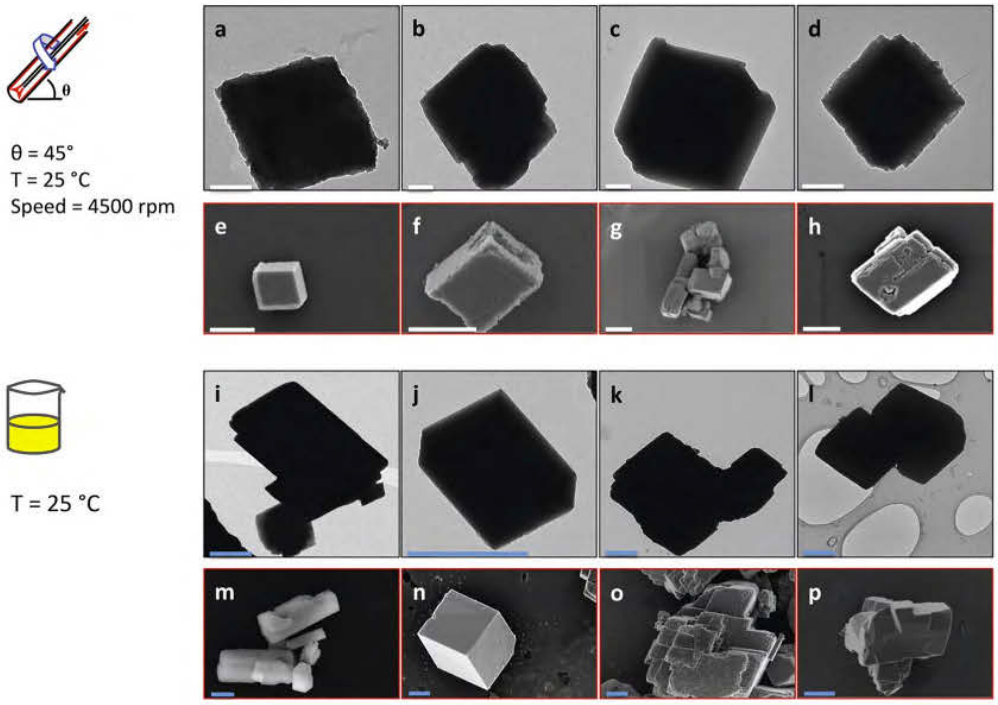

Figure 4 | Control of size, shape and morphology. TEM and SEM images of samples showing morphologies of calcite obtained at room temperature using the VFD at 4500 rpm and 45° tilt angle (a–h), and using batch processing (i–p). Scale bar for images (a)–(d) is 200 nm and 1 μm for the other images.

Stock solutions of $NaHCO_3$ and $CaCl_2$ were made in Milli-Q water to give a final concentration of 1 M. The reactants were prepared in 1 : 1, 1 : 2, 2 : 1, 1 : 3, 3 : 1, 1 : 10 and 10 : 1 ratios of HCO_3^- to Ca^{2+}. In the batch process, 15 mL of $CaCl_2$ solution with the target concentration was added drop wise to 15 mL of $NaHCO_3$ solution with the target concentration in a 50 mL conical flask. For the VFD under continuous flow, Fig. 1b, solutions of $NaHCO_3$ and $CaCl_2$ with the target concentrations were fed into the VFD at a flow rate of 1 mL/min using a peristaltic pump with the VFD set to the desired angle and at the desired temperature. The $CaCO_3$ obtained was filtered, washed with Milli-Q water and left to dry at room temperature.

Full methods and any associated references are available in the online version of the paper at www.nature.com/nature.

1. Millero, F. J. & DiTrolio, B. R. Use of thermodynamics in examining the effects of ocean acidification. *Elements* **6**, 299–303 (2010).
2. Cabemes, C., Cazenave, A. & Le Provost, C. Sea level rise during past 40 years determined from satellite and in situ observations. *Science* **294**, 840–845 (2001).
3. Baker, A. C., Glynn, P. W. & Riegl, B. Climate change and coral reef bleaching: An ecological assessment of long-term impacts, recovery trends and future outlook. *Est. Coast. Shelf Sci.* **80**, 435–471 (2008).
4. Addadi, L., Raz, S. & Weiner, S. Taking advantage of disorder: amorphous calcium carbonate and its roles in biomineralization. *Adv. Mater.* **15**, 959–970 (2003).
5. Weiss, J. M., Tuross, N., Addadi, L. & Weiner, S. Mollusc larval shell formation: amorphous calcium carbonate is a precursor phase for aragonite. *J. Exp. Zool.* **293**, 478–491 (2002).
6. Boulos, R. *et al.* Unzipping oyster shell. *RSC Adv.* **3**, 3284–3290 (2013).
7. Orr, J. C. *et al.* Anthropogenic ocean acidification over the twenty-first century and its impact on calcifying organisms. *Nature* **437**, 681–686 (2005).
8. Marubini, F., Ferrier-Pagès, C., Furla, P. & Allemand, D. Coral calcification responds to seawater acidification: a working hypothesis towards a physiological mechanism. *Coral Reefs* **27**, 491–499 (2008).
9. Steffen, W. *et al.* The Anthropocene: From global change to planetary stewardship. *AMBIO* **40**, 739–761 (2011).
10. Wahid, M. H., Eroglu, E., Chen, X., Smith, S. M. & Raston, C. L. Functional multi-layer graphene-algae hybrid material formed using vortex fluidics. *Green Chem.* **15**, 650–655 (2013).
11. Tong, C. L., Boulos, R. A., Yu, C., Iyer, K. S. & Raston, C. L. Continuous flow tuning of ordered mesoporous silica under ambient conditions. *RSC Adv.* **3**, 18767–18770 (2013).
12. Yasin, F. M. *et al.* Microfluidic size selective growth of palladium nano-particles on carbon nano-ionions. *Chem. Commun.* **48**, 10102–10104 (2012).
13. Yasmin, L., Chen, X., Stubbs, K. A. & Raston, C. L. Optimising a vortex fluidic device for controlling chemical reactivity and selectivity. *Sci. Rep.* **3**, 2282 (2013).
14. de Villiers, J. P. R. Crystal structures of aragonite, strontianite, and witherite. *Am. Mineral.* **56**, 758–767 (1971).
15. Markgraf, S. A. & Reeder, R. J. High-temperature structure refinements of calcite and magnesite. *Am. Mineral.* **70**, 590–600 (1985).
16. Wang, J. & Becker, U. Structure and carbonate orientation of vaterite ($CaCO_3$). *Am. Mineral.* **94**, 380–386 (2009).
17. de Leeuw, N. H. & Parker, S. C. Surface structure and morphology of calcium carbonate polymorphs calcite, aragonite, and vaterite: an atomistic approach. *J. Phys. Chem. B* **102**, 2914–2922 (1998).
18. McKinnon, J. J., Fabbiani, F. P. A. & Spackman, M. A. Comparison of polymorphic molecular crystal structures through Hirshfeld surface analysis. *Cryst. Growth Des.* **7**, 755–769 (2007).
19. Ogino, T., Suzuki, T. & Sawada, K. The formation and transformation mechanism of calcium carbonate in water. *Geochim. Cosmochim. Acta* **51**, 2757–2767 (1987).
20. Wray, J. L. & Daniels, F. Precipitation of calcite and aragonite. *J. Am. Chem. Soc.* **79**, 2031–2034 (1957).
21. Yoshioka, S. & Kitano, Y. Transformation of aragonite to calcite through heating. *Geochem. J.* **19**, 245–249 (1985).
22. Butler, M. F., Glaser, N., Weaver, A. C., Kirkland, M. & Butler, M. H. Calcium Carbonate Crystallization in the Presence of Biopolymers. *Cryst. Growth Des.* **6**, 781–794 (2006).
23. Kirboga, S. & Oner, M. Investigation of calcium carbonate precipitation in the presence of carboxymethyl inulin. *CrystEngComm* **15**, 3678–3686 (2013).
24. Finnemore, A. *et al.* Biomimetic layer-by-layer assembly of artificial nacre. *Nat. Commun.* **3**, 966 (2012).
25. Touaiti *et al.* Thermomechanical properties of $CaCO_3$-latex pigment coatings: Impact of modified dispersing agents. *Prog. Org. Coat.* **76**, 439–446 (2013).
26. Parakhonskiy, B. V., Haase, A. & Renzo, A. Sub-micrometer vaterite containers: synthesis, substance loading, and release. *Angew. Chem. Int. Ed.* **51**, 1195–1197 (2012).
27. Sand, K. K., Rodriguez-Blanco, J. D., Makovicky, E., Benning, L. G. & Stipp, S. L. S. Crystallization of $CaCO_3$ in water alcohol mixtures: Spherulitic growth, polymorph stabilization, and morphology change. *Cryst. Growth Des.* **12**, 842–853 (2012).
28. Ries, J. B., Anderson, M. A. & Hill, R. T. Seawater Mg/Ca controls polymorph mineralogy of microbial $CaCO_3$: A potential proxy for calcite-aragonite seas in Precambrian time. *Geobiology* **6**, 106–119 (2008).
29. Davis, K. J., Dove, P. M. & De Yoreo, J. The role of Mg^{2+} as an impurity in calcite growth. *Science* **290**, 1134–1137 (2000).
30. Liu, F. *et al.* Biomimetic fabrication of pseudohexagonal aragonite tablets through a temperature-varying approach. *Chem. Commun.* **46**, 4607–4609 (2010).
31. Adler, H. H. & Kerr, P. F. Infrared study of aragonite and calcite. *Am. Mineral.* **47**, 700–717 (1962).
32. Hetherington, P. PhD. Thesis, Process intensification: a study of calcium carbonate precipitation methods on a spinning disc reactor. University of Newcastle upon Tyne, (2006).
33. Northwood, D. O. & Lewis, D. Transformation of vaterite to calcite during grinding. *Am. Mineral.* **53**, 2089–2092 (1968).
34. Sekkal, W. & Zaoui, A. Nanoscale analysis of the morphology and surface stability of calcium carbonate polymorphs. *Sci. Rep.* **3**, 1587 (2013).
35. Wolf, G., Lerchner, J., Schmidt, H., Gamsjäger, H., Königsberger, E. & Shmidt, P. Thermodynamics of $CaCO_3$ phase transitions. *J. Therm. Anal.* **46**, 353–359 (1996).

Acknowledgments

Support of this work by the Australian Research Council, The Government of South Australia, Pearl Technologies Pty Ltd, and Centre for Microscopy, Characterisation and Analysis at the University of Western Australia and Adelaide University is greatly acknowledged. F. Zhang is thankful for the support of China Scholarship Council for his study in Australia. The authors thank Bob Northeast for the 3D drawing of the VFD.

Author contributions

R.A.B. and F.Z. carried out fluid flow experiments, R.A.B., F.Z. and E.S.T. carried out characterisation, A.D.M. carried out the Hirshfeld surface analysis, R.A.B., D.S. and C.L.R. designed the experiments and wrote the paper, and C.L.R. designed the microfluidic platform and coordinated the research.

Additional information

Supplementary information accompanies this paper at http://www.nature.com/scientificreports

Competing financial interests: The authors declare no competing financial interests.

How to cite this article: Boulos, R.A. *et al.* Spinning up the polymorphs of calcium carbonate. *Sci. Rep.* **4**, 3616; DOI:10.1038/srep03616 (2014).

Toxicology Research

COMMUNICATION

View Article Online
View Journal

Evaluating the effects of nacre on human skin and scar cells in culture†

Cite this: DOI: 10.1039/c4tx00004h

Received 6th January 2014,
Accepted 2nd May 2014

DOI: 10.1039/c4tx00004h

www.rsc.org/toxicology

Vipul Agarwal,[a] Edwin S. Tjandra,[a] K. Swaminathan Iyer,[a] Barry Humfrey,[b] Mark Fear,[c] Fiona M. Wood,[c] Sarah Dunlop[d] and Colin L. Raston*[e]

Pearl nacre, a biomineralisation product of molluscs, has growing applications in cosmetics, as well as dental and bone restoration, yet a systematic evaluation of its biosafety is lacking. Here, we assessed the biocompatibility of nacre with two human primary dermal fibroblast cell cultures and an immortalised epidermal cell line and found no adverse effects.

There are three main types of pearl oysters of the genus *Pinctada*: the "Akoya" pearl oyster called *Pinctada fucata*, the "Golden lipped" oyster *Pinctada maxima* and the "Black lipped" oyster named *Pinctada margaritifera*. Mollusc shells are mainly made up of two layers of calcium carbonate, comprising an outer layer of calcite and an inner layer of aragonite. Nacre (mother of pearl) in all oyster shells is a calcified structure that forms the lustrous inner layer. It is mainly composed of aragonite (~95–97%) tablets oriented in multiple layers, each surrounded by organic matrix.[1,2] This organic matrix makes up ~5% of the nacre composition and is mainly comprised of polysaccharides and proteins.[3] According to a European Commission report published in 2007 the cosmetic and toiletries industry in the EU, Japan, China and the US had a total market value of €136.2 billion.[4] The cosmetics industry maintains its edge by constantly developing novel topical skin treatments. A popular example is the use of all-natural or organic ingredients, such as fruit and plant extracts to offer wrinkle relief that mimics the painful and potentially dangerous side effects associated with invasive chemical remedies.[5] Clinically, topical treatments containing, for example, aloe vera, vitamin C, corticosteroids and tacrolimus are used with the aim of minimizing scarring.[6] Recently, there has been interest in the cosmetics industry in the use of nacre as a key ingredient.[7] Most of the formulations are reported to either use powdered pearl shell or powdered nacreous layer shell. Powdered shell and powdered nacre comprises of both organic and inorganic components. It is reported that nacre stores in its mineral-based organic structure a variety of bioactive molecules. Efficacy of this water soluble matrix (WSM) has been tested in a porcine burn injury model.[8] WSM was obtained by suspending powdered nacre in ultra-pure water and collecting the supernatant *via* precipitation of insoluble components by centrifugation. It was concluded that the active mineral based organic component has beneficial effects on the skin with enhanced wound healing.[8,9]

Nacre has also attracted attention for its potential in supporting bone grafting and bone regeneration. In culture under physiological conditions, nacre can transform to hydroxyapatite, the phosphorous rich main constituent of the mammalian bone framework.[10,11] Nacre and its WSM can also aid in osteogenic regeneration.[9,12–17] High phosphorous rich domains have been described at the interface between bone and implants made from *Margaritifera* shells which are biocompatible, biodegradable and osteoconductive and thus are thought to promote bone formation.[18] Furthermore, nacre powder has been used as an implantable material for reconstruction and regeneration of maxillary alveolar ridge bone in humans.[19] In this example, the implanted nacre dissolves gradually and is eventually replaced by the mature lamellar bone suggesting that the nacre acts as a biocompatible substrate for bone replacement.[19] The water soluble components of the crushed nacre have also been investigated for their potential in bone regeneration in a similar vein.[20,21] Lee *et al.*, demonstrated the wound healing potential of WSM component in a deep burn porcine skin model and showed enhanced collagen secretion and deposition at the injury site resulting in enhanced healing.[8] In another *in vivo* study using a rat skin incisional injury model, powdered nacre was implanted between the epidermis and dermis at the incisional site, with an aim of studying the effect of nacre on the synthesis of certain constituents of the dermal

[a]*School of Chemistry and Biochemistry, The University of Western Australia, Crawley, Australia*
[b]*Pearl Technology Pty Ltd, Geraldton, Australia*
[c]*Burn Injury Research Unit, School of Surgery, The University of Western Australia, Crawley, Australia*
[d]*School of Animal Biology, The University of Western Australia, Crawley, Australia*
[e]*School of Chemical and Physical Sciences, Flinders University, Bedford Park, Australia. E-mail: colin.raston@flinders.edu.au; Tel: +61 82017958*
†Electronic supplementary information (ESI) available. See DOI: 10.1039/c4tx00004h

extracellular matrix. It was concluded that implanted nacre increased collagen synthesis by dermal fibroblasts.[22] While extensive investigations have been carried out in bone, the evaluation of the biocompatibility of nacre with human skin cells is lacking. Thus the growing number of cosmetic formulations in the market with nacre as a key ingredient[7,23,24] clearly warrants a thorough assessment with human skin cells. Since scars are also common, and contain cells with a phenotype distinct from normal skin,[25] it is also important to test potential cosmetic ingredients with both cell types.

In the present study, we use nacre from the inner calcified layer of the shell of *Pinctada margaritifera* and report the *in vitro* toxicity assessment of the material on three cell types representing both epidermal and dermal layers of human skin. These were HaCaT cells, a human derived immortalised keratinocytes cell line, primary human dermal skin fibroblasts (HDF) and primary human scar fibroblasts (HSF).

Nacre used in the study was gently scraped[26,27] from the inner layer of the shell to avoid the post processing required in the case of powdered shell. SEM images (Fig. 1) confirmed that the nacre was composed of pseudo-hexagonal shaped aragonite tablets which have basal plane dimensions of 2–6 μm, and a thickness of 300–400 nm.[28] This structure is characteristic of previously reported nacre, which is a composite material consisting of alternating layers of mineral tablets separated by thin layers of biomacromolecular "glue".[29,30]

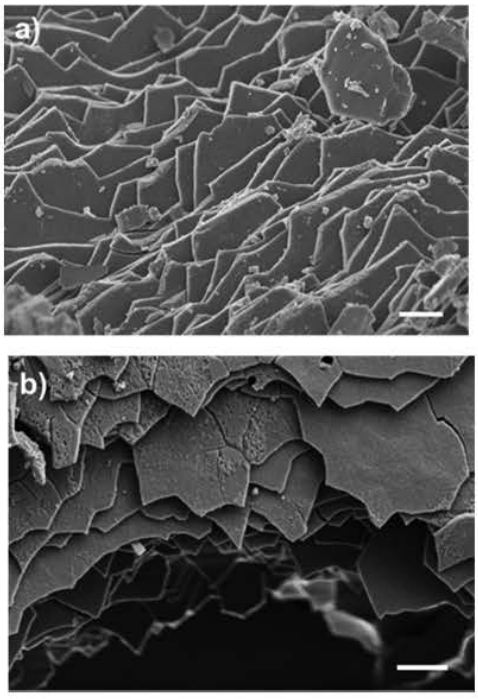

Fig. 1 Top view of the scrapped nacre, imaged using scanning electron microscopy (SEM). Scale bar (a) 1 μM and (b) 2 μM respectively. Sample was coated with 4 nm platinum prior to imaging.

To test the cytotoxicity of nacre, a live/dead assay was carried out (see ESI S1.4†). Cells were incubated with nacre in culture media at physiological conditions for 24 h to 72 h and were then stained for viability using calcein AM/ethidium bromide I solutions. Viable cells fluoresce green through the reaction of calcein AM with intracellular esterase, whereas non-viable cells fluoresce red due to the diffusion of ethidium homodimer across damaged cell membranes and binding with nucleic acids.

Fig. 2 shows live cells as the percentage of the total cells in human primary dermal skin fibroblast (HDF), human primary scar fibroblast (HSF) and human derived immortalised HaCaT cell cultures when exposed to various concentrations of nacre for 24 h and 72 h. Cytotoxicity of nacre was not observed for any of the concentrations examined in HDF cells (Fig. 2a). However, interestingly at a concentration of 2.5 mg ml^{-1} of nacre (highest concentration tested) there was a significant reduction in viability at both 24 and 72 hours in the HSF cells (Fig. 2b). This underlines the importance of testing both scar and normal skin cell types for cosmetic application. Toxicity was also observed at a concentration of 0.5 mg ml^{-1} in HaCaT cells (Fig. 2c), although this was only observed at 24 hours and

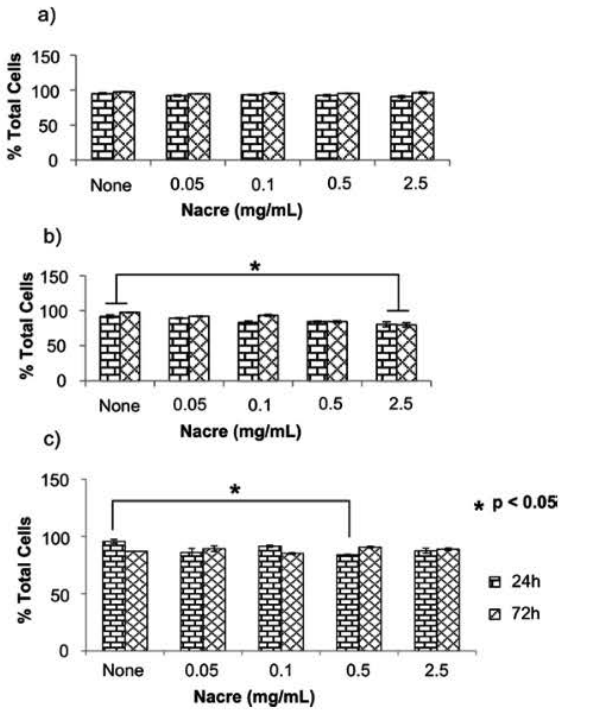

Fig. 2 Cell viability assays showing percentage of live cells in the culture post incubation with nacre. (a) Human dermal skin fibroblasts cells, (b) human scar fibroblasts cells and (c) human derived immortalised HaCaT cells were incubated with various concentrations of scrapped nacre and treated with calcein AM/ethidium bromide I to stain for live and dead cells. Both live and dead cells were counted using fluorescence microscopy. 'None' is the untreated control. Data presented as average ± SEM (n = 4). Significance was set at *p < 0.05 using bonferroni test in one way ANNOVA.

was no longer present at the 72 hour time point. These results are in line with the results obtained previously where constituents of nacre were shown to promote wound healing in a rat model[22] and deep burn porcine skin.[8] In both these studies, nacre has been shown to promote the recruitment of fibroblasts for restoration and coverage of the injury site while showing no apparent signs of cytotoxicity. It has also been shown to promote bone formation when implanted in the femur of sheep with midshaft hemidiaphysis resection of their femur *in vivo* reiterating the non-cytotoxic advantage of nacre.[31]

Fibroblasts have been reported to undergo morphological changes from dendritic to stellate shapes upon exposure to external cues caused by changes in actin polarisation and adhesion.[32,33] Cell morphology in fibroblasts is known to be influenced by cytokines such as transforming growth factor β which can potentially induce polymerisation of globular to filamentous actin.[34] Fibroblast morphology can also be modulated by extracellular matrix architecture during wound healing *via* cell–matrix interaction.[32] Such morphological change has been observed in cells undergoing oxidative stress.[35,36] In our study, we found similar changes in fibroblast morphology for both HDF and HSF cells at the highest concentration of nacre of 2.5 mg mL^{-1} (Fig. 3). Similar altered morphology was also observed for HaCaT cells (see ESI Fig. S1†). It could be postulated that the high concentration of nacre induces cellular stress, resulting in changes in the actin cytoskeleton and a more stellate morphology (Fig. 3i, iii, ii and iv). Cell area was calculated from the fluorescent images shown in Fig. 3 using Image J software.[37] It was found that both HDF and HSF had significantly larger cell areas ($p < 0.05$) when treated with 2.5 mg mL^{-1} of nacre (HDF: 2.79 ± 0.13 μm and HSF: 3.0 ± 0.19 μm respectively) as compared to the non-treated controls (HDF: 1.56 ± 0.08 μm and HSF: 1.54 ± 0.10 μm respectively) (see ESI Fig. S2†).

Altered fibroblast morphology has been thought to occur in response to various factors including aging,[38] strength of the extracellular matrix[39] or other etiologies that induce mechanical stress on the cell. Changes in morphology also commonly indicate oxidative as well as mechanical stress.[39] Therefore, we explored whether the morphological changes and increase in

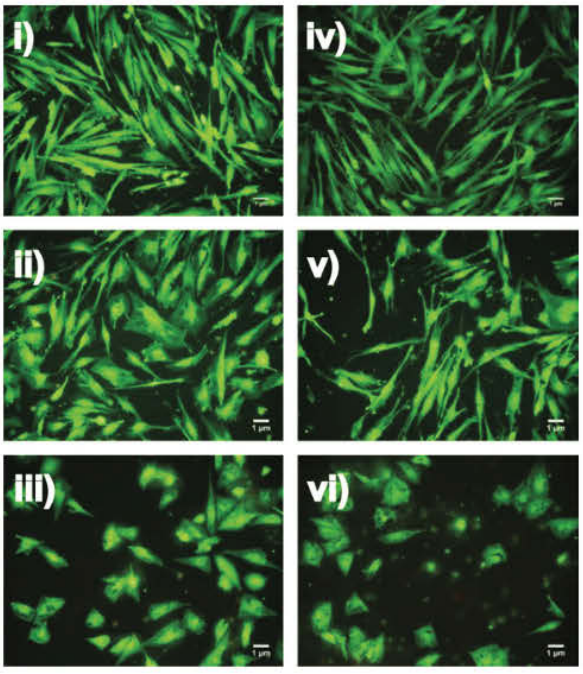

Fig. 3 Cell morphology post calcein AM staining and imaged using fluorescent microscopy. Cells were treated with various concentrations of nacre for 24 h, stained and imaged. (i) untreated (control) primary human dermal skin fibroblasts (HDF), (ii) HDF treated with 0.05 mg mL^{-1} nacre, (iii) HDF treated with 2.5 mg mL^{-1} nacre, and (iv), untreated (control) primary human dermal scar fibroblasts (HSF), (v) HSF treated with 0.05 mg mL^{-1} nacre and (vi) HSF treated with 2.5 mg mL^{-1} nacre. Scale bar 1 μm.

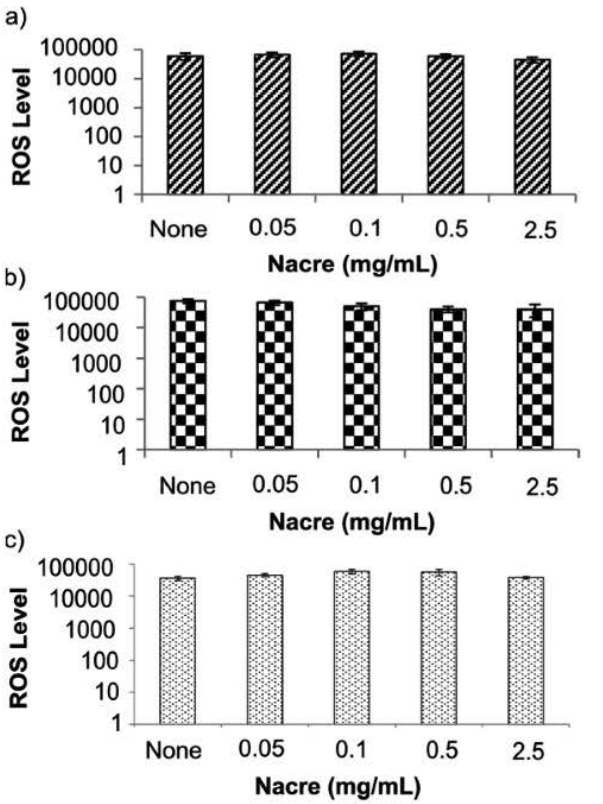

Fig. 4 Reactive oxygen species (ROS) assay showing ROS levels in cells stressed with various concentrations of nacre for 24 h. No significant stress was observed as a result of calcium (from nacre) induced oxidative stress at the concentrations studied. (a) Human dermal skin fibroblasts cells, (b) human scar fibroblasts cells and (c) human derived immortalised HaCaT cells were incubated with various concentrations of scrapped nacre for the specified period of time. Cells were then incubated with 2′,7′-dichlorodihydrofluorescein diacetate (DCFH-DA) solution which fluoresce in the presence of reactive oxygen species. 'None' is the untreated control. Data presented as average ± SEM (n = 3). Significance was set at *$p < 0.05$ using bonferroni test in one way ANNOVA.

cell area at the highest concentration of nacre in culture was a result of, or induced oxidative stress in, the cells. Oxidative stress was tested using the cell permeable fluorogenic probe 2′,7′-dichlorodihydrofluorescein diacetate (DCFH-DA). DCFH-DA is taken up by cells and is deacetylated by cellular esterases to non-fluorescent 2′,7′-dichlorodihydrofluorescein (DCFH) which is rapidly oxidised by reactive oxygen species (ROS) to highly fluorescent 2′,7′-dichlorodihydrofluorescein (DCF). The fluorescent intensity is proportional to the ROS levels within the cytosol (see ESI S1.5†). Cell responsiveness to the assay was carried out by stressing the cells with the H_2O_2 solution provided in the kit which was also used to generate the calibration curve (see ESI Fig. S3†). No changes in levels of reactive oxygen species were observed in any cell type at any concentration of nacre (Fig. 4). This is important as oxidative stress is known to be a significant contributor to skin damage and excessive scarring in previous studies.[40] It has been known that cells alter their morphology depending on their environment.[41,42] It is therefore hypothesized that the altered fibroblast morphology in the present case is mainly due to the regulation of cell motility through geometrical constraint in the presence of nacre. Indeed, it has been previously reported that when cells probe their physical surroundings, they acquire mechanical information or signals that help to determine the direction of migration, with a consequential change in cell morphology.[43]

Conclusions

We have established the biocompatibility of nacre using three human cell types representing the two primary layers of human skin, using immortalised keratinocytes from the epidermal layer and two primary human dermal cell cultures. The nacre used in the present study showed limited cytotoxicity at high concentrations in scar derived cells, with the morphology of the cells significantly changed by exposure at such concentrations of nacre. No apparent oxidative stress was evident in any of the cell types. Overall, the data support the use of low concentrations of nacre in aesthetic formulations, with the potential for high concentrations to cause changes in skin and/or scar cells which may have impact on efficacy.

The authors would like to thank the Australian Research Council and Pearl Technologies for funding the work under the grant number LP100100812. The authors would also like to acknowledge the Australian Microscopy & Microanalysis Research Facility at the Centre for Microscopy, Characterization & Analysis, The University of Western Australia, funded by the University, State and Commonwealth Governments.

Notes and references

1 J. H. E. Cartwright and A. G. Checa, *J. R. Soc. Interface*, 2007, **4**, 491–504.
2 F. Nudelman, E. Shimoni, E. Klein, M. Rousseau, X. Bourrat, E. Lopez, L. Addadi and S. Weiner, *J. Struct. Biol.*, 2008, **162**, 290–300.
3 Y. Oaki and H. Imai, *Angew. Chem., Int. Ed.*, 2005, **44**, 6571–6575.
4 D. G. f. E. a. I. European Commission, A Study of the European Cosmetics Industry, Report, European Commission, 2007.
5 P. M. Reddy, M. Gobinath, K. M. Rao, P. Venugopalaiah and N. Reena, *Int. J. Adv. Pharm. Nanotechnol.*, 2011, **1**, 121–139.
6 J. M. Zurada, D. Kriegel and I. C. Davis, *J. Am. Acad. Dermatol.*, 2006, **55**, 1024–1031.
7 Pearlcium, Genesis Framework – WordPress, vol. 2013, p. US.
8 K. Lee, H. Kim, J. Kim, Y. Chung, T. Lee, H.-S. Lim, J.-H. Lim, T. Kim, J. Bae, C.-H. Woo, K.-J. Kim and D. Jeong, *Mol. Biol. Rep.*, 2012, **39**, 3211–3218.
9 M. J. Almeida, C. Milet, J. Peduzzi, L. Pereira, J. Haigle, M. Barthélemy and E. Lopez, *J. Exp. Zool.*, 2000, **288**, 327–334.
10 Y. Guo and Y. Zhou, *J. Biomed. Mater. Res., Part A*, 2008, **86**, 510–521.
11 P. Westbroek and F. Marin, *Nature*, 1998, **392**, 861–862.
12 M. Lamghari, M. J. Almeida, S. Berland, H. Huet, A. Laurent, C. Milet and E. Lopez, *Bone*, 1999, **25**, 91S–94S.
13 M. Lamghari, H. Huet, A. Laurent, S. Berland and E. Lopez, *Biomaterials*, 1999, **20**, 2107–2114.
14 M. Lamghari, S. Berland, A. Laurent, H. Huet and E. Lopez, *Biomaterials*, 2001, **22**, 555–562.
15 F. Moutahir-belqasmi, N. Balmain, M. Lieberrher, S. Borzeix, S. Berland, M. Barthelemy, J. Peduzzi, C. Milet and E. Lopez, *J. Mater. Sci.: Mater. Med.*, 2001, **12**, 1–6.
16 D. Duplat, A. Chabadel, M. Gallet, S. Berland, L. Bédouet, M. Rousseau, S. Kamel, C. Milet, P. Jurdic, M. Brazier and E. Lopez, *Biomaterials*, 2007, **28**, 2155–2162.
17 C. Silve, E. Lopez, B. Vidal, D. Smith, S. Camprasse, G. Camprasse and G. Couly, *Calcif. Tissue Int.*, 1992, **51**, 363–369.
18 H. Liao, H. Mutvei, M. Sjöström, L. Hammarström and J. Li, *Biomaterials*, 2000, **21**, 457–468.
19 G. Atlan, N. Balmain, S. Berland, B. Vidal and É. Lopez, *C. R. l'Academie. Sci., Ser. III*, 1997, **320**, 253–258.
20 L. Pereira Mouriès, M.-J. Almeida, C. Milet, S. Berland and E. Lopez, *Comp. Biochem. Physiol., Part B: Biochem. Mol. Biol.*, 2002, **132**, 217–229.
21 M. Rousseau, H. Boulzaguet, J. Biagianti, D. Duplat, C. Milet, E. Lopez and L. Bédouet, *J. Biomed. Mater. Res., Part A*, 2008, **85**, 487–497.
22 E. Lopez, A. L. Faou, S. Borzeix and S. Berland, *Tissue Cell*, 2000, **32**, 95–101.
23 E. Lopez and A. E. Chemouni, *US Pat*, US10/089,982, 2005.
24 D. M. DeLaRosa, *US Pat*, US2008/0199533 A1, 2008.
25 C. Chipev and M. Simon, *BMC Dermatol.*, 2002, **2**, 13.
26 M. Norizuki and T. Samata, *Mar. Biotechnol.*, 2008, **10**, 234–241.
27 C. Ma, C. Zhang, Y. Nie, L. Xie and R. Zhang, *Tsinghua Sci. Technol.*, 2005, **10**, 499–503.

28 K. S. Katti, B. Mohanty and D. R. Katti, *J. Mater. Res.*, 2006, **21**, 1237–1242.
29 R. A. Boulos, C. Harnagea, X. Duan, R. N. Lamb, F. Rosei and C. L. Raston, *RSC Adv.*, 2013, **3**, 3284–3290.
30 E. S. Tjandra, R. A. Boulos, P. C. Duncan and C. L. Raston, *CrystEngComm*, 2013, **15**, 6896–6900.
31 S. Berland, O. Delattre, S. Borzeix, Y. Catonné and E. Lopez, *Biomaterials*, 2005, **26**, 2767–2773.
32 E. Tamariz and F. Grinnell, *Mol. Biol. Cell*, 2002, **13**, 3915–3929.
33 Q. M. Chen, V. C. Tu, J. Catania, M. Burton, O. Toussaint and T. Dilley, *J. Cell Sci.*, 2000, **113**, 4087–4097.
34 A. Moustakas and C. Stournaras, *J. Cell Sci.*, 1999, **112**, 1169–1179.
35 W. Malorni, F. Iosi, F. Mirabelli and G. Bellomo, *Chem. Biol. Interact.*, 1991, **80**, 217–236.
36 G. Bellomo, F. Mirabelli, M. Vairetti, F. Iosi and W. Malorni, *J. Cell. Physiol.*, 1990, **143**, 118–128.
37 T. J. Collins, *BioTechniques*, 2007, **43**, S25–S30.
38 J. Varani, M. K. Dame, L. Rittie, S. E. G. Fligiel, S. Kang, G. J. Fisher and J. J. Voorhees, *Am. J. Pathol.*, 2006, **168**, 1861–1868.
39 G. J. Fisher, T. Quan, T. Purohit, Y. Shao, M. K. Cho, T. He, J. Varani, S. Kang and J. J. Voorhees, *Am. J. Pathol.*, 2009, **174**, 101–114.
40 R. E. Barrow and M. R. K. Dasu, *J. Surg. Res.*, 2005, **126**, 59–65.
41 M. Dalby, M. Riehle, H. Johnstone, S. Affrossman and A. Curtis, *Tissue Eng.*, 2002, **8**, 1099–1108.
42 K. Burridge and M. Chrzanowska-Wodnicka, *Annu. Rev. Cell Dev. Biol.*, 1996, **12**, 463–519.
43 R. J. Petrie, A. D. Doyle and K. M. Yamada, *Nat. Rev. Mol. Cell Biol.*, 2009, **10**, 538–549.

OPEN

The Journal of Antibiotics (2015), 1–10

www.nature.com/ja

ORIGINAL ARTICLE

A new antibiotic with potent activity targets MscL

Irene Iscla[1], Robin Wray[1], Paul Blount[1], Jonah Larkins-Ford[2], Annie L Conery[2], Frederick M Ausubel[2], Soumya Ramu[3], Angela Kavanagh[3], Johnny X Huang[3], Mark A Blaskovich[3], Matthew A Cooper[3], Andres Obregon-Henao[4], Ian Orme[4], Edwin S Tjandra[5], Uwe H Stroeher[6], Melissa H Brown[6], Cindy Macardle[7], Nick van Holst[7], Chee Ling Tong[8], Ashley D Slattery[8], Christopher T Gibson[8], Colin L Raston[8] and Ramiz A Boulos[8]

The growing problem of antibiotic-resistant bacteria is a major threat to human health. Paradoxically, new antibiotic discovery is declining, with most of the recently approved antibiotics corresponding to new uses for old antibiotics or structurally similar derivatives of known antibiotics. We used an *in silico* approach to design a new class of nontoxic antimicrobials for the bacteria-specific mechanosensitive ion channel of large conductance, MscL. One antimicrobial of this class, compound 10, is effective against methicillin-resistant *Staphylococcus aureus* with no cytotoxicity in human cell lines at the therapeutic concentrations. As predicted from *in silico* modeling, we show that the mechanism of action of compound 10 is at least partly dependent on interactions with MscL. Moreover we show that compound 10 cured a methicillin-resistant *S. aureus* infection in the model nematode *Caenorhabditis elegans.* Our work shows that compound 10, and other drugs that target MscL, are potentially important therapeutics against antibiotic-resistant bacterial infections.
The Journal of Antibiotics advance online publication, 4 February 2015; doi:10.1038/ja.2015.4

INTRODUCTION

The overprescription of antibiotics and failure of patients to complete antibiotic treatment regimens have contributed to the emergence of bacterial multi-drug resistance (MDR). At the same time, the large costs involved in developing new drugs, exacerbated by a complicated drug approval and patent process,[1] have caused a dearth in new antibiotic research with many pharmaceutical companies choosing to focus their efforts on more profitable, higher volume drugs.[2,3] As a result, fighting MDR bacterial infections in patients is becoming increasingly difficult with treatment options becoming very limited.[4,5] Furthermore, there are relatively few novel small molecules in the antibiotic development pipeline.[6]

The mechanosensitive ion channel of large conductance (MscL) in bacteria is an attractive target for drug discovery because of its high level of conservation in bacterial species, and its absence from the human genome. Such level of conservation suggests that the channel has an important and conserved function, which has recently been highlighted as one of the top 20 targets for drug development.[7] In *Escherichia coli*, the transmembrane MscL channel consists of five identical subunits, each composed of 136 amino acids.[8,9] MscL has the largest pore size of any gated ion channel, estimated to be 28 Å when fully open.[10,11] Mechanosensitive channels have evolved to sense mechanical tension on the membrane and convert it into an electrochemical response. As such, they act as gatekeepers, protecting bacterial cells against lysis following acute decrease in the osmotic environment. Moreover, these channels can act as entry points for drugs and other small molecules into bacterial cells.

In this paper, we describe the *in silico* design of MscL ligands, which led to the discovery of a novel class of compounds with optimal binding to MscL. One of these ligands, 1,3,5-tris[(1E)-2′-(4″-benzoic acid)vinyl]benzene (referred to hereafter as **10**, Ramizol), is an effective antimicrobial against methicillin-resistant *Staphylococcus aureus* (MRSA).[12] Using microscopic analysis and other techniques, we show that the mechanism of action of **10** in Gram-positive and Gram-negative bacteria involves its interaction with MscL. We also show that **10** exhibits *in vivo* efficacy in a *Caenorhabditis elegans* nematode infection model. Moreover, **10** exhibits low levels of toxicity in addition to being a potent antioxidant,[13] potentially providing an additional benefit by reducing bacterial-induced inflammation.

RESULTS

In silico design of ligands targeting MscL

To explore the potential of MscL as a target for antibiotics, we developed a spatial map between the exposed oxygen atoms of amino acids, lining the gate of the MscL channel. This three-dimensional spatial map was used for the *de novo* design[14] of several potential

[1]Department of Physiology, UT Southwestern Med Ctr, Dallas, TX, USA; [2]Department of Molecular Biology, Massachusetts General Hospital, Boston, MA, USA; [3]Institute for Molecular Bioscience, University of Queensland, St Lucia, QLD, Australia; [4]Department of Microbiology, Immunology, and Pathology, Colorado State University, Fort Collins, CO, USA; [5]School of Animal Biology, The University of Western Australia, Crawley, WA, Australia; [6]School of Biological Sciences, Flinders University, Bedford Park, SA, Australia; [7]Flinders Medical Science and Technology, Immunology, Allergy and Arthritis, Flinders University, Bedford Park, SA, Australia and [8]Centre for NanoScale Science and Technology, School of Chemical and Physical Sciences, Flinders University, Bedford Park, SA, Australia
Correspondence: Paul Blount or Dr R Boulos, Centre for NanoScale Science and Technology, School of Chemical and Physical Sciences, Flinders University, Bedford Park, South Australia 5042, Australia.
E-mail: Paul.blount@UTSouthwestern.edu or ramiz.boulos@flinders.edu.au
Received 19 September 2014; revised 27 November 2014; accepted 15 December 2014

ligands capable of hydrogen bonding to the MscL channel amino acids as shown in Figure 1a. We calculated that one of these potential ligands, 1,2,4-tris[2′-(4″-phenol)ethyl]benzene (ligand 2), had the lowest docking energy (Figure 1b). We then further optimized the binding of ligand 2 using iterative *in silico* docking models to identify related structures with lower docking energies (Figure 1c). Specifically, the hydroxyl groups in ligand 2 were substituted with a variety of functional groups (aldehydes, amide cations, amino, carboxyl, chloride). With reference to Figure 1c, we found that the addition of carboxyl groups to the 'b', 'c' and 'd' positions resulted in the most favorable docking energies. This ligand, 8, was determined to have a free energy of binding equivalent to $\sim -55.94\,kJ\,mol^{-1}$, which is higher than previously screened candidates from the National Cancer Institute database. Thus, compound 8 and its analogs represent a potentially novel class of antimicrobials based on *p*-carboethoxy-tristyryl and *p*-carboethoxy-terastyrenyl benzene derivatives.

Compound 10 is a potent antibiotic against a range of Gram-positive bacteria

We further investigated a particular analog of compound 8: the symmetrical and fluorescent molecule **10**, which, based on preliminary disk diffusion studies, was found to be more effective than the other analogs[12] with the exception of 2,2′,2″-{[(1*E*,1′*E*,1″*E*)-benzene-1,3,5-triyltris(ethene-2,1-diyl)]tris(benzene-4,1-diyl)}triacetic acid, **11**, which was only discovered recently.[15] As shown in Table 1, **10** is a potent antimicrobial against a variety of *S. aureus* strains with minimum ICs (MICs) of $\sim 4\,\mu g\,ml^{-1}$. These *S. aureus* strains include a variety of drug-resistant MRSA, glycopeptide intermediate *S. aureus* (GISA) and vancomycin-resistant *S. aureus* (VRSA) strains, including a MRSA strain that is daptomycin-resistant. **10** was also effective against an MDR *Streptococcus pneumoniae* strain with a MIC of $4\,\mu g\,ml^{-1}$. In contrast, **10** was relatively inactive (MIC $>64\,\mu g\,ml^{-1}$) against *Enterococcus faecalis* VanA clinical isolate and *E. faecium* MDR-VanA ATCC 51559. **10** was also inactive against a variety of Gram-negative bacteria tested (*E. coli* ATCC 25922, *Klebsiella pneumoniae* ATCC 700603, *K. pneumoniae* ATCC 13883, *Acinetobacter baumannii* ATCC 19606 and *Pseudomonas aeruginosa* ATCC 27853) with an MIC > 64-$\mu g\,ml^{-1}$ (data not shown), but showed marginal activity against a *P. aeruginosa* polymyxin–resistant strain (MIC $64\,\mu g\,ml^{-1}$) and a *K. pneumoniae* BAA-2146 NDM-1-positive strain (MIC $64\,\mu g\,ml^{-1}$).

Compound **10** also showed no significant activity against *M. tuberculosis* strains H37Rv and TT372 grown in 7H9 medium (MIC $160\,\mu g\,ml^{-1}$). However, when H37Rv was grown in Proskauer and Beck medium or in glycerol-alanine-salts media, the MIC was $20\,\mu g\,ml^{-1}$ (Table 1). One possible explanation for this observation is that the 7H9 medium contains albumin. It is well established that high affinity of albumin to a wide range of structurally different drugs[16] can affect their bioavailability. If **10** does indeed bind to albumin,

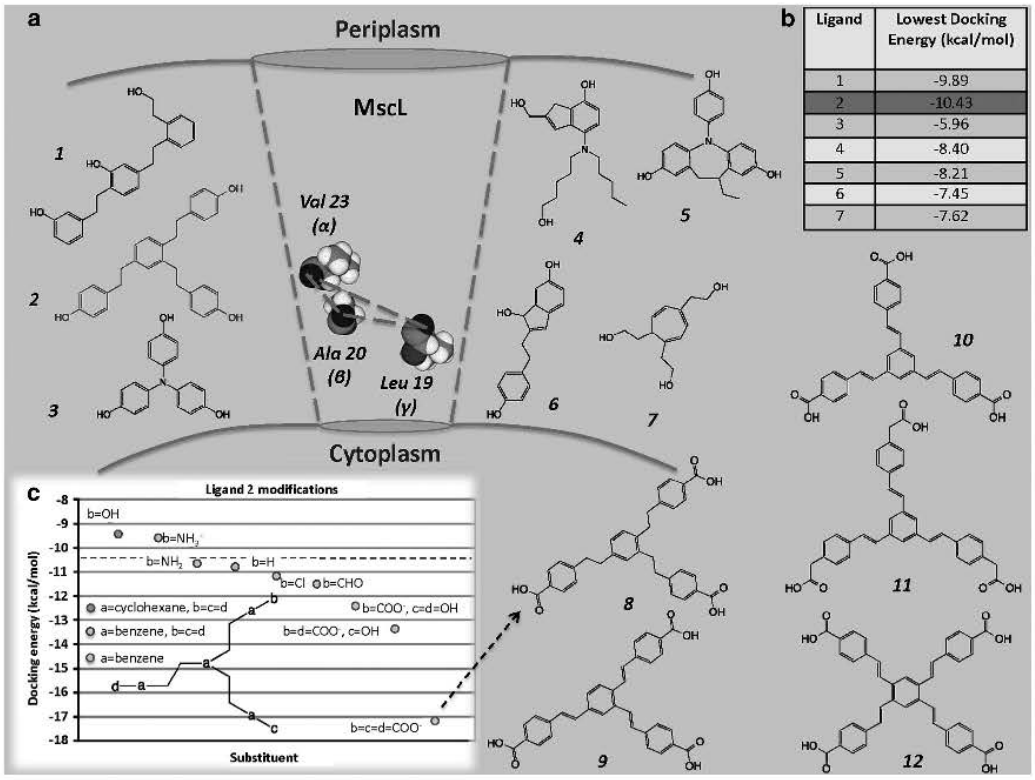

Figure 1 (**a**) Diagrammatic representation of target amino acids Leu19, Ala20 and Val23 in close proximity to the *E. coli* MscL channel gate, which were used for the *de novo* design of the designated ligands. (**b**) Docking energies (kcal mol^{-1}) of the ligands. (**c**) Iterative *in silico* docking of lead ligand 2, which gave rise to new class of antimicrobials including compounds 8–12. A full color version of this figure is available at *The Journal of Antibiotics* journal online.

Table 1 MIC data of antibiotics (μg ml^{-1}) against drug-resistant bacterial strains

Compound	*S. aureus MRSA clinical isolate*	*S. aureus MRSA ATCC 43300*	*S. aureus GISA NRS 17*	*S. aureus MRSA DapRSA clinical isolate*	*S. aureus GISA, MRSA NRS 1*	*S. pneum MDR ATCC 700677*
Vancomycin	1	1	4	2	4	1
Compound 10	8	8	4	4	4	4

Compound	*S. aureus NARSA VRS 3b*	*S. aureus NARSA VRS 4*	*S. aureus NARSA VRS 1*	*S. aureus NARSA VRS 10*
Vancomycin	64	>64	>64	>64
Teicoplanin	4	32	>64	64
Daptomycin	1	2	4	4
Dalbavancin	1	16	>64	>64
Telavancin	0.5	1	2	4
Compound 10	4	4	4	4

	M. tuberculosis H37Rv		*M. tuberculosis TT372*	
Compound	*GAS medium*	*P&B medium*	*7H9 medium*	*7H9 medium*
Rifampicin	<0.002	<0.002	<40	<40
Compound 10	20	20	160	160

Abbreviations: GAS, glycerol-alanine-salts; GISA, glycopeptide intermediate *S. aureus*; MDR, multi-drug resistant; MIC, minimum inhibitory concentration; MRSA, methicillin-resistant *Staphylococcus aureus*; NARSA, Network of Antimicrobial Resistance in *S. aureus*; P&B, Proskauer and Beck; VRS, vancomycin-resistant *S. aureus*. Comparison of efficacy of **10** and vancomycin against a panel of MRSA and glycopeptide intermediate *S. aureus*, and MDR *S. pneumonia*, comparison of efficacy of **10** and commercial antibiotics against a panel of vancomycin-resistant *S. aureus* from the Network of Antimicrobial Resistance in *S. aureus*, and comparison of efficacy of **10** and rifampicin against MDR *Mycobacterium tuberculosis* H37RV and TT372 strains. The 7H9 medium contains oleic acid, albumin, dextrose and catalase, which is needed for the growth of the bacteria. GAS medium has a final pH of 6.6 and the Proskauer and Beck (P&B) medium has a final pH of 7.4. A full color version of this table is available at *The Journal of Antibiotics* journal online.

it suggests that the structure of **10** may be further optimized to increase its bioavailability. For a detailed chart, see Supplementary Figure S1.

Compound 10 toxicity

We measured the cytotoxicity of **10** against a number of human tissue culture cell lines. The growth of NIH/3T3 and HaCaT cells was not affected by 50 μg ml^{-1} of **10**, and at 100 μg ml^{-1} only a marginal effect on growth was observed, whereas 500 μg ml^{-1} of **10** completely blocked the growth of these cells (Supplementary Figures S2a and b). Testing for 24 h on other cell lines such as HepG2 and HEK293 revealed no cytotoxicity up to 50 μg ml^{-1} of **10** (Supplementary Figures S2c and d). Therefore toxicity to eukaryotic cells is not seen until ~10 times the MIC against *S. aureus*.

Compound 10 acts through MscL

As **10** was specifically designed as a ligand for MscL, we sought evidence that the antimicrobial activity of **10** is a consequence of its interaction with the MscL channel. Even though **10** is not as effective against some Gram-negative species and strains, we reasoned that if the particular parental *E. coli* strain (FRAG-1) that was used to generate all of the mechanosensitive channel null strains was sensitive enough to **10**, we should be able to determine whether the potency of **10** is dependant on MscL. We therefore tested these strains. In addition, a variety of genetic and physiological tools are readily available in *E. coli* for the analysis of mechanosensitive channels making it the organism of choice for such experiments.

Growth inhibition assays of **10** were performed using *E. coli* MJF612[17] carrying an empty vector, expressing wild-type *E. coli* MscL (Eco MscL), expressing a MscL K55T mutant that is slightly more sensitive to tension,[9] expressing the MscL orthologues from *Clostridium perfingens* (CP MscL), or expressing the MscL orthologue from *S. aureus* (SA MscL). For concentrations of **10** in the 7.5–10 μg ml^{-1} range, all strains expressing *mscL* except the *mscL* homolog from *S. aureus* showed reduced growth in a pilot-experiment titration curve compared with the control strain carrying the empty vector (Figure 2a). These data suggest that at concentrations of ~7.5 μg ml^{-1}, MscL is required for the mediated growth inhibition of **10**. In contrast, at ~16.5 μg ml^{-1}, all strains were equally inhibited, suggesting that MscL is not the only target of **10** at concentrations greater than this concentration.

In a separate experiment, *E. coli* MJF612 expressing various *mscL* genes was grown to stationary phase in the presence of 13.5 μg ml^{-1} of **10**. *E. coli* MJF612 expressing the unrelated *E. coli* mechanosensitive channel of small conductance (MscS), which also detects membrane tension, was included to examine whether **10** has specificity for MscL. Cells expressing Eco MscL, Eco K55T MscL and *C. perfringens* MscL showed a decreased growth dependant on **10**, whereas cells containing an empty vector and those expressing SA MscL showed growth independent of **10** (Figure 2b). Bacteria expressing MscS were also sensitive to **10**, however the decrease in growth rate observed for the *E. coli* expressing MscS was only half of the strain expressing MscL. The observation that expression of SA MscL in *E. coli* does not confer sensitivity to **10** may not be surprising given that SA MscL is more difficult to gate when in *E. coli* membrane compared with being in its native membranes.[18] This is possibly due to the requirement of *S. aureus* endogenous lipid composition much like for the *M. tuberculosis* MscL.[19] These data show that MscL, and to a lesser extent MscS expression, affect the efficacy of the drug.

To determine whether **10** directly affects the activity of the MscL channel, we carried out patch-clamp experiments of native membranes using an *E. coli* 'giant' spheroplast preparation derived from strain PB104 (an *mscL* null mutant in which Eco MscL is over-expressed to enhance the number of channel activities observed[20]). The response of MscL to pressure across the patch was assessed before and after treatment with 25 μg ml^{-1} of **10**. As shown in Figure 2c,

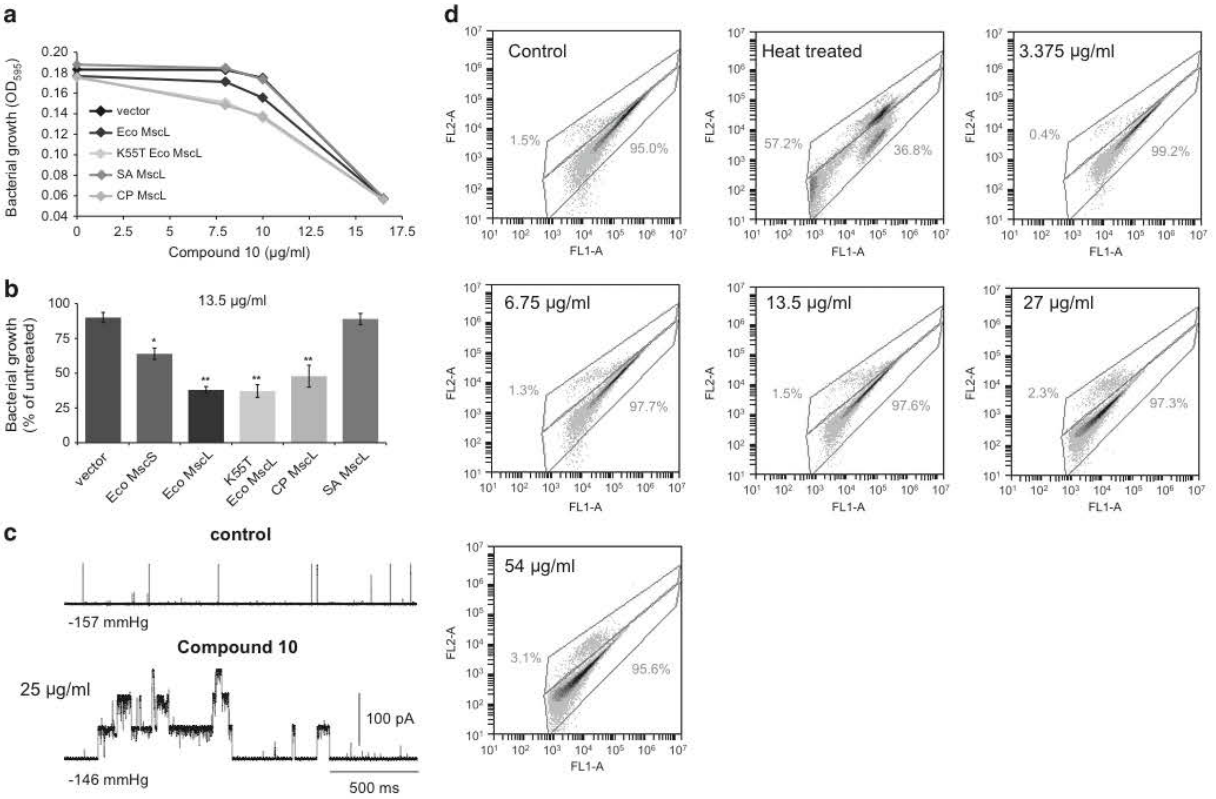

Figure 2 Mechanism of action studies. (**a**) Titration curve showing the effect of different concentrations of 10 on growth of E. coli MJF612 bacteria carrying an empty vector (dark blue) or expressing E. coli (Eco) MscL (red), K55T Eco MscL (green), S. aureus (SA) MscL (light blue) or C. perfingens (CP) MscL (orange). Note that the SA MscL data directly overlay the data for the vector-only-negative control. Each OD point presented is the average of four wells and all experiments are internally controlled. (**b**) The growth of cultures at stationary phase with or without at 13.5 μg ml − of 10 was measured for MJF612 bacteria carrying an empty vector (dark blue) or expressing Eco MscS (purple), Eco MscL (red), K55T Eco MscL (green), SA MscL (light blue) or CP MscL (orange). Bacterial growth is represented as a percentage of the untreated samples. $*P \leqslant 0.0045$, $**P \leqslant 0.0001$, One-way ANOVA and Dunnett's multiple comparison test against empty vector. (**c**) Effect of 10 on MscL channel activity in native bacterial membranes. MscL channel activity was measured before (top) and after the addition of 25 μg ml^{-1} of 10 to the bath (bottom). Channels were activated by negative pressure applied to the patch. The traces are from the same patch held at the pressures shown for each trace (bottom left). (**d**) Flow cytometry data of *E. coli* (FRAG-1) untreated, heat-treated at 60 °C for 20 min and treated with 10 at the designated concentrations. SYBR Green I was used as a DNA-staining agent and propidium iodide was used to detect membrane porosity. A full color version of this figure is available at *The Journal of Antibiotics* journal online.

characteristic MscL channel activities were easily seen, and a significant increase in the probability of channel opening was observed after treatment with **10**. A decrease in the pressure threshold needed to gate Eco MscL was also observed after 10 min incubation with **10** (82.9 ± 4.3 percentage of the pressure required to gate the untreated, $n = 5$, $P \leqslant 0.02$, Student *t*-test paired). No change in the pressure threshold required to gate MscS was observed in these patch-clamp experiments (97.7 ± 4.9 percentage of untreated, $n = 4$). As previously observed, such subtle increases in mechanosensitivity of MscL mutants in patch-clamp experiments can lead to significantly slower bacterial growth of strains harboring these mutants.[9,21]

To rule out the possibility that **10** simply disrupts bacterial cellular membranes at the concentration at which it is effective in the *E. coli* growth experiments (shown in Figure 2a, Figure 2b and the patch-clamp results shown in Figure 2c), we carried out flow cytometry experiments in which *E. coli* FRAG-1 expressing Eco MscL treated with **10** were stained with propidium iodide (PI) (to test for the intactness of membranes) and SYBR Green I to stain all the cells. These flow cytometry data revealed that the control sample had ~98.5% viability, as determined by the intensity of PI-stained cells (Figure 2d). As a control, cells were heated to 60 °C for 20 min, which resulted in ~57% of the cells being permeable to PI. As shown in Figure 2d, the integrity of the *E. coli* FRAG-1 membranes was not compromised with concentrations of **10** up to ~54 μg ml^{-1}. However, there was an almost 100-fold decrease in the intensity of the SYBR Green I as the concentration of **10** increased from ~3.4 to 54 μg ml^{-1}, suggesting a significant decrease in DNA content as a result of inhibition of growth and cell division.

Compound 10 causes morphological changes in *S. aureus*

On the basis of the observations from the patch-clamp experiments and the titration experiments above, we hypothesized that the opening of the MscL channel caused by **10** might result in changes in the size and shape of bacterial cells. Low-magnification scanning electron microscopy (SEM) of *S. aureus* ATCC 6538 showed a decrease in bacterial density and biofilm formation, concurrent with an increase in the concentration of **10** (Supplementary Figure S3). Bacterial size measurements revealed that bacteria treated

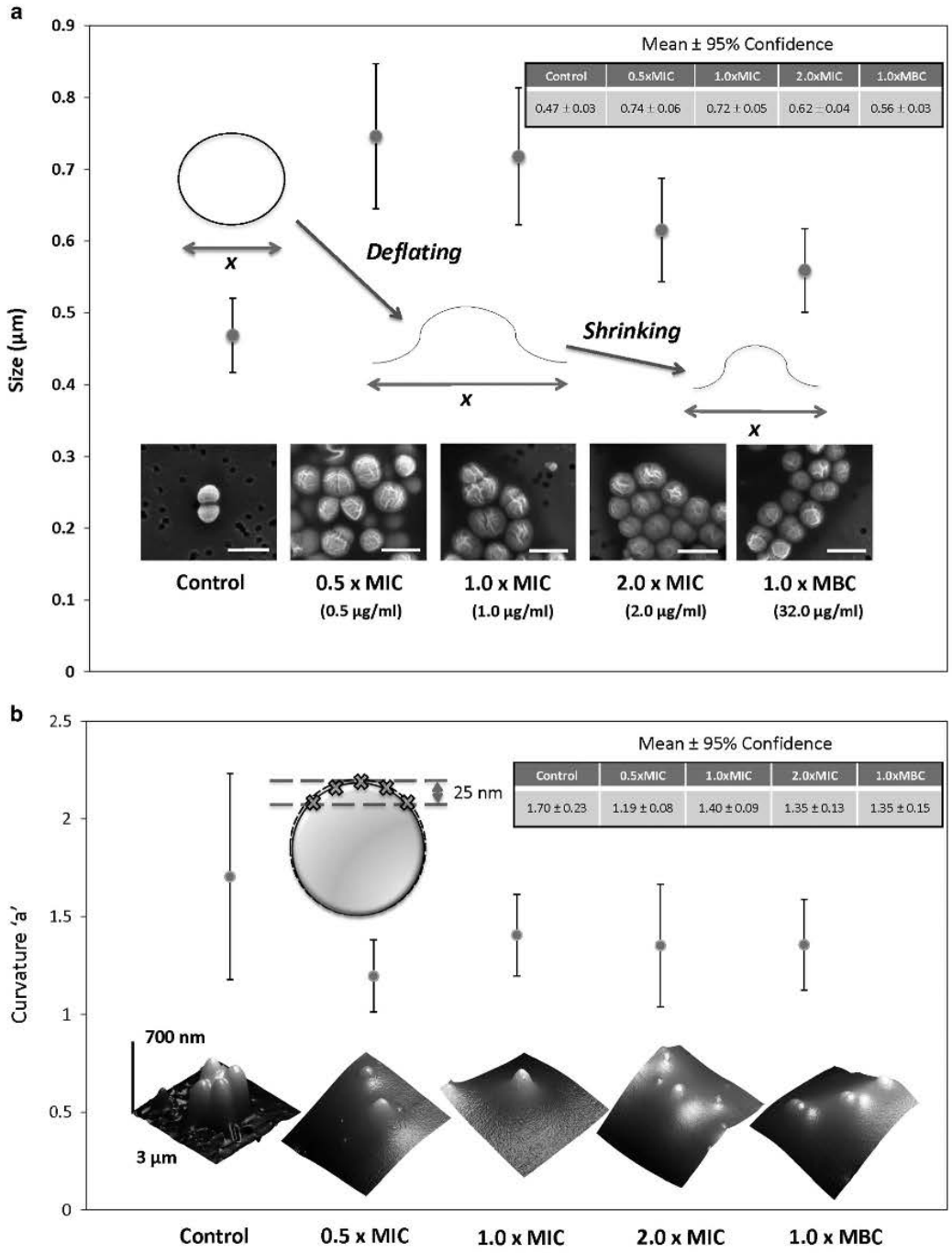

Figure 3 Microscopic analysis of *S. aureus* ATCC 29213 treated with **10** at different concentrations. (**a**) SEM images and size measurements of *S. aureus* with an inset showing the mean ± 95% confidence ($n=12$). Scale bar 1 μm and magnification ~×85 000. (**b**) The change in the 'a' parameter (representing bacteria curvature) is shown with representative 3D AFM images beneath (3 μm × 3 μm × 700 nm). The top 25 nm of an AFM scan was used as a basis for a parabolic equation fit $y=ax^2+bx+c$ to show the change in curvature after treatment with the drug. The inset shows the mean ± 95% confidence ($n=10$ for 1 × MBC and $n=20$ for other concentrations). A full color version of this figure is available at *The Journal of Antibiotics* journal online.

with 0.5 μg ml^{-1} were significantly wider than the control (Figure 3a). At concentrations of **10** >0.5 μg ml^{-1}, there was a gradual but significant reduction in the size of the bacteria. Moreover, untreated *S. aureus* showed a round and firm geometry with distinct surface features, which become distorted with increasing drug concentrations. Atomic force microscopy (AFM) also revealed a statistically significant change in morphology of the uppermost 25 nm region of *S. aureus* (see Figure 3b for illustration). This region

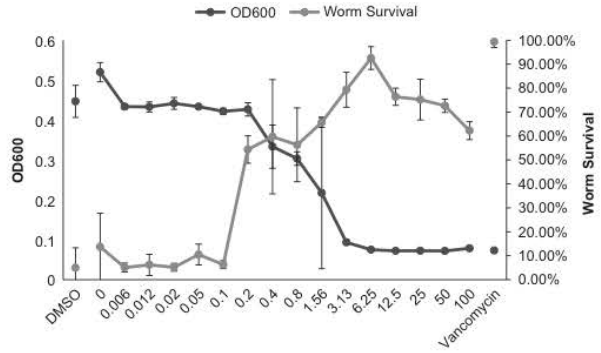

Figure 4 Percentage of surviving *C. elegans* as a function of **10** concentration and density of surviving bacteria as a function of **10** concentration in the absence of *C. elegans*. The percentage of worm survival is shown in red with the corresponding axis on the right and the growth of MRSA MW2 is shown in blue with the corresponding axis on the left. Concentrations are shown in $\mu g\,ml^{-1}$. The negative control with solvent DMSO is shown on the far left and the positive control with antibiotic vancomycin is shown on the far right. A full color version of this figure is available at *The Journal of Antibiotics* journal online.

was observed to be of narrow parabolic geometry in the control sample, which then flattened as the drug concentration increased (Figure 3b). The AFM and SEM results support each other, as the latter width measurement is inversely proportional to the measurement of the parabolic curvature parameter 'a'. These morphological changes are consistent with the spontaneous activation of MscL in the presence of **10** leading to solute loss and osmolytes and consequently a reduction in the size of *S. aureus*.

Compound 10 is effective in an animal model of *S. aureus* infection

Compound **10** has potent antibacterial activity *in vitro*, and accordingly we tested whether this activity would translate to *in vivo* models of infection. We examined the efficacy of **10** in treating the nematode *C. elegans* infected with MRSA strain MW2. Approximately 60% of the worms survived when treated with **10** at concentrations above 0.2 $\mu g\,ml^{-1}$ and >90% of the worms survived the MRSA infection at the most effective concentration of **10**, 6.25 $\mu g\,ml^{-1}$ compared with a 5% survival rate for the control (Figure 4). The range of effective concentrations (0.2–100 $\mu g\,ml^{-1}$) also corresponded to low bacterial counts *in vitro* as detected by measuring the OD at 600 nm (OD_{600}) in assay wells without the presence of worms.

DISCUSSION

Compound **10** is a potent antibiotic against drug-resistant Gram-positive bacteria with limited activity against Gram-negative species. However, it is worth noting that although **10** showed no apparent effect on *E. coli* ATCC 25922 (MIC > 64 $\mu g\,ml^{-1}$), it did show an inhibitory effect on the growth of *E. coli* MJF612 (MIC ~ 13.5 $\mu g\,ml^{-1}$) as shown in Figures 2a and b. The difference in effect is due to a strain variation, being previously observed for a number of fluoroquinolone antibiotics where in some cases the difference in susceptibility between the WT and the ATCC 25822 strains was over fourfolds.[22] The reduced activity against Gram-negative bacteria presumably arises from the presence of the lipopolysaccharide-containing outer membrane, which acts as a barrier to hydrophobic compounds such as **10**. Although **10** kills bacteria, it is nontoxic to mammalian cells. The lowest concentration at which any cytotoxicity has been observed in any cell line is 50 $\mu g\,ml^{-1}$, allowing for a tolerated therapeutic window between 4 and 50 $\mu g\,ml^{-1}$ for MRSA.

We have shown here that, the potency of the antimicrobial activity of **10** is dependent on MscL. These data are consistent with the *in silico* results, suggesting binding of the compound to the channel. **10** represents the first success at designing a drug with specificity to MscL. Some previous studies suggest that there are other antibacterial compounds that may have some influence on the channel; however, most of these studies did not show both an *in vivo* dependence upon MscL expression and a direct effect on channel activity. The bacterial toxin sublancin 168,[23] a glucosylated bacteriocin showed MscL-dependent activity against *Bacillus subtilis* and *S. aureus in vivo*, but there was no assessment of the role of MscS or any electrophysiological studies. Another group of antimicrobial agents (Parabens) has been reported to affect MscL as assayed by patch-clamp analysis, but there have been no *in vivo* studies to determine any MscL-dependent effects. Parabens affect MscS as well as MscL,[24,25] suggesting that they are nonspecific activators of membrane-tension-gated channels, as has been observed for several amphipaths.[26,27] Finally, MscL expression has recently been shown to increase streptomycin potency, and overall the effects appear to be specific for MscL, suggesting direct binding; the open channel may even serve as a route for streptomycin to get access to the cytoplasm.[21] **10** affects MscS- as well as MscL-expressing cells, suggesting it might have some amphipathic or nonspecific ability to activate bacterial membrane-tension-gated channels *in vivo*. However, in patch-clamp experiments, only MscL showed a decrease in the pressure threshold in the presence of **10**, in agreement with a facilitation to gate MscL. Hence, the predicted binding of **10** to MscL and the finding that MscL appears to be more affected than MscS as assayed by patch-clamp suggests that while there may be an amphipathic component to MscL activation by **10** *in vivo*, there may also be a more MscL-specific agonist action as well. In addition, the flow cytometry experiments show that there is no compromise to the integrity of the plasma membrane, consistent with the interpretation that **10** directly interacts with the channels. At last, microscopic imaging using SEM and AFM analysis reveal a significant change in bacterial cell morphology in bacteria treated with **10**, with the bacteria flattened and shrunk, which is consistent with MscL channel activation. Therefore, these data suggest that MscL is a target for **10**.

In vivo testing of **10** in an MRSA infection model in the nematode *C. elegans* has shown that the drug is an active antibiotic, rescuing the worms from the infection at a concentration of ~1.5 $\mu g\,ml^{-1}$ (Figure 4). The worm infection model represents a therapeutic window from 0.2 to 50 $\mu g\,ml^{-1}$, a range at which no toxicity is observed in human cell lines. This therapeutic window is better than that of FDA-approved antibiotics, such as tobramycin and gentamicin (therapeutic range of 4–10 $\mu g\,ml^{-1}$), amikacin (therapeutic range 20–30 $\mu g\,ml^{-1}$) and vancomycin (therapeutic range 20–40 $\mu g\,ml^{-1}$). The results highlight and address some of the preliminary challenges in antibiotic development and pave the way for future research and development for the antimicrobial compounds discussed herein, including resistance emergence testing, formulation of **10** and analogs thereof, in addition to investigating different routes of administration using different animal infection models.

METHODS

In silico design experiments

Autodock 3.05[28] was used for the *in silico* docking experiments as it is well documented and has a graphical user interface (Autodocktools) that is simple

to use. The atomic coordinates of the MscL protein from *E. coli* were obtained from a homology structure designed previously.[29] In this structure, the amino-acid residues of *M. tuberculosis* have been replaced with those of *E. coli* and the coordinates of the amino acids left unaltered. The Eco MscL structure used is a truncated version of MscL and has only 95 amino-acid residues (Met12 to Glu107), compared with the 136 amino-acid residues representing the whole protein. Past experiments suggest that the rest of the protein is not significant for the activity of MscL and therefore removing it was advantageous by saving computer power and significantly reducing the computational time. The Protein Data Bank file of the Eco MscL was loaded in Autodocktools and the water molecules removed. Polar hydrogens were added to the proteins and the charges and solvation parameters were added to the atoms of the macromolecule, and the file saved in Protein Data Bank file format with charges and solvation parameters included.

The ligands were built and saved in Brookhaven format[30] and Autodocktools was used to prepare the ligands for docking. The rigid root of the ligand was defined automatically and the maximum number of rotatable bonds was allowed. The number of active torsions was set to the number of rotatable bonds and the toggle activity of torsions allowed to move most atoms. The partial atomic charges were calculated[31] using the AM1 Hamiltonian, and the geometry of the ligand was optimized. These were entered into the Protein Data Bank file replacing the charges generated using Autodocktools.

The grid size and center used for the Autodock calculation (see Supplementary Table S1 for parameters used for docking) was restricted to the amino-acid residues near Ala20, as it has been shown that this is where parabens and eriochrome cyanine bind.[24] To narrow down the search for target amino acids, the amino acids that surround the docked ligands were determined. The amino-acid residues surrounding the ligands for most of the dockings ranged from Leu19 to Lys31. Hydrogen acceptor groups (namely oxygen atoms) were targeted in the protein side chain. Depending on where they occur, a ligand with hydrogen donor groups was then designed that can H-bond with the oxygen atoms. This approach was taken given that there were a limited number of amino acids with oxygen atoms exposed to the inside of the pore. This identified amino acids, Leu19, Ala20, Val23, Gly26 and Ala27, with oxygen atoms exposed to the inside of the pore. The oxygen atoms in Gly26 and Ala27 are slightly shielded by other amino acids. In addition, they point to the side rather than to the inside of the pore, and hence may not contribute significantly to hydrogen bonding.

It is also important to note that the geometry of these five amino acids is the same in the five subunits, as long as no more than one amino acid is considered to be in any subunit. Therefore, instead of visualizing these amino acids in one chain, they were visualized as an amino acid/subunit so that subunit 1 has Leu19, subunit 2 has Ala20, subunit 3 has Val23, subunit 4 has Gly26 and subunit 5 has Ala27.

As parts of the protein pore are narrower than others, it was important to design a pharmacophore that has a length less than the diameter of the pore at the position of all five amino-acid residues. If this is the case, then any one pharmacophore will, at most, bind to four amino acids. Owing to the fact that the most accessible oxygen atoms are in the following amino acids: Leu19, Ala20 and Val23, particular attention was given to these amino acids.

A *de novo* approach was undertaken to design a pharmacophore and seven ligands were constructed with three hydroxyl groups each (Figure 1a). These ligands were then docked with the Eco MscL. The assumption being that the closer the hydroxyl groups of a ligand to the spatial dimensions of the ketone groups in Eco MscL (Supplementary Table S2), the better the docking. This was not the case; nonetheless, the results showed exceptional docking energies for ligand 2, which was then used as a lead in an iterative docking process.

The hydroxyl groups in ligand 2 were replaced by various functional groups and the effect on docking energy was noted. The functional groups include: aldehydes, amide cations, amino, carboxyl and chlorines (Figure 1c). The carboxyl groups were deprotonated and were added, one at a time, until the carboxyl groups replaced all the hydroxyl groups. The four phenyl groups of ligand 2 were also replaced by cyclohexane groups. The parent compound was also included (which did not include the hydroxyl groups).

The best docking energy was observed with replacement of all hydroxyl groups for carboxyl groups with an overall charge of -3 on the molecule. This ligand has an exceptional free energy of binding equivalent to ~ -55.94 kJ mol^{-1}, which is higher than that previously reported.[6] MscL may not show an overall ion selectivity; however, the docking results show preferential binding to the mostly hydrophobic deprotonated tri-acid species.

Compound 10 synthesis

Drug synthesis was carried out using a procedure published previously[32] with some modifications. Ethyl acetate (20%) in hexane was used for monitoring the progress of the Heck cross-coupling reaction using thin layer chromatography and 20:80 ethyl acetate-dichloromethane for eluting the product using fine silica after tetrahydrofuran removal under vacuum. The product from the saponification reaction was collected by filtration and eluted in fine silica using a 20:80 methanol-tetrahydrofuran solvent system, followed by the addition of diethyl ether as an anti-solvent to wash the compound.

MIC assay

All compounds were prepared at 160 μg ml^{-1} in water from a stock solution of 20 mM of **10** in dimethyl sulfoxide (DMSO). The compounds, along with standard antibiotics, were serially diluted twofold using Mueller Hinton broth (MHB) in 96-well plates (nonbinding surface, Corning 3641, Tewksbury, MA, USA) using MHB. Concentrations of standards ranged from 64 μg ml^{-1} to 0.03 μg ml^{-1}, and concentrations of compounds ranged from 8 to 0.003 μg ml^{-1}, with final volumes of 50 μl per well. Gram-positive bacteria were cultured in MHB (Bacto Laboratories Pty Ltd, Mt Pritchard, NSW, Australia) at 37 °C overnight. Mid-log phase bacterial cultures were diluted to the final concentration of 5×10^5 CFU ml^{-1} (in MHB) and used with the diluted compounds to be tested. Plates were covered and incubated at 37 °C for 24 h, and MICs designated as the lowest concentration that showed no visible growth. Experiments were carried out in duplicate ($n = 2$), with vancomycin as a positive inhibitor control.

M. tuberculosis testing

Rifampicin and **10** were resuspended in DMSO and diluted to obtain a drug concentration of 160 μg ml^{-1}. Five microliter of this drug concentration (equivalent to 0.8 μg) was dispensed into a 96-well plate and serially twofold diluted in DMSO (final drug volume 5 μl). Thereafter, frozen aliquots of the bacterial strains H37Rv and Victor strain TT372 were thawed and suspended at 2×10^5 bacteria per ml in 7H9 media supplemented with oleic acid, albumin, dextrose and catalases (final albumin concentration of 5 g l^{-1}). Two hundred microliter of these bacterial suspensions were added to each well in 96-well plates, containing either compound (final drug concentration: 4 μg ml^{-1}). Plates were incubated at 37 °C for 7 days, when 20 μl of Alamar Blue reagent were added to each well. Plates were incubated for an additional 2 days at 37 °C, when absorbance was evaluated in a microtiter plate reader at 570 nm. Bacterial absorbance was normalized to the blank absorbance and compared with the positive control (untreated bacteria). Data were graphed as percent inhibition. A similar procedure was carried out for *M. tuberculosis* H37Rv grown in glycerol-alanine-salts medium and Proskauer and Beck medium at a pH 7.4. At concentration $\geqslant 80$ μg ml^{-1}, **10** precipitated in glycerol-alanine-salts medium pH 6.6. However, no precipitation was observed at lower concentrations (40–5 μg ml^{-1}) where it also inhibited bacterial growth.

NIH/3T3 and HaCaT cytotoxicity assay

HaCaT immortalized keratinocytes and NIH/3T3 fibroblasts were seeded as 1.5×10^3 cells per well in a 96-well plate in 50 μl media (Dulbecco's modified Eagle's medium/F12+GlutaMAX from Gibco (Mulgrave, VIC, Australia) with 10% v/v foetal bovine serum and 1% v/v penicillin/streptomycin). Cells were incubated for 2 h at 37 °C, 5% CO_2 to allow cells to attach to the plates. **10** was prepared in DMSO and diluted 20 times in culture media, giving a final concentration of 1 mg ml^{-1} with 5% DMSO. Fifty microliter of each dilution was added into 50 μl of culture medium in triplicates to reach the final concentrations. The cells were incubated with the compounds overnight at 37 °C, 5% CO_2. After the incubation, MTS(3-(4,5-dimethylthiazol-2-yl)-5-(3-carboxymethoxyphenyl)-2-(4-sulfophenyl)-2H-tetrazolium, inner salt) (Promega, Australia, Alexandria, NSW, Australia) (60 μl) was added to each well. The plates were then incubated for 3 h at 37 °C, 5% CO_2. Sixty microliter

from each well was transferred to a new plate and the absorbance was then read at 490 nm using EnSpire 2300 Multimode Plate Reader. Results are presented as the average percentage of control ± s.d. for each set of duplicate wells. The difference between the experiment and the blank is recorded as normalized mean. For each treatment, the experiment was carried out in triplicate for each time point, at 0, 24, 48 and 72 h. Time 0 starts after overnight incubation.

HepG2 and HEK293 cytotoxicity assay

10 was prepared in DMSO at 20 mM. It was diluted 200 times in culture media, giving a final concentration of 50 μg ml^{-1} with 0.5% DMSO. Hepatocellular carcinoma (HepG2 ATCC HB-8065) and human embryonic kidney cells (HEK293 ATCC CRL-1573) cells were seeded as 1.5×10^4 cells per well in a 96-well plate in a final volume of 100 μl in Dulbecco's modified Eagle's medi (Gibco-Invitrogen, Waltham, MA, USA), in which 10% or 1% of foetal bovine serum was added. Cells were incubated for 24 h at 37 °C, 5% CO_2 to allow cells to attach. All tested compounds were diluted from 2.5 mg ml^{-1} to 0.38 μg ml^{-1} in threefold dilutions. Then, 10 μl of each dilution was added into 90 μl of culture medium in triplicates. Colistin and Tamoxifen were used as the controls. The cells were incubated with the compounds for 24 h at 37 °C, 5% CO_2. After the incubation, 3-(4,5-Dimethylthiazol-2-yl)-2,5-diphenyltetrazolium bromide (Invitrogen) was added to each well to a final concentration of 0.4 mg ml^{-1}. The plates were then incubated for 2 h at 37 °C, 5% CO_2. Medium was removed, and crystals were resuspended in 60 μl of DMSO. The absorbance was then read at 570 nm using a Polarstar Omega instrument. The data were then analyzed by Prism software. Results are presented as the average percentage of control ± s.d. for each set of duplicate wells using the following equation: Percent viability = $(ABS_{TEST} - ABS_{5\%DMSO}/ABS_{UNTREATED} - ABS_{5\%DMSO}) \times 100$.

Strains and cell growth

Constructs were inserted in the PB10d expression vector[9,33–35] and the *E. coli* strain MJF612, which is null for MscL, MscS and MscS homologs (FRAG-1 *ΔmscL::cm, ΔmscS, ΔmscK::kan, ΔybdG::aprΔ*)[17] were used as a host for all experiments. Unless stated otherwise, cells were grown in citrate-phosphate defined medium consisting of (per liter: 8.57 g of Na_2HPO_4, 0.87 g of K_2HPO_4, 1.34 g of citric acid, 1.0 g of NH_4SO_4, 0.001 g of thiamine, 0.1 g of $Mg_2SO_4.7H_2O$, 0.002 g of $(NH_4)_2SO_4.FeSO_4.6H_2O$) plus 100 μg ml^{-1} ampicillin.

In vivo growth inhibition experiments

E. coli strain MJF612 was used as a host for Eco MscL (MscL), K55T Eco MscL (K55T MscL), *C. perfringens* MscL, SA MscL and *E.coli* MscS (MscS) constructs in the PB10d expression vector. Overnight cultures were grown in citrate-phosphate defined medium pH 8 plus 100 μg ml^{-1} ampicillin with shaking at 37 °C. The following day, cultures were diluted 1:40 in the same media and grown for 30 min before inducing expression with 1 mM isopropyl β-D-1-thiogalactopyranoside. After 30 min of induction, all cultures were adjusted to an OD_{600} of 0.08. The cultures were then diluted 1:3 into pre-warmed citrate-phosphate defined medium pH 8 containing 100 μg ml^{-1} ampicillin plus **10**. Cultures were loaded in 96-well plates (190 μl per well), sealed with a breathable film, and incubated at 37 °C for 16 h without shaking. The OD_{595} of the cultures was measured using a Multiskan Ascent (Thermo Scientific Inc., Waltham, MA, USA).

Electrophysiology

E. coli giant spheroplasts were generated as previously described[20] from PB104 strain (*ΔmscL::Cm*)[34] expressing Eco MscL. Patch-clamp experiments were performed in the inside–out configuration, at room temperature under symmetrical conditions in a buffer at pH 6.0 (200 mM KCl, 90 mM $MgCl_2$, 10 mM $CaCl_2$ and 5 mM HEPES). Patches were excised, and recordings were performed at 20 mV (for simplicity the patch traces openings are shown upward). Data were acquired at a sampling rate of 20 kHz with 10 kHz filtration using an AxoPatch 200B amplifier (Molecular Devices, Sunnyvale, CA, USA). A piezoelectric pressure transducer (World Precision Instruments, Sarasota, FL, USA) was used to measure the pressure throughout the experiments. After taking three separate pressure threshold measurements in regular patch buffer for control, a 25 μg ml^{-1} solution of **10** was perfused to the bath and channel sensitivity within the same patch was measured subsequently every 10 min.

Flow cytometry experiments

Bacterial cultures were prepared from a single colony of *E. coli* FRAG-1 grown on Lysogeny Broth media. The single colony was added to 8.5 ml of filtered MHB (0.2 μM Minisart, Sartorius Stedim) to which **10** (3.375 μg ml^{-1} to 54 μg ml^{-1} in doubling concentrations) was added. The cultures were incubated overnight at 37 °C with shaking in 2 ml volumes before analysis, at which point SYBR Green I (10 × final in MHB) and PI (10 μg ml^{-1} final in H_2O) were added. Cells were incubated for 5 min, prior to analysis. The heat-treated sample was exposed to 60 °C for 20 min before adding SYBR Green I and PI and incubated for 5 min.

An Accuri C6 Flow Cytometer was used for the flow cytometer experiments. The fluidics rate was set to Medium (35 μl min^{-1}) and the threshold limit was set on FL1 (530/30) to a value of 800. Samples were run and 30 000 events collected. Sample data were analyzed using the CFlow software. FL2-A (585/60) (Em_{max} 605 nm, PI) was plotted on the *y* axis versus FL1-A (530/30) (Em_{max} 521 nm, SYBR Green I) on the *x* axis. No gates were applied and fluorescence compensation was not required.

Sample preparation for microscopy

The bacterial strain *S. aureus* ATCC 6538 was grown overnight at 37 °C on Muller–Hinton Agar (Oxoid, Thermo Fisher Scientific Inc., Waltham, MA, USA). The bacteria were harvested and the OD of bacteria suspended in MHB was adjusted to ~0.5 MacFarlane units so as to give 5×10^7 CFU ml^{-1}. Bacteria were then aliquoted into 10 ml tubes and various amounts of **10** at 1 mg ml^{-1} dissolved in DMSO were added to give a final concentration ranging from 32 μg ml^{-1} to 0.5 μg ml^{-1} (twofold serial dilutions). Bacterial numbers were enumerated using the Miles–Misra method in which serial dilutions of 10 μl samples from each culture were spread onto nutrient agar in duplicate. After incubation at 37 °C for 24 h, the colonies were counted.

S. aureus ATCC 6538 cultures were treated as above and incubated overnight. Cultures were loaded into sterile disposable syringes and filtered through a 0.2-μm isopore polycarbonate hydrophilic filter (Millipore, Billerica, MA, USA). Bacteria on filters were fixed in 4% paraformaldehyde/1.25% glutaraldehyde in phosphate-buffered saline and 4% sucrose (pH 7.2) for 15 min. The fixative was removed with a sterile pipette and the filters washed in a washing buffer composed of 4% sucrose in phosphate-buffered saline for 5 min. The washing buffer was then removed and the bacteria were post-fixed in 2% OsO_4 in water for 30 min. The OsO_4 were then pipetted out into an osmium waste bottle and the bacteria were washed in a washing buffer composed of 4% sucrose in phosphate-buffered saline for 5 min. The bacteria were then dehydrated in four consecutive different concentrations of ethanol, 70% ethanol (1 change of 10 min), 90% ethanol (1 change of 10 min), 95% ethanol (1 change of 10 min) and 100% ethanol (3 changes of 10 min). After removing the ethanol, the bacteria were critical point dried in hexamethyldisilazane (2 changes of 15 min) and then mounted on a stub and platinum coated (10 nm). Carbon paint was then applied to the edges of the stub making contact with the filter to improve conductivity and reduce sample charging.

Scanning electron microscopy analysis

SEM was carried out using a FEG Quanta 450 microscope at an accelerating voltage of 3–7 Kv and a working distance of 10 mm. The specimens were observed using a secondary electron detector under high-vacuum conditions. Images were captured at high definition at ~×85 000 magnification and a scan rate of 100 ms per frame.

Atomic force microscopy analysis

AFM images were acquired in air using a Bruker Dimension FastScan AFM with a Nanoscope V controller, operating in PeakForce Tapping mode. Bruker ScanAsyst Air probes with a nominal tip radius of 2 nm and nominal spring constant of 0.4 N m^{-1} were used. Imaging parameters including set-point, scan rate (1–2 Hz) and feedback gains were adjusted to optimize image quality and minimize imaging force. Images were analyzed using the Bruker Nanoscope Analysis software (version 1.4). The AFM scanner was calibrated in the x, y and

z directions using silicon calibration grids (Bruker model numbers PG: 1 µm pitch, 110 nm depth and VGRP: 10 µm pitch, 180 nm depth).

After acquiring the images, 20 bacteria per sample were chosen at random and a cross-section was drawn through the apex of each bacteria. The shape of the uppermost 25 nm of each bacteria was analyzed by fitting the parabolic function $y = ax^2+bx+c$, and extracting the coefficient 'a', which represents the curvature of the parabola. Higher 'a' values describe a narrow apex geometry, whereas low 'a' values describe a flatter apex with lower curvature. The analysis was restricted to the uppermost 25 nm in order to ensure that all of the samples were analyzed in the same manner, as many of the bacteria are embedded in organic matter to varying degrees, which restricts the analysis region in each case.

C. elegans infection model

The *C. elegans* infection assay was carried out as previously described.[36] A stock solution of **10** in DMSO (10 mg ml^{-1}) was prepared. Dilution series consisting of 1:10 dilution (from 100 µg ml^{-1}) and a 1:2 dilution (from 100 µg ml^{-1}) were tested. To prepare a 1:10 dilution series, 5 µl of 100 µg ml^{-1} of **10** was diluted into 45 µl of liquid media with 1% DMSO. This was repeated for all dilutions. To each well, 20 µl of compound containing liquid media was added followed by the addition of 35 µl of MRSA and 15 µl media containing 15 worms. Vancomycin at 20 and 100 µg ml^{-1} were used as positive controls and DMSO was used as a negative control. After infection and co-incubation with compound for 4 days, bacteria were washed out and the worms were stained with Sytox Orange dye and imaged. The ratio of stained to unstained worm area was used to measure worm death. Prior to washing, an OD_{600} measurement was taken to assess the bacterial growth.

Full methods and any associated references are available in the online version of the paper at www.nature.com/nature.

CONFLICT OF INTEREST

RAB declares ownership of the intellectual property licensed to Boulos & Cooper Pharmaceuticals Pty Ltd. The remaining authors declare no conflict of interest.

ACKNOWLEDGEMENTS

The *in vivo* growth inhibition experiments and the electrophysiology experiments were supported by Grant I-1420 of the Welch Foundation, Grant RP100146 from the Cancer Prevention & Research Institute of Texas, and Grants AI08080701 and GM061028 from the National Institutes of Health. The *C. elegans* experiments were supported by grant P01 AI083214 from the National Institutes of Health. II is supported by Grant 12SDG8740012 from the National American Heart Association. The funding bodies had no role in study design, data collection and analysis, decision to publish or preparation of the manuscript. The content is solely the responsibility of the authors and does not necessarily represent the official views of the National Institutes of Health. MAB, JXH, SR and AK were supported by a Wellcome Trust Seeding Drug Discovery Award (094977/Z/10/Z), and MAC by an NHMRC Principal Research Fellowship (APP1059354). UHS is supported by NHMRC Project Grant 535053. We gratefully acknowledge support of this work by the Australian Research Council and the Government of South Australia. RAB gratefully acknowledges supervision from Allan J McKinley during his Honors year when the modeling work was undertaken. SEM analysis was carried out at Adelaide Microscopy and AFM studies were carried out using facilities in the School of Chemical and Physical Sciences, Flinders University. Both of these microscopy facilities are supported by the Australian Microscopy and Microanalysis Research Facility (AMMRF). Flow Cytometry experiments were carried out at Flow Cytometry Immunology facility at Flinders Medical Centre. Ramizol is a Trademark fully registered in Australia.

Author contributions: RW and II conducted the *in vivo* growth inhibition studies and the electrophysiology, JlF and AlC carried out the *C. elegans* infection work, SR, AK and JXH conducted the susceptibility testing of MDR *S. aureus* and *S. pneumonia*, and cytotoxicity of HEK293 and HepG2 cells, AO carried out the susceptibility testing of *M. tuberculosis*, EST carried out the cytotoxicity studies on NIH/3T3 and HaCaT cells lines, UHS conducted experiments on the effect of **10** on viable counts of *S. aureus* and supplied cultures for microscopy, NVH carried out the flow cytometry experiments, RAB carried out the *in-silico* studies, synthesis of **10** and prepared the samples for microscopy, ClT and RAB carried out the scanning electron microscopy analysis, ADS, CTG and RAB carried out the atomic force microscopy analysis, II, PB, AlC, JLF, FMA, MAB, UHS, MHB, AO, CLR and RAB wrote the manuscript, PB, FMA, IO, MHB, MAC, NVH, CM and RAB designed the experiments, and RAB coordinated the research.

1 Katz, M. L., Mueller, L. V., Polyakov, M. & Weinstock, S. F. Where have all the antibiotic patents gone? *Nat. Biotechnol.* **24**, 1529–1531 (2006).
2 Christoffersen, R. E. Antibiotics—an investment worth making? *Nat. Biotechnol.* **24**, 1512–1514 (2006).
3 Clardy, J., Fischbach, M. A. & Walsh, C. T. New antibiotics from bacterial natural products. *Nat. Biotechnol.* **24**, 1541–1550 (2006).
4 Prasad, S. & Smith, P. Meeting the threat of antibiotic resistance: building a new frontline defence. *Australian Government Office of the Chief Scientist*. http://www.chiefscientist.gov.au/wp-content/uploads/OPS7-antibioticsPRINT.pdf (2013).
5 Piddock, L. J. Antibiotic action: helping deliver acation plans and strategies. *Lancet Infect. Dis.* **13**, 1009–1011 (2013).
6 Butler, M. S. & Cooper, M. A. Antibiotics in the clinical pipeline in 2011. *J. Antibiot.* **64**, 413–425 (2011).
7 Barh, D. *et al.* A novel comparative genomics analysis for common drug and vaccine targets in Corynebacterium pseudotuberculosis and other CMN group of human pathogens. *Chem. Biol. Drug. Des.* **78**, 73–84 (2011).
8 Boulos, R. A. Antimicrobial dyes and mechanosensitive channels. *A. Van Leeuwenhoek* **104**, 155–167 (2013).
9 Prole, D. L. & Taylor, C. W. Identification and analysis of putative homologues of mechanosensitive channels in pathogenic protozoa. *PLoS One* **8**, doi:10.1371/journal.pone.0066068 (2013).
10 Corry, B. *et al.* An improved open-channel structure of MscL determined from FRET confocal microscopy and simulation. *J. Gen. Physiol.* **136**, 483–494 (2010).
11 Wang, Y. *et al.* Single molecule FRET reveals pore size and opening mechanism of a mechano-sensitive ion channel. *eLife* **3**, doi:10.7554/eLife.01834 (2014).
12 McKinley, A. J., Riley, T. V., Lengkeek, N. A., Stewart, S. G. & Boulos, R. A. Antimicrobial Compounds. US20120329871 A1 (2012).
13 James, E. *et al.* A novel antimicrobial reduces oxidative stress in cells. *RSC Adv.* **3**, 7277–7281 (2013).
14 DeGrado, W. F. & Summa, C. M. De novo design and structural characterization of proteins and metalloproteins. *Annu. Rev. Biochem.* **68**, 779–819 (1999).
15 Boulos, R. A. *et al.* Inspiration from old dyes: tris(stilbene) compounds as potent Gram-positive antibacterial agents. *Chem. Eur. J.* **19**, 17980–17988 (2013).
16 Quinlan, G. J., Martin, G. S. & Evans, T. W. Albumin: biochemical properties and therapeutic potential. *Hepatology* **41**, 1211–1219 (2005).
17 Schumann, U. *et al.* YbdG in Escherichia coli is a threshold-setting mechanosensitive channel with MscM activity. *Proc. Natl Acad. Sci.* **107**, 12664–12669 (2010).
18 Yang, L. M., Zhong, D. & Blount, P. Chimeras reveal a single lipid-interface residue that controls MscL channel kinetics as well as mechanosensitivity. *Cell. Rep.* **3**, 520–527 (2013).
19 Zhong, D. & Blount, P. Phosphatidylinositol is crucial for the mechanosensitivity of Mycobacterium tuberculosis MscL. *Biochemistry* **52**, 5415–5120 (2013).
20 Blount, P., Sukharev, S. I., Moe, P. C., Martinac, B. & Kung, C. *Mechanosensitive Channels of Bacteria*, vol. 294, 458–482. Academic Press: San Diego, CA, USA, 1999.
21 Iscla, I., Wray, R., Wei, S., Posner, B. & Blount, P. Streptomycin potency is dependent on MscL channel expression. *Nat. Commun.* **5**, doi:10.1038/ncomms5891 (2014).
22 Schedletzky, H., Wiedemann, B. & Heisig, P. The effect of moxifloxacin on its target topoisomerases from *Escherichia coli* and *Staphylococcus aures*. *J. Antimicrob. Chemother.* **43**, 31–37 (1999).
23 Kouwen, T. R. *et al.* The large mechanosensitive channel MscL determines bacterial susceptibility to the bacteriocin sublancin 168. *Antimicrob. Agents Chemother.* **53**, 4702–4711 (2009).
24 Nguyen, T., Clare, B., Hool, L. C. & Martinac, B. The effects of parabens on the mechanosensitive channels of *E. coli*. *Eur. Biophys. J.* **34**, 389–395 (2005).
25 Kamaraju, K. & Sukharev, S. I. The membrane lateral pressure-perturbing capacity of parabens and their effects on the mechanosensitive channel directly correlate with hydrophobicity. *Biochemistry* **47**, 10540–10550 (2008).
26 Martinac, B., Adler, J. & Kung, C. Mechanosensitive ion channels of E. coli activated by amphipaths. *Nature* **348**, 261–263 (1990).
27 Perozo, E., Kloda, A., Cortes, D. M. & Martinac, B. Physical principles underlying the transduction of bilayer deformation forces during the mechanosensitive channel gating. *Nat. Struc. Mol. Biol.* **9**, 696–703 (2002).
28 Morris, G. M. *et al.* Automated docking using a Lamarckian genetic algorithm and an emperical binding free energy function. *J. Comput. Chem.* **19**, 1639–1662 (1998).
29 Nguyen, T., Clare, B., Guo, W. & Martinac, B. The effects of parabens on the mechanosensitive channels of *E. coli*. *Eur. Biophys. J.* **34**, 389–395 (2005).
30 *Spartan '02*, Wavefunction, Inc.: Irvine, CA, USA, 2002.
31 *Gaussian 98*, Gaussian, Inc.: Pittsburgh, PA, USA, 1998.
32 Lengkeek, N. A. *et al.* The synthesis of fluorescent DNA intercalator precursors through efficient multiple heck reactions. *Aust. J. Chem.* **64**, 316–323 (2011).

33 Moe, P. C., Levin, G. & Blount, P. Correlating a protein structure with function of a bacterial mechanosensitive channel. *J. Biol. Chem.* **275**, 31121–31127 (2000).
34 Blount, P., Sukharev, S. I., Schroeder, M. J., Nagle, S. K. & Kung, C. Single residue substitution that change the gating properties of a mechanosensitive channel in *Escherichia coli*. *Proc. Natl Acad. Sci. USA* **93**, 1652–11657 (1996).
35 Blount, P. *et al*. Membrane topology and multimeric structure of a mechanosensitive channel protein of *Escherichia coli*. *EMBO J.* **15**, 4798–4805 (1996).
36 Rajamuthiah, R. *et al*. Whole animal automated platform for drug discovery against multi-drug resistant *Staphylococcus aureus*. *PLoS ONE* **9**, doi:10.1371/journal.pone.0089189 (2014).

Supplementary Information accompanies the paper on The Journal of Antibiotics website (http://www.nature.com/ja)